Electrochemiluminescent & Amperometric Detection of DNA & DNA Damage

by

Lynn Dennany B.Sc. (Hons)

A Thesis presented at Dublin City University for the degree of Doctor of Philosophy

Supervisior:

Prof. Robert J. Forster

School of Chemical Sciences

August 2004

I hereby certify that the material, which I now submit for assessment on the programme of study leading to the award of doctor of philosophy, is entirely of my own work and has not been taken from the work of others, save and to the extent that such work has been cited and acknowledged within the text of my work.

Signed: Lynn Denneny ID: 97157163

Date: 8th Sept '04

Acknowledgements:

I would like to thank lots of people, these are just a few.

My supervisor Prof. Robert Forster for all his support, advice and endless enthusiasm throughout my time here. I also wish to thank Prof. James Rusling for letting me visit and work in his lab and for all his input during my stay in UCONN, and subsequently through emails.

To the present members of the Forster research group, Darragh, for being there for me right from the start, and Tommy (Thomas F. McEvoy) for all your help and of course all the nights out, you're both the best, Elena, Fabio, Johan, Javed and Richard, and to the past members, Lorraine, Darren, Sonia, Mary and Jenni for all your help when I first started. To everyone in DCU who I've gotten drunk with, asked for help, gone for coffee and everything else, it's made the last three years what they've been. A special shout out to Blánaid, for everything you've done for me both in and out of college. And a big thank you to, the champions of the chemistry football tournament, all the members of the McEvoy Team, Ray, Petes, Nigel, Gavin, and Andrea. To all the usual suspects, Orla, Eadaoin, Susan, Martina, Aoife, Daniel, Shane, John, Micheal, Clare, Frankie, Karl, and all the rest, I just can't fit you all in, as well as those with whom I worked in UCONN, especially, Maricar, Jing, Liping, Erwin and Ivy.

To all my family, despite not having a clue what I've been doing for the last few years have supported and encouraged me. So a special thanks to Mam, Dad, Alan, Suzanne, Gran, Deirdre, Joan and the rest of the bunch. A huge big thank you to Kieran for helping to keep me sane and keep me going right up til the end. I couldn't have done it without you.

Table of Contents

Abstract

Some ruthenium and osmium complexes and metallopolymers have been synthesised and characterised using viscosity, spectroscopic and electrochemical techniques. The obtained results showed that the photochemical and electrochemical properties of the monomeric complexes, *i.e.* $M(bpy)_3^{2+}$ and $M(bpy)_2(pic)_2^{2+}$, where bpy is 2,2'bipyridyl and pic is 4-picoline, accurately predict the properties of the analogous polymeric material, $M(bpy)_2(PVP)_{10}^{2+}$, where PVP is poly-4-vinylpyridine. However, the excited state lifetimes and quantum yield of photoluminescence are considerable lower for the polymeric materials than for the analogous $M(bpy)_3^{2+}$ complexes.

The $Ru(bpy)_2(PVP)_{10}^{2+}$ polymer is an effective mediator for the oxidation of the DNA base guanine using thin films of these materials on electrode surfaces. The film thickness and electrode potential were systematically varied in both sulphuric acid and PBS electrolyte showing that charge transport through the film is a diffusion-like process and the charge transport diffusion coefficient, D_{CT} is approximately 2×10^{-11} cm^2s^{-1}. This charge transport rate is independent of the concentration of the electrolyte, indicating an open porous layer structure. The osmium metallopolymer, $Os(bpy)_2(PVP)_{10}^{2+}$, was also shown to be an effective mediator for the oxidation of the biomarker 8-oxoguanine. The characteristics of this metallopolymer as a thin film were also investigated, yielding similar results to the ruthenium analogue.

ECL was demonstrated in solution phase via annihilation between the electrogenerated 3+ and 1+ forms of the compounds. The ECL spectrum for $Ru(bpy)_2(PVP)_{10}^{2+}$ was similar to the photoluminescence, suggesting that the same orbitals are responsible for the emission, whether the excited state was formed electrochemically or photochemically. The ECL efficiencies (ϕ_{ECL}) followed the same order as the photoluminescent efficiencies (ϕ_p). The effects of quenchers and self quenching as well as the temperature dependence of the luminescence was investigated, yielding information on the quenching constant, k_q, and the activation energies for both the monomeric and polymeric materials. Electrodes modified with thin films containing one or both of the redox polymers and DNA were used for dual amperometric and electrochemiluminescent detection of DNA damage, either by the formation of adducts by chemically generated damage or oxidative DNA damage, for use as a toxicity screening sensor. This system provides fast and accurate responses to the production of DNA adducts, which cause disruption of the DNA helical structure and to oxidative DNA damage in comparison to the methods already in use. The combined amperometric and electrochemiluminescent detection provided a more sensitive and selective sensor for this type of analysis. Immobilisation of the chemiluminescent reagent has a number of advantages over solution-phase ECL-based systems; conserves reagent, is simpler and more cost effective and has an additional level of selectivity. It also allowed for the utilisation of thin films containing both the redox polymers and DNA, which resulted in quick easy analysis of potential toxins.

CHAPTER 1

THEORETICAL FRAMEWORK

AND

SURVEY OF LITERATURE

"Quoting one is plagiarism, quoting many is research"

Anonymous

1.1 Deoxyribonucleic Acid (DNA):

1.1.1 The Structure of DNA:

DNA was identified as the molecular material that makes up genes in the mid 1940s by Avery, MacLeod and McCarty.[1] By the mid 1950s Crick and Watson,[2,3] using data from Franklin and Wilkins, had determined the structure of DNA.

The simplest way of looking at the structure of DNA is as two strands of molecular polymers. These wind around each other to form a double helix. Each of these strands of DNA is made up of monomers known as nucleotides. These nucleotides join together, or polymerise, to form the polymer DNA. The nucleotide itself is quite a complex molecule, consisting of three distinct components: a sugar, a nitrogenous base and phosphoric acid.[4] In DNA there are only four types of nitrogenous bases, and so only four types of monomer exist. It is also in these bases that the information stored in the DNA molecule is found, as it is the order of these bases in a DNA strand that ultimately determines the protein that is being encoded by a particular stretch of DNA. Thus, the sequence of these bases determines an individual's genetic make-up.

The four bases can be separated into two groups, each group having two members, Figure 1.1. The simplest bases are the pyrimidines, which have a single ring structure. The two forms found in DNA are thymine (T) and cytosine (C). The other two bases are called purines, which contain two rings in their structure. Guanine (G) and adenine (A) are the purines found in DNA.[4]

Once the nucleotides polymerise a polynucleotide is formed. Crick and Watson realised that DNA consisted of two polynucleotide strands, which run in opposite directions.[2,3] Further, these strands were wound around each other to form a double helix. The sugars and phosphate groups effectively form the staging of the helix and make two continuous strands from one end to the other. Sticking out from this staging and, more importantly, pointing inwards, are the bases. What Crick and Watson also realised was that the bases come into contact with each other and therefore each step of the staircase is actually two bases, attached by hydrogen bonding.[2,3]

The interactions seen on the steps of the DNA are shown in Figure 1.2. As can be seen, thymine on one strand always bonds to adenine while cytosine bonds to guanine. Therefore, once the sequence of bases on one strand is known, the sequence of the other strand is also known. The two strands are said to be complementary to each other, and the phrase 'complement strand' is often used. The second point to notice is that there are three hydrogen bonds between guanine and cytosine, while there are only two hydrogen bonds between adenine and thymine.[5]

If a model is made of the DNA molecule, it becomes apparent that the helix has a regular pattern. The helix is approximately 20 Å wide, and has two grooves running around and along it. One groove is referred to as the major groove, and the other is the minor groove. A simplified diagram is shown in Figure 1.3.

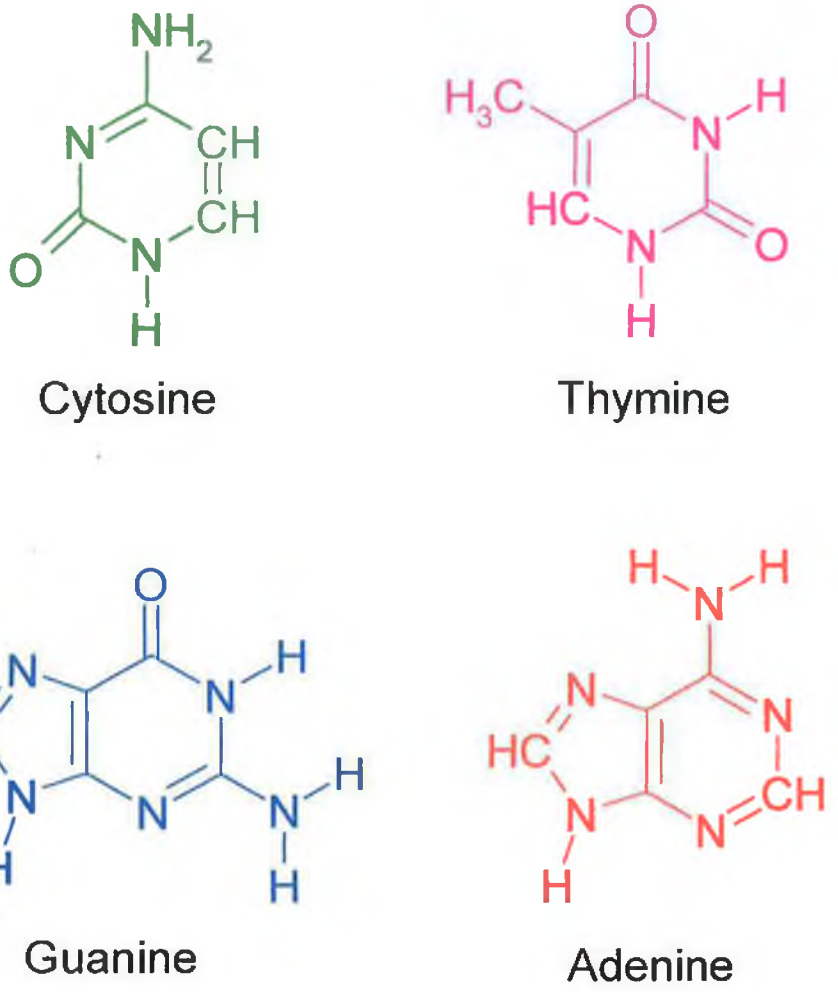

Figure 1.1: *The four bases found in DNA, the two pyrimidines bases; thymine (T) and cytosine(C), and adeneine (A) and guanine (G) the two purine bases.*

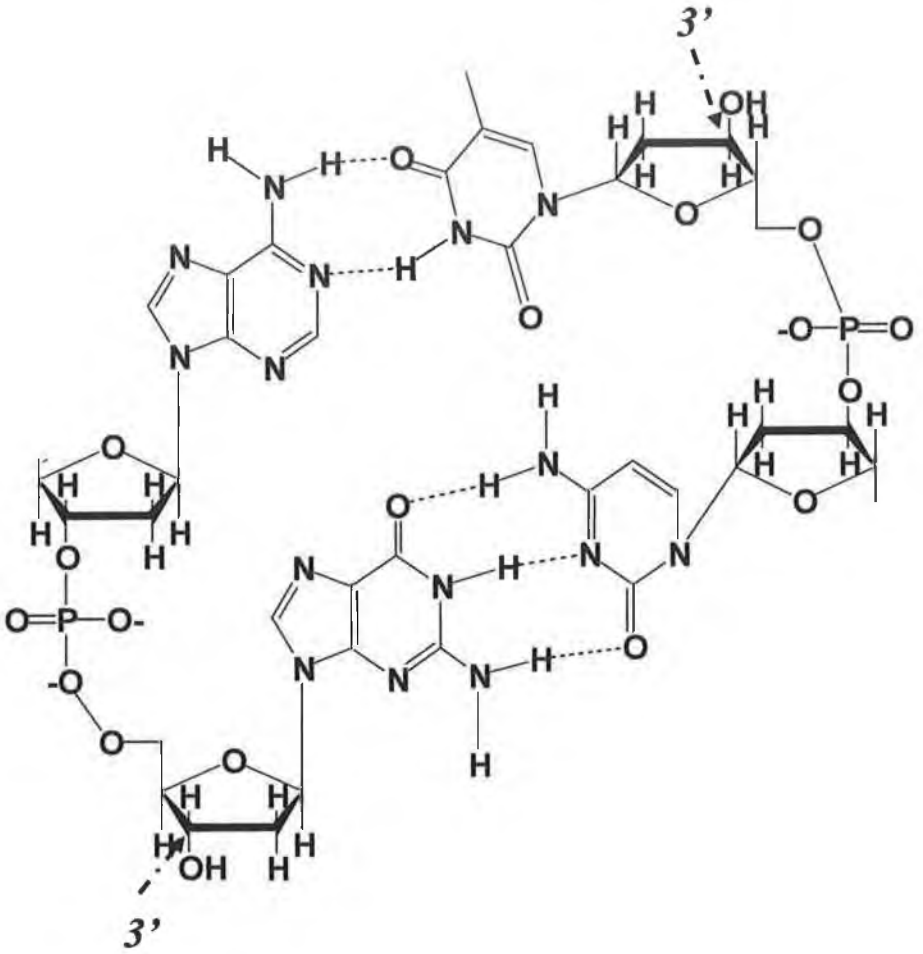

Figure 1.2: *Hydrogen bonding seen between bases in the DNA molecule.*

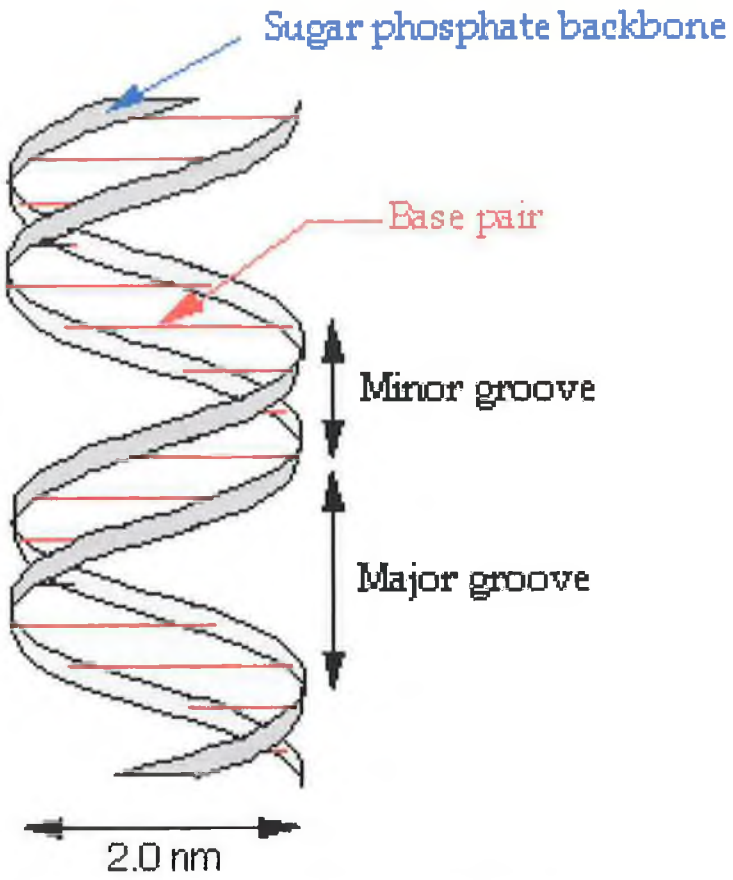

Figure 1.3: A diagram of the double helix.

1.1.3 The Role of Guanine in DNA Damage:

The oxidation and electrophilic alkylation of nucleic acids has been the focus of considerable research in toxicology, because the resulting lesions are suspected of leading to aging and cancer.[16] A major target for oxidants is guanine (G); as the base with the lowest ionisation potential of the four DNA bases,[17,18] it is the most likely site for damage to occur. Guanine certainly undergoes more reactions than the other three physiological bases. The oxidation of guanine leads to among other oxidation products, 8-oxoguanine, which has a lower fidelity in the replication process and enhances the probability for adenine incorporation into the complementary strand.[19] Thus, under conditions of oxidative stress, mutations from guanine-cytosine (G:C) base pairs into thymine-adenine (T:A) base pairs occur. Under UV irradiation[20] and in the presence of certain oxidants,[21] the first step of the oxidation process is the formation of a guanine radical cation ($G^{+\bullet}$). The guanines in GG and GGG sequences delocalise the charge among all the guanine bases, thereby lowering the potential. Because of the lower ionisation potential in comparison to single guanines,[22] the positive charge should migrate from the single $G^{+\bullet}$ to the G clusters if long-distance electron transport through DNA is possible.[20,21,23] Consequently, mutations will occur predominantly at G clusters. This is very dangerous, since several hot spot codons of p53 tumour suppressor genes contain GG sequences[20,21] making them prone to mutations. A more recent study also showed that the sites of mutation in p53 that are linked to lung cancer are the same sites at which benzo[a]pyrene adducts are formed, providing a strong link between smoking and lung cancer.[24] Smoking has also been linked to male infertility again due to its reaction with guanine.[8-11] Because of this, investigations into determining the possibility of charge transfer from a single $G^{+\bullet}$ to a GGG cluster have been carried out by Giese.[25] This group developed an assay that enabled site-selective oxidation of single G bases. The efficiency of the charge transport, measured using electrochemical techniques, diminished dramatically with increasing number of A:T base pairs between $G^{+\bullet}$ and GGG. However, in DNA strands where Gs are located

between the $G^{+\bullet}$ and GGG sequence, long-distance charge transport occurred by a multistep hopping mechanism.

1.1.4 Action of Styrene Oxide on DNA:

Chemical pollution of the environment comes with industrialization. Pollutants from factories and exhausts from automobiles contaminate the air we breathe and the water we drink, and endanger people's health. Also, certain chemicals or substances produced or used in the workplace may put people at an increased risk of developing certain types of cancers. It has been estimated that 85% of all cancers are caused by environmental pollutants.[26] At the same time, hundreds of thousands of new chemicals are generated each year. If these chemicals are aimed at commercial development, toxicity testing becomes more and more important. It is essential to quickly identify and characterize the toxicity of chemicals and pollutants, thus reducing the uncertainties in the assessment of human exposure.

Damage to DNA by chemicals and their metabolites constitutes a major toxicity mechanism.[27] The interaction between DNA and chemicals can lead to structural changes of the DNA double helix or chemical modification of DNA, which may cause serious mutations and induce various diseases.[28,29] In this study, the action of styrene and its metabolite, styrene oxide, a known carcinogen, was used as the model damage agent.

Styrene 7,8-oxide (SO) is a major metabolite of styrene,[30] a widely used chemical monomer. It is produced from the action of cytochrome P450 enzymes in the liver on styrene, shown in Figure 1.4. The formation of epoxides from alkenes, including, e.g. ethylene and propylene, is mainly mediated by CYP-dependent monooxygenases. This occurs by incorporating an atom of molecular oxygen into the substrate.[31] Even though this process is the first step in transforming lipophilic chemicals to excretable form, certain chemicals are activated by this to their ultimate carcinogenic form. Styrene is metabolised to styrene oxide (SO), by several enzymes, specifically CYP2B6 followed by CYP1A2, CYP2E1 and CYP2C8.[32] It has been shown to form DNA adducts *in vitro* and *in vivo* which may

be the cause of the mutagenic and carcinogenic properties of the chemical.[33,34,35,36] Under physiological conditions, the main alkylation sites for mono-substituted epoxides, such as styrene oxides, are the ring nitrogens at N7-guanine,[37,38,39,40] their structure is shown in Figure 3.8. This reaction takes place through the β carbon of the epoxides by S_N2 type reaction mechanisms. Although alkylation occurs preferentially at this site, other adducts have also being identified including those at the N2- and O6-guanine, N1- and N6-adenine and N3-cytosine, but to a much lesser extent.[42,41] The site of alkylation of the DNA constituents is mainly determined by the ionic character of the substrate.[42] Thus, alkyl epoxides that are not able to stabilise an ionic charge to any great extent, like aliphatic alkyl epoxides, react predominantly at ring nitrogen positions in DNA bases. As already stated, under physiological conditions the main alkylation sites are 7-guanine, 1- and 3-adenine, and 3-cytosine, in contrast, SO and BMO, butadiene monoxide, modify also exocyclic groups.[37,39,43,44] The reaction mechanisms of nucleoside alkylation have been studied using optically active epoxides. In the case of ring-nitrogen substitution, the reaction through the β-carbon has been found to follow direct displacement by S_N2 type of reaction mechanism.[45,46] In contrast, under neutral conditions the exocyclic sites open the epoxide in SO only at the α-carbon, resulting in both inverted and retained stereochemistry, indicating prominent S_N1 type of nucleophilic attack. [45,47]

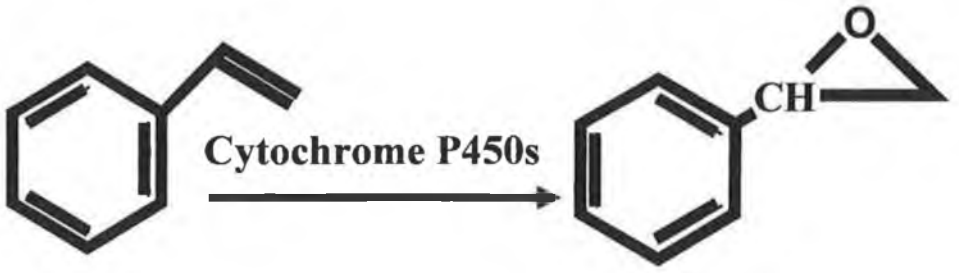

***Figure 1.4**: Formation of styrene oxide.*

The formation of adducts by the reaction of styrene oxide with the DNA bases disrupts the helical structure of DNA. This disruption causes the DNA to

uncoil, forming a structure that is more single stranded in character. Once uncoiled the DNA bases can react more readily with complexes such as $Ru(bpy)_3^{2+}$. DNA adducts represent the most direct measure of the biological effect of a potential carcinogen.[46,47,48] The adducts may trigger a cascade of complex processes leading to mutagenesis and carcinogenesis, as illustrated in simplified form in Figure 1.5.[49] It was earlier assumed that DNA adducts play a role predominantly in the initiation phase of carcinogenesis. The recent evidence of genetic lesions in multiple steps of cancer development suggests that DNA adducts are involved in many stages of ontogenesis. The reasons for the particular importance of DNA adducts measured in qualitative and quantitative ways using properly characterized internal and external standards were clearly elucidated by Hemminki.[50] Moreover, DNA adducts represent an individual measure of metabolic as well as DNA repair capacity. An additional reason to use styrene as a model compound is its unique capacity to act as both an alkylating and aralkylating agent, giving rise to a wide spectrum of various DNA adducts. Different kinds of adducts at different sites of the DNA bases exhibit different biological properties, which may result in different kinetics of formation and removal, different rates of the repair process and therefore, in different degrees of biological significances and mutagenic potencies.

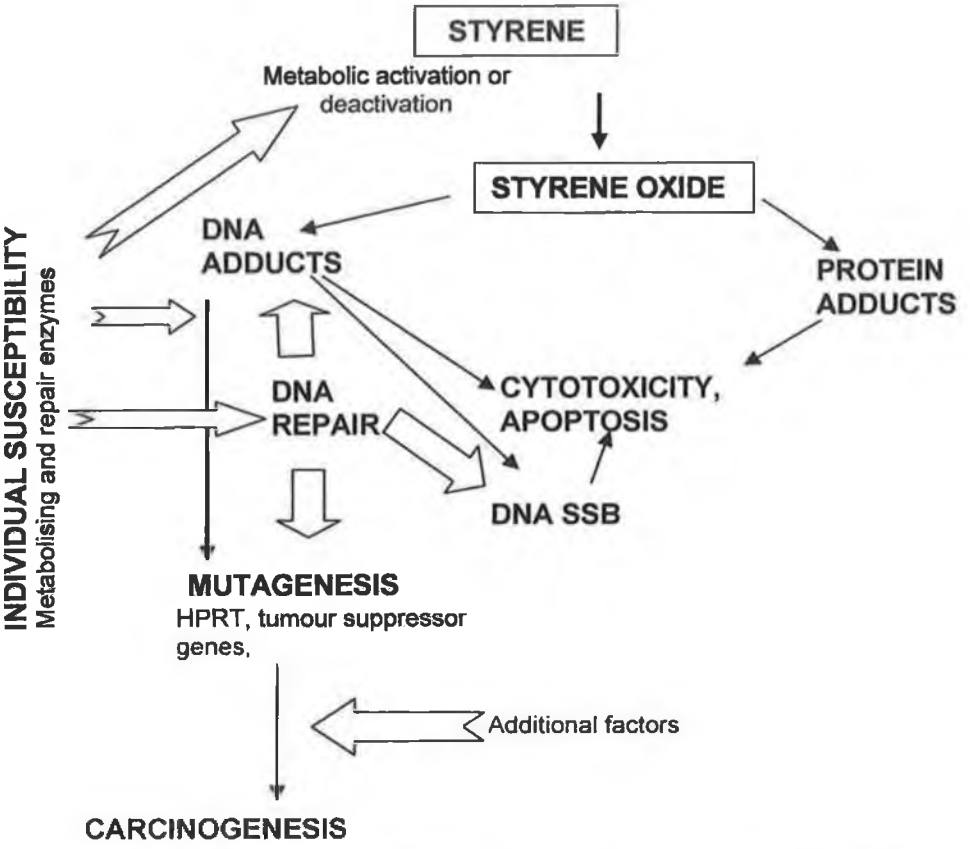

Figure 1.5: *Cascade of processes leading to mutagenesis and carcinogenesis. Adapted from reference 41.*

Most epoxide-alkylation in DNA has been shown to take place at 7-guanine and 3-adenine, leading to potentially mutagenic apurinic sites. The 7-guanine and 3-adenine adducts are expected to result in GC→TA and AT→TA transversions, respectively, since DNA polymerase preferentially adds an adenine opposite to an apurinic site.[51] Such mutations have indeed been found in SO-treated hypoxanthine-guanine phosphoribosyl transferase (*hprt*) mutant clones[52] and in PO-treated *Salmonella hisG46* and *hisG428*.[53] AT→TA transversions have also been identified at the *hprt* locus in mice splenic T cells exposed to BD, whereas exposure to BMO and DEB produced more GC→TA transversions.[54] It has been shown that in genomic DNA the steady state of apurinic/apyrimidic sites is ~1 lesion per 10^5 nucleotides.[55] In humans, the adduct levels induced by the epoxides studied could be expected in level up to few adducts per 10^8 nucleotides and in experimental animals few adducts per 10^6 nucleotides. Therefore, the mutagenic role of the apurinic sites originating from the 7-guanine or 3-adenine adducts induced by these epoxides can be considered rather small, especially because the apurinic/apyrimidic sites are constantly being repaired. The repair mechanism therefore has the ability only to repair damage in a particular range. So low adduct formation can be repaired, a high adduct formation results in the death of the cell, but the formation of adducts between these ranges can remain undetected by the repair mechanism and it is cumulative affect of these adducts that is responsible for carcinogenicity.

Even though formed to lower extent, substitution at base-pairing sites of DNA can be expected to be more mutagenic as compared to the 3-adenine or 7-guanine adducts. The dominating type of SO-induced *hprt*-mutation was the AT→GC transition[52] and short term animal studies on BD have shown the mutations at the AT base pairs to be the predominant ones.[56] These mutations are likely related to 1- or N^6-alkylation of adenine residues. The AT→GC transition was observed in a site-specific mutation study in which a SO adduct at N^6-adenine was inserted in *N-ras* gene codon 61. However, the N^6-adenine adduct showed a rather low miscoding potential,[57] probably because the adduct has still the

possibility for base-pairing with thymine residues. The same transition was also observed in a study by Carmical et al.[58] where RR enantiomer of BDE was inserted at the N^6-position of adenine within the *N-ras* codon 61. Interestingly, the corresponding SS enantiomer yielded exclusively AT→CG mutations.[58] It appears that the N^6-adenine adducts are not responsible for the mutagenesis associated with the exposure BD or styrene metabolites. More likely mutagenic candidates are the 1-adenine adducts, or the corresponding deaminated 1-hypoxanthine adducts,[59] since they occupy a central Watson–Crick base pairing site disrupting the normal hydrogen-bonding.

Since the guanine adducts are most likely to be formed from these reactions, they can useful as biomarkers of exposure to the studied epoxides. The major advantage of 7-substituted guanines is their high concentration relative to the concentration of other adducts formed. But because of their lower mutagenicity they can be mainly used as a surrogate marker for other promutagenic adducts. The reaction of styrene oxide on DNA also produces several DNA-SO adducts, as previously stated this can also be useful for toxicity testing. The DNA-SO adducts disrupt the helical structure of DNA allowing, for example, the guanines present be more readily available for other reactions, therefore providing a distinct difference in response for intact DNA and damaged DNA. This is the type of system utilised in this study.

1.1.5 Oxidative DNA Damage:

Oxidative damage is also of particular interest in this study. Oxidative damage can occur from a variety of sources, including γ-irradiation, photoionisation, reactive oxygen species (ROS) and a variety of chemicals.

Oxygen is essential for normal respiratory function; however, it has many toxic effects. These effects, as with many damaging pathways, may vary with the type of organism, its age, physiological state and diet. The majority of the damaging effects of oxygen can be attributed to the formation of O_2 radicals *in vivo*. With over 20 ROS adducts identified, and the availability of ROS *in vivo*, antioxidant defences have evolved to protect against ROS. Levels of oxidative stress are therefore extremely important, since only intermediate levels of the oxidative base lesion are likely to have a mutagenic effect. Both very high and very low levels of base lesions are repaired by the defence mechanisms.

Hydroxyl radicals are probably the most noxious of the ROS generated from O_2 and react directly with all known biomolecules at diffusion limited rates, $\sim 10^7$–$10^{10} M^{-1}s^{-1}$. This is possible due to its unique characteristics in comparison to other ROS. It is the most electrophilic radical to which DNA is normally exposed. It has a strong tendency for both addition across a double bond and hydrogen abstraction. It also has high thermokinetic reactivity. As such, all components of the highly electron dense DNA strand are subject to $^{\bullet}OH$ attack. At least five groups of damage by this radical may be generated, including oxidised bases, abasic sites, DNA-DNA intrastrand adducts, strand breaks and DNA-protein cross links.

A large number of lesions caused by the action of $^{\bullet}OH$ radicals have been reported for the purine bases in DNA. Purine $^{\bullet}OH$ adducts demonstrate a phenomenon called "redox ambivalence", *i.e.*, they are mesomeric structures that are easily oxidised and easily reduced. Therefore, the relative yields of each lesion formed cannot be obtained using a mass balance. $^{\bullet}OH$ adds to C4, C5 and C8 of

guanine. C8OH is probably the most studied adduct, and is one that exhibits redox ambivalence. Reduction of C8OH gives a formamidopyrimidine (FAP_y), while oxidation results in 8-oxoguanine. Interestingly, the adducts formed at C4 and C5 decay back to form the guanine, in a type of "auto repair mechanism". Therefore, although addition at C8 accounts for only 25% of the $^{\bullet}OH$ addition, it is the only lesion which causes significant base adducts. Hydrogen extraction from a guanine sugar can cause a cyclic adduct with the guanine base sugar itself, 8,5'-cyclo-2'-deoxyguanosine. This reaction is, however, suppressed in the presence of oxygen, as it reacts with the sugar radical before it can cyclise. The lesions generated by $^{\bullet}OH$ addition to guanine are shown in Figure 1.6.

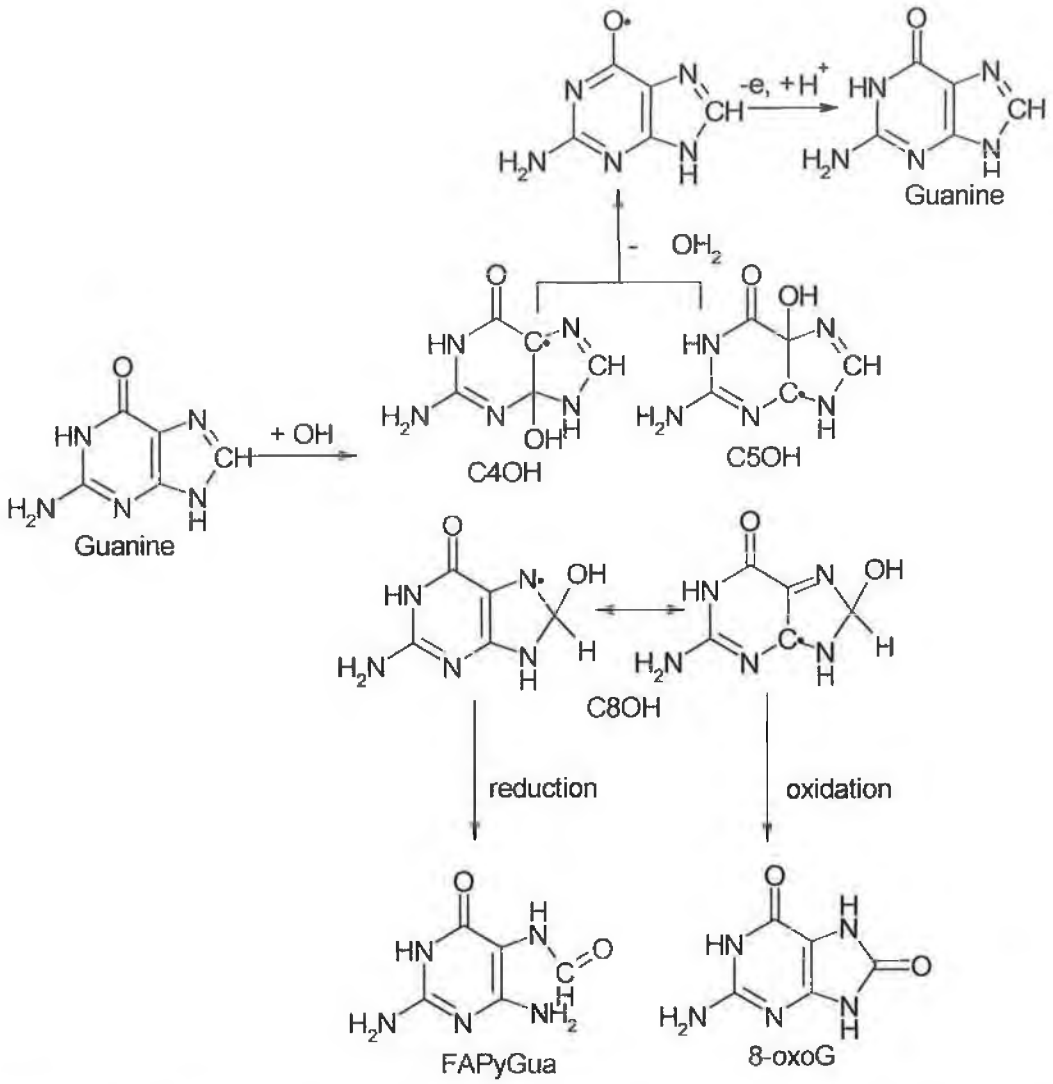

Figure 1.6: *Guanine lesions generated by attack of •OH. Adapted from reference 60.*

$^{\bullet}$OH on average travels a maximum of 3 nm (about 5-10 molecular diameters) before it reaches a molecule with which to react. It cannot, however, cross biological membranes; as such, it can only inflict damage on DNA if it is generated in very close proximity to the duplex. H_2O_2, a precursor for $^{\bullet}$OH, can cross biological membranes and so if a metal catalyst is localised very close to DNA, $^{\bullet}$OH can be generated close enough to inflict oxidative damage. The major endogenous source of $^{\bullet}$OH within cells is the transition metal mediated Fenton reaction. H_2O_2 is ubituous in the human body as it is a by-product of enzymatic reactions.

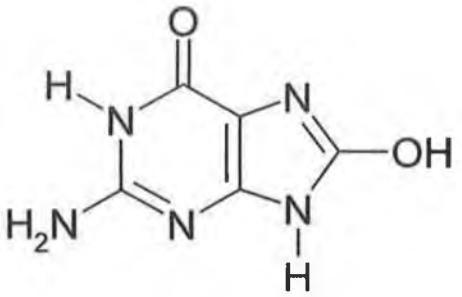

6-keto, 8-enol form

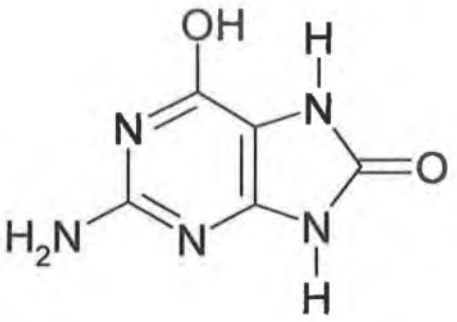

6-enol, 8-keto form

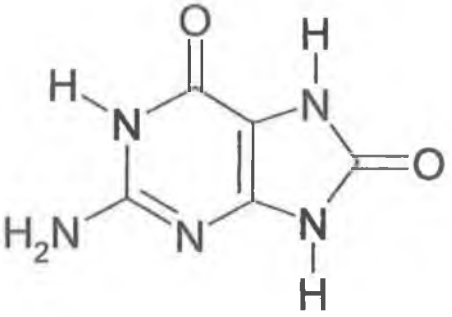

6,8-diketo form

Figure 1.7: *Chemical structures of 8-oxoguanine. The 6,8-diketo is the most stable form of the molecule.*

The main oxidative adduct examined in this study is 8-oxoguanine. 8-oxoG was first reported in 1984 by Kasai and Nishimura. It can be formed via the mediation of hydroxyl radials in the Udenfriend system (ascorbic acid, Fe^{II}, EDTA, O_2). It differs from its parent base guanine in that it has an ionisation potential approximately 0.5 V lower than guanine. The oxidation of guanine to form 8-oxoG has been well studied, and based on electrochemical studies, it has been established that it involves a two proton ($2\ H^+$), two electron ($2\ e^-$) oxidation. The reaction is a proton-coupled electron transfer (PCET), *i.e.,* both a proton and an electron are removed in a single step.

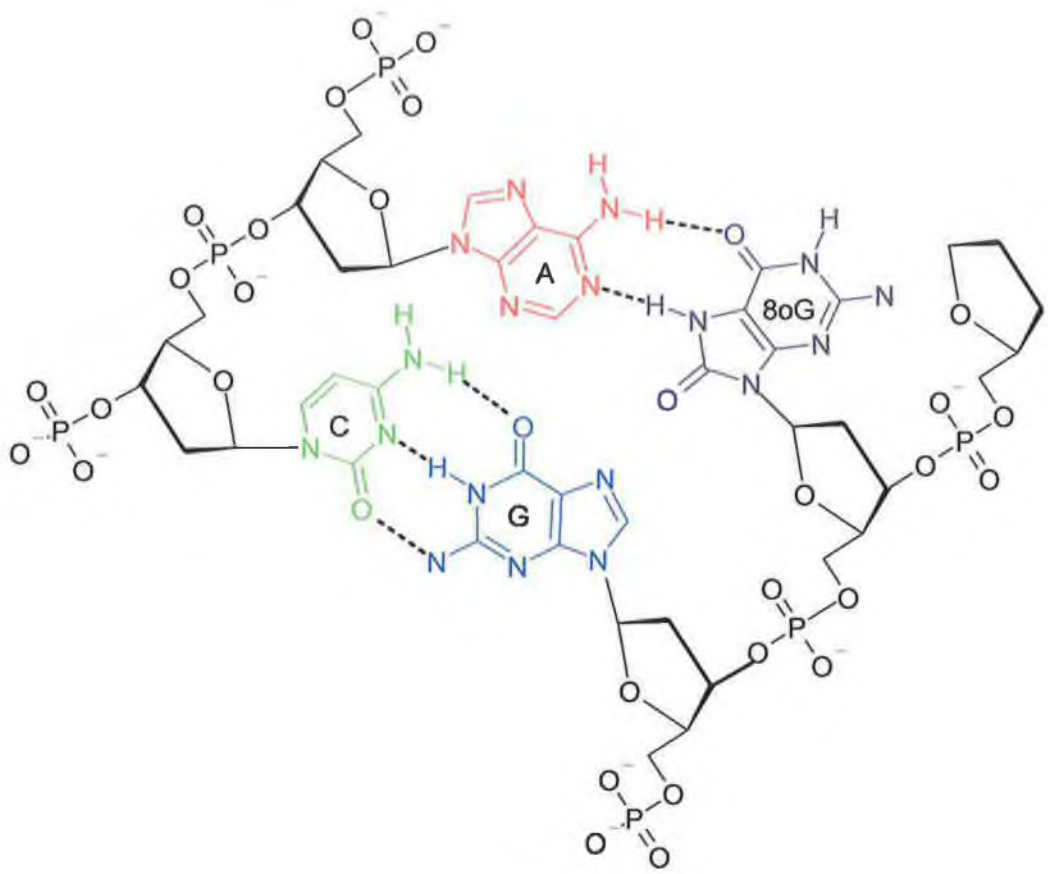

Figure 1.8: *Watson-Crick base pair C:G and Hoogsten base pair A:8-oxoG in the DNA double helix.*

Once guanine has been converted to 8-oxoG, the 8-oxoG is incorporated into the double helix with very few structural perturbations; however, 8-oxoG directs the incorporation of the DNA base adenine, A, as well as cytosine. It was reported that in 99% of cases, C was incorporated opposite 8-oxoG, and so in these cases there was no long term effects of guanine oxidation. However, in the other 1% of cases A was incorporated opposite 8-oxoG, resulting in a G $\rightarrow$ T substitution, which has been implicated in carcinogenesis. The oxidation of guanine alters the hydrogen bonding functionality of the bases, so the 8oxoG has the same pattern of hydrogen bond acceptors/donors as T, as shown in Figure 1.8.

It is clear therefore that 8-oxoG, one of the primary oxidation products of guanine, can be formed and has mutagenic effects.

1.2 Electrochemical Approaches to DNA Damage Detection:

Sequence-selective detection of analyte DNA sequences have been reported using a variety of electrochemical sensors, or biosensors, based on voltammetric, and electrogenerated chemiluminescent measurements.[61,62,67] Indeed, the electrochemical voltammetric oxidation of DNA[69,] is attractive for rapid, inexpensive assays in comparison with chromatographic or electrophoretic analysis of hydrolysed samples. While they are separation based techniques they can provide detailed molecular information on DNA damage,[63] especially when coupled with mass spectroscopy,[63,64] they are limited by long sample preparation times and high costs.

The voltammetric method has been used to detect DNA hybridisation on electrode surfaces.[64-66] The detection principle relies on changes in peak current or potential of a redox-active molecule that selectively binds with DNA. Mikkelsen *et al*, covalently immobilised single-stranded DNA on a glassy carbon surface via the formation of amide bonds between activated carboxylate groups on the electrode surface and the amine group of the deoxyguanine residues of oligonucleotide probes.[65,66] The formation of double stranded DNA was monitored by changes in the voltammetric peak current of $Co(bpy)_3^{3+}$, a DNA minor groove-binder. Interfacial DNA hybridisation results in preconcentration of $Co(bpy)_3^{3+}$ on the electrode surface, resulting, in turn, in an increase in oxidation current.

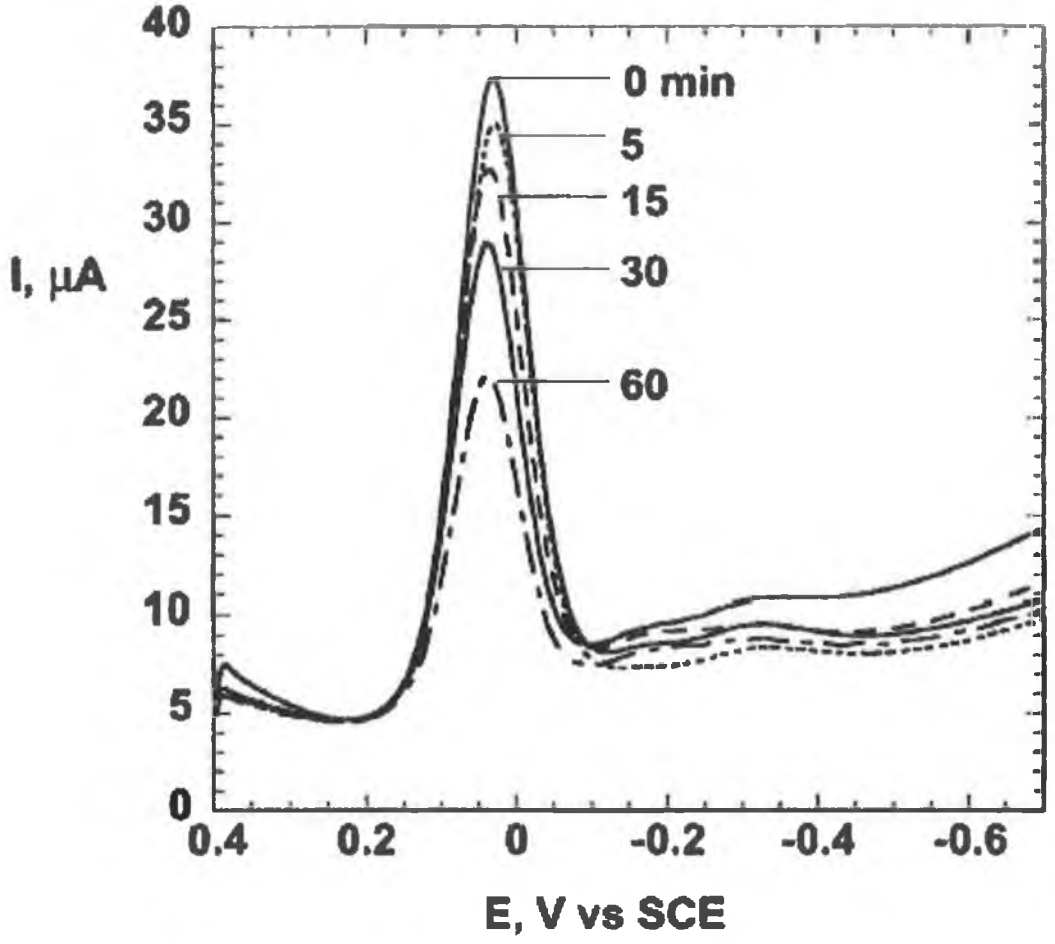

Figure 1.9: *SWV of PDDA/ST ds-DNA(Mb/ST ds-DNA)$_2$ films on rough pyrolytic graphite (PG) reacted at 37 °C with 4% styrene and 2 mM H_2O_2 at pH 5.5 and then transferred to 20 μM $Co(bpy)_3^{3+}$ in pH 5.5 buffer. Adapted from reference 67.*

Another development in this area was studied by Palacek and co-workers.[68] They employed adsorption of DNA on mercury and carbon electrodes, and showed that single stranded DNA was much more easily oxidised than double stranded DNA, since single stranded DNA is not protected by the shielding effect of the helical structure.[68,69] Adsorptive voltammetry on mercury electrodes was used to detect DNA damage from strong acids,[70] methylating agents,[71] and hydroxyl radicals.[72,73] Damage from ionising radiation was detected on mercury electrodes by adsorptive linear sweep voltammetry[74] and adsorptive AC voltammetry[75] in DNA solutions, and by using chronopotentiometry with DNA adsorbed onto carbon electrodes.[76]

A recent study reported detection by direct oxidation of damaged DNA films on graphite electrodes using derivative square-wave voltammetry.[77] Calf Thymus DNA films gave near featureless backgrounds and oxidation peaks developed as the film was incubated with styrene oxide, which forms known covalent adducts with guanosine in DNA[78] leading to abnormal molecular genetic events.[79] This method detected adducts which resulted from the reaction of styrene oxide with DNA.

It had been shown that nucleic acids could be detected in solution via catalytic oxidation of guanine bases using $Ru(bpy)_3^{2+}$ as the mediator.[80] In solution, $Ru(bpy)_3^{2+}$ exhibits a reversible redox couple at +1.05V, similar to the oxidation potential observed for guanosine.[17,18] Addition of guanine-containing DNA to a solution of $Ru(bpy)_3^{2+}$ therefore leads to a catalytic enhancement in oxidation current according to a two-step mechanism;

$$Ru(bpy)_3^{2+} \rightarrow Ru(bpy)_3^{3+} + e^- \quad \textbf{(1)}$$

$$Ru(bpy)_3^{3+} + DNA \rightarrow DNA_{ox} + Ru(bpy)_3^{2+} \quad \textbf{(2)}$$

where DNA_{ox} represents a DNA molecule where guanine has undergone a one-electron oxidation.[81]

Thorp *et al.*, also investigated the kinetics of this reaction and concluded that only guanosine bases in DNA were oxidised, and that the rate of oxidation and thus, the catalytic current depends on the DNA structure and base sequence.[80,82,83,84] The oxidising metal complexes mediate the electrochemical oxidation of guanine nucleotides in polymeric DNA and oligonucleotides. This catalysis results in an enhancement in cyclic voltammograms that yields the rate constant for oxidation of guanine by the metal complex. Due to the fact that the cationic transition metal mediators interact in the minor groove of DNA, intimate contact between the mediator and guanine is precluded by the unique structure of the double helix. The accessibility of electrons to guanine is influenced by the nature of the base opposite guanine, the electron-transfer rate constant can therefore be used to identify the paired (or mismatched) base.[80] The oxidation rate constants follow the trend G(single strand) > GA > GG > GT > GC. These mismatches are all distinguishable from each other.

Subsequent work showed that sequences of guanines in the DNA strand also affected the rate constants.[84] The GG doublet and GGG triplet have lower ionisation potentials than that of guanine, and as such can be used as a "hole trap" in the study

of DNA-mediated electron transfer. The study indicated that the increased electron donor reactivity is primarily due to the favourable placement of the electronegative N7 atom of the base, these results in a relative increase in current on going from G to GG to GGG as shown in Figure 1.10. These results may also support the finding that triplet guanines are more prone to damage since they are more reactive and act as electron traps in the DNA structure.

The use of ECL in the detection of DNA has also been studied. The main focus of EC detection systems which utilise ECL do so either by using a cofactor such as TPrA (tri-*n*-propylamine), or a label to produce the ECL[114-117]. The emission produced from TPrA arises from the energetic electron transfer reaction between electrogenerated DNA-$Ru(phen)_3^{3+}$ and an intermediate in the oxidation of TPrA. The use of labels to detect DNA by ECL is described in the following sections.

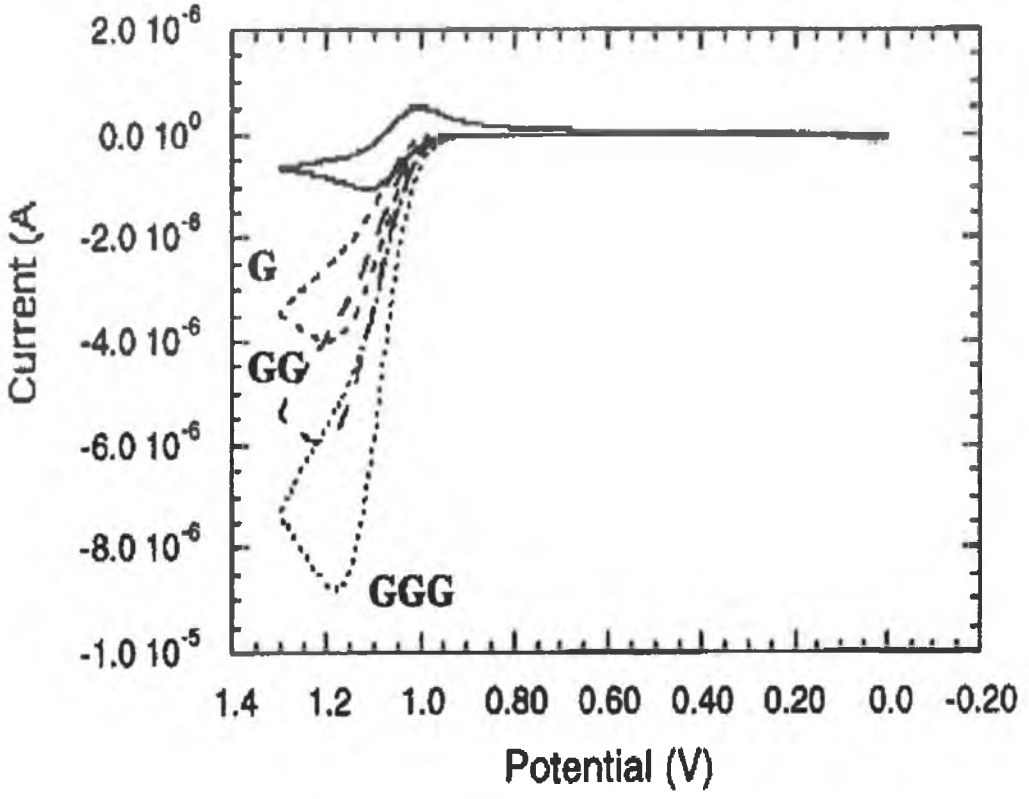

Figure 1.10: *Cyclic voltammograms of $Ru(bpy)_3^{2+}$ (25 μM) in the presence of 75 μM DNA in 50 mM sodium phosphate buffer with 700 mM NaCl. Cyclic voltammograms shows added sequences to the single stranded forms of G15 (G, short dashed), GG16 (GG, long dashed), and GGG17 (GGG, dotted). The solid line is a CV of $Ru(bpy)_3^{2+}$ only. Adapted from reference 84.*

1.3 *Electrochemical Methods Used to Study Polymer Modified Electrodes:*

1.3.1 Cyclic Voltammetry:

Cyclic voltammetry (CV) involves monitoring the current response of a small stationary electrode in an unstirred solution which is excited by a triangular potential wave form.[85] This technique has found widespread application in the investigation of modified electrode processes.[86] Cyclic voltammetry can be utilised to determine the diffusion coefficient, D_{CT}, the extent of electro-activity of modifying layer or the feasibility of mediated oxidation of a particular analyte.

In cyclic voltammetry the potential applied to the working electrode is first swept in a forward direction, stopped at a desired potential, then a reverse sweep returns the potential to its initial value and then repeated for a defined number of cycles. The potential range of these sweeps is chosen to drive redox switching of an analyte and the current (I) is recorded as a function of the potential (E). The current response resulting from electron transfer between the analyte and the electrode and is associated with a change in the oxidation state of the electroactive analyte.[139] The measured values in this I vs. E plot are the anodic and cathodic peak potentials $E_{p,c}$ and $E_{p,a}$; the anodic and cathodic peak currents $I_{p,c}$ and $I_{p,a}$; and the half-peak potentials, which are the potentials $E_{p/2,c}$ and $E_{p/2,a}$, at which the cathodic and anodic currents reach half their peak values. The independent variables are the voltage scan rate and the range of potential over which the scan is made. The former is the most important parameter in a diagnostic sense, although proper selection of scan range can often eliminate interferences from other processes. How these parameters or quantities of interest are established is illustrated in Figure 1.11.[87]

Characterising modifying layers under conditions of finite diffusion has received considerable attention. This is the condition in which the redox composition of the layer is in thermodynamic equilibrium with the electrode potential, (*i.e.*, the Nernst condition), it will be observed for all electrochemical reversible reactions at sufficiently slow cyclic voltammogram scan rates, such that all electroactive centres undergo redox transformation on the time scales considered.

For the typical theoretical response for a cyclic voltammogram of an electrochemically reversible couple that is confined on the electrode surface. The peaks for surface-confined species are sharp and symmetrical unlike those for freely diffusing species. This behaviour is due to the presence of a fixed amount of redox active species at the electrode, which is not altered by the complications of mass transfer. When a potential is applied to a surface modified electrode the current rises from essentially zero to a peak value and then back to zero. For an ideal system no peak-to-peak separation is expected.

An ideal reversible voltammetric process involving a surface bound reactant has the following features;

$$i_p = \frac{n^2 F^2 A \Gamma \nu}{4RT} \quad \textbf{(3)}$$

$$E_{p,c} = E_{p,a} \quad \textbf{(4)}$$

$$FWHM = \frac{90.6}{n} mV \quad \textbf{(5)}$$

$$\frac{i_{p,c}}{i_{p,a}} = 1 \quad \textbf{(6)}$$

where FWHM is the full width at half maximum, n is the number of electrons passed, F is Faraday constant, Γ the total electroactive coverage, A is the electrode area, ν is the scan rate, R the gas constant and T is temperature. These are shown in Figure 1.11.

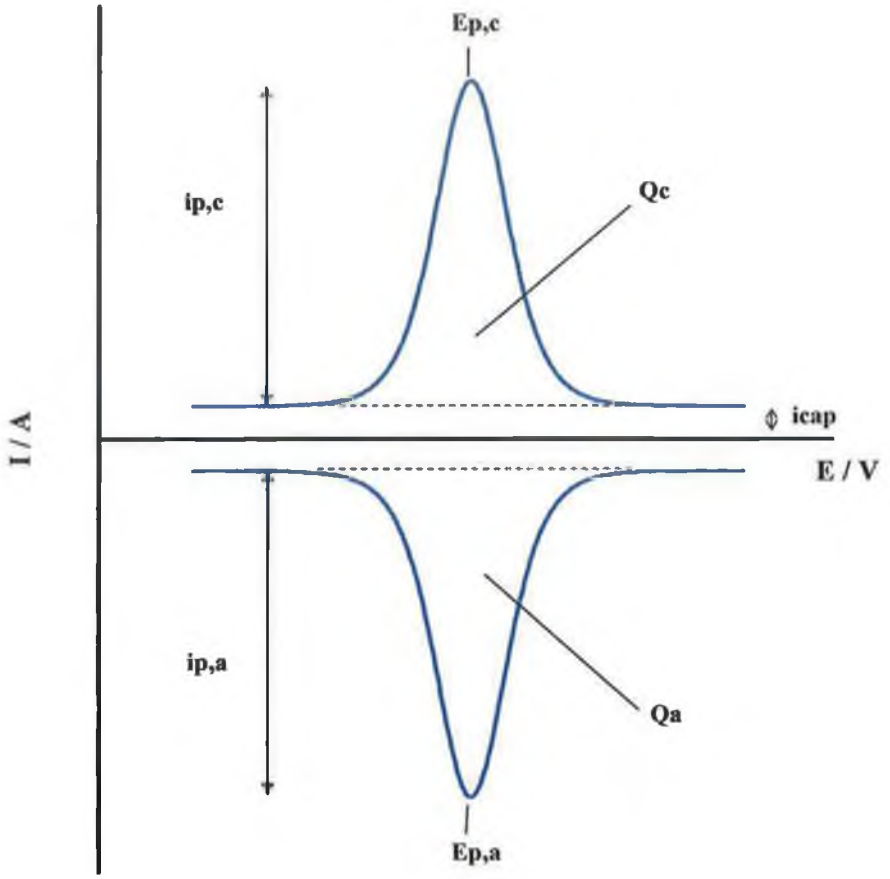

Figure 1.11: *Cyclic voltammogram of a chemically modified electrode with a monolayer of an electrochemically reversible mediator. i = current, E = potential, p = peak, c = cathodic, a = anodic, cap = capacative.*

Under these conditions of exhaustive oxidation/reduction of the modifying layer the Faradaic charge, Q, under the current potential curve gives the quantity Γ (mol cm^{-2}) according to the expression;

$$\Gamma = \frac{Q}{nFA} \qquad (7)$$

Charge measurements, which use a simple current baseline as in Figure 1.12, assume that any dispersion in double layer capacitance current, accompanying alterations in surface ionic charge caused by reduction or oxidation is insignificant.

For a polymer or thicker film under these conditions of finite diffusion, a plot of scan rate versus peak current will be linear. At higher scan rates where there is sufficient time to only electrolyse part of the total number of redox sites during each linear scan, a transistion to semi-infinite diffusion control occurs and a $\nu^{1/2}$ dependence on peak current is observed. Under these semi-infinite conditions the following behaviour is observed;

$$\Delta E_p = \frac{57}{n} mV \text{ (at 25 } ^0\text{C)} \qquad \textbf{(8)}$$

1.3.2 Chronoamperometry:

In potential step experiments the potential of the working electrode is changed instantaneously, and either the current-time (chronoamperometry) or the charge-time (chronocoulometry) response is recorded.[88]

A potential step at a redox polymer film modified electrode produces a current-time decay which can reflect the diffusion rate of electrochemical charge. Thus under the condition $D_{ct}\tau/d^2 << 1$, e.g. at sufficiently small times where semi-infinite diffusion prevails, the decay of current from a large potential step (completely across the wave) should conform to the Cottrell equation;

$$i(t) = \frac{nF'AD_{ct}^{1/2}C}{\pi^{1/2}t^{1/2}} \qquad (9)$$

The apparent charge transport diffusion coefficient can thus be evaluated if C is known, by plotting i(t) verses $t^{-1/2}$.

Accurately determining D_{ct} requires a diffusional response and the absence of migrational effects (i.e. movement of species under the influence of an electric field) Perturbation of the diffusion current by other components manifests itself as a non-zero intercept on the short time portion of the Cottrell plot or as a peak in a plot of $it^{1/2}$ verses $t^{1/2}$.[89]

It should be noted that although the accepted mechanism for charge transport in redox polymer films is a succession of electron transfer self exchange reactions (i.e. electron hopping) between neighbouring redox sites, this process is often not rate determining. Since the charge on the electroactive centre is altered during redox switching, a flow of counter ions and associated solvent necessarily accompanies electron transport. Also, some segmental polymer chain motion may be necessary in order to juxtapose redox centres. Therefore, apart from the intrinsic thermal barrier to electron transfer, the rate limiting process may be the rate of ion

diffusion required to maintain electroneutrality or the rate of polymer chain movement.[89] Two of these processes are mutually opposed; rapid electron diffusion is most favoured by a high concentration of oriented sites, while rapid ion diffusion is favoured by swollen films in which the void volume is high. It has been reported that optimal charge transport rates are therefore observed for intermediate loadings of redox sites.[90]

A steady-state dual-electrode ring disk technique has been utilised in order to decouple the two transport processes. This method effectively freezes out the counter-ion contribution and hence enables the contribution from electron exchange to be determined.

Impedance spectroscopy has also been used to evaluate D_{ct}. Since this technique is based on the response of the system to a small applied sinusoidal potential with variable frequency, which is normally superimposed on a D.C. potential, only a tiny fraction of the total number of redox groups is active during the measurement and correspondingly small quantities of counter-ions are transferred across the film / solution interface to preserve electroneutrality. This technique has been compared with chronoamperometry and shown to yield similar charge transport values[91].

1.3.3 Homogeneous Charge Transport:

In most films, electrochemical charge transport is thought to occur by electron self exchange reactions between neighbouring oxidised and reduced sites. This electron hopping process is mathematically representable by diffusion laws in which the charge transport diffusion coefficient, D_{ct}, is introduced as a measure of its rate. However, this is only one of many factors which effects charge transport. Other factors include ion transport and heterogeneous electron transfer.

The concentration profile of fixed oxidised and reduced sites within the film depends on the dimensionless parameter $D_{ct}\tau/d^2$, where τ is the experimental time scale, (related to the time for a potential scan to traverse the wave), and d is the polymer layer thickness. When $D_{ct}\tau/d^2 >> 1$, all electroactive sites within the film are in equilibrium with the electrode potential, and the surface type behaviour described previously is observed. In contrast, when $D_{ct}\tau/d^2 << 1$, the oxidising scan direction is switched before reduced sites at the film's outer boundary are oxidised. This is the semi infinite electrochemical charge diffusion condition, here the $\nu^{1/2}$ dependence of the peak current is seen. The peak current is given by the same equation as that used for species dissolved in solution and diffusing to the electrode surface, *i.e.*, the Randles-Sevcik equation;

$$i_p = 2.69x10^5 n^{3/2} A D_{ct}^{1/2} \nu^{1/2} C \qquad \textbf{(10)}$$

where C is the concentration of electroactive sites within the film. This equation is routinely used for evaluation of D_{ct} using cyclic voltammetry at relatively high scan rates (typically > 50 mV/s).

1.3.4 Mediated Electron Transfer:

Electrochemical reactions, unlike homogeneous chemical reactions, have rate constants that are dependent on the applied over-potential of the electrode; this is normally an exponential relationship as described by Butler-Volmer kinetics. At the potential where iso-energetic conditions are satisfied, i.e., where the energy of the electron and the donating / accepting orbital are equal, electron transfer should be in equilibrium, this is the thermodynamic formal potential, E°, of the redox couple.

Frequently however it is required to apply potentials in excess of those predicted purely on the basis of thermodynamics in order to drive a particular reaction. This extra driving force is known as the activation over-potential and is a result of the excess free energy required to surmount the activation energy barrier for the electron transfer.

Applying a large activation over-potential is undesirable in electroanalysis; since it greatly increases the number of interferences that may be electroactive in the measurement cycle. Mediated electron transfer or electrocatalysis is a process which seeks to provide lower energy of activation pathways by mediating electron transfer to the analyte through a suitable redox species as described by the following equations:

$$\mathbf{A - e^- \rightarrow B} \qquad \mathbf{(11)}$$

$$\mathbf{B + S \rightarrow A + P} \qquad \mathbf{(12)}$$

Where A and B are the reduced and oxidised forms of the mediator respectively and S and P are the substrate and product. In addition to lowering overpotential, electrocatalysis can improve sensitivity and lower limits of detection as a result of increased reaction rates.

For true electrocatalysis the Gibbs free energy function (ΔG^0) for the catalytic reaction must be negative, this is given by the formula;

$$\Delta G^0 = -n\ F\ \Delta E^0 \qquad (13)$$

where ΔE^0 is the difference between the formal potential of the substrate and that of the electrocatalyst. As ΔG^0 must be negative for mediation of oxidation reactions, the half-wave potential of the redox catalyst must be negative of the formal potential of the substrate and for catalysis of reduction reactions the reverse situation must exist. Also it can be seen that the driving force for the mediated reaction is determined by the magnitude of the ΔE^0 term.[92]

The catalysis of electrochemical reactions is perhaps the main motivation for many of the investigations carried out on redox polymer coated electrodes in recent years. Considerable advances have been made during the last decade in the development of polymer based electrocatalysis[93] for both chemical and biological sensors. The primary motivation for these investigations is that polymer modified electrodes combine the advantages of monolayer derivatised electrodes with homogeneous catalytic systems, i.e., a high local concentration of catalytic sites, despite the total amount of catalyst being small, easy separation of the reaction products from the catalyst and a three dimensional dispersion of the reacting centres.

1.3.5 Square Wave Voltammetry (SWV):

Square Wave Voltammetry (SWV) belongs to the family of pulsed voltammetric methods, which was invented by Ramaley and Krause.[94,95] It was popularised by Osteryoung and co-workers.[96,97,98] It has proven to be a useful method to investigate redox reactions with overlapping waves. The excitation waveform applied to the cell is a square wave potential superimposed to a staircase potential, shown in Figure 1.12. This is a differential technique, where the current is sampled at the end of each forward and reverse half cycle thus minimizing the interference from non-faradaic current and is displayed as a "net" current. The interference due to a dissolved species such as oxygen will be limited due to the fact that SWV is a purely subtractive technique.[99]

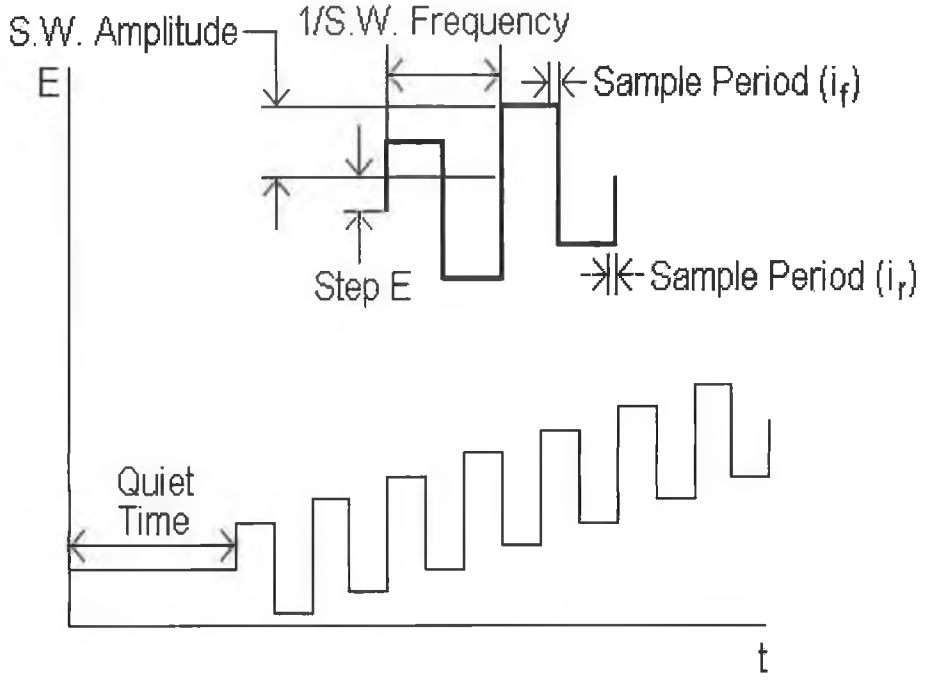

Figure 1.12: *The square wave curve. Adapted from*
http://chem.ch.huji.ac.il/~eugeniik/square_wave_voltammetry.html

Osteryoung and O'Dea have proposed the broad diagnostic use of SWV in a way similar to that for which cyclic voltammetry has been so successful.[86,98] Indeed SWV does have a high information content, especially when one considers the voltammograms of forward and reverse currents, ad it has the power to interrogate electrode processes over a wide potential span in a reasonable time. Its strength with respect to CV are derived especially from its ability to suppress the background. In general, systems can be examined at substantially lower concentrations than with CV. Moreover, there is normally much less distortion of the response by the background, so that fitting of data to theoretical models can be done with greater accuracy. On the whole, SWV is better than CV for evaluating quantitative parameters for systems that are understood mechanistically. SWV also has weakness with respect to CV, namely, for most practitioners CV is more intuitively interpretable in chemical terms. Also, because the reversal in CV covers a large span of potentials, it can more readily highlight linkages between processes occurring at widely separated potentials. Finally, CV offers a considerably wider range of time scales than SWV.

For practical analysis, SWV is generally the best choice among all pulse methods, because is offers background suppression with the effectiveness of DPV, sensitivity slightly greater than that of DPV, much faster scan times, and applicability to a wider range of electrode materials and systems.

1.4 Electrochemiluminescence; Principles, Occurrence and Applications:

1.4.1 General Principles:

Chemiluminescence (CL) is a powerful analytical technique that exhibits high sensitivity and selectivity.[100] Electrogenerated chemiluminescence (ECL) has important advantages over more conventional CL, in that reagents needed for the reaction are produced *in situ* when required at the electrode. The reaction can therefore be controlled and manipulated by controlling the applied potential. Indeed this increased interest is reflected in the number of reviews[101,102,103,104,105,106,107,108,109,110,111] that report the usefulness of ECL detection methods and its analytical applications.

ECL can arise from organic as well as inorganic substances and can be produced by annihilation reactions between reduced and oxidised forms of the same species or by using a co-reactant that forms an energetic oxidant or reductant on bond cleavage.[100] AC as well as DC electrolysis may be used and the precursors may be generated sequentially at the electrode by CV or potential step techniques or simultaneously at a rotating ring disk[112] or double band electrode.

As stated previously, the precursors participating in the homogeneous electron transfer leading to the light emitting excited state are generated at electrodes through heterogeneous electron transfer reactions. In organic ECL systems,[100] these precursors are often in the form of oxidised and reduced radical ions, whereas in inorganic systems they are simply the reduced and/or oxidised forms of the parent complex. The oxidised precursor represents a 'hole' in the highest occupied molecular orbital (HOMO) which enhances its oxidative properties, while the reduced form represents an electron in the lowest unoccupied molecular orbital (LUMO), which enhances its capacity for reduction. In all cases the homogeneous reaction between these precursors is characterised by very fast ($\sim 10^{10}$ $M^{-1}s^{-1}$) very exoergic (typically 2-4 eV) electron transfer.[136] Also, as both

radicals may be quite unstable; their reaction with each other usually demands very rapid sequential or simultaneous generation of both species.

As can be seen from Figure 1.13, there are two possible paths for the homogeneous reaction between the two radicals. Firstly, the electron transfer may take place from the HOMO of the reduced radical to the LUMO of the oxidised one (B). This is the path most favoured thermodynamically. However, if electron transfer is sufficiently rapid, this means that a large amount of energy would have to be dissipated which can not be achieved over a very short time scale in vibrational modes, which is very difficult for the reacting system. Here a kinetic manifestation of the Franck-Condon principle comes into play, and the path to electronically excited products becomes relatively attractive, because its demand for mechanical accommodation is not nearly so great.[136]

The luminescent path involves electron transfer between the LUMO of the reduced radical and the slightly less energetic LUMO of the oxidised radical (A). In this case only a small amount of energy needs to be dissipated in mechanical modes, this satisfies the Franck-Condon principle and leads to the formation of an excited state product, which emits light on relaxation, forming the stable ground state products.

The requirements for reactions leading to ECL have also been explained within the frame work of the Marcus theory of electron transfer,[113] which predicts that for an electron transfer reaction, the rate constant k_{et} depends on the standard free energy of reaction ΔG^0, according to the expression;

$$RT\frac{d\ln(k_{et})}{d(-\Delta G^0)} \approx \frac{1}{2}\left[1+\frac{\Delta G^0}{\lambda}\right] \qquad \textbf{(14)}$$

where λ is the solvent re-organisational energy. Thus, for low to moderate $-\Delta G^0$ values an increase in $\ln(k_{et})$ with increasing ΔG^0 is expected. A maximum value of

k_{et} can be obtained for $\Delta G^0 = -\lambda$ and for reactions in which $|-\Delta G^0| > \lambda$ an inverse behaviour is observed in which the rate decreases with increasing driving force. Thus, the lack of significant direct reaction to the ground state for homogeneous reactions in ECL systems is rationalised as an example of slow electron transfers to be expected for highly exergonic reactions in the inverted region of the Marcus theory.

With this kinetic requirement in mind and the aforementioned Franck-Condon limitation on the dissipation of high energy in mechanical modes, it is possible to understand why electrochemiluminescent systems choose an electron transfer pathway which leads to the formation of excited states rather than the thermodynamically more favoured direct production of ground state products.

For most ECL systems, which involve annihilation, the intensity of the light emission is controlled by three main factors; the rate of the annihilation reaction, N (mol s^{-1}), the efficiency of production of the excited state (Φ_{ES}) and the efficiency of light emission from the excited state (Φ_f). These are linked by the following formula:

$$I_{ECL} = \Phi_f \Phi_{ES} N \qquad \textbf{(15)}$$

where I_{ECL} is intensity in einsteins s^{-1}. The product of Φ_f and Φ_{ES} is often termed the overall ECL efficiency (Φ_{ECL}) and is defined as the number of photons emitted per redox event. It can be measured experimentally using the following expression:

$$\Phi_{ECL} = \frac{\int_0^t FI_{ECL}\,dt}{\int_0^t i_{a,c}\,dt} = \frac{\int_0^t FI_{ECL}\,dt}{Q_{a,c}} \qquad \textbf{(16)}$$

in which the total ECL intensity integrated over a finite period of time t, multiplied by the Faraday F, is divided by $i_{a,c}$, which is equal to the total anodic or cathodic charge Q.[114] Φ_{ECL} strictly approaches the luminescence efficiency Φ_f, but apart from in the case of some ruthenium chelates it is generally found to be considerably lower. This can be attributed to at least two reasons[115]; (i) The instability of the oxidation and/or reduction products which participate in the reaction leading to the excited state. (ii) The competition between the reaction leading to the excited state product and that leading to the ground state product.

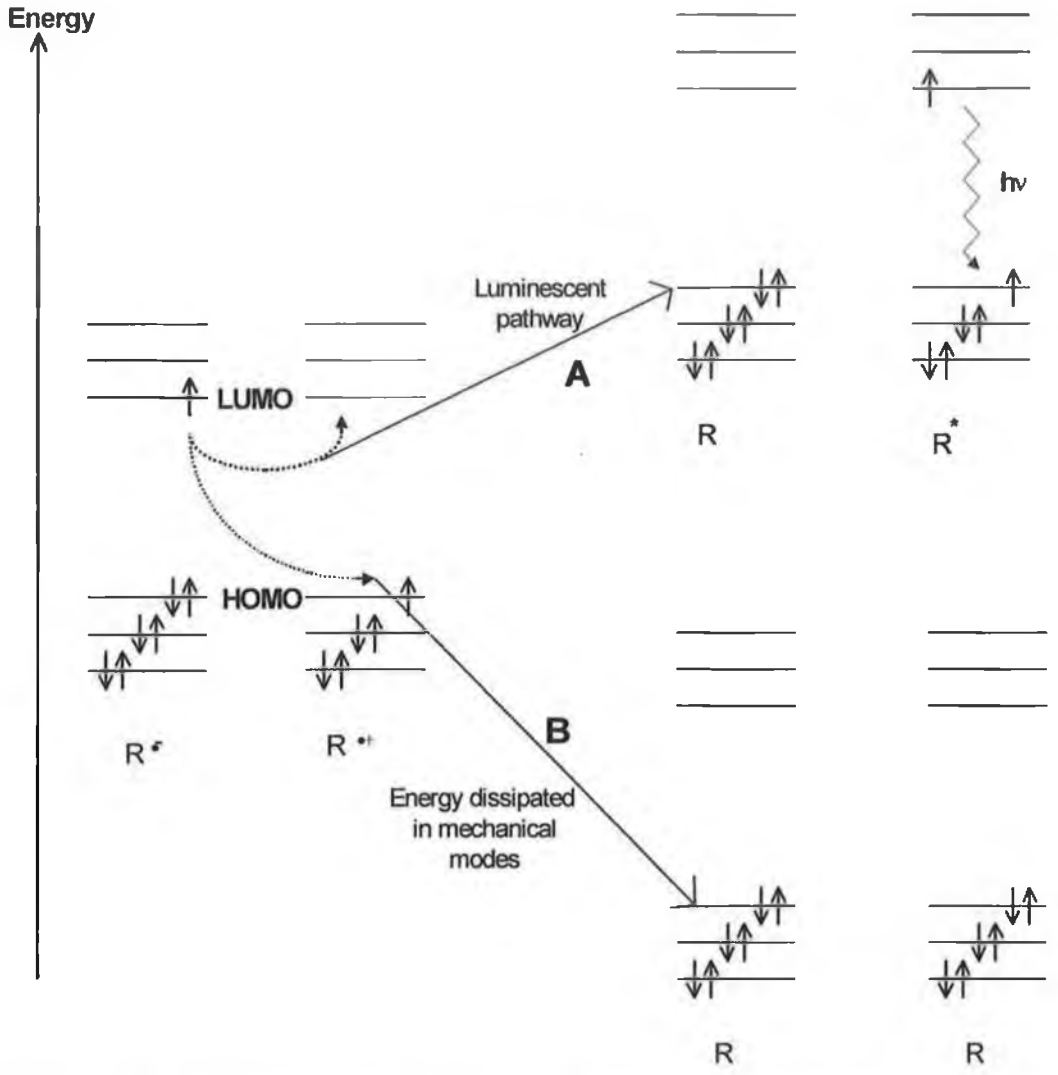

Figure 1.13: *Molecular orbital diagram showing two alternative pathways for electron transfer between oxidised and reduced precursors* R^- *and* R^+*. (A) Formation of an excited state and (B) direct population of ground state products. Adapted from reference 136.*

There are at least five main pathways by which ECL can occur. These pathways are;

(i) S-Route: Reactions between oxidised and reduced precursors leading to the direct formation of an excited (usually singlet) state. This is known as the S-route and the system in this case is said to be energy sufficient. A typical S-route system is the polyaromatic hydrocarbon; 9,10-diphenylanthracene (DPA). The radical cation and the anion of this species are produced by applying a double potential step to a platinum electrode in a solution of DPA dissolved in MeCN or DMF using a tetrabutylammonium salt as supporting electrolyte.[43] The reaction proceeds as follows;

$DPA - e^- \longrightarrow DPA^{\bullet+}$ (electro-oxidation) **(17)**

$DPA + e^- \longrightarrow DPA^{\bullet-}$ (electro-reduction) **(18)**

$DPA^{\bullet+} + DPA^{\bullet-} \longrightarrow DPA + {}^1DPA^*$ (electron transfer) **(19)**

${}^1DPA^* \longrightarrow DPA + h\nu$ (chemiluminescence) **(20)**

where ${}^1DPA^*$ is the excited singlet state. Emission is observed at λ_{max} = 420nm. The energy supplied by the ion annihilation reaction (reaction 19 above) is sufficient to directly populate the emitting singlet state.

(ii) T-Route: When radical annihilation reaction is 'energy deficient' and therefore unable to produce an excited singlet state directly, then an excited triplet may be formed, which may be able to generate a singlet for efficient light emission through triplet-triplet annihilation. This indirect pathway is known as the T-route. An example of the T-route is the DPA-TMPD ECL system, (where TMPD is N,N,N',N'-tetramethyl-p-phenylenediamine). In this system the following reactions take;

$TMPD - e^- \longrightarrow TMPD^{\bullet+}$ **(21)**

$$TMPD^{\bullet+} + DPA^{\bullet-} \longrightarrow 3DPA^{*} + TMPD \qquad \textbf{(22)}$$

$$2\,{}^{3}DPA^{*} \longrightarrow DPA + {}^{1}DPA^{*} \qquad \textbf{(23)}$$

and followed by reaction 21. As can be seen from Figure 1.14 only the non-emitting triplet is energetically accessible following reaction 22, therefore the energy for the population of first excited singlet comes from reaction 23 where the energy from two electron transfers is pooled to provide sufficient energy.

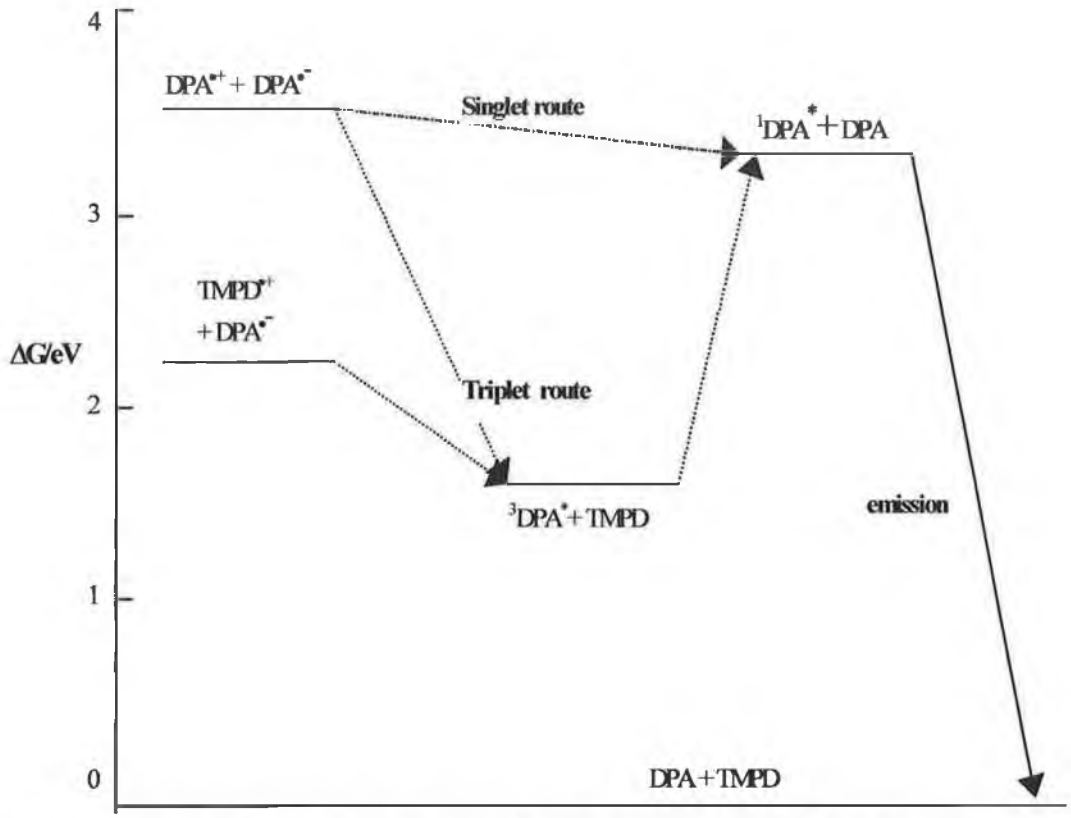

Figure 1.14: *Energy level diagram for DPA and DPA-TMPD ECL systems.*

(iii) E-Route: In the two previous types of ECL considered, the annihilation reaction leading to the formation of the emitting species is said to proceed *via* a charge transfer or encounter complex. There is a third type where this molecular complex itself is responsible for emission. If the excited complex emitter is formed from two like molecules, it is known as an eximer, and if formed from two unlike molecules, it is an exiplex.[116] The mechanism involving emission originating from these types of complexes is sometimes known as the E-route.

For example, the ECL of pyrene[116](Py) plus TMPD produces a bimodel spectral emission with peaks at *ca.* 400nm from $^1Py^*$, and *ca.* 480nm from the Py_2^* eximer:

$$Py^{\bullet-} + TMPD^{\bullet+} \longrightarrow {}^3Py^* + TMPD \qquad \textbf{(24)}$$

$$^3Py^* + {}^3Py^* \longrightarrow {}^1Py^* + Py \qquad \textbf{(25)}$$

$$^3Py^* + {}^3Py^* \longrightarrow Py_2^* \qquad \textbf{(26)}$$

where $^1Py^*$ and $^3Py^*$ represent the excited singlet and triplet states of pyrene respectively and Py_2^* represents the eximer.

(iv) A S-route system which involves direct population of triplets by homogeneous reaction between electrogenerated precursors, followed by phosphorescence to give ground state products. This path is most often encountered with transition metal complexes such as ruthenium(tris)bipyridine, $Ru(bpy)_3^{2+}$. Here, spin allowed excited states undergo rapid deactivation due to spin-orbital coupling and emission originates from the lowest energy excited state via energy sufficient routes. The life-time of this species being too short to take part in subsequent annihilation reactions, emission comes as phosphorescence from the spin-forbidden excited state.

If a solution of $Ru(bpy)_3^{2+}$ in acetonitrile (ACN) is subjected to a cyclic double step potential alternating between oxidation and reduction potential of the

complex, an orange emission is observed from the vicinity of the electrode (λ_{max} = 610 nm). The reaction sequence is as follows;

$$Ru(bpy)_3^{2+} + e^- \rightarrow Ru(bpy)_3^{+} \quad \textbf{(27)}$$

$$Ru(bpy)_3^{2+} - e^- \rightarrow Ru(bpy)_3^{3+} \quad \textbf{(28)}$$

$$Ru(bpy)_3^{+} + Ru(bpy)_3^{3+} \rightarrow Ru(bpy)_3^{2+} + [Ru(bpy)_3^{2+}]^* \quad \textbf{(29)}$$

$$[Ru(bpy)_3^{2+}]^* \rightarrow Ru(bpy)_3^{2+} + h\nu \quad \textbf{(30)}$$

Since the excited state triplet from which emission occurs is directly populated, the system is energy sufficient and is therefore classed as an S-Route system.[128]

(v) Homogeneous reactions of electrogenerated precursors with electron donors/acceptors present in solution can also result in ECL[154]. For instance, if a strong oxidising or reducing agent, such as oxalate ($C_2O_4^{2-}$) or peroxodisulphate ($S_2O_8^{2-}$) is introduced into solution in the $Ru(bpy)_3^{2+}$ system described above, then only half the oxidation-reduction cycle need be applied. However, it should be noted that being a strong oxidising/reduction agent is a necessary, but not sufficient condition for a co-reactant to produce ECL in these cases.[154]

1.4.2 Analytical Applications:

There are many different types of inorganic ECL systems. However, investigations into inorganic ECL have mainly concentrated on ruthenium chelates, particularly $Ru(bpy)_3^{2+}$ and its derivatives. This is due to the intrinsic and sometimes exceptional properties of these complexes, namely that they can emit luminescence at room temperature in aqueous solutions, and undergo reversible one-electron transfer reactions at easily attainable potentials, leading to sufficiently stable reduced or oxidised species. The efficiency of excited state production (Φ_{ES}) under certain conditions also nears 100%.[114]

The electrochemiluminescence of $Ru(bpy)_3^{2+}$ was first demonstrated by Tokel and Bard in 1972.[117] Though chemiluminescence of the chemically oxidised (3+) species had previously been reported.[118] The authors showed that on cycling the potential of a Pt electrode between the first oxidation and reduction potentials of a solution of the complex dissolved in acetonitrile, the same characteristic emission could be produced. It was proposed that the reduction step leading to the +1 species involved addition of an electron to the LUMO (π^* orbital), while the oxidation step leading to the +3 species involved in the removal of an electron from the HOMO (d-orbital). The enthalpy of the charge transfer reaction between these two species was calculated from the peak potentials and it was noted that the reaction was quite sufficient to populate the excited triplet state of the complex. ECL was also demonstrated for oxidation of the +1, 0 and -1 complexes using 10-methylphenothiazine as a co-reactant.

Following on from this, Rubenstien and Bard have reported intense ECL from $Ru(bpy)_3^{2+}$ in aqueous solution using strong reductants. The emission was produced at a platinum electrode in solutions of the complex dissolved in 0.1 M H_2SO_4 in the presence of mM concentrations of oxalate when the potential was held at a sufficiently positive value to oxidise $Ru(bpy)_3^{2+}$. The mechanism of the ECL

reaction was reported to involve a highly reducing intermediate $CO_2^{\bullet-}$, formed on oxidation of oxalate by $Ru(bpy)_3^{3+}$.

$$Ru(bpy)_3^{2+} - e^- \rightarrow Ru(bpy)_3^{3+} \quad \textbf{(31)}$$

$$Ru(bpy)_3^{3+} + C_2O_4^{2-} \rightarrow Ru(bpy)_3^{2+} + C_2O_4^{\bullet-} \quad \textbf{(32)}$$

$$C_2O_4^{\bullet-} \rightarrow CO_2 + CO_2^{\bullet-} \quad \textbf{(33)}$$

$$Ru(bpy)_3^{3+} + CO_2^{\bullet-} \rightarrow [Ru(bpy)_3^{2+}]^* + CO_2 \quad \textbf{(34)}$$

$$[Ru(bpy)_3^{2+}]^* \rightarrow Ru(bpy)_3^{2+} + h\nu \quad \textbf{(35)}$$

another possible route following reaction 33 was:

$$Ru(bpy)_3^{2+} + CO_2^{\bullet-} \rightarrow Ru(bpy)_3^{+} + CO_2 \quad \textbf{(36)}$$

$$Ru(bpy)_3^{+} + Ru(bpy)_3^{3+} \rightarrow Ru(bpy)_3^{2+} + [Ru(bpy)_3^{2+}]^* \quad \textbf{(37)}$$

followed by reaction 35.

It was noted that production of the excited state by direct reaction of $Ru(bpy)_3^{3+}$ with $C_2O_4^{2-}$ was not possible since the free energies of the $Ru(bpy)_3^{2+/3+}$ and $C_2O_4^{2-}$ / CO_2 are insufficient.

The complex $Ru(bpz)_3^{2+}$(where bpz is 2,2`-bipyrizine) has been shown to produce ECL[119,120] with efficiencies similar to that of $Ru(bpy)_3^{2+}$ ($\Phi_{ECL} \sim 4\%$ at room temperature). Redox processes were shifted approximately 0.5 V toward more positive potentials compared to the corresponding bpy species and it was noted that this could prove useful in ECL in aqueous media where proton reduction interferes at negative potentials. The temperature dependence of Φ_{ECL} was also studied; the similarity between it and Φ_f in the lower temperature range suggested very efficient excited state formation by reaction between the 3+ and 1+ form of the complex and that ECL efficiency was only limited by the luminescence quantum yield at these temperatures.

The electrochemiluminescent determination of peroxydisulphite ($S_2O_8^{2-}$) in aqueous solution using electrogenerated $Ru(bpz)_3^+$ has been described.[121] The method was shown to be highly specific and to have a linear range of 10^{-9} - 10^{-3} M, using a rotating disk as working electrode.

Two ruthenium chelates which have been shown to give higher ECL efficiencies than that of $Ru(bpy)_3^{2+}$ are $Ru(dp\text{-}bpy)_3^{2+}$ and $Ru(dp\text{-}phen)_3^{2+}$ (where dp-bpy is 4,4`- diphenyl-2,2`-bipyridine and dp-phen is 4,7-diphenyl-1,10-phenantroline).[122] Efficiencies were measured using $Ru(bpy)_3^{2+}$ as a relative standard (5.0%) and were found to be 14% and 24% for the dp-bpy and dp-phen[123] complexes respectively.

Enhanced ECL in bimetallic ruthenium species has been described,[124] $[(bpy)_2Ru]_2(bphb)^{4+}$, where bphb is 4-bis(4'-methyl-2,2'-bipyridin-4-yl)benzene, displayed an ECL efficiency higher than $Ru(bpy)_3^{2+}$ at 16 %, and far higher than its monometallic analogue. The enhanced luminescent properties of this species was ascribed to a weak electronic coupling between metal centres, and the bipyridine like environment conferred by the bridging ligand.

Recent studies have shown that at oxide covered tantalum electrodes, electrochemically generated solution-phase hot electrons (i.e., electrons at an energy far above the Fermi energy of a phase) are detectable by virtue of their reaction with $Ru(bpy)_3^{3+}$ to produce its excited state.[125,126]

$Ru(bpy)_3^{2+}$ exhibits intense ECL with a range of co-reactants, both oxidants and reductants, which is relatively insensitive to the presence of oxygen and impurities. This makes the system a very attractive means of detection, and there are numerous such methods published in the literature for determination of a wide variety of analytes.[127] These have been extensively reviewed.[128,110,111,109]

The $Ru(bpy)_3^{2+}$/oxalate system has also been used to determine oxalate in synthetic urine,[129] high oxalate concentrations in blood and urine is known to accompany a number of maladies including renal failure, vitamin deficiency and intestinal diseases. ECL intensity was linearly related to oxalate concentration over the range of 10^{-6}-10^{-4} M. This region encompasses the concentrations found in normal blood and urine. $Ru(bpy)_3^{2+}$ itself has been determined in the presence of oxalate and persulphite to levels as low as 10^{-13} M, which allowed the authors to suggest its implementation as a novel ECL label.[130]

Other organic species which have been determined using $Ru(bpy)_3^{2+}$ ECL include hydroxyl carboxylic acid,[131] monohydric alcohols,[132] both of which produce the excited state through broadly similar mechanisms to oxalate.

Solution phase $Ru(bpy)_3^{2+}$ ECL has been used in flow injection analysis to quantify aliphatic amines,[133] which act as reducing agents in a manner analogous to oxalate. It is found that ECL emission from the reaction with amines increases in the order $1° < 2° < 3°$ amines. Primary amines have only been detected by prior derivitisation with divinylsolfone, with which they undergo a cycloaddition reaction resulting in the formation of the alicyclic tertiary amine.[134]

The mechanism for the reaction of amines with $Ru(bpy)_3^{2+}$ to produce its excited state is thought to be as follows:[133,135]

$$Ru(bpy)_3^{2+} \longrightarrow Ru(bpy)_3^{3+} + e^- \quad \textbf{(38)}$$

$$R(CH_3)NCH_2\text{-}R` \longrightarrow R(CH_3)N^{\bullet+}CH_2\text{-}R` + e^- \quad \textbf{(39)}$$

$$R(CH_3)N^{\bullet+}CH_2\text{-}R` \longrightarrow R(CH_3)NC^{\bullet}H\text{-}R` + H^+ \quad \textbf{(40)}$$

$$R(CH_3)NC^{\bullet}H\text{-}R` + Ru(bpy)_3^{3+} + H_2O \longrightarrow [Ru(bpy)_3^{2+}]^* + R(CH_3)NH + R`CHO \quad \textbf{(41)}$$

$$[Ru(bpy)_3^{2+}]^* \longrightarrow Ru(bpy)_3^{2+} + h\nu \quad \textbf{(42)}$$

Danielson *et al.* have looked at a large number of amines with respect to their potential for producing ECL.[133] They found a strong inverse correlation between ECL intensity and first ionisation potential, and also noted that the loss of a non-bonding electron for the electron transfer reaction leading to ECL was favoured.

Knight and Greenway have reviewed the relationship between structural attributes of tertiary amines and ECL activity with $Ru(bpy)_3^{2+}$.[135] Among the most important features were as follows; a hydrogen atom attached to the α-carbon is usually essential. Electron withdrawing or donating substituents close to the radical centre tend to modulate ECL intensity due to a stabilising or destabilising effect on the radical intermediate (which participates in the reaction leading to the excited state). Resonance stabilisation of the radical intermediate reduces its reactivity and thus ECL intensity (as is the case with aromatic amines), the molecular geometry and the radical species may also be a factor.

ECL detection has been developed for use in immunoassays and DNA probe analysis.[136,137,138] $Ru(bpy)_3^{2+}$can be easily modified by attaching reactive groups to the bipyridyl ligands to form active labels for proteins, nucleic acids and other biological molecules. Figure 1.15 shows the structure of the ECL labels used by Origen and Perkin-Elmer in their respective technologies. The approach has many distinct advantages, namely that problems of sample handling, disposal and life-time inherent in radioammunoassays are eliminated, since no radioactive isotope is used. Detection limits are extremely low, normally sub-picomolar, (a limit of 5 x 10^{-20} moles was reported for the HIV-1 *gag* gene), the linear dynamic range is greater than six orders of magnitude, the labels are extremely stable and can be stored for over a year at room temperature and their small size allows multiple labelling of the same molecule without affecting the immunoreactivity or hybridisation of the probes.

ECL technology has recently been commercially developed for the clinical diagnostics market.[169] Assays have been developed for a wide variety of applications such as pregnancy, thyroid diseases, infectious diseases.[170] The sensitive detection of biotoxiods and bacterial spores such as anthrax in soil has also been described.[171] In this technology, ECL detection is combined with conventional antigen-antibody reactions which take part on streptavidin coated magnetic particles. The sample is combined with a reagent containing biotinylated antibody and a second ruthenium labelled antibody. During incubation the antibodies capture the target molecules, the microparticles are then added and during a second incubation period the biotinylated antibody attaches to the streptavidin coated particles (see Figure 1.16). Next the sample is drawn into the ECL measuring cell along with a buffer containing tripropylamine. A magnet located under the electrode captures the microparticles at the electrode surface and all unbound reagent is washed from the cell. The magnet is then removed and a potential is applied to the electrode, initiating ECL emission.

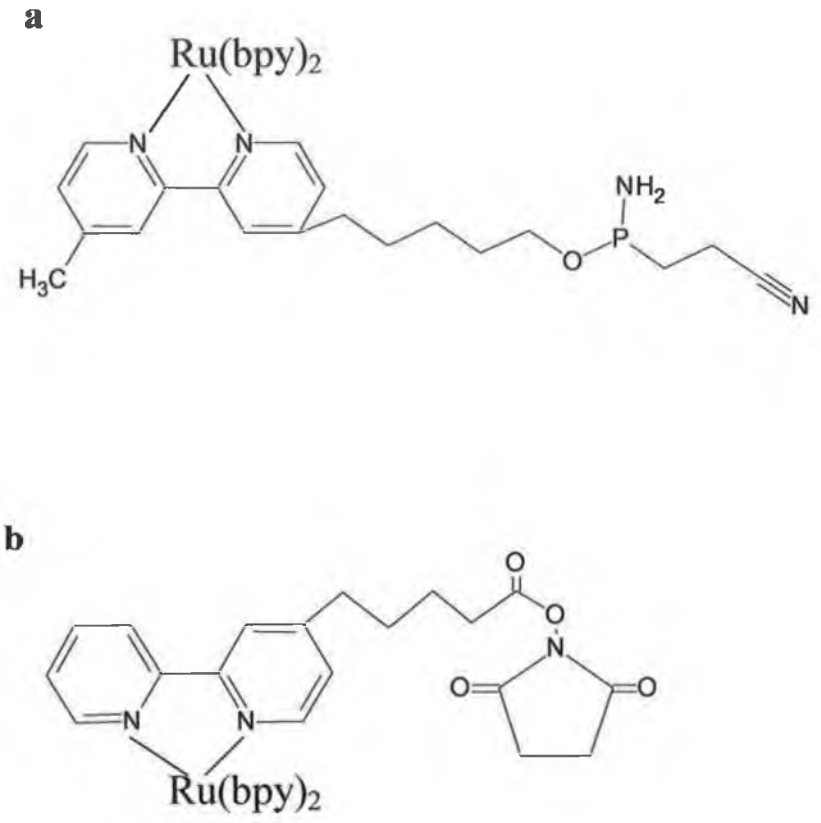

Figure 1.15: *Structure of the ECL labels used by Oriel (a) and Perkin-Elmer (b) for immunoassays and DNA probe analysis.*

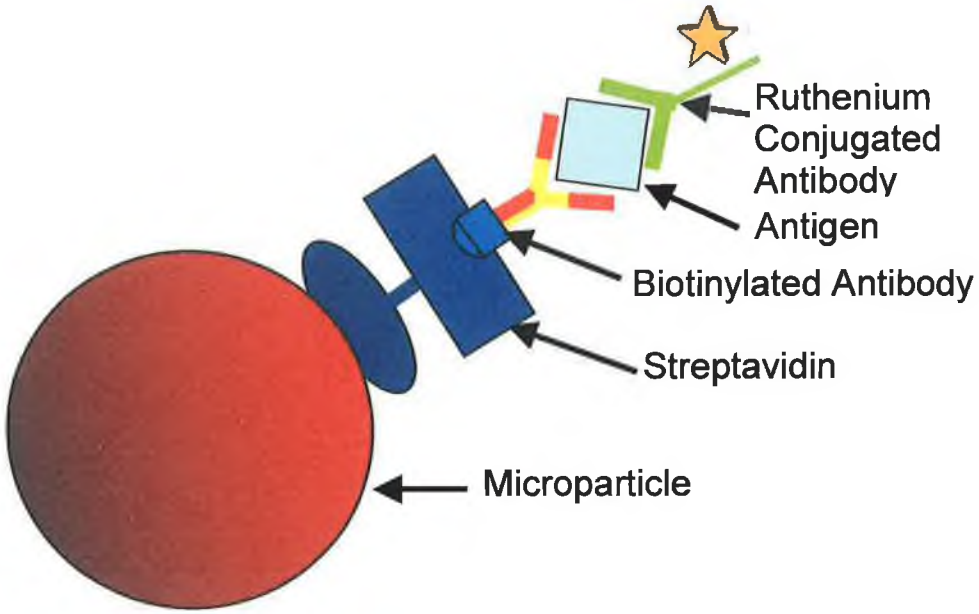

Figure 1.16: *Basis of Elecsys® ECL immunoassay technology. From reference 117.*

ECL can also be generated from a modified electrode. Again, the most studied example of this is that of $Ru(bpy)_3^{2+}$ electrostatically incorporated into the ion exchange polymer, Nafion, first reported in 1980.[139] The catalytic oxidation of oxalate in aqueous electrolyte was demonstrated, accompanied by a corresponding light emission characteristic of the ruthenium complex. Generation of ECL in the absence of oxalate or similar co-reactants, by repetitive pulsing between the 1+ and 3+ states of the complex in solutions containing >20% acetonitrile was also demonstrated. However, the emission intensity rapidly decayed due to extensive dissolution of the film in these media.

Following on from this the analytical usefulness of ECL arising from modified electrodes was investigated. One example used $Ru(bpy)_3^{2+}$ immobilised in Nafion at the electrode surface within the context of a flow injection analysis (FIA) system to quantify oxalate, alkylamines and NADH.[140] ECL intensity was linearly proportional to oxalate concentration over four decades, but the limit of detection, though still quite low at 1 μM, was somewhat higher than that for the corresponding solution phase experiment. Antibiotics containing amine functionalities were also shown to be suitable analytes and selectivity studies using compounds frequently found in biological matrices revealed few significant interferences. Working curves for NADH detection showed good linearity over a wide concentration range with a good limit of detection of 1 μM.[140]

ECL systems are finding interesting applications in other areas besides analysis. For example in the visualisation and characterisation of electrode surfaces. Through magnification of ECL patterns recorded at carbon electrodes it was possible to show the location, size and shape of electron transfer active regions.[141] Similarly the chemical architecture of carbon fibre microelectrodes was characterised after electrochemical treatment to produce different levels of surface oxides.[142] Wightman *et al.* have used the ECL of DPA to generate images of microelectrodes with dimensions in the micrometer range,[143] revealing features of their surface topography. Anodised glassy carbon electrodes which were

microderivatised to render tiny areas more electrochemically active have also been visualised using luminol ECL imaging.[144] Luminol ECL was also used to reveal the spatial distribution of adsorbed poly(phenylene oxide) on platinum electrodes.[145] An interesting application of ECL imaging has been the visualisation of electrohydrodynamic convective patterns in thin layer electrochemical cells.[146] Recently, scanning electrochemical microscopy (SECM) has been used in conjunction with ECL. by generating $Ru(bpy)_3^{2+}$ ECL at an SECM tip it was possible to image a microelectrode array consisting of 30 μm Au bands.

The observation of discrete chemical reaction events in solution has been achieved by single photon detection of the ECL of DPA. [147,148] The chemical reactions were restricted to a 20 femtolitre volume adjacent to a microelectrode by the use of high speed potential pulses. The possibility of single molecule detection using ECL at an SECM tip has also been discussed.[149]

There have been several other uses and suggested uses for ECL systems besides analysis. For example there has been some interest in the application of ECL active species in display devices,[150,151] and as discussed previously, light emitting diodes. The prospect of electrochemical pumping of laser dyes has been discussed since ECL systems first began to be investigated in detail, [152,153] and recently electrochemically produced laser action has been realised for solutions of DPA in a thin layer cell consisting of mirror and half mirror Pt electrodes on quartz substrates, 2-7 μm apart.[154]

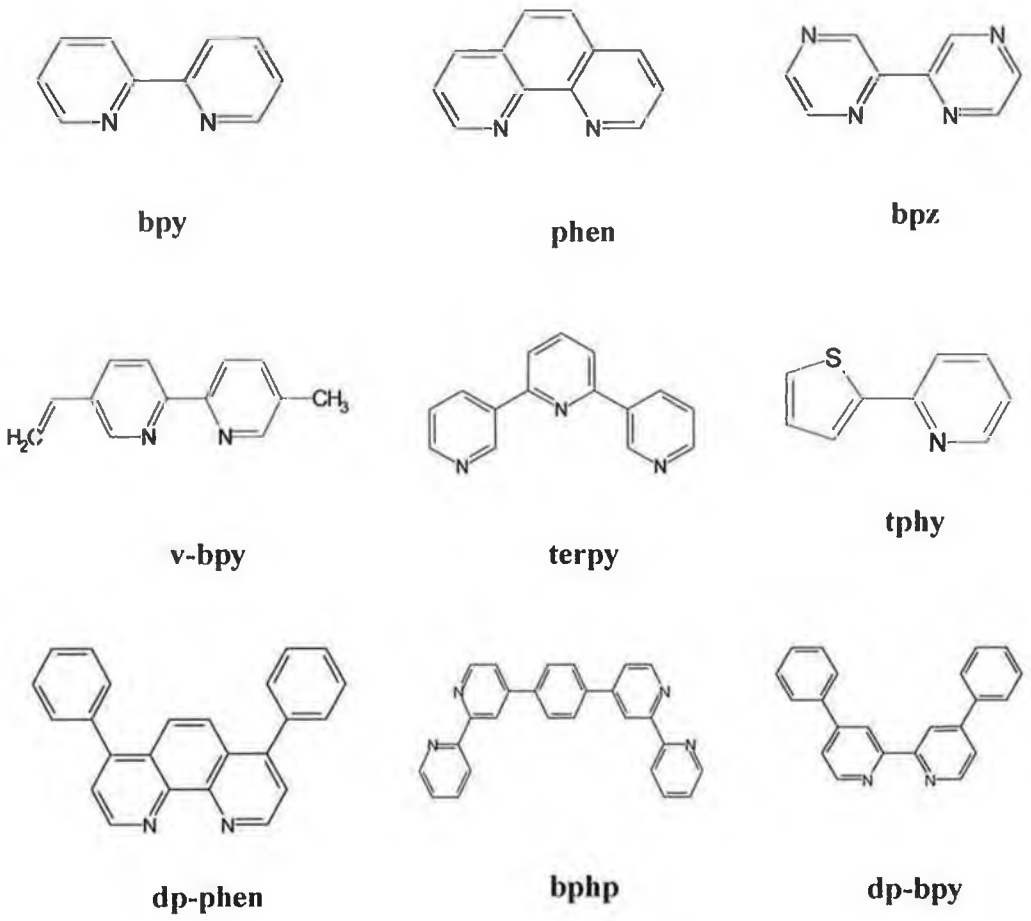

Figure 1.17: *Structures of the ligands of some of the ECL active inorganic complexes mentioned in the text. bpy =2,2'bipyridyl, phen = phenanthroline, bpz = 2,2'bipyrizine, v-bpy = 4-vinyl, 4-methyl,2,2'bipyridyl, terpy = 2,2'2-terpyridyl, tphy = 2-(2-thienyl)-2-pyridine, dp-phen = diphenyl phenanthroline, bphp = 4-bis(4'-methyl-2,2'-bipyridin-4-yl)benzene and dp-bpy = diphenyl bipyridyl.*

Extension of $Ru(bpy)_3^{2+}$ ECL to osmium systems has been somewhat limited due to the larger spin-orbit coupling in osmium systems that results in shorter excited state lifetimes and weaker emission efficiencies.[155,156,157] However, the electrogenerated chemiluminescence of a family of bipyridine and phenantroline complexes of Osmium has been reported.[158] The fluorescent abilities of these types of compound had previously been reported to be comparable to or even greater than that of $Ru(bpy)_3^{2+}$.[159] Also they were reported to undergo reversible oxidation/reduction within an accessible potential window, thus, it was reasoned that these complexes could represent a new family of strongly electrochemiluminescent materials. Potential steps were used, in acetronitrile solutions of the complexes to generate ECL by annihilation reactions between oxidised (3+) and reduced (1+) precursors, and external oxidants (N-methylphenothiazine) and reductants (anthraquinone) were also effective in producing ECL. Of the ten compounds tested $Os(bpy)_2$diphos, where diphos is 1,2-bis-diphenylphosphinoethane, gave the best ECL efficiency, but this was lower than expected on the basis of its quantum yield of fluorescence emission, and considerably lower than that of $Ru(bpy)_3^{2+}$.

ECL of $Os(phen)_2(dppene)^{2+}$, where phen is 1,10-phenanthroline and dppene is bis(diphenylphosphino)ethene) has also been reported.[160] It was shown to produce ECL in mixed CH_3CN/H_2O (50:50 v/v) and aqueous (0.1 M KH_2PO_4) solutions with tri-*n*-propylamine (TPrA) as an oxidative-reductive coreactant. The incorporation of phosphine ligands into the framework of osmium polypyridyl systems resulted in excited state photoluminescent lifetimes in excess of 200 ns.[161] The development of osmium based sensors shows many advantages over the ruthenium systems, mainly, the osmium systems are more photostable than their ruthenium analogues. The ECL emission quantum efficiency for this system is 2-fold greater than $Ru(bpy)_3^{2+}$ in aqueous solutions. This can prove useful in diagnostic or environmental applications in which greater sensitivity and detection limits than those of $Ru(bpy)_3^{2+}$ can provide are required. The lower potentials

required to excite osmium systems may also be of benefit in DNA diagnostic applications.

Osmium complexes of the general formula $Os(L)_3^{2+}$, where L = 2,2`-bipyridine, 1,10-phenantroline and 2,2`-bipyrizine, were examined[162] with a view to finding a useful ECL tag with an emission wavelength considerably different from that of $Ru(bpy)_3^{2+}$, (the availability of tags at different wavelengths would allow multiple tests to be carried out simultaneously). Of the three, the bipyrazine complex gave the most promising results with an emission maximum at 700 nm and an excited state life-time of 0.24 μs.

Advances in organic light-emitting diodes have triggered intensive research effort towards the development of efficient solid-state electroluminescent materials. In this pursuit several osmium complexes have been synthesised and characterised. Among these are compounds of the structure $[Os(bpy)_2L]^{2+}$. This type of complex, unlike $Os(bpy)_3^{2+}$, can show very intense room temperature luminescence with an emission quantum yield three orders of magnitude greater than that of $Os(bpy)_3^{2+}$. For example when L is *cis*-1,2-bis(diphenylphosphino)ethylene. For this compound the greater emission quantum yield can be correlated with the strong π-back bonding ability of the phosphine ligand through the energy gap theorem.[163]

The photoluminescent properties and electronic structures of several other Os(II) complexes have also been investigated.[164] From these studies in was concluded that Os(II) complexes with high triplet state photoluminescent efficiency can be used as the emitting layer of organic EL devices, extending the material's range and providing a new approach to improving the EL efficiency.

1.5 Conclusion:

In conclusion, the vast number of new chemicals being produced everyday can have drastic effects on our DNA and subsequently on our health, as outlined in this review. It is therefore necessary to have a method to detect the damage, if any, caused by these chemicals. Although there are already many methods in use to perform this task, they are often expensive and time consuming. As can be clearly seen in this review a faster and more economical alternative to these methods is electrochemical detection. Although EC detection may not offer as detailed results as mass spectroscopy, for example, it is more time efficient and as such can be used for preliminary data into the toxicity of a new compound. A more in-depth analysis could then be preformed to obtain the exact mechanism of DNA damage once a compound was shown to produce a negative result from its reaction with DNA.

By utilising two methods simultaneously a much more sensitive procedure can be obtained. The many advantages of several methods are discussed here, however, due to its inherent selectivity and sensitivity, ECL and electrochemical analysis are logical choices for this system. Incorporating ECL with either cyclic voltammetry or square wave voltammetry can be useful as a quick and efficient method of toxicity screening of any new chemical produced.

1.6 References:

1 Avery, OTC; MacLeod, M.; McCarty, M.; *J. Exper. Medicine*, **1944**, *79*, 137-158.

2 Watson, J.D.; Crick, F.H.C.; *Nature*, **1953**,*171*, 737-738.

3 Watson, J.D.; Crick, F.H.C.; *Nature,* **1953**, *171*, 964.

4 Hancock, J.T.; Pallister, C.J.; (Ed), *Molecular Genetics*, Reed Educational and Professional Publishing Ltd., **1999**, Ch. 2.

5 Watson, J.D.; *The Double Helix,* Atheneum, London, **1968**

6 Schena, M.; Shalon, D.; Davis, R.W.; Brown, P.O.; *Science,* **1995,** *270*, 467-470.

7 Brown, A.P.; Anson, F.C.; *Anal. Chem.*, **1977**, *49*, 1585.

8 Shen, H.-M.; Ong, C.-N.; *Free Radical Biol. Med.*, **2000**, *28(4),* 529-536.

9 Zenzes, M.T.; Bielecki, R.; Reed, T.E.; *Fertility and Sterility*, **1999**, *72(2),* 330-335.

10 Shen H.-M.; Chia S.-E.; Ong, C.-N.; *J. Andrology,* **1999**, *20(6),* 718-723.

11 Hughes, C.M.; McKelvey-Martin, J.; Lewis, S.E.M., *Mutagenesis*, **1999**, *14*, 71-75.

12 Zhang, Y.-J.; Weksler, B.B.; Wang, L.; Schwartz, J.; Santella, R.M., *Athyerosclerosis,* **1998**, 140(2), 325-331.

13 Otteneder, M.; Lutz, W.K., *Mut. Res. Mol. Mech. Mutagenesis,* **1999**, *424*, 237-247.

14 Ahmed, F.E.; *J. Envir. Sci. Health: C,* **2000**, *18*, 75-125.

15 Santella, R.M.; *Cancer Epid. Biomarkers & Preventation*, **1999**, *8(9),* 733-739.

16 Strauss, B.S.; *Cancer Res.*, **1992**, *52*, 249-253.

17 Seidel, C.A.M.; *J. Phys. Chem.*, **1996**, *100*, 5541-5553.

18 Steenken, S.; Jovanoic, S.V.; *J. Am. Chem. Soc.,* **1997**, *119*, 617-618.

19 Halliwell, B.; Gutteridge, J.M.C.; *Free Radicals in Biology and Medicine: 2nd Ed.:* Oxford University Press: Oxford, **1989**, Ch. 2.53, Ch. 8.

20 Sies, H; Schulz, W.A.; Steenken, S.; *J. Photocehm. Photobiol. B,* **1996**, *32*, 97-102.

21 Wolf, P.; Jones, G.D.D.; Candeias, L.P.; O'Neill, P.; *Int. J. Radiat. Biol.*, **1993**, *64*, 7-18.

22 Sugiyama, H.; Saito, I.; *J. Am. Chem. Soc.*, **1996**, *118*, 7063-7068

23 Saito, I; Nakamura, T.; Nakatani, K.; Yoshioka, Y.; Yamaguchi, K.; Sugyiama, H.; *J. Am. Chem. Soc.*, **1998**, *120*, 12686-12687.

24 Denissenko, M.F.; , Pao, A.; Tang, M.-S.; Pfeifer, G.P.; *Science*, **1996**, *274*, 430.

25 Giese, B.; *Acc. Chem. Res.*, **2000**, *33*, 631-636.

26 Lewis, R. J. Sr., *Carcinogenically Active Chemicals - A Reference Guide*, Van Nostrand Reinhold: New York, 1991.

27 Singer, B.; Grunberger, D., *Molecular Biology of Mutagens and Carcinogens*; Plenum: New York, 1983.

28 Hemminki, K., *Carcinogenesis*, **1993**, *14*, 2007-2012.

29 Hemminki, K., *Carcinogenesis*, **1993**, *14*, 355-360.

30 *Monographs on the evaluation of carcinogenic risks to humans, No. 60, Some industrial chemicals*, IARC, Lyon, 1994; pp. 45-213 and 233-346, IARC, Lyon, 1993; K. Hemminki.

31 F.P. Guengerich, *Toxicol. Lett.* **1994**, *70*, 133–148.

32 T. Nakajima, E. Elovaara, F.J. Gonzalez, H.V. Gelboin, H. Vainio, T. Aoyama, *Characterization of human cytochrome P450 isozymes responsible for styrene metabolism*. In: M. Sorsa, K. Peltonen, H. Vainio, K. Hemminki (Eds.), *Butadiene and Styrene: Assessment of Health Hazards, IARC Scientific Publication* **No. 127**, International Agency for Research on Cancer, Lyon, 101–108.

33 K. Hemminki, P. Vodicka, *Toxicol. Lett.*, **1995**, *77*, 153-161.

34 S. M. Rappaport, K. Yeowell-O'Connell, *Toxicol. Lett.*, **1999**, *108*, 117-126.

35 M. Otteneder, U. Lutz, W. K. Lutz, *Mutat. Res.*, **2002**, *500*, 111-116.

36 M. Koskinen, L. Vodickove, P. Vodicka, SC. Warner, K. Hemminki, *Chem.-Biol. Interact.*, **2001**, *138*, 111-124.

37 C. Qiun, A. Dipple, *Chem. Res. Toxicol.,* **1995**, *8*, 389-395.

38 R. R. Selzer, A. A. Elfarra, *Arch. Biochem. Biophys.,***1997**, *343*, 63-72.

39 T. Barlow, A. Dipple, *Chem. Res. Toxicol.,* **1999,** *12*, 883-886.

40 M. Koskinen, D. Calebiro, K. Hemminki, *Chem.-Biol. Interact.,***2000**, *126*, 201-213.

41 K. Savela, A. Hesso, K. Hemminki, *Chem.-Biol. Interact.,* **1986**, 235.

42 T. Barlow, A. Dipple, *Chem. Res. Toxicol.* **1998**, *11*, 44–53.

43 F. Latif, R.C. Moschel, K. Hemminki, A. Dipple, *Chem. Res. Toxicol.* **1988**, *1*, 364–369.

44 T. Barlow, A. Dipple, *Chem. Res. Toxicol.* **1999**, *12*, 883–886.

45 I. Neagu, P. Koivisto, C. Neagu, R. Kostiainen, K. Stenby, K. Peltonen, *Carcinogenesis* **1995**, *16*, 1809–1813.

46 A.R. Collins, *Mol. Aspects Med.* **1998**, *19*, 359–432.

47 K. Hemminki, M. Koskinen, H. Rajaniemi, C. Zhao, *Regulat. Toxicol. Pharmacol.* **2000**, *32*,264–275.

48 F.P. Perera, I.B. Weinstein, *Carcinogenesis,* **2000** , *21*,517–524.

49 Vodicka, P.; Koskinen, M.; Arand, M.; Oesch, F.; Hemminki, K.; *Mutation Res.,* **2002**, *511*, 239-254.

50 K. Hemminki , *Environ. Health Perspect.* **1997**, *105 (Suppl. 4)*, 823–827.

51 L.A. Loeb, B.D. Preston, *Annu. Rev. Genet.* **1986**, *20*, 201–230.

52 T. Bastlová, A. Podlutsky, *Mutagenesis* **1996**, *11*, 581–591.

53 J.B. Guttenplan, W. Kosinska, F.L., *Environ. Mol. Mutagen.* **1994**, *23*, 23.

54 J.E. Cochrane, T.R. Skopek, *Carcinogenesis* **1994**, *15*, 719–723.

55 J. Nakamura, J.A. Swenberg, *Cancer Res.* **1999**, *59*,2522–2526.

56 (a) S.C. Sisk, L.J. Pluta, J.A. Bond, L. Recio, *Carcinogenesis* **1994**, *15*,471–477.

(b) L. Recio, K.G. Meyer, *Environ. Mol. Mutagen.* **1995**, *26*,1–8.

(c)L. Recio, S. Sisk, K. Meyer, L. Pluta and J.A. Bond, *Toxicology* **1996**, *113*,106–111.

(d) A.M. Steen, K.G. Meyer, L. Recio, *Mutagenesis* **1997**, *12*,359–364.

57 G.J. Latham, L. Zhou, C.M. Harris, T.M. Harris, R.S. Lloyd, *J. Biol. Chem.* **1993**, *268*, 23427–23434.

58 R. Carmical, *Environ. Mol. Mutagen.* **2000**, *35*, 48–56.

59 T. Barlow, J. Takeshita, A. Dipple, *Chem. Res. Toxicol.* **1998**, *11*, 838–845.

60 Breen, A.P.; Murphy, J.A.; *Free Radical Biol. Med.,* **1995**, *18*, 1033 – 1077.

61 Dennany, L.; Forster, R.J.; Rusling, J.F.; *J. Am. Chem. Soc.,* **2003**, *125*, 5213.

62 Dennany, L.; White, B.; Symth, M.; Forster, R.J.; Rusling, J.F.; *J. Am. Chem. Soc.,* **2004**, *in press.*

63 Cadet, J.; Weinfeld, M.; *Anal. Chem.,* **1993**, *65*, 675A-682A.

64 Schrader, W.; Linscheid, M.; *Arch. Toxicol.,* **1997**, *71*, 588-595.

65 Millan, K.M.; Mikkelsen, S.R.; *Anal. Chem.,* **1993**, *65*, 2317.

66 Millan, K.M.; Saraullo, A.; Mikkelsen, S.R.; *Anal. Chem.,* **1994**, *66*, 3830.

67 Zhou, L.; Yang, J.; Estavillo, C.; Stuart, J. D.; Schenkman, J. B.; Rusling, J. F. *J. Am. Chem. Soc.*, in press

68 Palecek, E.; Boublikova, P.; Jelen, F.; *Anal. Chim. Acta,* **1986**, *187*, 99-107.

69 Palecek, E.; *Electroanalysis,* **1996**, *8*, 7-14.

70 Jelen, F.; Fojta, M.; Palecek, E.; *J. Electroanal. Chem.,* **1997**, *427*, 49-56.

71 Jelen, F.; Tomschik, M.; Palecek, E.; *J. Electroanal. Chem.,* **1997**, *423*, 141-148.

72 Fojta, M.; Palecek, E.; *Anal. Chim. Acta,* **1997**, *342*, 1-12.

73 Fijta, M.; Stankove, V.; palecek, E.; Koscielniak, P.; Mitas, J.; *Talanta,* **1998**, *46*, 155-161.

74 Sequaris, J.-M.; Valenta, P.; *Int. J. Radiat. Res.,* **1982**, *42*, 407-415.

75 Sequaris, J.-M.; Valenta, P.; *J. Electroanal. Chem.,* **1987**, *227*, 11-20.

76 Wang, J.; Rivas, G.; Ozsoz, M.; Grant, D.H.; Cai, X.; Parrado, C.; *Anal. Chem.,* **1997**, *69*, 1457-1460.

77 Mbindyo, J.; Zhang, Z.; Stuart, J.D.; *Anal. Chem.,* **2000**, *72*, 2059-2065.

78 Pauwels, W.; Vodiceka, P.; Servi, M.; Plna, K.; Veulemans, H.; Hemminki, K.; *Carcinogenesis,* **1996**, *17*, 2673-2680.

79 Latham, G.J.; Lloyd, R.S.; *J. Biol. Chem.,* **1994**, *268*, 28427-28530.

80 Johnson, D.H.; Glasgow, K.C.; Thorp, H.H.; *J. Am. Chem. Soc.,* **1995**, *117*, 8933.

81 Ontko, A.C.; Armistead, P.M.; Kirus, S.R.; Thorp, H.H.; *Inorg. Chem.,* **1999**, *38*, 1842-1846.

82 Farrer, B.T.; Thorp, H.H.; *Inorg. Chem.,* **2000**, *39*, 44-49.

83 Yang, I.V.; Thorp, H.H.; *Inorg. Chem.,* **2000**, *39*, 4969-4976.

84 Sistare, M.F.; Codden, S.J.; Heimlich, G.; Thorp, H.H.; *J. Am. Chem. Soc.,* **2000**, *122*, 4742-4749.

85 Southampton; *Electrochemistry Group: Instrumental Methods in Electrochemistry,* John Wiley & Sons, Inc, New York, **1985**, Ch. 2, pp. 49.

86 Brown, A.P.; Anson, F.C., *Anal. Chem.,* **1977**, *49,* 1585.

87 Skoog; Holler; Nieman; *Principles of Instrumental Analysis: Fifth Edition,* Harcourt Brace & Company, **(1998)**, pp. 650-660.

88 Southampton electrochemistry group *Instrumental methods in electrochemistry* Wiley, New York, **1985**, Ch.2, 49.

89 Kelly, D. M. ; Vos, J. G. *Electroactive polymer electrochemistry, Part 2: Methods and applications,* Plenum press, New York, **1996**, Ch. 8, p.191.

90 Forster, R. G.; Vos, J. G. *Electrochim. Acta.* **1992**, 37, 159.

91 Larsson, H.; Sharp, M. *J. Electroanal. Chem.* **1995**,381, 133.

92 Saveant, J. M. *Acc. Chem. Res.* **1980**, 13, 323.

93 Tee, Y.; Janda, P.; Zhang, J.; Pietro, W.J.; Lever, A. B. P. *J. Porphyrins and Phthalocyanines* **1997**, 1, 3.

94 Ramaley, L., Krause, M.S., *Anal. Chem.*, **1969**, *41*, 1362-1365.

95 Ramaley, L., Krause, M.S., *Anal. Chem.*, **1969**, *41*, 1365-1369.

96 Osteryoung, J., *Accts. Chem. Res.,* **1993**, *26*, 77.

97 Osteryoung, J. and Osteryoung, R.A., *Phil. Trans. Roy. Soc. London Ser. A,* **1981**, *302*, 315.

98 Osteryoung, J., O'Dea, J.J., *Electroanal. Chem.,* **1986**, *14*, 209.

99 Strobel, H. A.; Heineman, W. R., *Chemical Instrumentation: A Systematic Approach, 3rd Edition*, John Wiley & Sons: New York, 1989.

100 (a) Knight, A.W.; Greenway, G.M.; *Analyst* **1994**, *119*, 879-890.
(b) Knight, A.W.; *Trends Anal. Chem.,* **1999**, *18 (1)*, 47-62.
(c) Fähnrich, K.A.; Pravda, M.; Guilbault, G.G.; *Talanta*, **2001**, *54*, 531-559.
(d) Park, S-M.; Tryk, D.A.; *Reviews Chem. Interactions,* **1981**, *4*, 43-79.

101 Fahnrich, K.A.; Pravda, M.; Guilbault, G.G.; *Talanta*, **2001**, *54*, 531-559.

102 Fleet, B.; Keliher, P.N.; Kirkbright, G.F.; Pickford, C.J.; *Analyst*, **1969**, *94*, 847.

103 Herejk, J.; Holzbecher, Z.; *Chem. Listy*, **1984**, *78*, 1254.

104 Greenway, G.M.; *Trends Anal. Chem.*, **1990**, *9*, 200.

105 Rozhitskii, N.N.; *J. Anal. Chem. USSR*, **1992**, *47*, 1288.

106 Velasco, J.G.; *Electroanalysis*, **1991**, *3*, 261.

107 Kricka, L.J.; Stanley, P.E.; *Luminescence*, **1999**, *14*, 107.

108 Knight, A. W.; Greenway, G. M.; *Analyst* **1994**, *119*, 879.

109 Knight, A.W.; *Trends Anal. Chem.,* **1999**, *18 (1),* 47.

110 Lee, W.Y.; *Mikrochim. Acta*, **1997**, *127,* 19.

111 Gerardi, R.D.; Barnett, N.W.; Lewis, S.W.; *Anal. Chim. Acta,* **1999**, *378*, 1.

112 Maloy, J.T.; Prater, K.B.; Bard, A.J.; *J. Am. Chem. Soc.*, **1971**, *93*, 5959.

113 Jonah, C. D. ; Matheson, M. S.; Meisel, D. *J. Am. Chem. Soc.* **1978**, *100*, 1449.

114 Wallace, W. L.; Bard, A. J. *J. Phys. Chem.* **1979**, *83,* 1355.

115 Bolletta, F.; Bonafede, S. *Pure and Appl. Chem.* **1986**, *56*, 1229.

116 Campell, A.K., *Chemiluminescence* Horwood, England, **1988**, 516.

117 Tokel, N. E.; Bard, A. J. *J. Am. Chem. Soc.* **1972**, *94*, 2862.

118 Hercules, D. M.; Lyth, F.E.; *J. Am. Chem. Soc.* **1966**, *88*, 4745.

119 Velesco, J. G.; Rubenstein, I.; Cruchley, R. J.; Lever, A. B. P.; Bard, A. J., *Inorg. Chem.* **1983**, *22*, 822.

120 Velesco, J. G. *J. Phys. Chem.* **1988**, *92*, 2202.

121 Yamashita, K.; Nishida, S. Y.; Harima, Y; Segawa, A. *Anal. Chem.* **1991**, *63*, 872.

122 MCCord, P.; Bard, A. J. *J. Electroanal. Chem.* **1991**, *318*, 91.

123 Kapturkiewicz, A. *Chem. Phys. Lett.* **1995**, *236*, 389.

124 Richter, M. M.; Bard, A. J.; Kim, W.; Schmehl, R. H. *Anal. Chem.* **1998**, *70*, 310.

125 Sung, Y. E.; Gaillard, F.; Bard, A. J. *J. Am. Chem. Soc.* **1998**, *102*, 9797.

126 Sung, Y. E.; Bard, A. J. *J. Am. Chem. Soc.* **1998**, *102,* 9806.

127 bookmark error

128 Rozhitskii, N.N.; *J. Anal. Chem. USSR,* **1992**, *47*, 1288.

129 Rubenstein, I.; Martin, C. R.; Bard, A. J. *Anal. Chem.* **1983**, *55*, 1580.

130 Ege, G.; Becker, W.G.; Bard, A. J. *Anal. Chem.* **1984**, *56*, 2413.

131 Chen, X.; Chn, w.; Jiang,Y.; Jia, L.; Wang, X.; *Microcheem. J.,* **1998**, *59*, 427.

132 Chen, X.; Sata, M.; Lin, Y.; *Microchem. J.,* **1998**, *58*, 13.

133 Noffsinger, J. B.; Danielson, N. D. *Anal. Chem.* **1987**, *59*, 865.

134 Uchicura, K; Kirishawa, M. *Anal. Sci.* **1991**, *7*, 803.

135 Knight, A.W.; Greenway, G.M.; *Analyst*, **1996**, *121*, 101R.

136 Holeman, J. A.; Danielson, N. D. *Anal. Chim. Acta.* **1993**, *277*, 55.

137 Yocoyama, K.; Sasaki, S.; Ikebukuro, K.; Taceuchi, T.; Karube, I.;Tokitsu,Y.; Masuda, Y. *Talanta,* **1994**, *41*, 1035.

138 Jamieson, F.; Sanchez, R. I.; Dong, L.; Leland, J. K.; Yost, D.Martin, M. T. *Anal. Chem.* **1996**, *68*, 1298.

139 Rubenstein, I.; Bard, A. J. *J. Am. Chem. Soc.* **1980**, *102*, 6642.

140 Downey, T. M.; Neiman, T. A. *Anal. Chem.* **1992**, *64*, 261.

141 Engstrom, R. C.; Johnson, K. W.; Desjarlais, S. *Anal. Chem.* **1987**, *59*, 670.

142 Hopper, P.; Kuhr, W. G. *Anal. Chem.* **1994**, *66*, 1996.

143 Wightman, R. M.; Curtis, C. L.; Flowers, P. A.; Maus, R. G.; McDonald, E. M. *J. Phys. Chem.* **1998,** *102*, 9991.

144 Ratcliff, B. B.; Klancke, J. W.; Koppang, M. D.;Engstrom, R. C.; *Anal. Chem.* **1996**, *68*, 2010.

145 Engstrom, R. C.; Nohr, P. L.; Vitt, J. E. *Colloids and Surfaces A* **1994**, *93*, 221.

146 Orlic, M.; Rosenmund, J.; Doblhofer, K.; Ertl, G. *J. Phys. Chem.* **1998**, *102*, 1397.

147 Collinson, M. M.; Wightman, R. M. *Science* **1995**, *268*, 1883.

148 Wightman, R. M.; Ritchie, E. *Abstr. Pap. Am. Chem. Soc.* **1997**, 213:179-Phys, Part 2.

149 Bard, A. J.; Fan, F-R. F. *Acc. Chem. Res.* **1996**, *29*, 572.

150 Laser,D.; Bard, A. J. *J. Electrochem. Soc.* **1975**, *122*, 632.

151 Igasari, R.; Nosaka, Y.;Miyama, A.; Kaneko, M.; Yokoyama, M. *J. Electrochem. Soc.* **1988**, *135*, 2987.

152 Measures, R. M. *Appl. Opt.* **1975**, *14*, 909.

153 Heller, C. A.; Jernigan, J. L. *Appl. Opt.* **1977**, *16*, 61.

154 Horiuchi, T.; Niwa, O.; Hatakenaka, N. *Nature* **1998**, *394*, 659.

155 Creutz, C., Chou, M., Netsel, T.L., Okumura, M., Sutin, N., *J. Am. Chem. Soc.* **1982**, *102*, 1309.

156 Kober, E.M., Meyer, T.J., *Inorg. Chem.,* **1982**, *21*, 3967.

157 Ouyang, J., Bard, A.J., *Bull. Chem. Soc. Jpn.,* **1988**, *61*, 17.

158 Abruna, H. D. *J. Electroanal. Chem.* **1984**,*175*, 321.

159 Casper, J. V.; Kober, E. M.; Sullivan, B. P.; Meyer, T.J. *J. Am. Chem. Soc.* **1982**, *104*, 630.

160 Bruce, D., Richter, M.M., Brewer, K.J., *Anal. Chem.,* **2002**, *74*, 3157-3159.

161 Brewer, R.G., Jensen, G.E., Brewer, K.J., *Inorg. Chem.,* **1994**, *33*, 124.

162 Chi-woo Lee; Ouyang, J.; Bard, A. J. *J. Electroanal. Chem.* **1988**, *244*, 319.

163 Bernhard, S., Gao, X., Malliaras, G.G. Abruna, H.D., *Adv. Mater.*, **2002**, *14*, 433-436.

164 Gao, F.G., Bard, A.J., *Chem. Mater.,* **2002**, *14*, 3465-3470.

CHAPTER 2

SYNTHESIS AND CHARACTERISATION OF RUTHENIUM AND OSMIUM CONTAINING METALLOPOLYMERS AND COMPLEXES: ELECTROCHEMICAL AND PHOTOPHYSICAL PROPERTIES.

"If I had only known, I would have been a locksmith."

Albert Einstein

2.1 *Introduction:*

Metallopolymers constitute a class of materials that is attracting increased attention because of their widespread application.[1,2,3] Much attention has been paid to polymers containing poly(pyridyl) complexes of ruthenium(II) and osmium(II).[4,5,6,7] There is a well-developed background of synthetic chemistry for both ruthenium and osmium complexes of this type and they have many attractive properties such as chemical stability in a range of oxidation states and facile electrochemistry as well as many interesting photochemical properties.[8] The attachment of ruthenium and osmium polypyridyl complexes to the electrode surface using polymeric matrices can be achieved by electrostatically incorporating charged complexes into cationic/anionic polymer films, though the stability of such systems is frequently compromised by leaching of the redox species from the layer.[9,10,11,12] Alternatively, the reductive polymerisation of vinyl-containing metal complex monomers can lead to the formation of films of varying thickness but extensive cross-linking is a feature of these materials.[13,14,15] Preparing metallopolymers through covalent attachment of the metal centre to a pre-formed polymer backbone offers many advantages, including synthetic control, reproducibility and a high level of structural control. An important feature of all these approaches is that it enables the redox and excited state behaviour of the monomeric analogues to be compared with polymeric materials.

The synthetic procedures available for labelling polymers with covalently attached metal centres offer considerable flexibility, for example, the choice of solvent, reaction time or temperature will determine whether the mono or bis substituted product is favoured,[16] *i.e.* $[M(bpy)_2(POL)_nCl]^+$ or $[M(bpy)_2(POL)_n]^{2+}$, where bpy is 2,2'-bipyridyl and POL is the polymer backbone. Polymer backbones that have been utilised include poly-(4-vinylpyridine) (PVP)[17], poly(N-vinylimidazole) (PVI)[18], poly-4-vinylpyridine/polystyrene copolymers (PVP/PS), and more recently polystyrene with amide linkage.[19,20] Materials of different metal loadings ranging from 1:5 (n = 5, one metal complex per 5 monomer units) to 1:25

are normally used though more dilute loadings have been considered.[21] While the ligands in the complexes used as starting materials are almost exclusively bpy, the use of 2,2',2-terpyridine (terpy) has also been investigated.[22] However, because of the unfavourable bite angle of the terpy ligand these materials suffer from decreased photostability compared to their bpy analogues. A great advantage of these preformed polymer materials is that because they can be dissolved, they can be characterised and investigated in great detail as solution phase species as well as in an immobilised state.[23] Conventional spectroscopic and electrochemical methods can be used to probe the nature of the co-ordination sphere around the metal centre, while elemental analysis, molecular weights and thermal methods have also been used in characterisation of these materials.[24]

2.2 *Apparatus and Reagents:*

Ultraviolet-visible spectra were carried out in HPLC grade ethanol or acetonitrile using a UV-Visible Cary 50 Scan spectrophotometer and data displayed and analysed using a personal computer containing Cary Win UV software. Emission spectra were recorded using a Perkin Elmer LS-50 luminescence spectrometer, equipped with a red sensitive Hamamatsu R928 detector. For room temperature measurements 1cm quartz cells were used while for low temperature (77 K) a quartz cell cooled with liquid nitrogen was utilised.

Excited state life-times of the polymer immobilised on ITO and in solution were measured using the third harmonic (355 nm) of a spectron Q-switched Nd-Yag laser for excitation, (10 ns pulse duration, 20 mJ per pulse). Emission was detected in a right angled configuration to the laser using an Oriel model IS520 gated intensified CCD operated at 20 °C, coupled to an Oriel model MS125 spectrograph. Initially solutions were deaerated for 20 min using argon or nitrogen prior to use, however, to accommodate comparisons with data obtained from films.

Proton nuclear magnetic resonance (NMR) spectra were obtained using a Bruker ACF 400 MHz spectrometer. Measurements were carried out in DMSO.

High performance liquid chromatography (HPLC) was carried out using a Varian 9002 HPLC pump equipped with a 20 μL injection loop and a particil SCX radical PAK ion exchange cartridge. A Varian 9050 variable wavelength UV-Vis detector, used at a detection wavelength of 280 nm and interfaced with a personal computer was used for detection. The mobile phase consisted of 80:20 (v/v) HPLC grade acetonitrile:water and 0.1 $LiClO_4$ (Sigma) employed as an ion-pairing agent. Flow rates of between 1.8 and 3 cm^3min^{-1} were utilised.

Chronoamperometry and cyclic voltammetry were carried out using a conventional three-electrode assembly. The potentiostat used was a CH instruments

model 660. Working electrodes were 3 mm diameter glassy carbon disks shrouded in Teflon, which was cleaned by polishing with alumina on a felt pad, followed by sonication in distilled deionised water for 30 min. The electrode was modified with the polymer by drop-casting a 1% ethanolic solution of the polymer onto the electrode and allowing the solution to air dry. Potentials were measured versus Ag/AgCl reference electrode. The counter electrode was a 1 cm^2 platinum flag. All electrochemical measurements were carried out at room temperature. The solvent employed for the solution phase cyclic voltammetry was 0.1 M H_2SO_4 or PBS. All solutions were degassed using nitrogen or argon prior to measurement.

Cis-[Ru(bpy)$_2$Cl$_2$]

The method employed for synthesis was based on that used by Sullivan.[25] $RuCL_3$ and $LiCl.H_2O$ were heated at reflux in DMF under N_2. To this solution 2,2'-bipyridyl was added slowly and the mixture allowed to reflux under a nitrogen environment for a further 8 h. After cooling, acetone was added to the purple solution, which was left overnight. The dark purple crystalline product was isolated, washed firstly with a minimum amount of ice-cold water to remove any Ru-CO complex formed by the degradation of DMF,[26] then with diethyl ether and allowed to air dry.

HPLC, cyclic voltammetry, NMR and UV-visible spectroscopy were carried out to confirm the purity of the product. HPLC of $Ru(bpy)_2Cl_2$ showed a single peak. Integration of this peak showed 95% purity. These results and the single redox couple observed at 0.38 V using cyclic voltammetry confirm the identity of the compound. (See Figures 2.1, 2.2, 2.3 and 2.4).

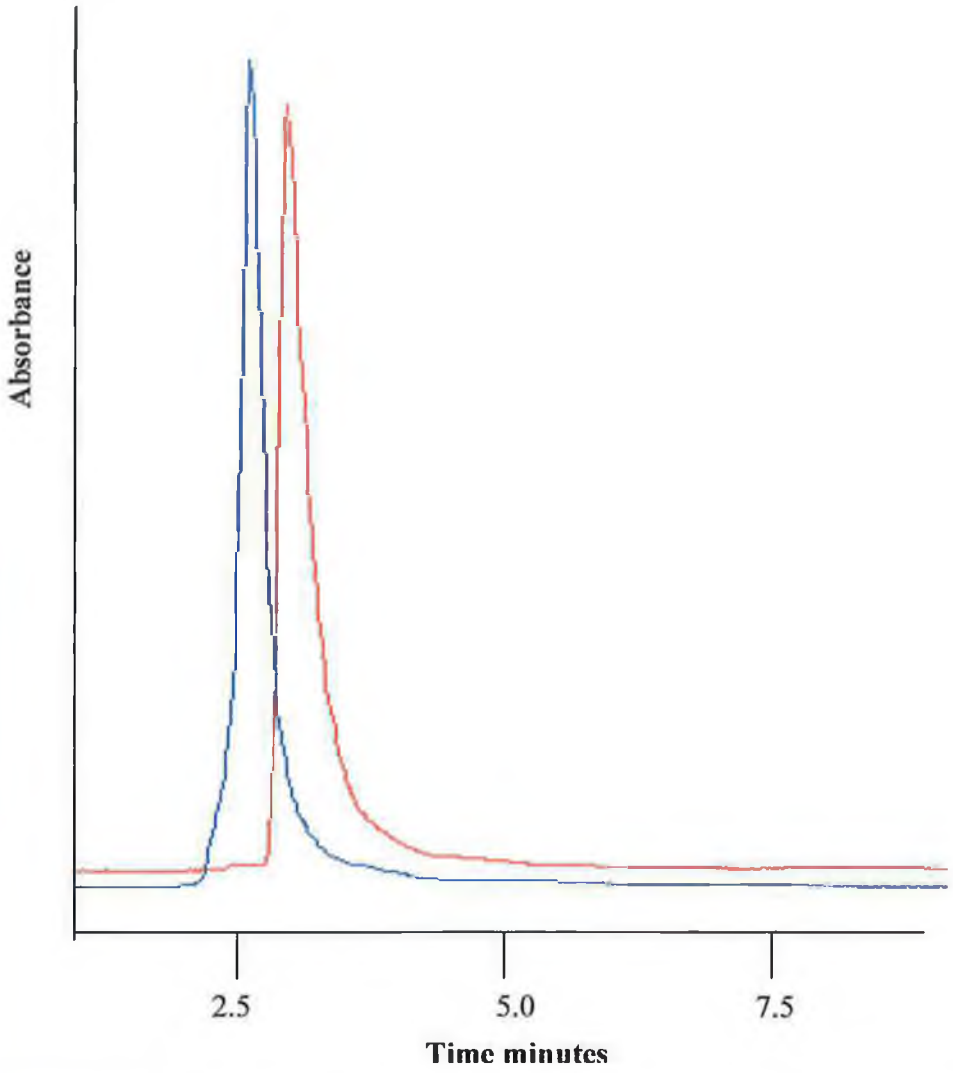

Figure 2.1: *HPLC chromatogram of $Ru(bpy)_3^{2+}$ and $Ru(bpy)_2Cl_2$, 280 nm was used as the detection wavelength. Mobile phase used was 80:20 (v/v) acetonitrile:H_2O and 0.1 M $LiClO_4$ employed as an ion-pairing agent. A flow rate of 2 ± 0.2 $cm^3 min^{-1}$ was utilised. Plots offset for clarity.*

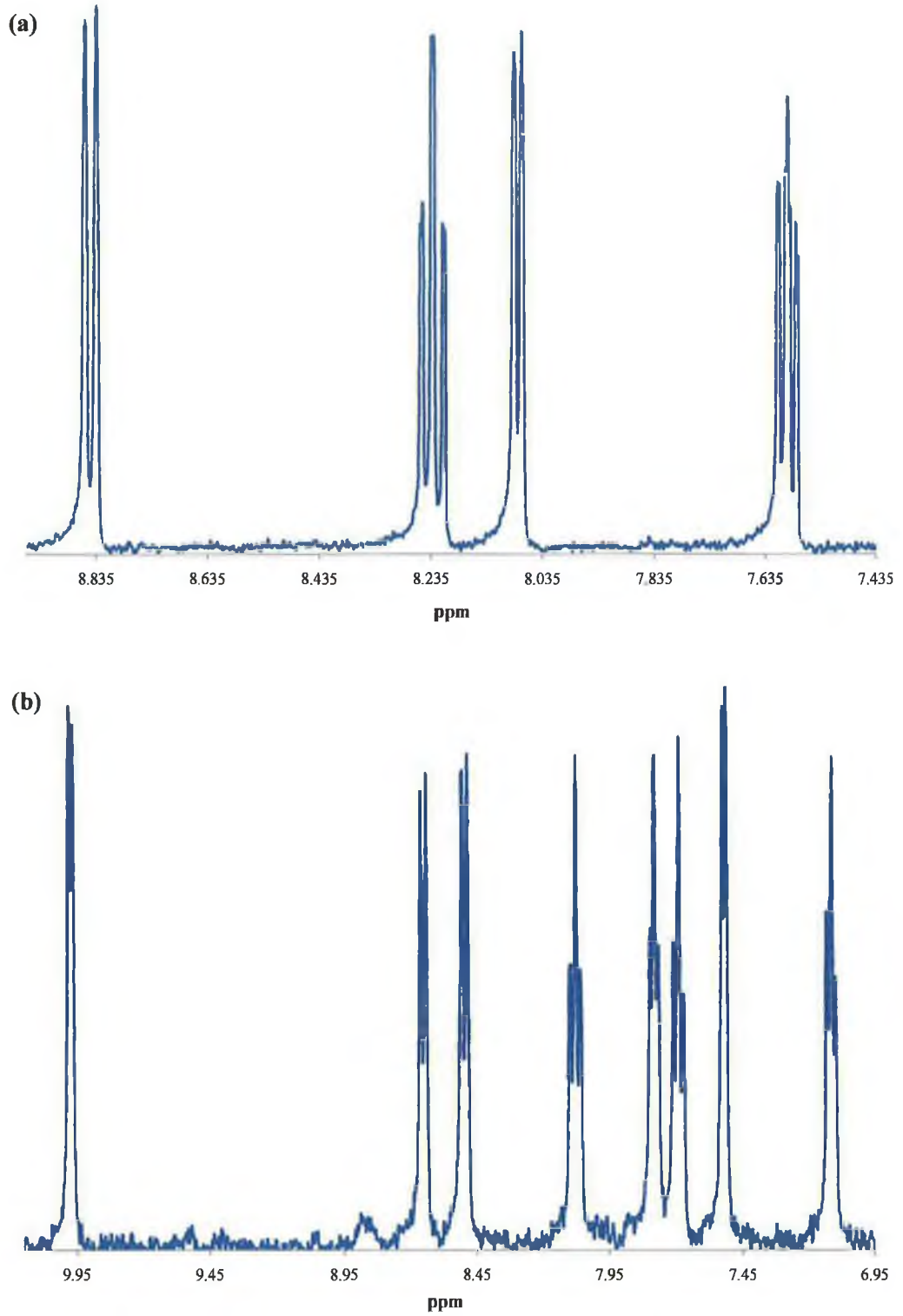

Figure 2.2: *NMR of (a) $Ru(bpy)_3^{2+}$ in d-acetone and (b) $Ru(bpy)_2Cl_2$ in DMSO.*

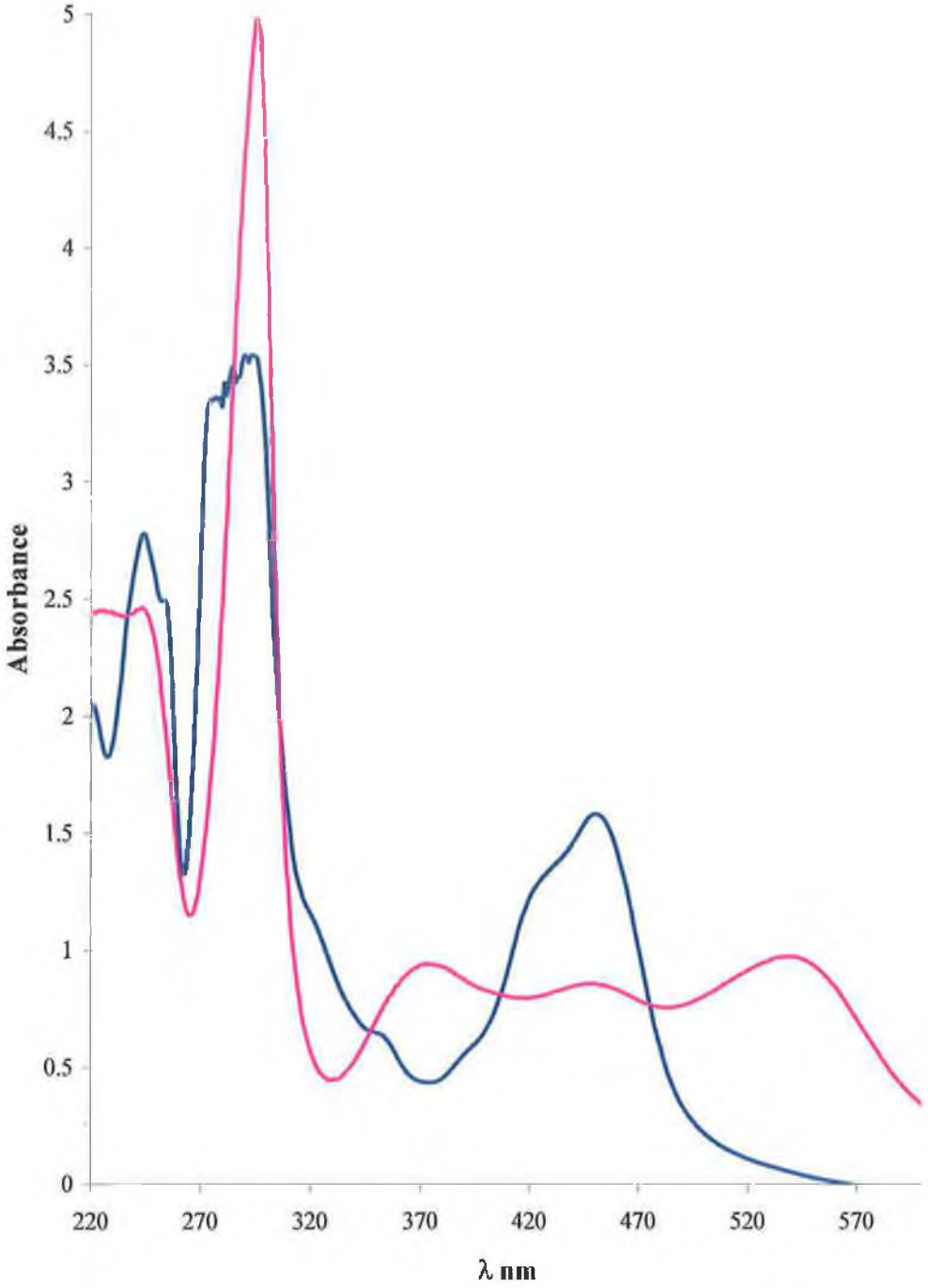

Figure 2.3: *UV-visible absorption spectra of $Ru(bpy)_3^{2+}$ (blue), $Ru(bpy)_2Cl_2$ (pink) dissolved in ethanol. Concentrations of 100 μM where used.*

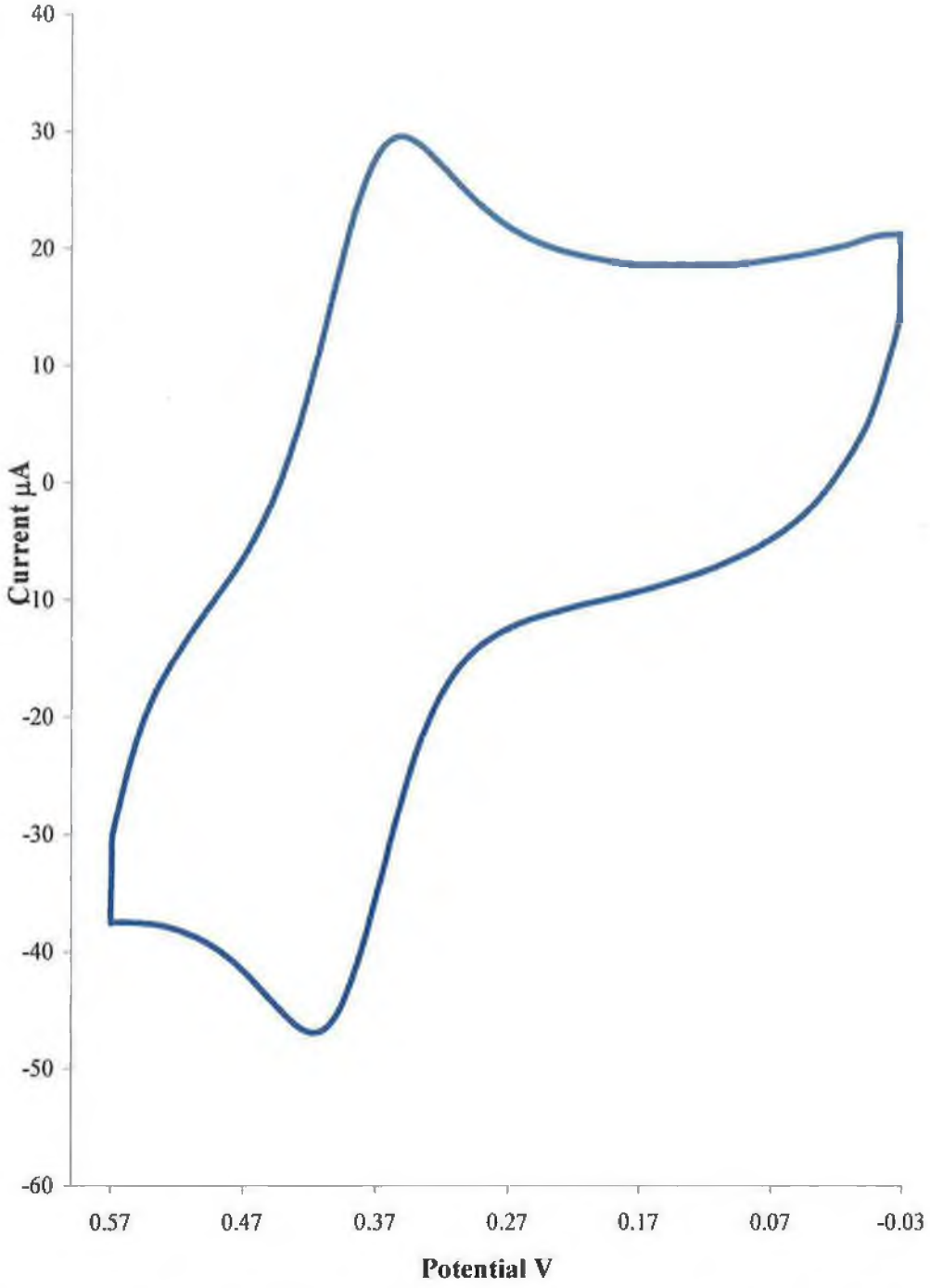

Figure 2.4: *Cyclic voltammetric response of a glassy carbon electrode to 5 mM* $Ru(bpy)_2Cl_2$ *dissolved in 0.1 M* H_2SO_4. *Scan rate was 500* mVs^{-1}.

Cis-[Os(bpy)$_2$Cl$_2$]

Cis-[Os(bpy)$_2$Cl$_2$] was prepared as described in the literature[27]. K_2OsCl_6 and 2,2-bipyridyl were refluxed for approximately 45 min in ethylene glycol. To this saturated sodium dithionite solution was added. The solid was then extracted and washed using distilled water and diethyl ether.

The product was characterised by cyclic voltammetry, UV-Visible spectroscopy and NMR. Figure 2.5 shows the NMR spectrum of the complex. The cyclic voltammogram showed a single redox peak at ~0 V vs. Ag/AgCl, also shown in Figure 2.6. These results, plus the UV spectrum confirmed the identity of the compound.

Poly(4-vinylpyridine)

4-vinylpyridine was purified by vacuum distillation at 70°C. The colourless monomer was then degassed with nitrogen and bulk polymerised for 4 h using the free radical initiator 2,2'-azobisisobutylronitrile (AIBN) at a mole ratio of 500:1 (monomer:initiator). The product was purified by repeated precipitation in diethyl ether and dried *in vacuo*. Viscometry was used in order to determine the molecular weight of the polymer (see Section 2.3.2).

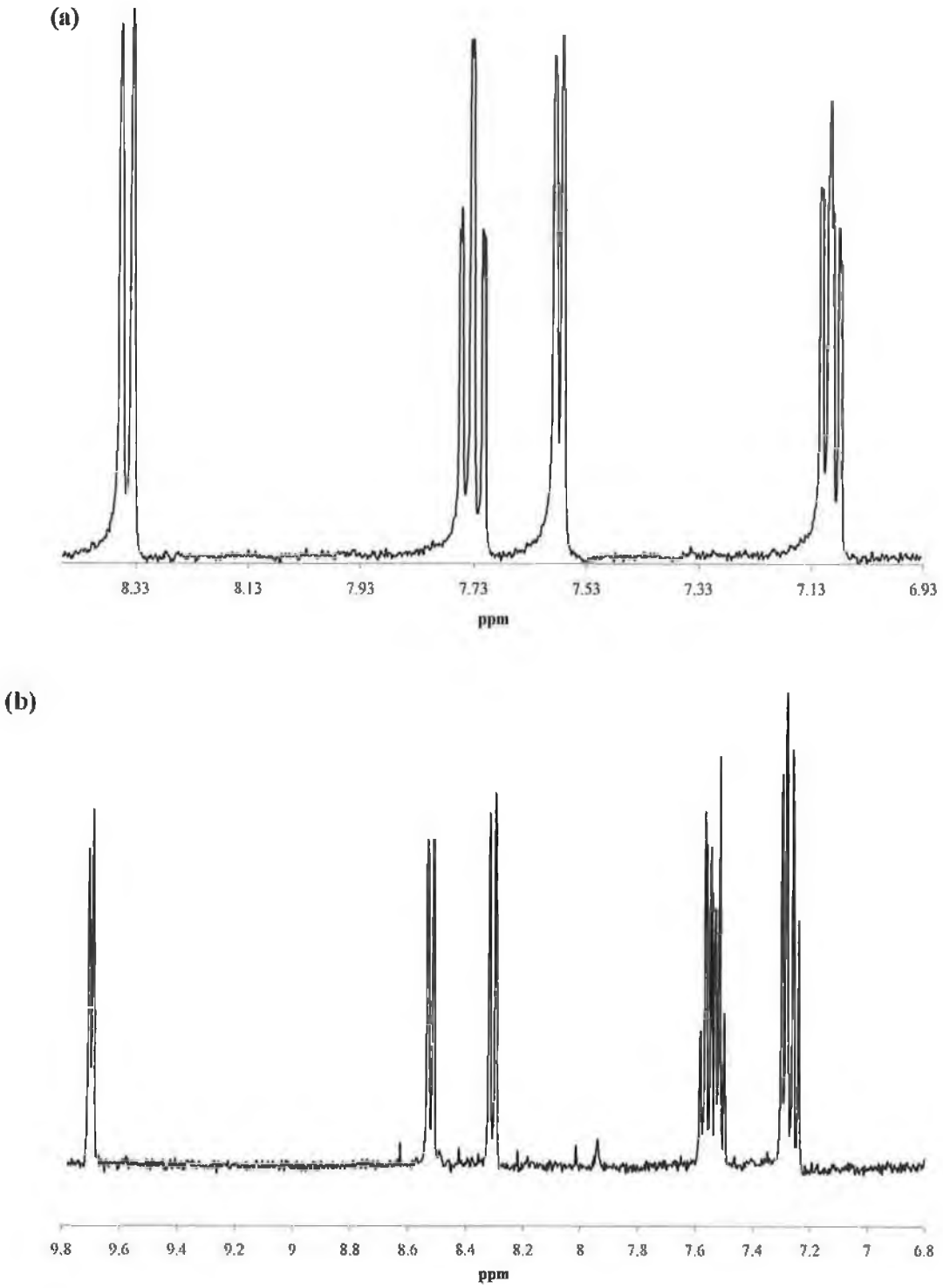

Figure 2.5: *NMR of (a) $Os(bpy)_3^{2+}$ in d-acetone and, (b) $Os(bpy)_2Cl_2$ (above) in DMSO.*

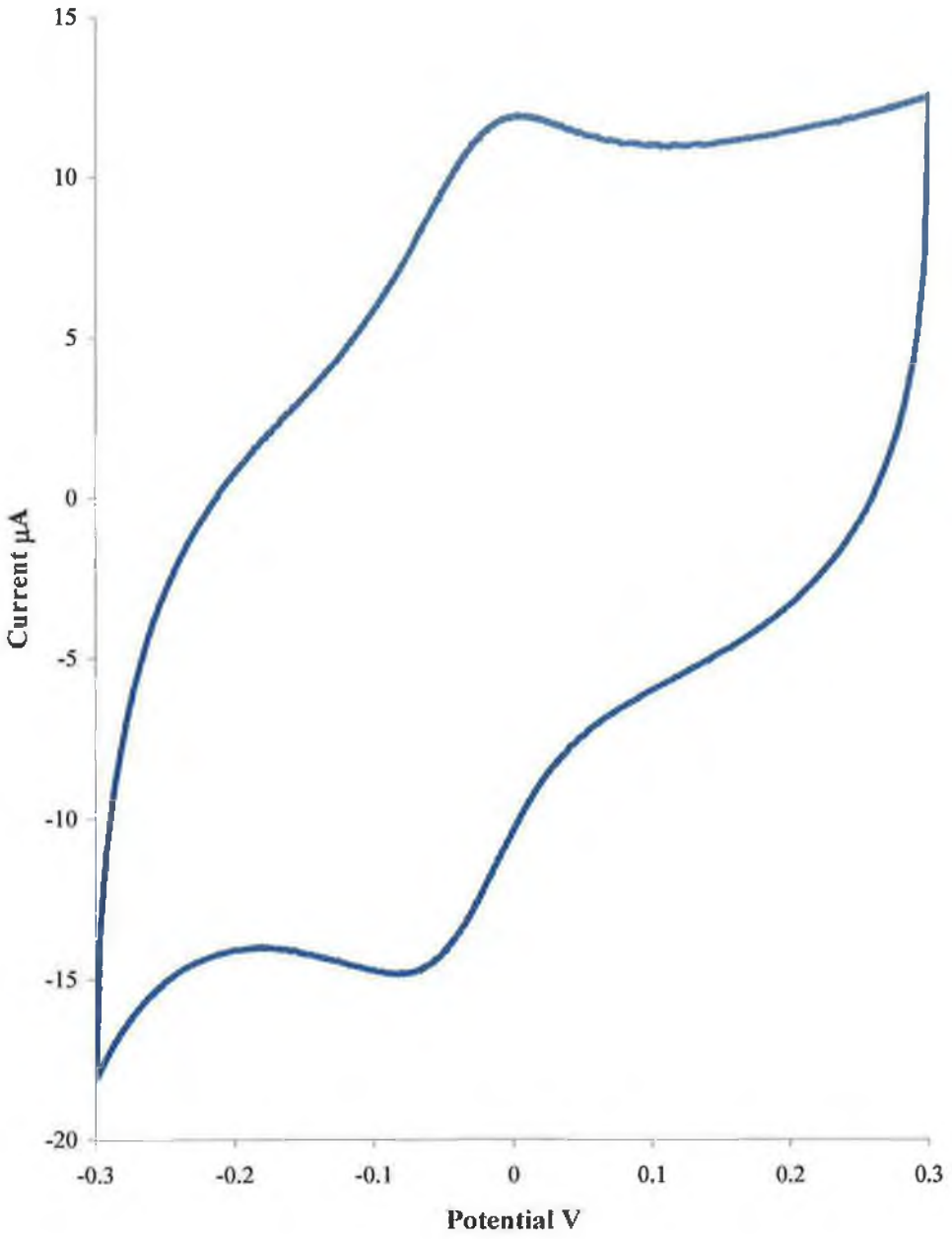

Figure 2.6: *Cyclic voltammogram of 50 µM $Os(bpy)_2Cl_2$ dissolved in 0.1 M $LiClO_4$. Scan rate was 50 mVs^{-1}.*

[Ru(bpy)$_3$(PF$_6$)$_2$]

Ruthenium tris(bipyridyl) was synthesised according to a literature method[28] and characterised by HPLC, UV, cyclic voltammetry and NMR. (See Figure 2.1, 2.2, 2.3 and 2.6).

[Os(bpy)$_3$(PF$_6$)$_2$]

Osmium tris(bipyridyl) was synthesised following the method described in the literature and characterised by voltammetry and NMR.[29] The NMR data is shown is Figure 2.5 while the cyclic voltammogram is shown in Figure 2.8.

Cis-[Ru(bpy)$_2$(H$_2$O)](ClO$_4$)$_2$

The bis-aquo complex was prepared by heating cis-Ru(bpy)$_2$Cl$_2$ in a minimum volume of water for 0.5 h and was precipitated by addition of a five molar excess of $LiClO_4$, followed by refrigeration for 1 h. The product was isolated and dried by suction. Its UV-visible spectrum was consistent with a bis-aquo co-ordinated structure.[30]

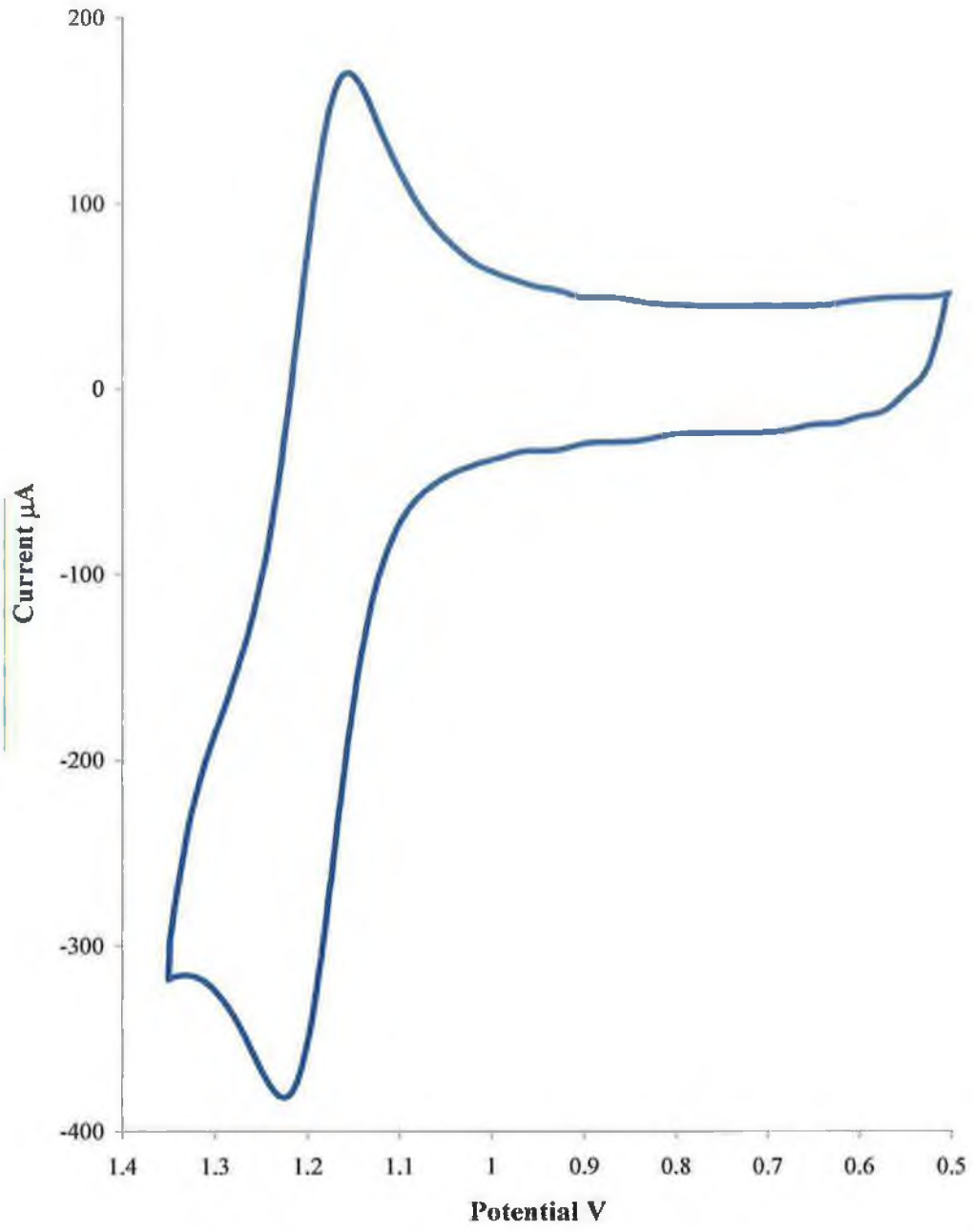

Figure 2.7: *Cyclic voltammetric response of a glassy carbon electrode to 5 mM* $Ru(bpy)_3^{2+}$ *dissolved in 0.1 M* H_2SO_4. *Scan rate was 5* mVs^{-1}.

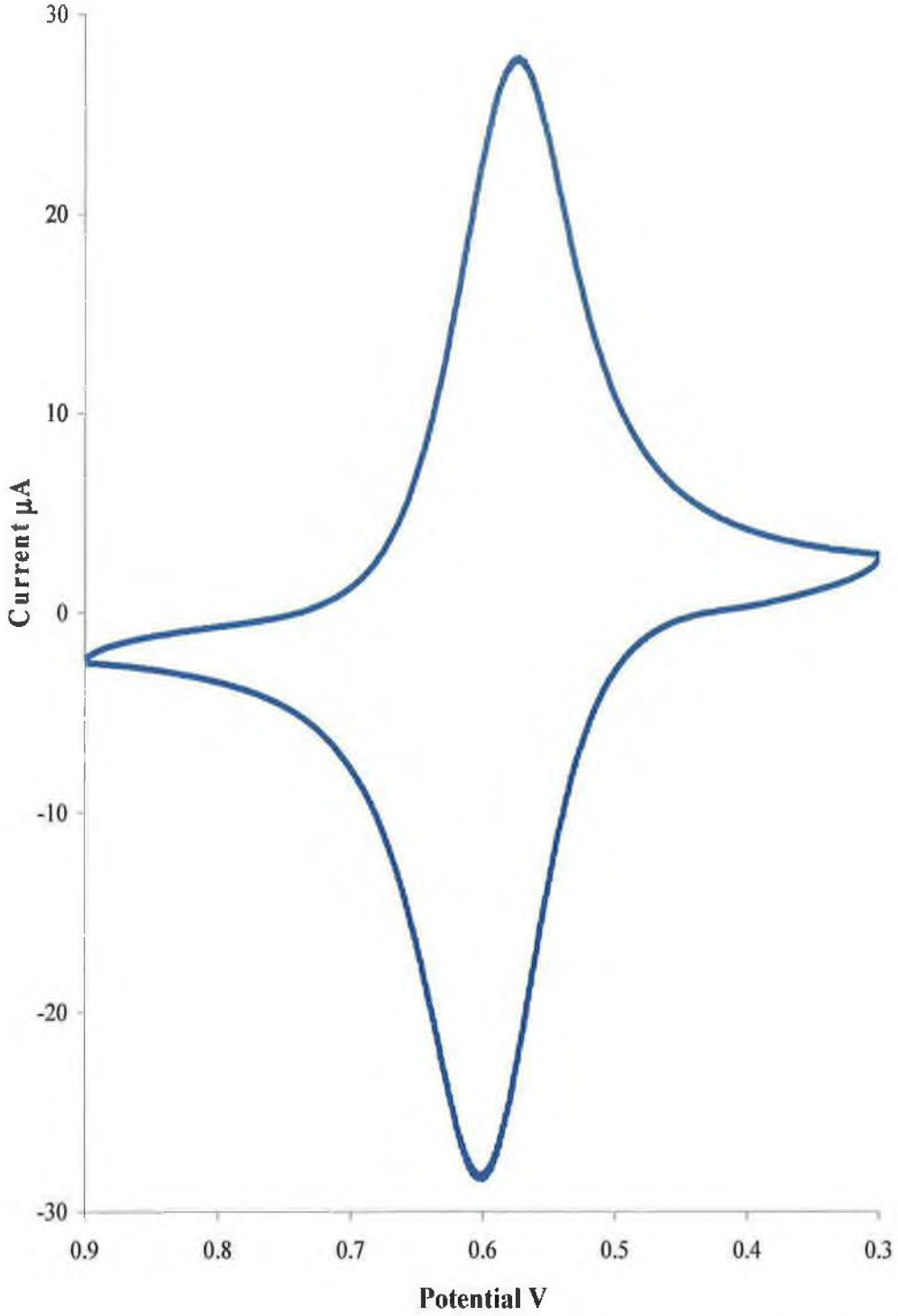

Figure 2.8: *Cyclic voltammetric response of a glassy carbon electrode to 0.5 mM* $Os(bpy)_3^{2+}$ *dissolved in 0.1 M* H_2SO_4. *Scan rate was 5* mVs^{-1}.

$[Ru(bpy)_2(PVP)_{10}](ClO_4)_2$

The bis substituted metallopolymer was prepared by refuxing cis-$[Ru(bpy)_2(H_2O)](ClO_4)_2$ with a ten fold excess of PVP, (Aldrich), in order to give the structure shown in Figure 2.10. The reflux was performed in the dark in 80:20 ethanol:water for up to 72 h and was constantly monitored by UV-visible spectroscopy and cyclic voltammetry. The product was solvent stripped into pure ethanol and precipitated in diethyl ether.[31]

$[Ru(bpy)_2(PVP)_{10}Cl](ClO_4)_2$

The monosubstituted material shown in Figure 2.9 was formed using a similar procedure as that used for $[Ru(bpy)_2(PVP)_{10}]^{2+}$ except that $Ru(bpy)_2Cl_2$ was used as the starting material and no water was added to the reaction mixture.

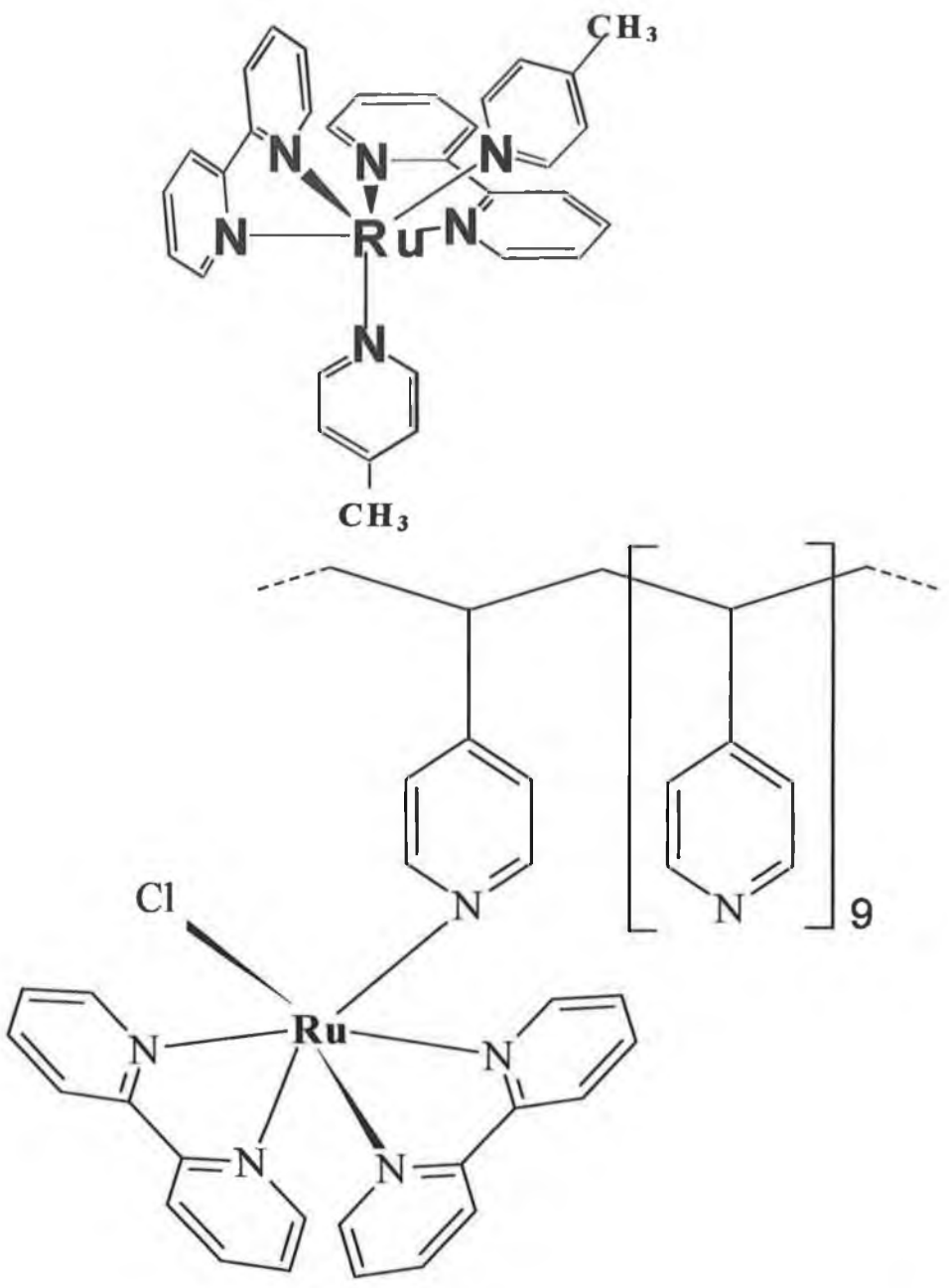

Figure 2.9: *Structure of the redox complexes* $[Ru(bpy)_2(pic)_2]^{2+}$ *(top) and* $[Ru(bpy)_2(PVP)_{10}Cl]^{+}$ *(bottom).*

cis-[Ru(bpy)$_2$(pic)$_2$](PF$_6$)$_2$

The model complex was prepared by refluxing $Ru(bpy)_2Cl_2$ with a 10 molar excess of the ligand (4-picoline) in 50:50 ethanol:H_2O for 24 h in the dark. The complex was precipitated with ammonium hexafluorophosphate, filtered, washed and recrystallised from 60:40 acetone:H_2O. Typical yields were 80-90% and characterisation was performed using uv-visible spectroscopy, and cyclic voltammetry (see Figures 2.14 and 2.22).

[Os(bpy)$_2$(PVP)$_{10}$]Cl$_2$

Cis-$[Os(bpy)_2Cl_2]$ was dissolved in ethanol. H_2O was added and the solution was boiled for approximately one hour. A ten fold excess of PVP, dissolved in a minimum value of ethanol was added. The final solvent composition was 80:20 H_2O:ethanol. The solution was allowed to reflux for at least 10 days and was continuously monitored using cyclic voltammetry. The structure of this compound is shown in Figure 2.11. Characterisation was performed using uv-visible and emission spectroscopy and cyclic voltammetry (see Figures 2.15, 2.18 and 2.34).

[Os(bpy)$_2$(PVP)$_{10}$Cl]Cl$_2$

This was prepared in the same manner as the bis-substituted complex described above, although no H_2O was needed and shorter reflux times were utilised. The perchlorate salt was prepared by addition of 2 M of lithium perchlorate to the ethanolic solution of the metallopolymer. The polymer was then recovered by filtration. The product was solvent stripped into pure ethanol and precipitated in diethyl ether.[31]

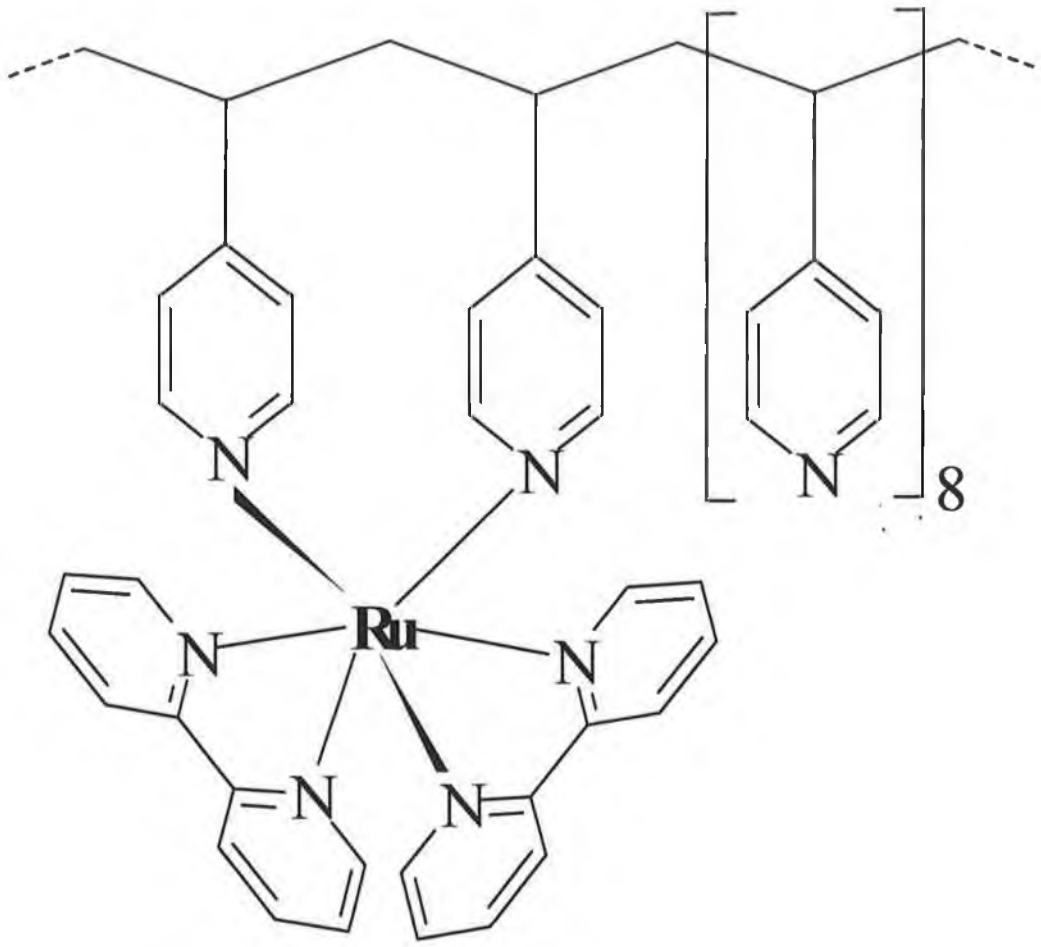

Figure 2.10: *Structure of the redox polymer* $[Ru(bpy)_2(PVP)_{10}]^{2+}$

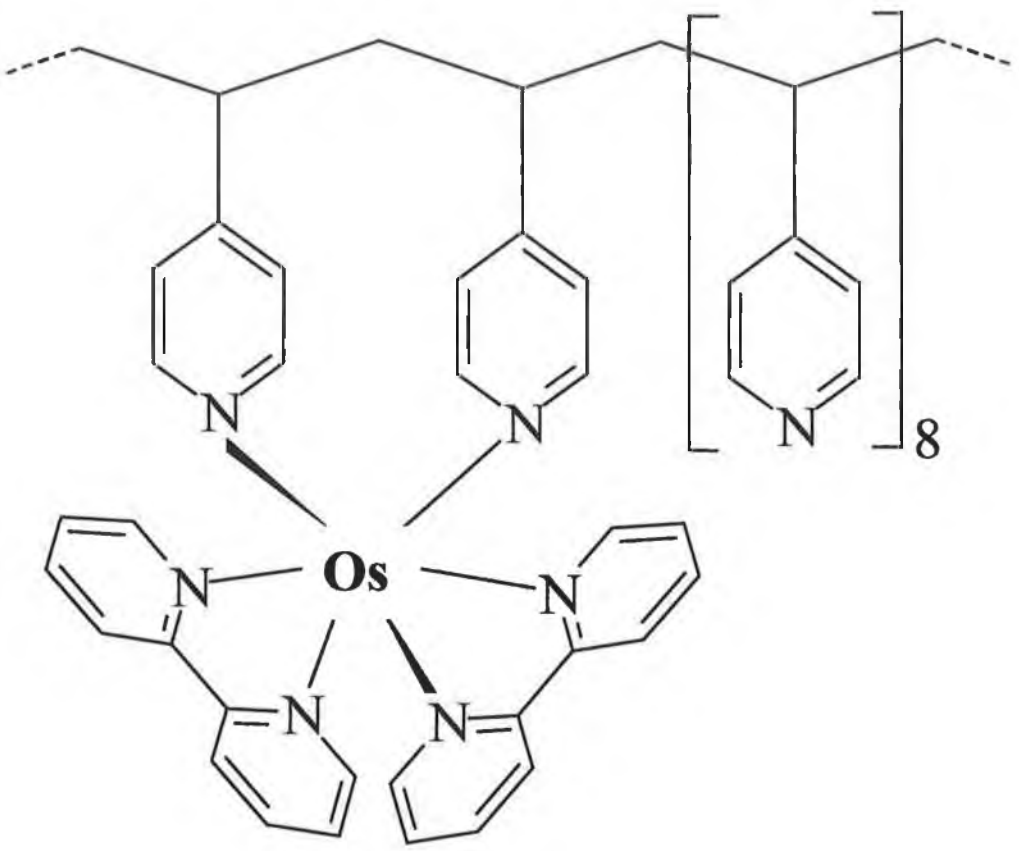

Figure 2.11: *Structure of the redox polymer* $[Os(bpy)_2(PVP)_{10}]^{2+}$.

2.3 *Characterisation:*

2.3.1 *General:*

The synthesis of the redox polymer containing poly(pyridyl) metal compounds by covalent attachment of the metal complex to a polymer backbone is based on the different lability of the chloride ligands in the complex $[M(bpy)_2Cl_2]$, M = Ru, Os.[16,32] The removal of the first chloride occurs readily by refluxing in methanol or ethanol, removal of the second chloride requires aqueous-solvent mixtures, or longer refluxing times in ethylene glycol.[33,34,35,36,37,38] Consequently, for the synthesis of the bis substituted material, $[M(bpy)_2(PVP)_n]^{2+}$, water must be added to the reaction mixture. For this synthesis, it had been discovered that using the bis-aquo complex, $[M(bpy)_2(H_2O)_2]^{2+}$, as a starting material was the most successful strategy, as it reduced reaction times and gave rise to only negligible amounts of the mono-substituted product. The overall reaction for both reaction schemes can be summarised as follows, substituting osmium for ruthenium where necessary:[24]

$$Ru(bpy)_2Cl_2 + H_2O \rightarrow [Ru(bpy)_2(H_2O)Cl]^+ + Cl^- \quad \textbf{(1)}$$

$$[Ru(bpy)_2(H_2O)Cl]^+ + H_2O \rightarrow [Ru(bpy)_2(H_2O)_2]^{2+} + Cl^- \quad \textbf{(2)}$$

$$[Ru(bpy)_2(H_2O)_2]^{2+} + PVP \rightarrow [Ru(bpy)_2(H_2O)(PVP)]^{2+} + H_2O \quad \textbf{(3)}$$

$$[Ru(bpy)_2(H_2O)(PVP)]^{2+} \rightarrow [Ru(bpy)_2(PVP)_n]^{2+} \quad \textbf{(4)}$$

It was noted that when these metal complexes are reacted with a preformed polymer, soluble polymers can be obtained.[24] It should be noted that a single inter-chain crosslink would double the effective molecule weight of the bis coordinated material. As already stated, since these materials are soluble, they can be characterised in solution and their application as electrode modifiers is facilitated.

The synthesis of $[Os(bpy)_2(PVP)_{10}]^{2+}$ can be described in the same way as the ruthenium analogue (equations 1-4), but because of the inertness of osmium complexes, longer reflux times were required.

The synthetic flexibility of the procedure is evident since materials with different metal to polymer ratios can be prepared easily by adding the appropriate amounts of reactants. The polymer backbone can be changed provided it has a pendant coordinating group, and the nature of the metal centre can also be varied. The metal loading of the materials described here is based on the quantity of starting material employed, assuming complete reaction. The metal loading for both the ruthenium and osmium metallopolymers throughout the study is 1:10, metal:backbone.

2.3.2 Polymer Molecular Weight Determination:

Although there is no evidence that molecular weight has a strong influence on the electrochemical properties of the electroactive coating, it has been shown that higher molecular weight materials adhere much better to the electrode surface and enhance the lifetime of the modified electrode.[6] The use of hydrodynamic techniques such as viscometry for the determination of the molecular weight of polymers is well established.[39] The formula which relates a polymer solution viscosity to molecular weight is the Mark-Houwink equation:

$$[\eta] = KM^a \qquad (5)$$

also,

$$[\eta] = \lim_{c \to 0} \frac{\left(\eta/\eta^*\right) - 1}{c} \qquad (6)$$

where $[\eta]$ is the intrinsic viscosity at infinite dilution, η/η^* is the viscosity of the solution divided by the viscosity of the pure solvent (for which the respective efflux times can be substituted) K and a are the Flory constants, which depend on the identity of the solvent and polymer and M is the polymer molecular weight. K and a have previously been evaluated as 2.5×10^{-4} and 0.68 respectively for ethanolic solutions, these values imply a semi coiled structure of the polymer.[40] Ethanolic solutions of PVP in the concentration range 0.2-1.0 % were prepared and the efflux time of each through a viscometer which was thermostated at 25 ±0.5 ^{0}C was measured. A plot of $[(\eta/\eta^*)-1]/c$ versus concentration c, (see Figure 2.12), was extrapolated to infinite dilution and gave the value of the intrinsic viscosity $[\eta]$ to be 0.5582 cm^3/g. Substituting this value into the Mark-Houwink equation gives a molecular weight of approximately 90,000 $gmol^{-1}$ for the uncoordinated PVP back-bone.

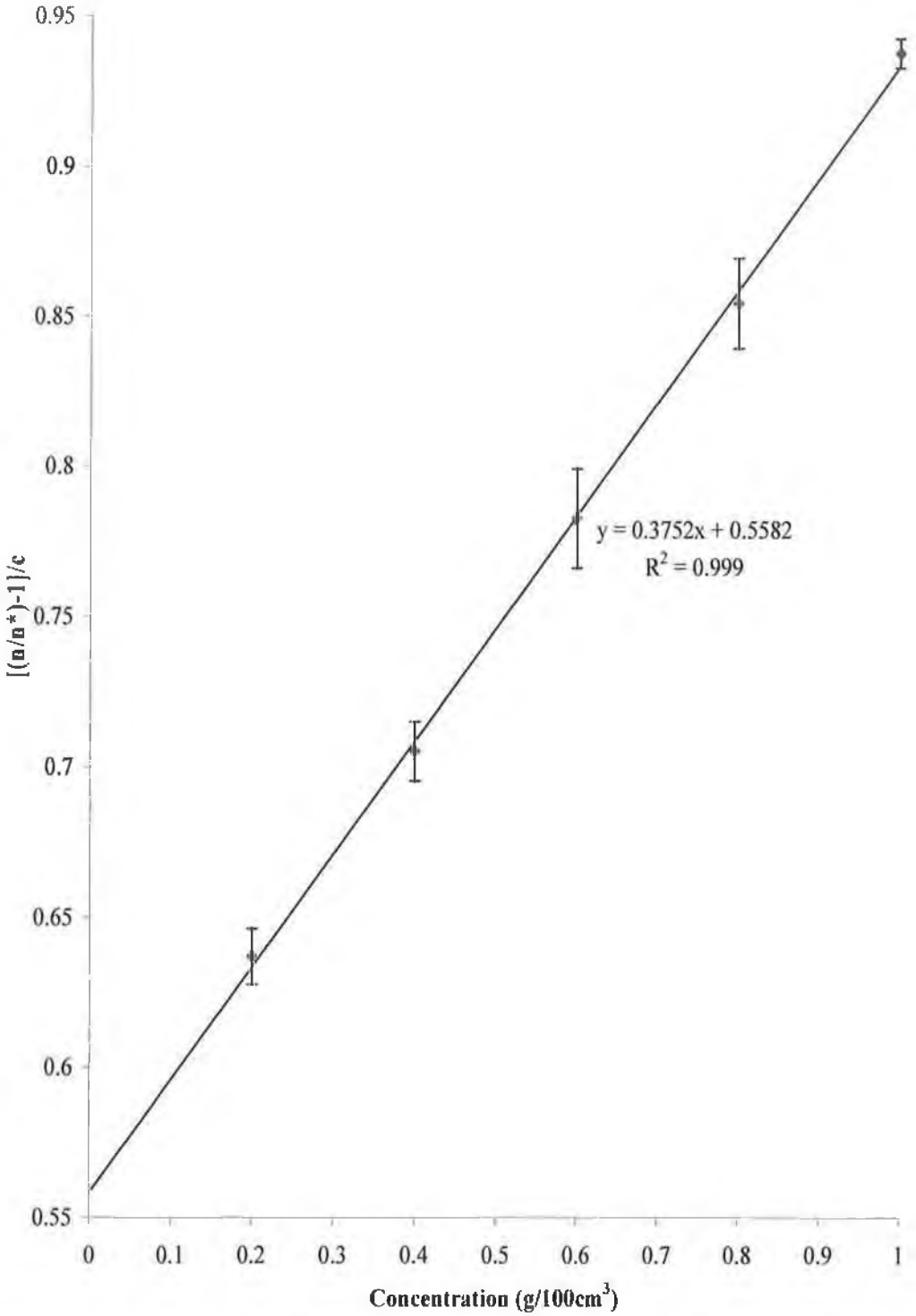

Figure 2.12: *Concentration dependence of the viscosity of ethanolic solutions of PVP at 25 ^{0}C. Error bars represent triplicate results.*

2.3.3 Spectroscopic and Photophysical Properties:

Ruthenium(II) compounds are stable low-spin d^6 species which can be oxidised at the metal or reduced by addition of an electron in a ligand π^* orbital. The most important photophysical properties of ruthenium poly(pyridyl) complexes are depicted in Figure 2.13. The absorption spectrum of these species is characterised by intense absorption bands in the visible region, which are assigned to metal to ligand charge transfer (MLCT) transitions.[16] Emission is dominated by a closely spaced manifold of at least three triplets charge transfer states, but at ambient temperatures[41] these can be viewed as occurring from a single state (^{3}MLCT). Due to spin orbital coupling, fast intersystem crossing occurs from the singlet to triplet state with an efficiency of unity, followed by emission from the triplet state to the ground state (k_r) or radiationless deactivation[42] to the ground state (k_{nr}). An alternative deactivation is population of the ^{3}MC (metal centred) state. If this occurs the electron occupies an anti-bonding metal-based orbital, resulting in distortion of the metal ligand axes and weakening the Ru-N bonds. This may cause photodecomposition of the complex, which manifests itself as ligand loss followed by co-ordination of a substitute ligand, often solvent or electrolyte.[5,43]

For a ruthenium containing metallopolymer, the nature of the co-ordination sphere around the central atom is of prime importance since it determines the redox potential and photophysical properties of the material obtained. Electronic spectroscopy has proven useful in the characterisation of these species. In particular, the position of the lowest absorption maxima and the wavelength of emission are often characteristic of a particular ruthenium moiety. Ruthenium poly(pyridyl) compounds typically exhibit two bands in the visible region of the spectrum. As previously stated, these have been assigned to metal to ligand charge transfer (MLCT) transitions from the metal localised orbital, Ru ($d\pi$), to the ligand localised orbital, bpy (π^*) orbitals. The positions of the absorption maxima are governed by the δ-donor and π-acceptor properties of the ligands. A ruthenium complex with a strong δ-donating ligand such as chloride is electron rich and the

MLCT band is present at a lower energy. This also results in a lower oxidation potential for the compound.[24,44]

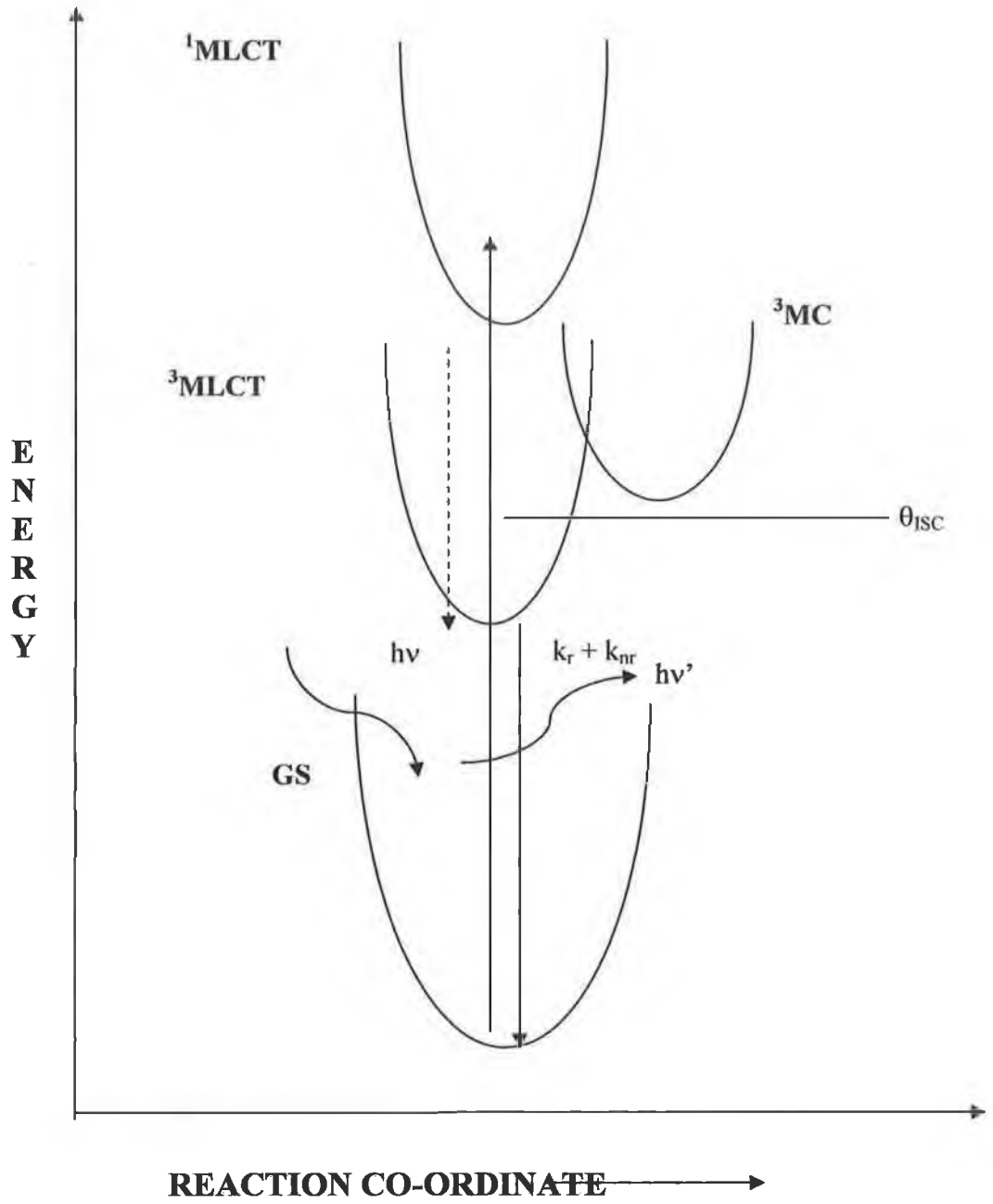

Figure 2.13: *Photophysical process of ruthenium polypyridyl compounds.*

2.3.4 UV-Visible Spectroscopy:

Figure 2.14 shows the UV-visible absorption spectra of $[Ru(bpy)_2PVP_{10}]^{2+}$, $[Ru(bpy)_2(pic)_2]^{2+}$ and $Ru(bpy)_3^{2+}$. These were obtained to assist in the characterisation of the polymer. Since the spin allowed metal to ligand charge transfer (^{1}MLCT) absorption maxima at 345 and 460nm are indicative of the $[Ru(N)_6]^{2+}$ coordination-sphere and corresponds closely to the UV-Vis spectrum of the $[Ru(bpy)_2(pic)_2]^{2+}$ model complex. The bands between 200 and 300nm correspond to $\pi \rightarrow \pi^*$ transitions associated with the pyridine units. The spectra obtained correspond to those obtained in previous characterisations of this metallopolymer.[24]

Through comparison of the UV-Vis spectrum of the ruthenium complexes, the $[Ru(N)_6]^{2+}$ coordination sphere of the ruthenium centre in the polymeric material is verified. The visible region MLCT bands $d \rightarrow \pi^*$ transitions, for the polymer occur at 460 nm, while the shoulders at 322 and 344 nm in the spectrum of $Ru(bpy)_3^{2+}$, are metal centred (MC) transitions.[45] The remaining bands in the ultraviolet region of the spectrum are assigned to ligand centred (LC) π-π^* transitions.[45]

The UV-visible spectrum of $[Ru(bpy)_2(PVP)_{10}Cl]^+$ showed an MLCT transition at the longer wavelength of 498 nm, this is characteristic of the $Ru(N)_5$ coordination sphere and the observation that λ_{max} is of longer wavelength reflects the strong electron donor properties of ruthenium.[46] Spectroscopic data for all the compounds studied are presented in Table 2.1.

Compound	*λmax (nm) Absorbance*[a]	*λmax (nm) Emission*[a] *(298K)*	*λmax (nm) Emission*[a] *(77K)*	ϕ_p *(%)*[b]	*τ ns*
$[Ru(bpy)_3]^{2+}$	290,452	605	586	6.2	855
$[Ru(bpy)_2(PVP)_{10}]^{2+}$	341,460	612	594	0.94	60
$[Ru(bpy)_2(PVP)_{10}Cl]^{+}$	440,498	704	680		
$[Ru(bpy)_2(pic)_2]^{2+}$	331,461	614	597	0.094	~40
$[Os(bpy)_3]^{2+}$	378,462,553	766	749	0.038	45
$[Os(bpy)_2(PVP)_{10}]^{2+}$	342,441,556	765	752		35
$[Os(bpy)_2(PVP)_{10}Cl]^{+}$	364,431,486,730				
$[Os(bpy)_2(pic)_2]^{2+}$	347,393,442,610	756	748		20

Table 2.1: *Spectroscopic data for the osmium and ruthenium metallopolymers and complexes studied.*

[a] *Measured in ethanol*

[b] *Photoluminescent quantum yield (ϕ_p) measured at 298 K in acetonitrile, using $Ru(bpy)_3^{2+}$ as relative standard, described later.*

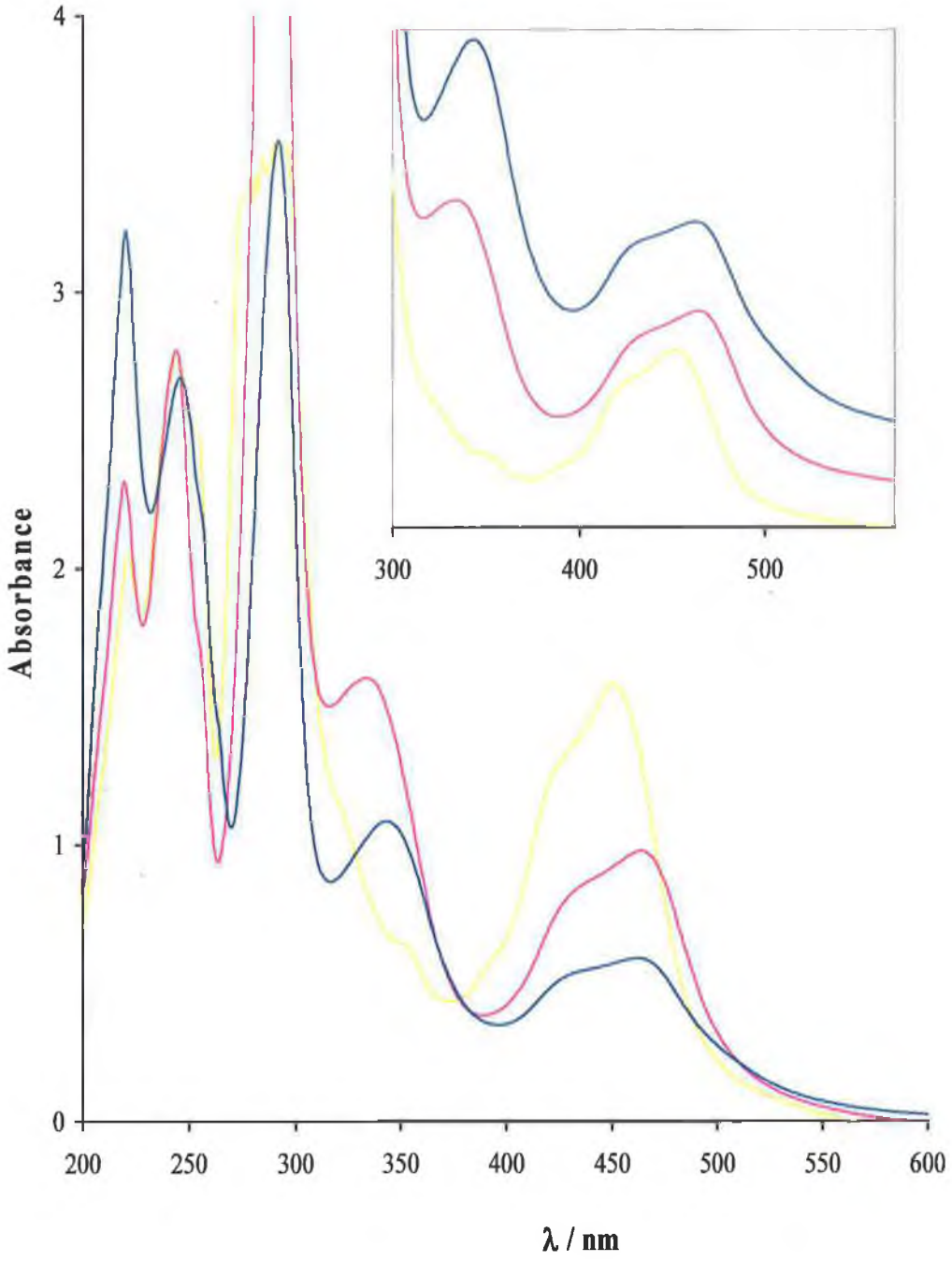

Figure 2.14: *UV-visible absorption spectra of* $[Ru(bpy)_2(PVP)_{10}]^{2+}$ *(blue),* $[Ru(bpy)_2(pic)_2]^{2+}$ *(pink) and* $Ru(bpy)_3^{2+}$ *(yellow) dissolved in ethanol. Concentrations of 100 μM where used. The insert shows an expanded and offset view of the visible region of the spectra.*

The ground state absorption and photophysical properties of numerous polypyridyl complexes of Os(II) have been examined, particularly by Meyer and coworkers. Although the electronic spectrum of $Os(bpy)_3^{2+}$ appears to have been studied first by Crosby *et al.*, [47] at least so far as spectral assignments of both absorption and fluorescence properties are concerned. The strong absorption band system in the visible was attributed to charge transfer.

Figure 2.15 presents the absorption spectra of $Os(bpy)_3^{2+}$, $[Os(bpy)_2(pic)_2]^{2+}$ and $[Os(bpy)_2(PVP)_2]^{2+}$ in ethanolic solution at ambient temperature. In the ultra-violet region of the spectrum a sharp absorption band is observed at approximately 290 nm. This band arises from a bpy based π-π^* transition. The absorption features in the visible region, broad bands between 350 and 550 nm, involve a series of closely lying excited states which arise from Os(5d) $\rightarrow$ bpy(π^*) charge transfer transition. As such, these bands are associated with metal–to-ligand-charge-transfer (MLCT) bands (d-π^*), indicated in the spectrum by the broad bands. The MLCT excited states can be further characterised as being predominantly triplet states containing an appreciable amount of singlet character as a consequence of spin-orbit coupling, which can also be a contributing factor to the broadness of the bands. The metal-ligand interaction is stronger for osmium complexes over their corresponding ruthenium analogues, subsequently resulting in a larger ligand-field splitting for osmium complexes. The position of these intense bands is governed by both the position of the anti-bonding orbital (π^*) in respect to the d-orbital for the metal.

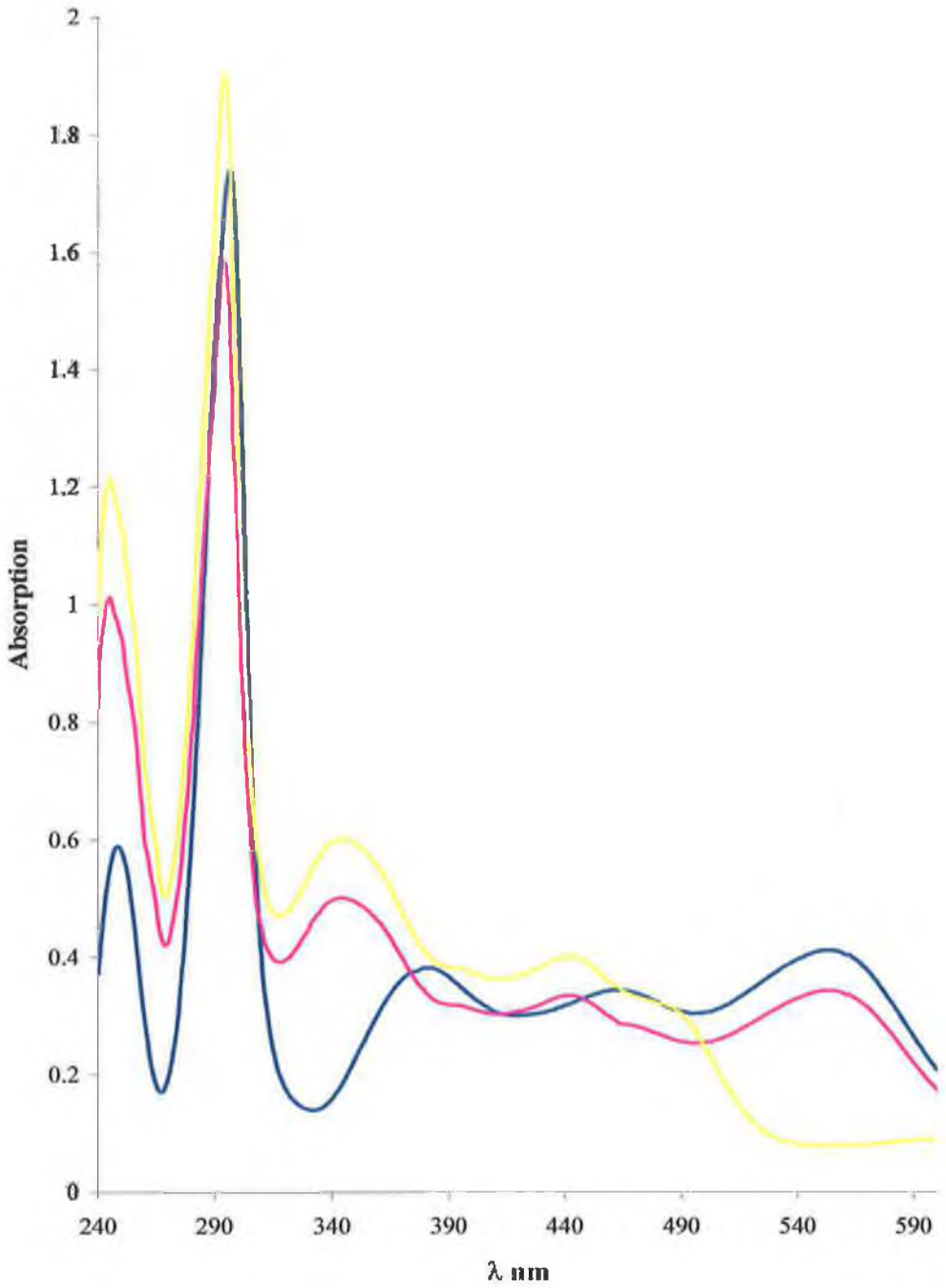

Figure 2.15: *UV-visible absorption spectra of* $[Os(bpy)_2(PVP)_{10}]^{2+}$ *(pink),* $[Os(bpy)_2(pic)_2]^{2+}$ *(yellow) and* $Os(bpy)_3^{2+}$ *(blue) dissolved in ethanol. Concentrations of 100 μM where used.*

2.3.5 Emission Spectroscopy:

Further evidence of the $Ru(N)_6$ nature of the co-ordination sphere is provided by the luminescence spectra of the polymer, the model complex and $Ru(bpy)_3^{2+}$ shown in Figure 2.16, which all display the characteristic emission maximum at approximately 600 nm. The mono-substituted complex showed only very weak luminescence and its wavelength was shifted to a lower energy (704 nm) relative to its bis-substituted analogue.

Figure 2.17 shows the vibrational fine structure observed in the emission spectra of the polymer and model complex at low temperature. The position of the emission maximum is shifted by approximately 20 nm on going from 298 to 77 K and a shoulder is evident at about 640 nm for both compounds. The location of the peaks in this spectrum closely to the emission spectrum[42] of $Ru(bpy)_3$ in EtOH/MeOH glass at 77 K. The vibrational structure is assigned to a perturbed skeletal vibration of the aromatic ring, due to the removal of the π^* electron.[16]

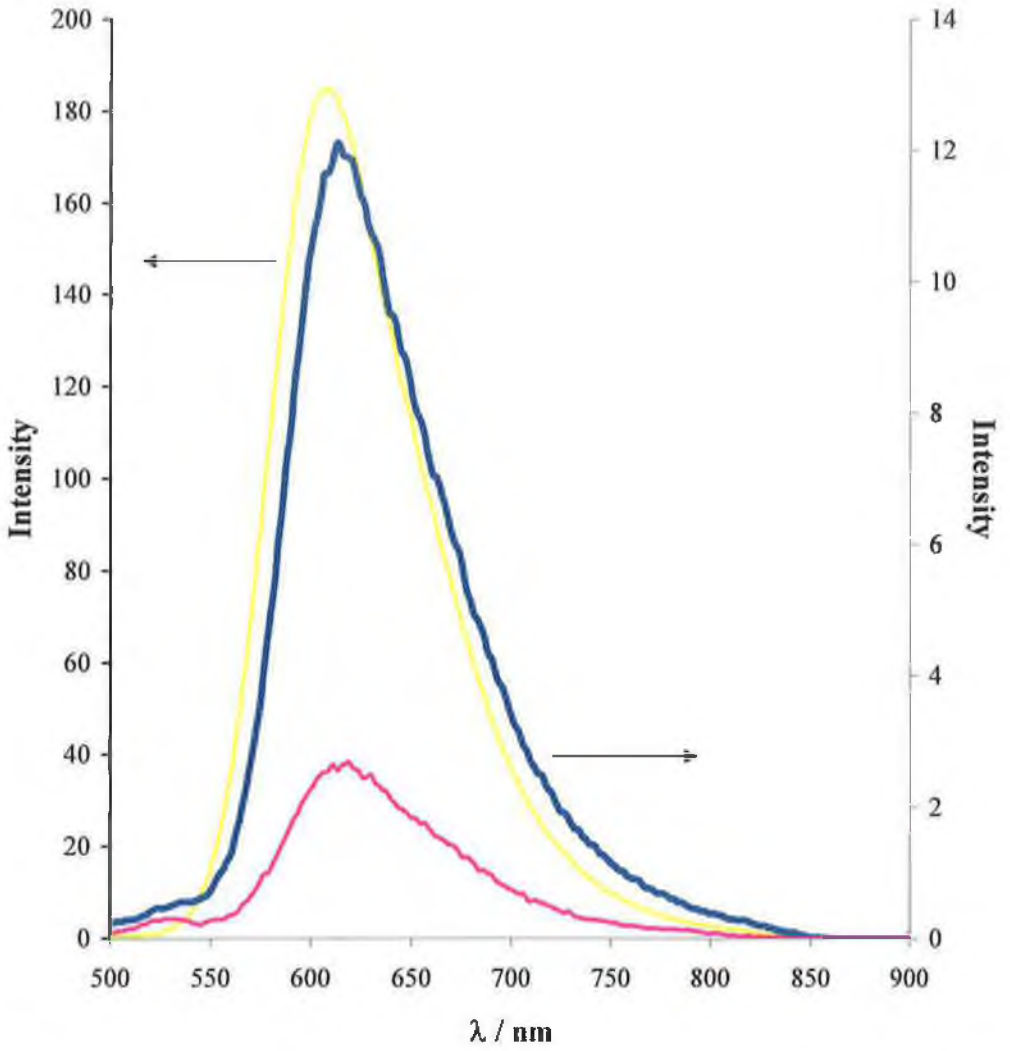

Figure 2.16: *Emission spectra of 100 μM* $[Ru(bpy)_2(PVP)_{10}]^{2+}$ *(blue) and 100 μM* $[Ru(bpy)_2(pic)_2]^{2+}$ *(pink) and 50 μM* $Ru(bpy)_3^{2+}$ *(yellow) measured in ethanol at 298 K.*

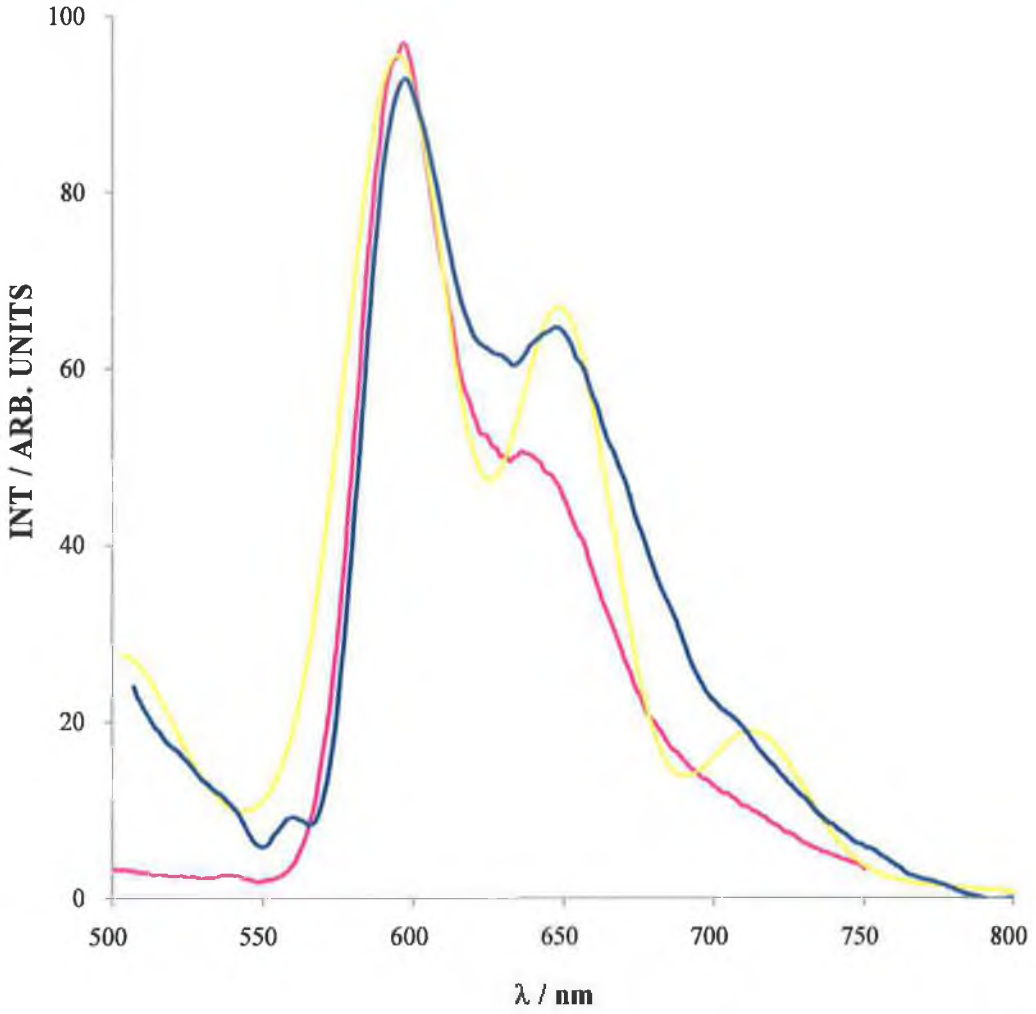

Figure 2.17: *Low temperature emission spectra of 100 μM* $[Ru(bpy)_2(PVP)_{10}]^{2+}$ *(blue) and 100 μM* $[Ru(bpy)_2(pic)_2]^{2+}$ *(pink) measured in EtOH/MeOH at 77 K. The second derivative guassian peak fit spectrum for the polymer is shown in yellow.*

Figure 2.18 shows the emission spectrum of some selected Os(II) polypyridyl complexes. In general, their absorption and emission are at a higher wavelength with respect to their ruthenium analogues. The luminescence spectra shown displays the characteristic emission maximum at approximately 750 nm. This strongly suggests the presence of the $[OsN_6]Cl_2$ moiety in the polymer, so that two nitrogen units from the polymer backbone are bound to the osmium centre. These observations are in agreement with the synthetic conditions employed.

Figure 2.18 also shows the vibrational fine structure observed in the emission spectra of the Os(II) complexes at low temperature. As with its ruthenium analogue, there is a slight shift of λ_{max} to a lower wavelength of approximately 10 – 15 nm on going from 298 to 77 K.

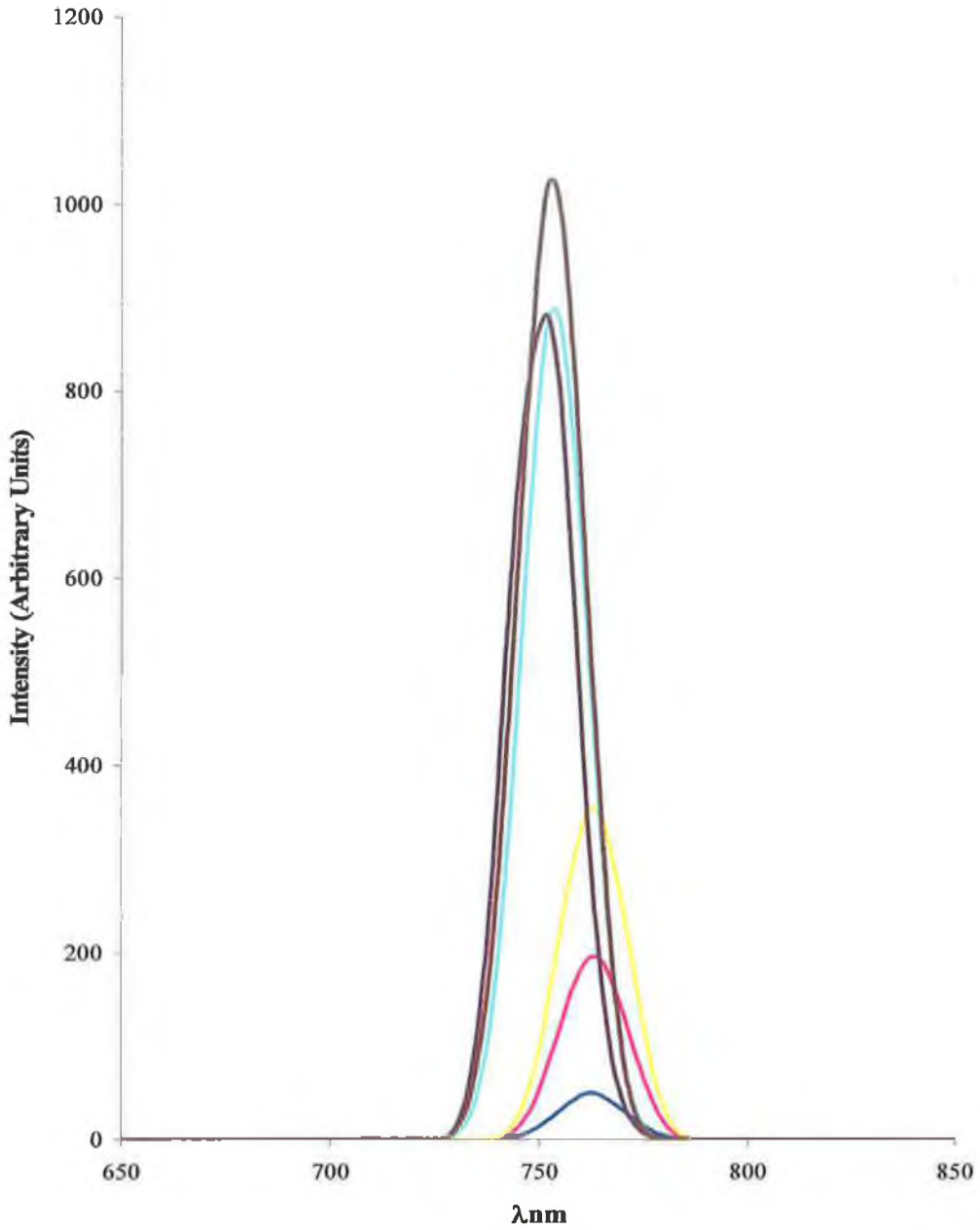

Figure 2.18: *Emission spectra of 100 μM $[Os(bpy)_2(PVP)_{10}]^{2+}$ (pink) and 100 μM $[Os(bpy)_2(pic)_2]^{2+}$ (blue) and 50 μM $Os(bpy)_3^{2+}$ (yellow) measured in ethanol at 298 K. Low temperature emission spectra of 100 μM $[Os(bpy)_2(PVP)_{10}]^{2+}$ (light blue) and 100 μM $[Os(bpy)_2(pic)_2]^{2+}$ (purple) and $Os(bpy)_3^{2+}$ (brown) measured in EtOH/MeOH at 77 K.*

2.3.6 *Photoluminescent Quantum Yields (ϕ_p) and Excited State Lifetimes (τ):*

The excited state lifetime and quantum efficiency are important parameters from the point of view of sensor sensitivity, since they directly influence the ECL intensity.[48,49] Relative photoluminescent quantum yields (ϕ_p) were measured in deaerated ACN or DMF (Argon, 20 minutes) (10^{-4} – 10^{-5} M) using the following relationship[42]:

$$\phi_P = \phi_{ref}\left(I_{sample} A_{ref} / I_{ref} A_{sample}\right) \qquad (7)$$

where I is the area under the emission spectrum and A is the absorbance for the sample and reference, obtained under identical experimental conditions, with $Ru(bpy)_3^{2+}$ as standard, $\phi_{ref} = 0.062$ (ACN), 0.063 (DMF).[42]

The fluorescence life-time of a substance usually represents the average amount of time the species remains in the excited state prior to its return to the ground state. Fluorescence is usually a unimolecular process and therefore the excited state population established by an impulse of exciting light will generally decay exponentially according to first order kinetics.[50] The impulse response function I(t) will have the form:

$$I(t) = I_0 e^{-kt} \qquad (8)$$

where k represents the overall relaxation rate and I_0 is simply a scaling factor. Since the fluorescence life-time (τ) is by definition the time required for the excited state population to decay to 1/e or ~37 % of its initial value, it follows that:

$$\tau = \ln 2 / k \qquad (9)$$

and τ can therefore be determined graphically from the slope of a plot of ln(I) verses t.

Figure 2.19 shows typical emission decay for the model complex $Ru(bpy)_2(pic)_2^{2+}$ in acetonitrile; single exponential decays were typically observed for this compound with lifetimes of the order of 40 ns.

The fluorescent lifetime of the polymer in solution phase and also the lifetime of the emitting state within thin films of the polymer immobilised on transparent ITO slides in contact with the electrolyte were measured using the laser spectroscopic system and are shown in Figures 2.20.

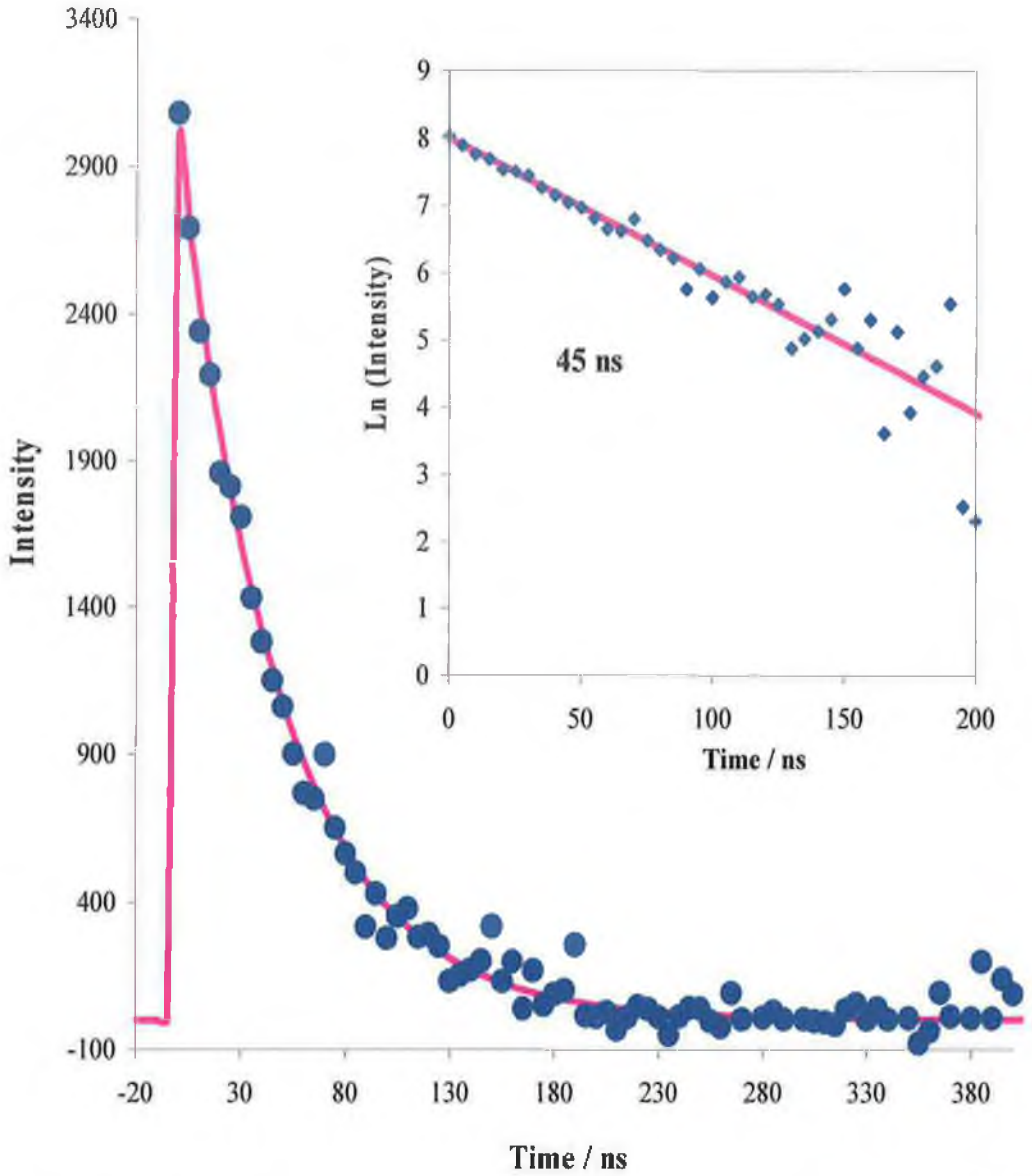

Figure 2.12: *Emission decay for a 10^{-4} M solution of $[Ru(bpy)_2(pic)_2]^{2+}$ in acetonitrile monitored at 614 nm following the application of a 10 ns laser pulse of 355 nm light.*

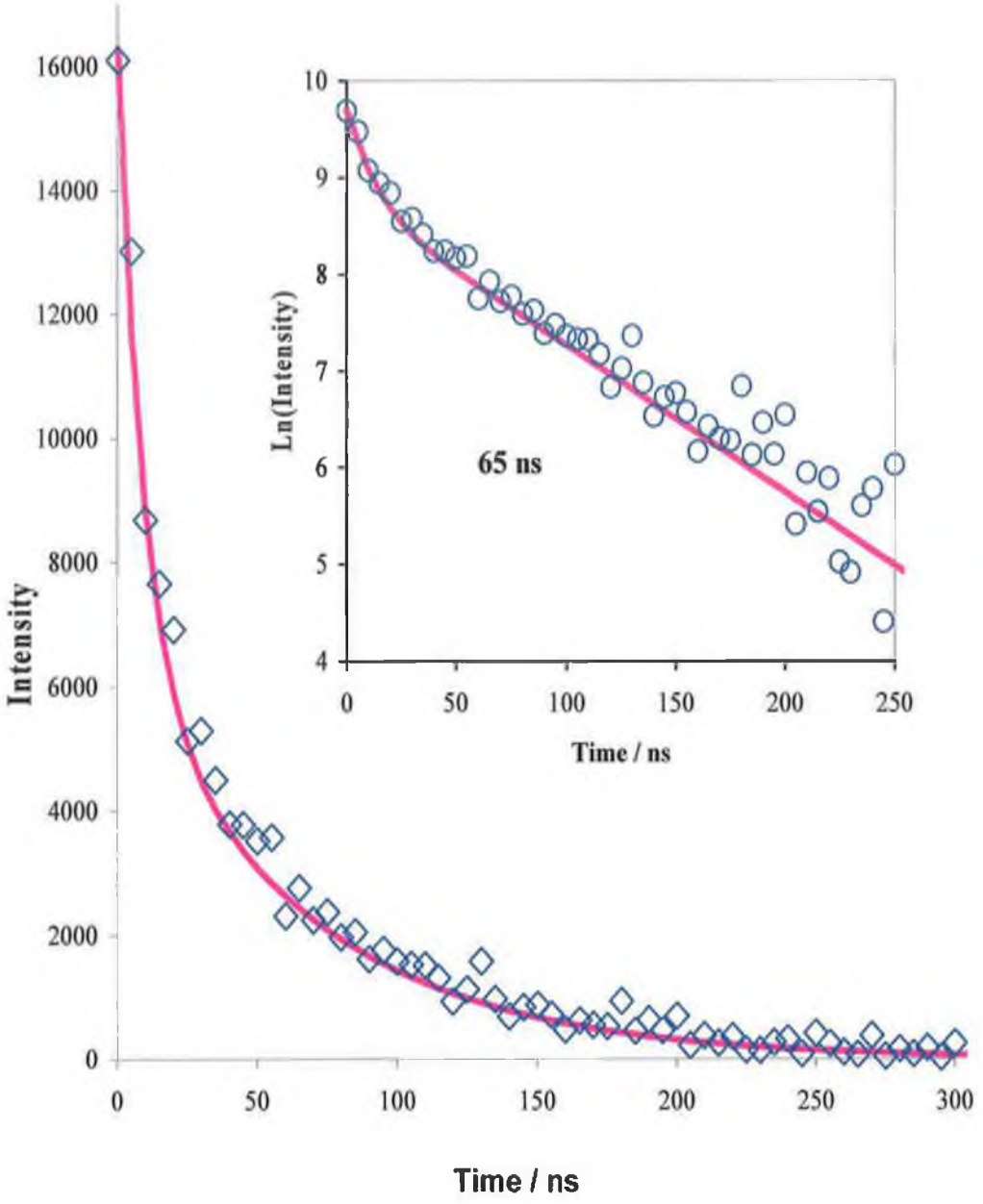

Figure 2.13: *Emission vs. time transient of* $[Ru(bpy)_2(PVP)_{10}]^{2+}$ *film deposited on ITO (*$\Gamma \sim 10^{-9}$ *mol* cm^{-2}*) in contact with 0.1 M* H_2SO_4*. The emission was monitored at 612 nm.*

Determinations of emission quantum yields and lifetimes for a series of structurally related complexes allows quantitative assessment of the importance of the non-radiative decay processes in these complexes. In the limit of large energy separation between the initial and final states with small differences in their equilibrium geometries (known as the weak coupling limit) the *energy gap law* predicts that the non-radiative decay rates k_{nr} to decrease exponentially with increasing energy separation;

$$k_r \propto \exp(-E_{em}) \qquad \textbf{(10)}$$

where E_{em} is the room temperature emission maximum. For radiative rates, Einstein's law predicts that the radiative rate constants vary as the third power of the excited state energy;

$$k_r \propto E_{em}^{3} \qquad \textbf{(11)}$$

Meyer *et. al.* have determined the radiative (k_r) and non-radiative (k_{nr}) decay rates of MLCT excited stated in an extended series of mixed ligand Os(II) complexes. These decay rate constants are obtained from the measured excited state lifetime and quantum yields as;

$$k_r = \Phi/\tau \qquad \textbf{(12)}$$

And

$$k_{nr} = 1/\tau - k_r \qquad \textbf{(13)}$$

Figure 2.21 shows that emission decays for the osmium polymer in acetonitrile are typically single exponentials with lifetimes of approximately 35 ns. As already stated, due to the energy gap law, it was expected that the lifetimes for the osmium complexes would be short lived in comparison to their ruthenium analogues.

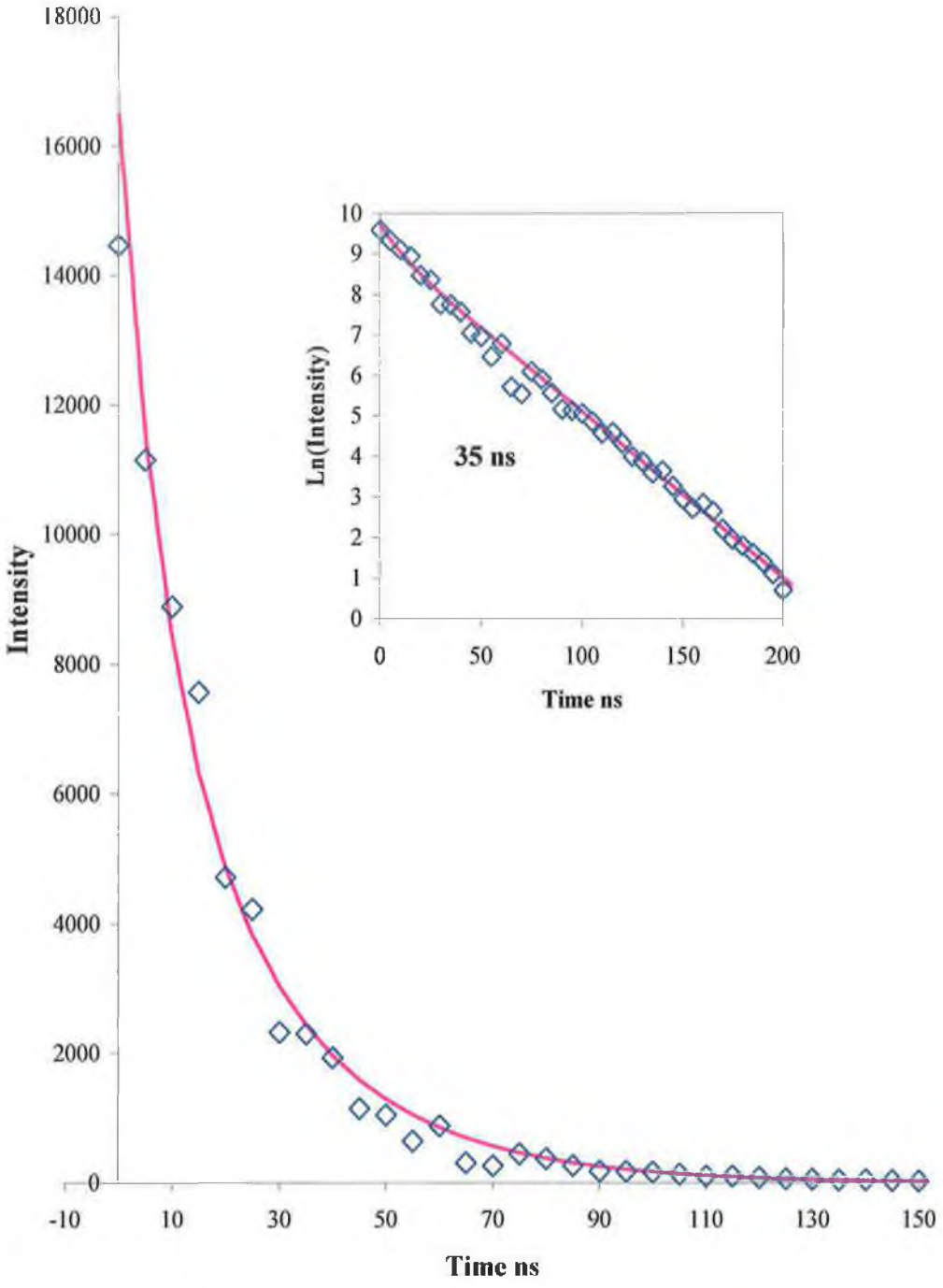

Figure 2.21: *Emission vs. time transient for the osmium metallopolymer film deposited on ITO ($\Gamma \sim 10^{-9}$ mol cm^{-2}) in contact with 0.1 M H_2SO_4. The emission was monitored at 765 nm following the application of a 10 ns laser pulse of 380 nm.*

2.4 Electrochemical Properties:

Figure 2.22 shows a cyclic voltammogram of a 1 mM solution of $[Ru(bpy)_2(pic)_2]^{2+}$ dissolved in ACN containing 0.1 M $TBABF_4$ as supporting electrolyte at a platinum electrode. Peak potentials for the different waves for this and the other species investigated, are given in Table 2.2. By analogy with the voltammetric behaviour of $Ru(bpy)_3$[51] and similar ruthenium complexes, the peaks centred at approximately $E_{1/2}$ = 1.2 V are attributed to the metal centred Ru^{2+} / Ru^{3+} redox couple and those at -1.44 and -1.64 V are bpy based reductions to the +1 and 0 charged species respectively.

A further, irreversible reduction wave was also observed at approximately -2.2 V, presumably due to the -1 charged species. However, scanning to this limit invariably resulted in poorly defined return peaks for the voltammogram as a whole, presumably due to following chemical reactions and electrode fouling.

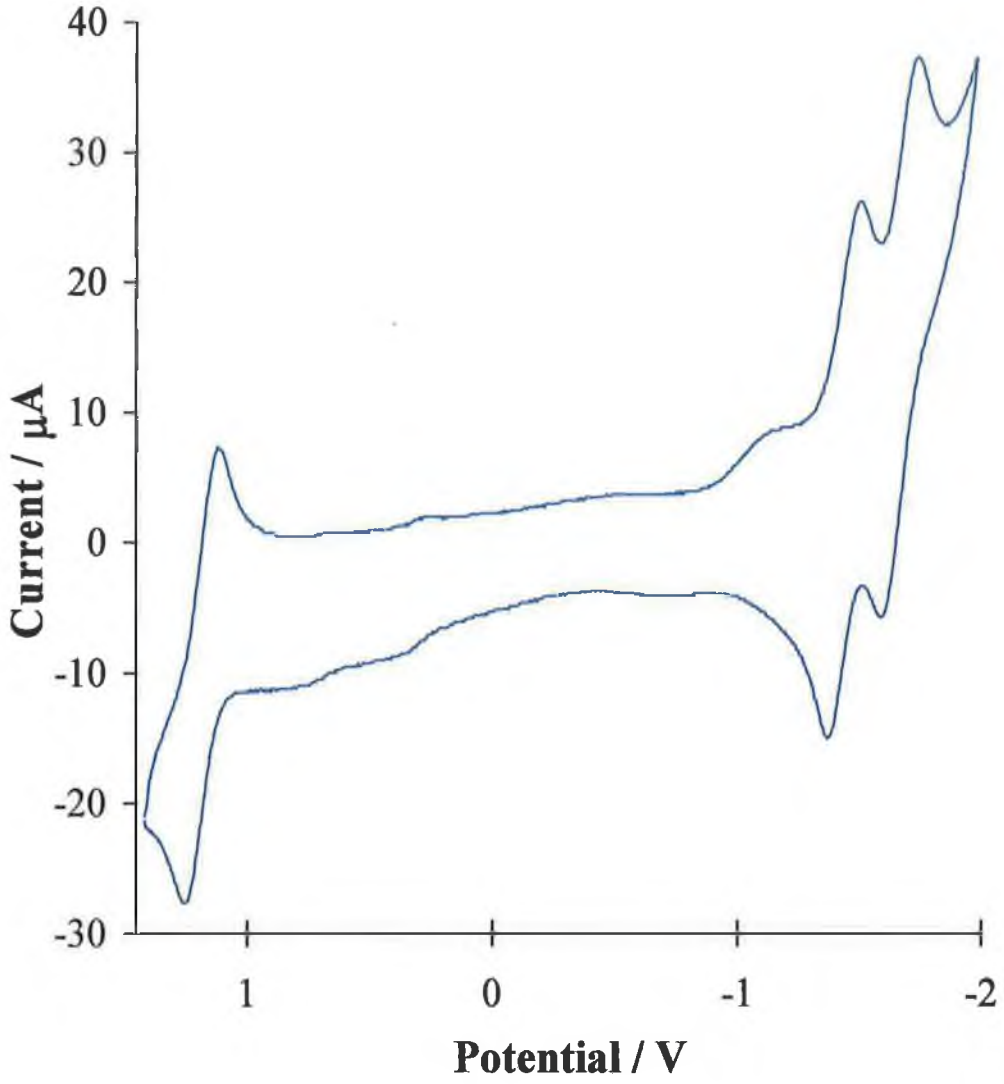

Figure 2.22: *Typical cyclic voltammetric response of 3 mm diameter platinum electrode to 1 mM* $[Ru(bpy)_2(pic)_2]^{2+}$ *in acetonitrile / 0.1 M* $TBABF_4$. *Scan rate 1* Vs^{-1}.

The metallopolymers $[Ru(bpy)_2(PVP)_{10}]^{2+}$ and $[Ru(bpy)_2(PVP)_{10}Cl]^{+}$ showed formal oxidation potentials for ruthenium at 1.26 and 0.77 V respectively in acetonitrile. The absence of peaks in the region of 0.8 V in the $[Ru(bpy)_2(PVP)_{10}]^{2+}$ CV shows that there was no significant formation of the mono-substituted species during synthesis of this material. The lower oxidation potential of $[Ru(bpy)_2(PVP)_{10}Cl]^{+}$ is due to the electron donating effect of the electro-donating chlorine substituent. This is consistent with δ donating properties, a ligand with weaker δ donating properties will donate less electron density into the metal centre resulting in more stabilised d orbitals and consequently higher oxidation potentials. As such the chlorine will increase the δ donor properties of the ligand back-bone and lower the oxidation potential. The cyclic voltammograms for both polymers are shown in Figure 2.23. Scanning in the negative potential region showed irreversible peaks, presumably due to bipyridine reduction, centred at -1.5 V for the mono-substituted and -1.35 V in the case of the bis substituted species.

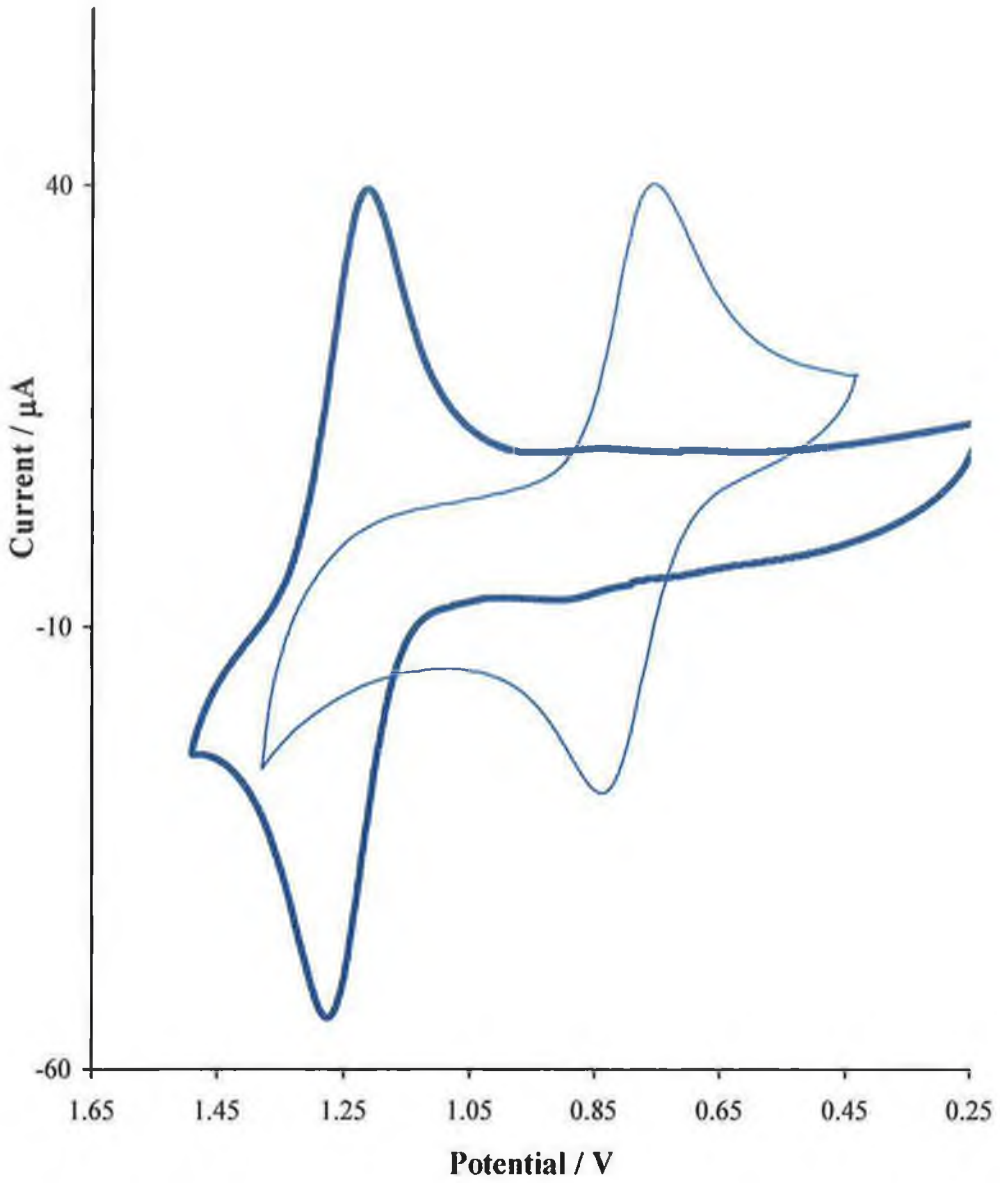

Figure 2.23: *Cyclic voltammetry of* $[Ru(bpy)_2(PVP)_{10}]^{2+}$ *(thick line), and* $[Ru(bpy)_2(PVP)_{10}Cl]^{+}$ *(thin line),as thin layers on glassy carbon (3 mm diameter), at 0.1 V* s^{-1}*. The electrolyte is 0.1 M* $TBABF_4$ *in ACN.*

A cyclic voltammogram of a conductive indium-tinoxide (ITO) coated glass slide coated electrode modified with a thin layer of $[Ru(bpy)_2(PVP)_{10}]^{2+}$ in 0.1 M H_2SO_4 is shown, compared with the theoretical response in Figure 2.24. The cyclic voltammetry exhibits a number of features characteristic of surface bound redox sites; the peak to peak separation between anodic and cathodic waves is close to zero at low scan rates, the full width at half maximum (FWHM) is approximately 90 mV and a plot of peak current versus scan rate is linear up to a scan rates of about 30 mVs^{-1} indicating finite charge transport diffusion conditions on these long time-scales. The onset of semi-infinite diffusional charge transport is evident at scan rates above 50 mVs^{-1} here a square root dependence on scan rate is seen and the C.V. shows distinctive diffusional tailing. In addition to these features, the ratio of $i_{p,a}/i_{p,c}$ is unity, indicating that the kinetics for the forward and back reaction are the same. These results demonstrate the close to ideally reversible voltammetry behaviour of immobilised layers of this redox polymer in contact with sulphuric acid electrolyte.

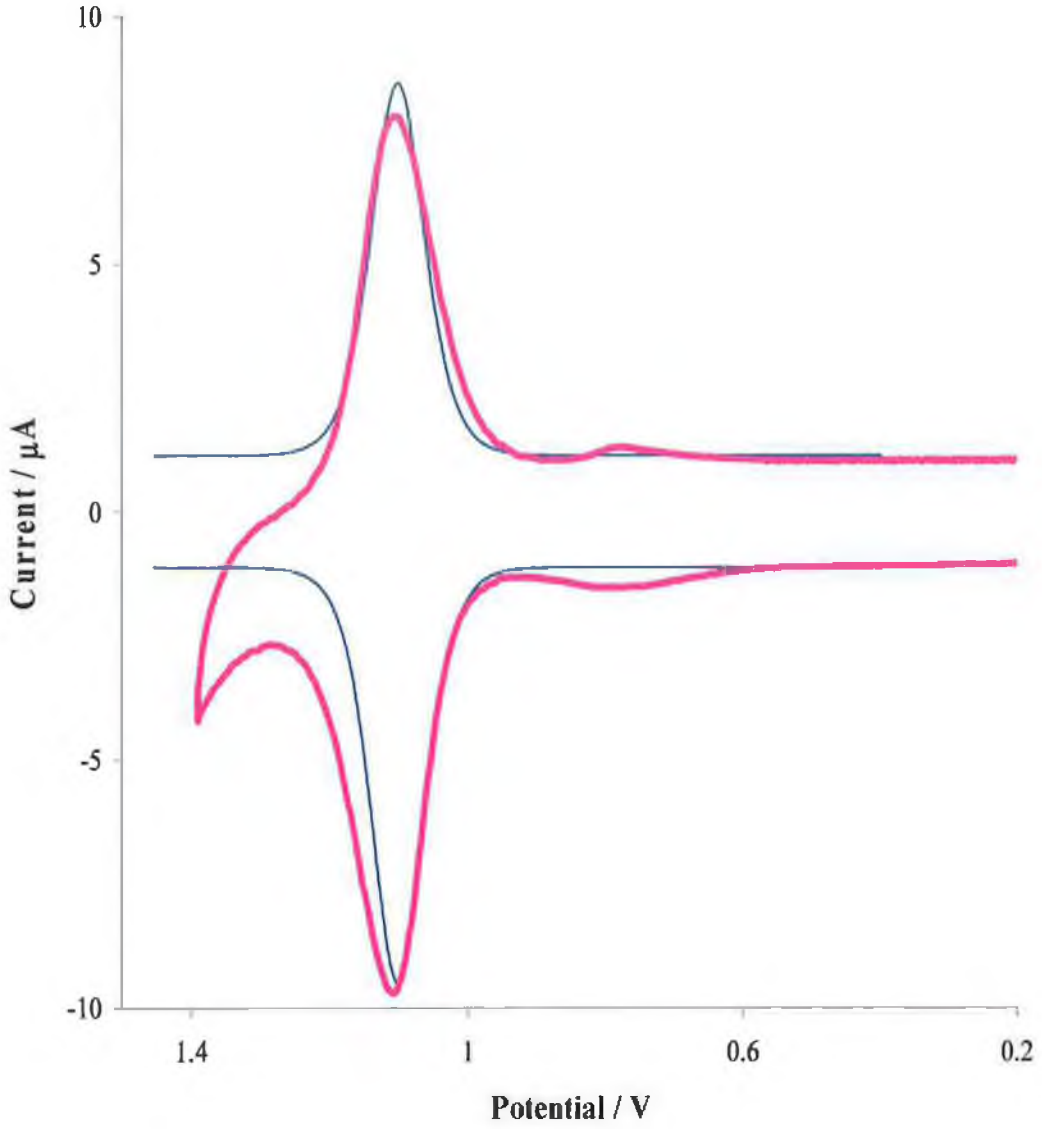

Figure 2.24: *Cyclic voltammogram of thin layer of* $Ru(bpy)_2(PVP)_{10}]^{2+}$ *coated on ITO slide,* (5×10^{-9} *mol* cm^2), *in contact with 0.1 M* H_2SO_4 *at a scan rate of 5* mVs^{-1}. *The thin line represents the theoretical response for a surface confined species at this coverage and scan rate.*

Ruthenium(II) compounds are stable low-spin d^6 species which can be oxidised or reduced. Upon excitation, it will return to the ground state often by emission of a photon. Emission is dominated by a closely spaced manifold of at least three triplet charge transfer states at ambient temperature ($MLCT^3$). Due to spin orbital coupling, fast intersystem crossing occurs from the singlet to triplet state with an efficiency of unity, followed by emission from the triplet state to the ground state (k_r) or radiationless deactivation to the ground state (k_{nr}). An alternative deactivation pathway following absorption to the triplet excited state is population of a metal centred (MC) orbital leading to photo-induced ligand substitution. If this occurs the electron occupies an anti-bonding metal based orbital, resulting in distortion of the metal ligand axes and weakening the Ru-N bonds. This may cause photodecomposition of the complex, which manifests itself as ligand loss followed by coordination of a substitute ligand, often solvent or electrolyte. Photodecomposition of this type has been observed to some degree in this study. Figure 2.25 shows a cyclic voltammogram of a thin film of $[Ru(bpy)_2(PVP)]^{2+}$ deposited on a conductive indium-tinoxide (ITO) coated glass slide following exposure to ambient light for five to six hours. The appearance of an additional redox couple at ~ 0.8V is consistent with the formation of a mono-substituted product[52] *via:*

$$^*[Ru(bpy)_2(PVP)_2]^{2+} + L \longrightarrow [Ru(bpy)_2(PVP)(L)]^{2+} \quad \textbf{(14)}$$

where L may be H_2O or SO_4^{2-}

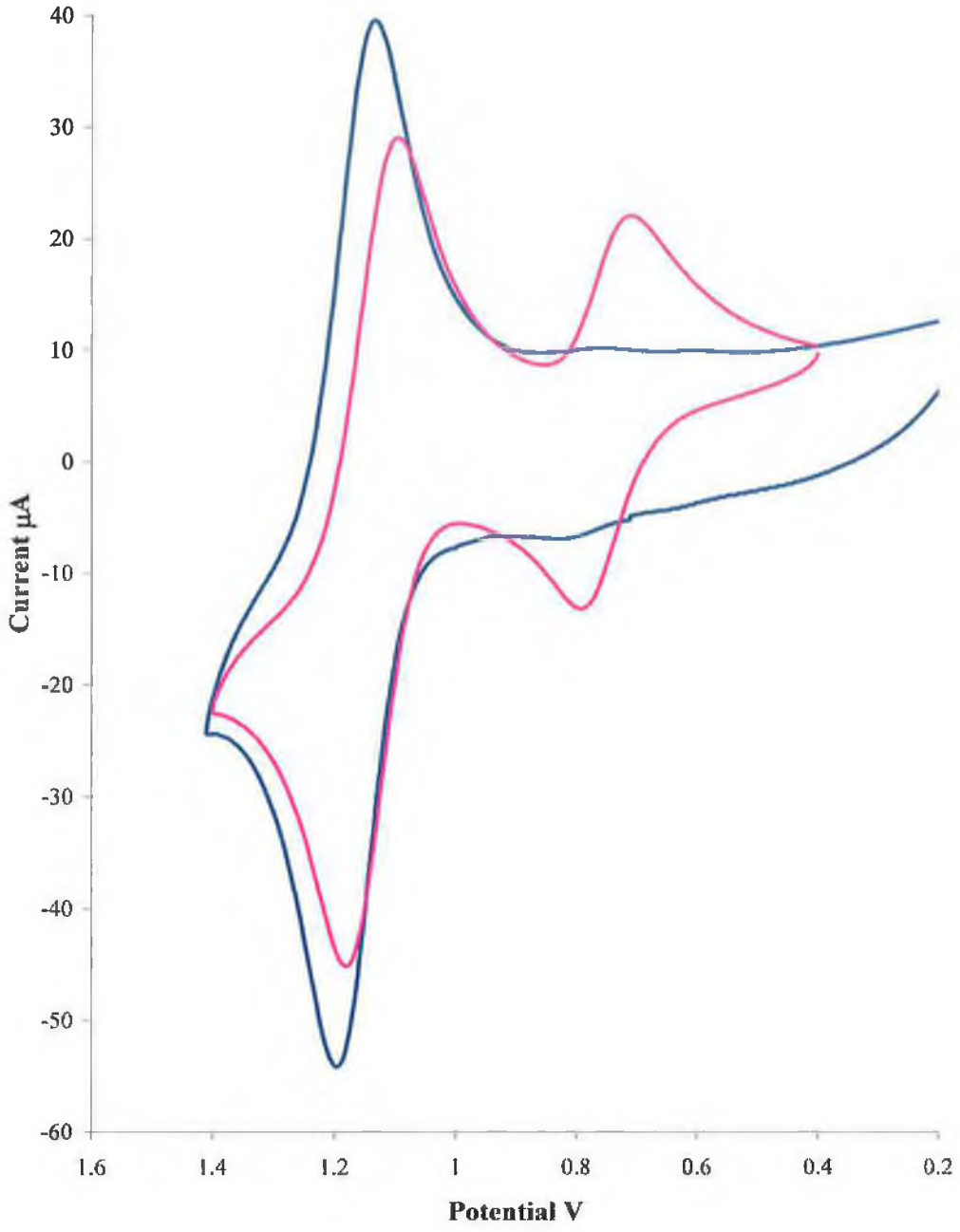

Figure 2.25: *Result of photo degradation, for polymer on ITO before (blue), and after (pink), 4 – 5 hrs exposure to ambient light. Scan rate 100 mVs^{-1}, surface coverage 5 x 10^{-9} mol cm^{-2}.*

A similar investigation was carried out on the osmium complexes. As with the ruthenium polymers, the voltammetric behaviour of $Os(bpy)_3^{2+}$ was compared with similar osmium complexes in order to confirm the identity of the redox couples. The peaks centred at approximately $E_{1/2}$ = 0.8 V were attributed to the metal centred Os^{2+}/Os^{3+} redox couple and those at ~ -1.25 V and –1.6 V are ligand based reductions to the +1 and 0 charged species, respectively (Table 2.2).

The metallopolymer $[Os(bpy)_2(PVP)_{10}]^{2+}$ and $[Os(bpy)_2(PVP)_{10}Cl]^{+}$ showed formal potentials for the Os(II/III) couples at 0.78 and 0.56 V respectively in acetonitrile. The absence of a peak at ~ 0.6 V in the cyclic voltammogram of $[Os(bpy)_2(PVP)_{10}]^{2+}$ shows that there are no significant amount of the mono substituted complex present. As with their ruthenium analogues, the lower oxidation potential of the mono-substituted complex is due to the chlorine substituent. The cyclic voltammograms for the osmium complexes showed characteristics of surface bound redox sites, which were previously discussed.

Compound	*E^0 (V vs. Ag/AgCl)[a]*		
	Oxidation	*Reduction*	
$[Ru(bpy)_3]^{2+}$	1.251	-1.41	-1.61
$[Ru(bpy)_2(pic)_2]^{2+}$	1.187	-1.44	-1.641
$[Ru(bpy)_2(PVP)_{10}]^{2+}$	1.26	-1.35	*
$[Ru(bpy)_2(PVP)_{10}Cl]^{+}$	0.77	-1.5	*
$[Os(bpy)_3]^{2+}$	0.76	-1.28	-1.632
$[Os(bpy)_2(pic)_2]^{2+}$	0.73	-1.32	-1.55
$[Os(bpy)_2(PVP)_{10}]^{2+}$	0.75	-1.26	-1.65
$[Os(bpy)_2(PVP)_{10}Cl]^{+}$	0.56	-1.34	*

Table 2.2: *Redox potentials of the osmium and ruthenium metallopolymers and complexes studied.*

[a] *Measured in acetonitrile*

* *poorly defined second ligand reduction process.*

Most of the polypyridine complexes of Os(II) that have been investigated so far are remarkably stable photochemically. This photochemical stability is a direct consequence of larger values of 10Dq as compared to Ru(II), which raises the energies of the low-lying dd states beyond significant thermal population at room temperature. The absence of low-lying dd states is also evidenced by relatively temperature independent lifetimes for the Os complexes, at least above 200 K. At these temperatures, the series of low-lying MLCT states that constitute the "MLCT state" reach a sufficient thermal population to behave as a single state.

Photosubstitution, however, has been noted in some osmium complexes with high energy emitting MLCT states, such as $[Os(bpy)_2(Me_2SO)_2]^{2+}$ which, for example, has its lowest energy absorption band at 400 nm and its emission maximum at 537 nm in acetonitrile. The complexes utilised here showed little or no photodecomposition at least when solutions or thin films are exposed to ambient light for periods up to 8 hours.

2.5 *Charge Transport Properties:*

2.5.1 *Introduction:*

Voltammetric detection of a solution species normally depends on that species being reduced or oxidised at the electrode surface. Frequently, slow electrode kinetics cause the redox reaction to occur at a more positive or negative potential than predicted on the basis of thermodynamics. Figure 2.26 shows that modification of electrode surfaces with redox centres that can mediate charge transfer to the analyte may reduce this overpotential.

Relatively, electrodes modified with thick polymer films can also increase the rate of reaction over that observed at unmodified electrode surfaces. The primary benefit of these systems is that they combine the advantages of monolayer derivatised electrodes with those of homogeneous catalytic systems, *i.e.* a high local concentration of catalytic sites despite the total amount of catalyst being small, easy separation of the reaction products from the catalyst and a three dimensional dispersion of the reacting centres.

For optimum sensor performance based on mediated charge transfer the reaction should proceed throughout the entire polymer film, which implies that high permeability of the film to the analyte is essential and charge transport through the film must be rapid.

Theoretical approaches for predicting and optimising the response of electrocatalytic redox polymer modified electrodes have been developed to a considerable extent.[53] Unfortunately, the exploitation of the theory has been limited in the field of electroanalysis.

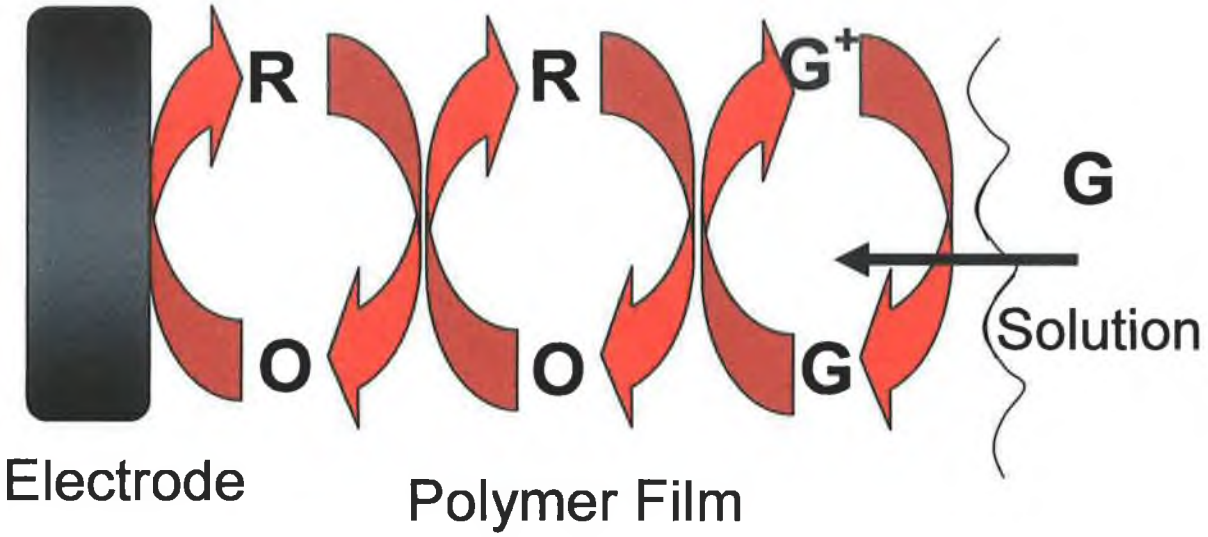

Figure 2.26: *A model for the mediated reduction of G, guanine by the O/R redox couple immobilised in a polymeric film at the electrode surface.*

2.5.2 General:

The theoreical voltammogram in Figure 2.27 exhibits a number of features characteristic of a reversible redox reaction.[54] The peaks for surface confined species are sharp and symmetrical unlike those of freely diffusing reactants. This behaviour is due to the presence of a fixed amount of redox active material at the electrode surface which is not hindered by the complications of mass transfer. When a potential is applied to a surface modified electrode the current rises from essentially zero to a peak value and then back to zero. For an ideal system no peak to peak separation is expected, $|(I_p)_a/(I_p)_c| \approx 1$, Figure 2.27 illustrates that the voltammetric behaviour for the ruthenium system is close to these theoretical expections. The peak current for a surface confined reactant under finite diffusion control is given by;

$$i_p = \frac{n^2F^2}{4RT}\nu A\Gamma \qquad \textbf{(15)}$$

where Γ is the surface coverage, ν is the scan rate, A is the area of the electrode, F is the Faraday constant, n is the number of electrons involved in the electrode reaction, R is the gas constant and T is the temperature in kelvin. The area under the voltammetric peak, corrected for any background current, represents the charge associated with the reduction or oxidation of the adsorbed species and can be used to calculate Γ according to;

$$\Gamma = \frac{Q}{nFA} \qquad \textbf{(16)}$$

where Q is the charge either the anodic or cathodic peak in coulombs. For an ideal Nernstian reaction under Langmuir isotherm conditions where no interaction occurs between adsorbates or at least they are concentration independent, a surface confined species will follow the relationship;

$$\Delta E_{p1/2} = 3.53\frac{RT}{nF} = \frac{90.6}{n} mV \qquad at\ 25\ ^0C \qquad (17)$$

and,

$$E_{pa} = E_{pc} \qquad or \qquad \Delta E_p \approx 0 \qquad (18)$$

where $E_{p1/2}$ is the full width at half maximum (FWHM) which is close to the theoretical value of 90.6 mV expected for a reaction involving a surface confined reactant and the transfer of a single electron. The features are also shown in Figure 2.21 for the ruthenium metallopolymer utilised in this study. Moreover, the peak current varies linearly with the square root of the scan rate, 100 mV≤v≤500 mVs^{-1}. These observations as seen as in Figure 2.28, indicate that the voltammetric behaviour of these polymer films is close to that expected for an ideally reversibly system under finite diffusion control at relatively slow scan rates.

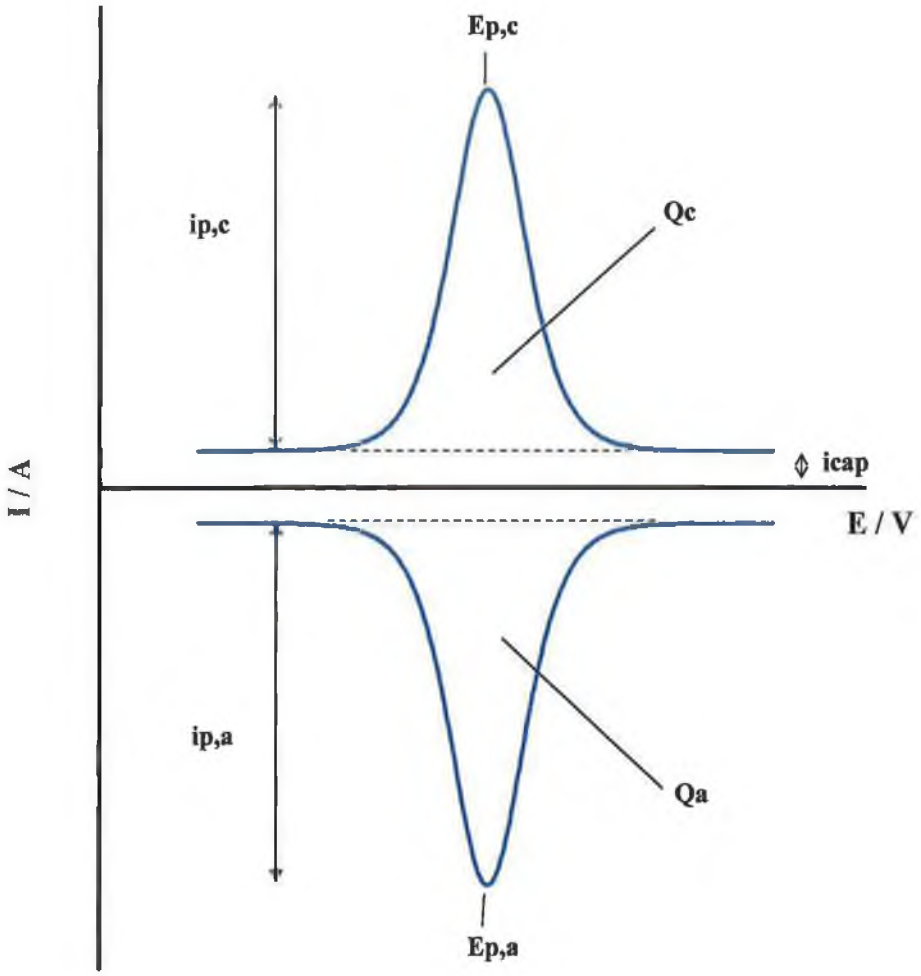

Figure 2.27: *Cyclic voltammogram showing theoretical response for an electrochemically reversible couple that is confined on the electrode surface.*

Figure 2.28 shows the voltammetric response of a thin layer of a $[Ru(bpy)_2(PVP)_{10}]^{2+}$ polymer film on a glassy carbon electrode at a slow scan rate where the supporting electrolyte is 20 mM PBS. The voltammogram shows a number of the characteristics described above. The full width at half maximum (FWHM) is close to the theoretical value of 90.6 mV expected for a reaction involving a surface confined reactant and the transfer of a single electron. The metallopolymer showed formal potentials for the Ru(II/III) redox couples at ~1.05 V. For all scan rates, the ratio of the anodic to cathodic peak currents is unity, indicating that the electron transfer reaction is chemically reversible. These results indicate that the voltammetric behaviour of these polymeric films in PBS electrolyte is close to ideal over this range of scan rates.

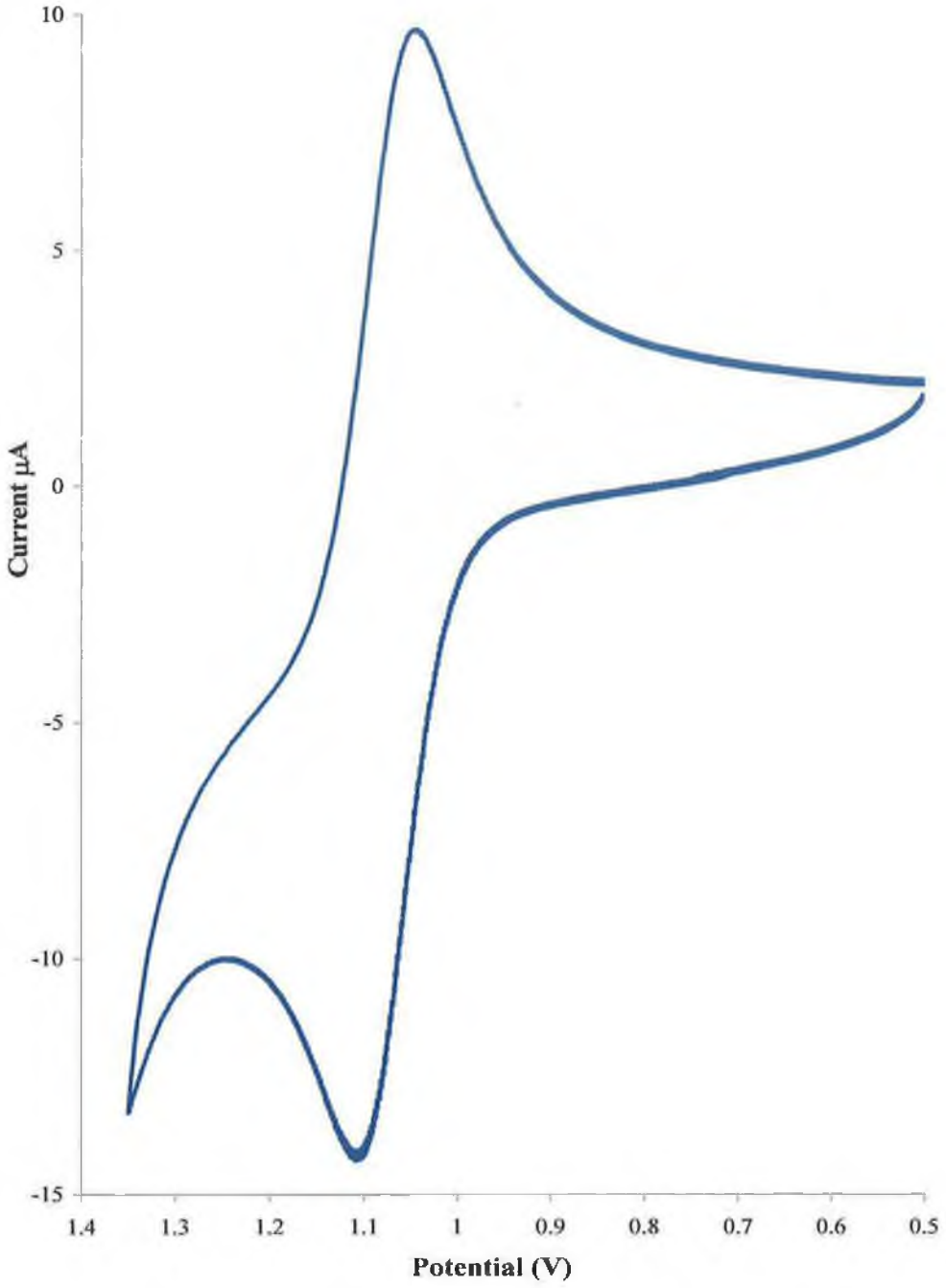

Figure 2.28: *Typical cyclic Voltammogram of a ruthenium metallopolymer thin layer (Γ = 2.78 x 10^{-8} Mol cm^{-2}) on glassy carbon in contact with 20 mM PBS electrolyte. The working electrode is modified 3 mm glassy carbon electrode. The scan rate is 5 mVs^{-1}.*

The formal potential of the M(II/III) redox couple of the metallopolymers coated as thin films on glassy carbon electrodes have been listed in Table 2.2. A typical cyclic voltamogramm of the mixed metal film is given in Figure 2.29. The film was prepared by drop casting a 0.2% ethanolic solution of 50:50 w/w $Ru(bpy)_2(PVP)_{10}^{2+}$: $Os(bpy)_2(PVP)_{10}^{2+}$ onto the electrode surface and allowing it to dry. As expected the osmium analogue of the ruthenium metallopolymer shows a reversible redox couple at a less positive potential. The redox potentials obtained for the metals in mixed metallopolymer films are in close agreement with those obtained for single metallopolymer films, formal potentials within ± 0.04 and ± 0.02 for ruthenium and osmium metallopolymers respectively, as well as producing similar currents to those obtained for each metallopolymer individually. This coupled with the fact that the wave form remains undistorted suggests little interaction exists between the metal centres. A similar behaviour has been reported for electropolymerised metal bipyridyl systems[55].

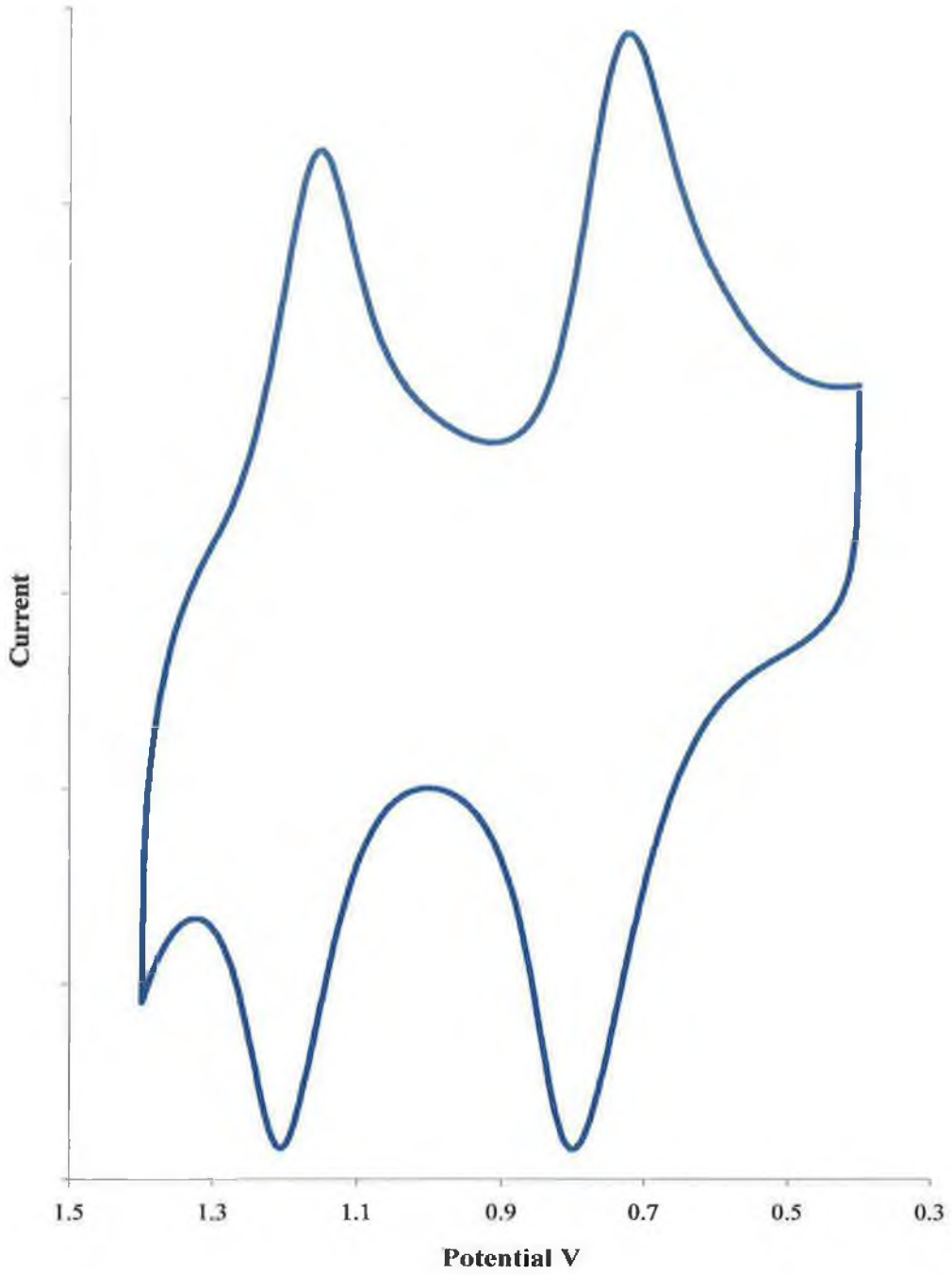

Figure 2.29: *Typical cyclic Voltammogram of a mixed ruthenium/osmium metallopolymer thin layer (Γ_{total} = 2.65 x 10^{-8} mol cm^{-2}) on glassy carbon in, 20 mM PBS electrolyte. The working electrode is modified 3 mm glassy carbon electrode. The scan rate is 5 mVs^{-1}.*

2.5.3 Evaluation of Charge Transport Diffusion Coefficients:

The sensitivity of this sensor will ultimately be dictated by the rate at which the Ru^{3+} sites can be regenerated. Therefore, it is important to determine the rate of charge transport through the film leading to the conversion of the inactive Ru^{2+} centres into the mediating Ru^{3+} centres. D_{ct} the rate of charge movement through the film is characterised by the charge transport apparent diffusion coefficient. D_{ct} characterises the movement of charge through the film. This parameter can be obtained from a plot of i_p vs. $v^{1/2}$ under semi-infinite linear diffusion controlled conditions. This response is predicted to be linear by equation 28, usually favoured by relatively higher scan rates.

The rate of charge transport through the polymer can be quantified by measuring D_{ct} using cyclic voltammetry or chronoamperometry. The lower limit on the range of useful scan rates in cyclic voltammetry is dictated by the requirement that the depletion layer thickness be significantly less than the overall film thickness, while the upper scan rate is limited by the rate of heterogeneous electron transfer across the electrode layer interface or ohmic drop effects. In this study, these conditions are met for $100 \geq v \geq 500$ mVs^{-1} and plots of peak current varied linearly with the square root of scan rate over this range, typical cyclic voltammetric scan rate dependency and Randles-Sevcik plots are shown in Figure 2.31.

Chronoamperometry experiments conducted on a tens of milliseconds timescale were also used to evaluate D_{ct}, in all cases linear Cottrell were observed. The concentration of redox centres within layers of $[Ru(bpy)_2(PVP)_{10}]^{2+}$ has previously been evaluated for a 1 in 10 loading of this polymer[12], the value of 0.8 M, was used for calculation of both D_{ct}(CV) and D_{ct}(CA) in this study. A frequent observation for metallopolymers of this type is that the diffusion coefficient as measured by chronoamperometry is frequently larger than that obtained using cyclic voltammetry. This difference may reflect a systematic variation in the density of the

redox centres through the film thickness with preferential swelling close to the film/electrolyte interface causing an increased inter-site separation and lower rates of charge transport.[56] This interpretation is supported by previously reported neutron scattering measurements by Hillman *et al.*[57,58] Since the redox composition of a significantly larger fraction of the layer is switched in the slower cyclic voltammetry experiments than in chronoamperometry, the similar D_{CT} values suggest that movement of charge compensating counter ions through the film is quite facile. This observation is supported by the work of Meyer *et al.*[59] which suggests that bis coordination of metal centres to a polymer back-bone imposes structural rigidity on the matrix causing adjacent redox sites to maintain their fixed relative positions and leading to quite an open and porous layer structure.

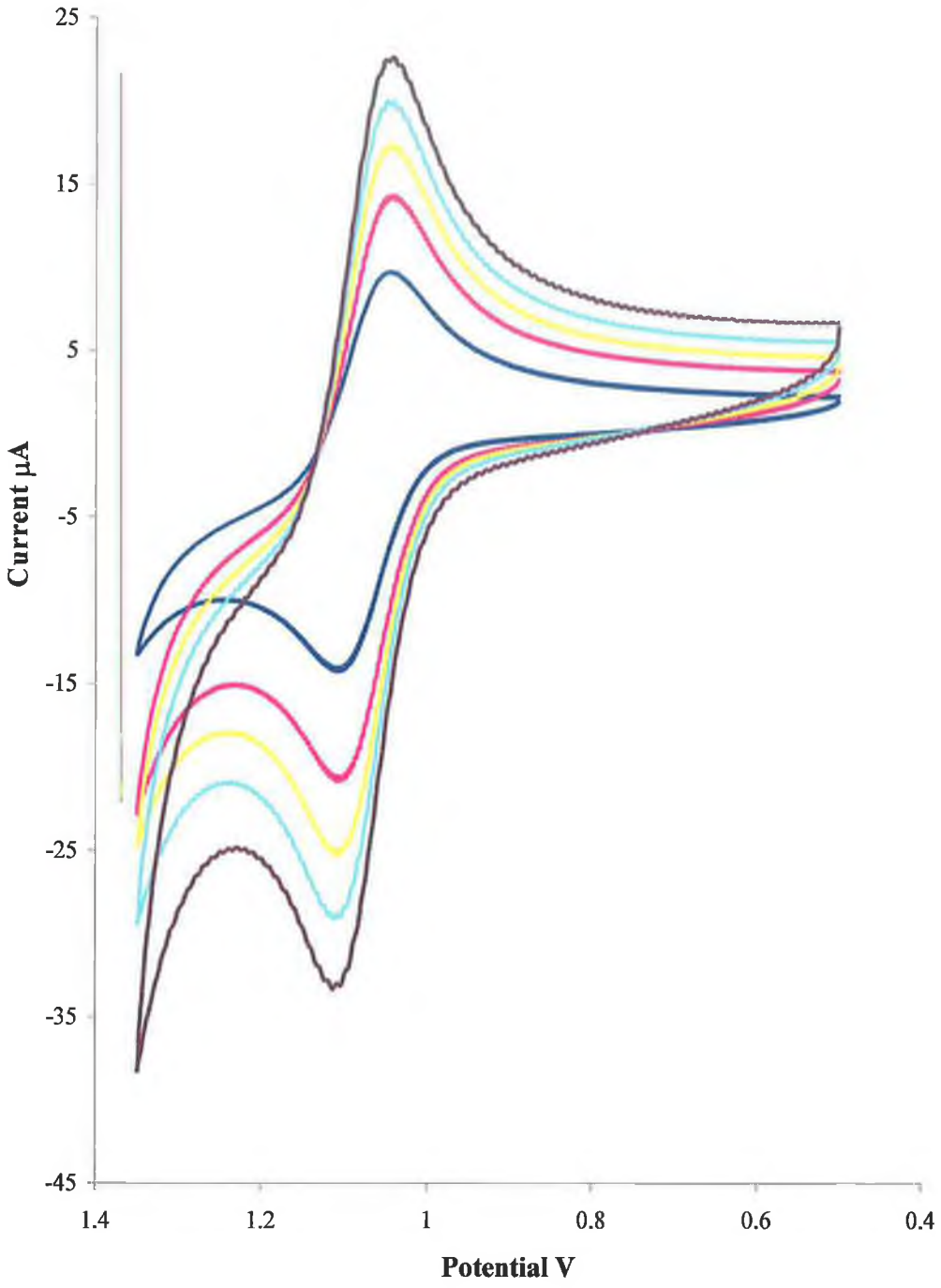

Figure 2.30: *Scan rate dependency of the metallopolymer in PBS electrolyte for* $[Ru(bpy)_2(PVP)_{10}]^{2+}$, $100 < \nu < 500\ mVs^{-1}$.

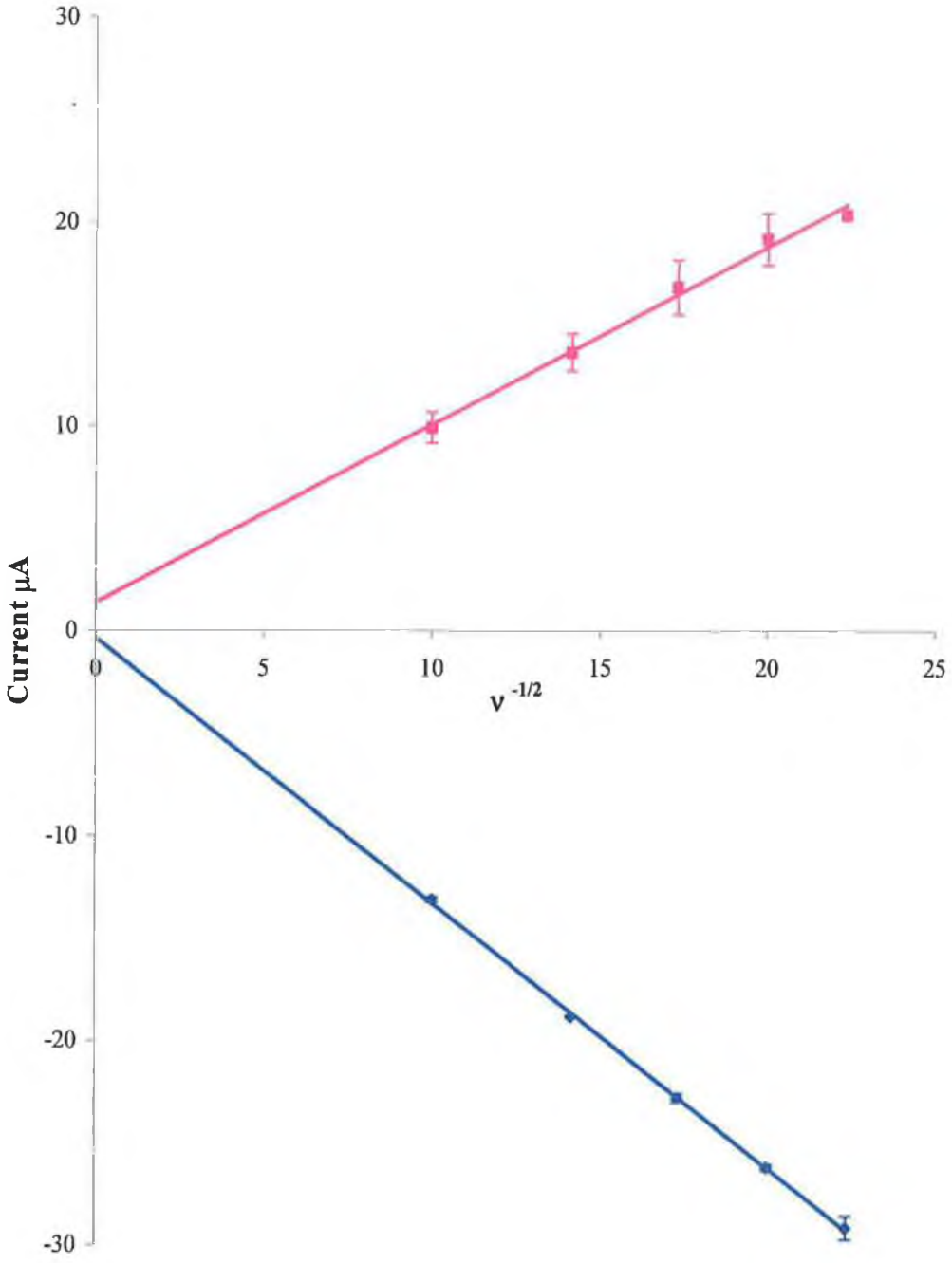

Figure 2.31: *Randles-Sevich plots for* $[Ru(bpy)_2(PVP)_{10}]^{2+}$ *in 20 mM PBS,* $100 < \nu < 500\ mVs^{-1}$.

Table 2.3: *Variation of charge transport diffusion coefficient (D_{ct}) for a high surface coverage of the electrode by the polymer film (≈2.8 x 10^{-8} Mol cm^{-2}) as measured by both cyclic voltammetry and chronoamperometry. Values for both anodic and cathodic branches are given.*

[PBS] Mol L^{-1}	*D_{ct}(CA) Anodic $10^9 cm^2 s^{-1}$*	*Dct(CV) Cathodic $10^9 cm^2 s^{-1}$*	*E^0 V vs Ag/AgCl*	*D_{ct}(CA) Anodic 10^9 $cm^2 s^{-1}$*	*D_{ct}(CA) Cathodic 10^9 $cm^2 s^{-1}$*
0.02	5.0	6.7	1.105	4.2	2.7
0.05	1.0	1.3	1.093	2.7	1.6
0.1	4.6	3.9	1.061	0.9	1.0
1	6.6	7.6	1.055	4.3	5.1

Table 2.4: *Variation of charge transport diffusion coefficient (D_{ct}) for a low surface coverage of the electrode by the polymer film (≈1.2 x 10^{-9} Mol cm^{-2}) as measured by both cyclic voltammetry and chronoamperometry. Values for both anodic and cathodic branches are given.*

[PBS] Mol L^{-1}	D_{ct}(CA) Anodic 10^9 cm^2s^{-1}	Dct(CV) Cathodic 10^9 cm^2s^{-1}	E^0 V vs Ag/AgCl	D_{ct}(CA) Anodic 10^9 cm^2s^{-1}	D_{ct}(CA) Cathodic 10^9 cm^2s^{-1}
0.02	3.5	4.3	1.093	2.8	1.0
0.05	4.8	0.9	1.114	0.9	3.5
0.10	1.0	5.6	1.075	1.1	4.1
1.00	5.2	0.7	1.066	5.2	6.8

Tables 2.3 and 2.4 summarises the D_{ct} values observed as the concentration of the PBS supporting electrolyte is systematically varied. These data show that the homogeneous charge transport rates are insensitive to electrolyte concentration, with no significant variation in D_{ct} occurring as the concentration is increased from 0.02 to 1 M. A shift in the formal potential could be indicative that ion transport is rate limiting or that ion coupling processes, which affect the E^0, have occurred. However, this is not the case. The negligible shift in both the magnitude of the D_{CT} and the value of the formal potential indicate that ion pairing is not rate limiting. Also, in both PBS and sulphuric acid electrolyte charge compensating ions freely diffuse through the polymer film maintaining electronuetrality.

Impedance analysis could provide a more detailed insight into whether ionic or electronic resistance is in fact the rate limiting step. A study to investigate if charge transport is controlled via counter-ion displacement or if electron hopping is rate determining would also provide an in-depth understanding of this type of film.

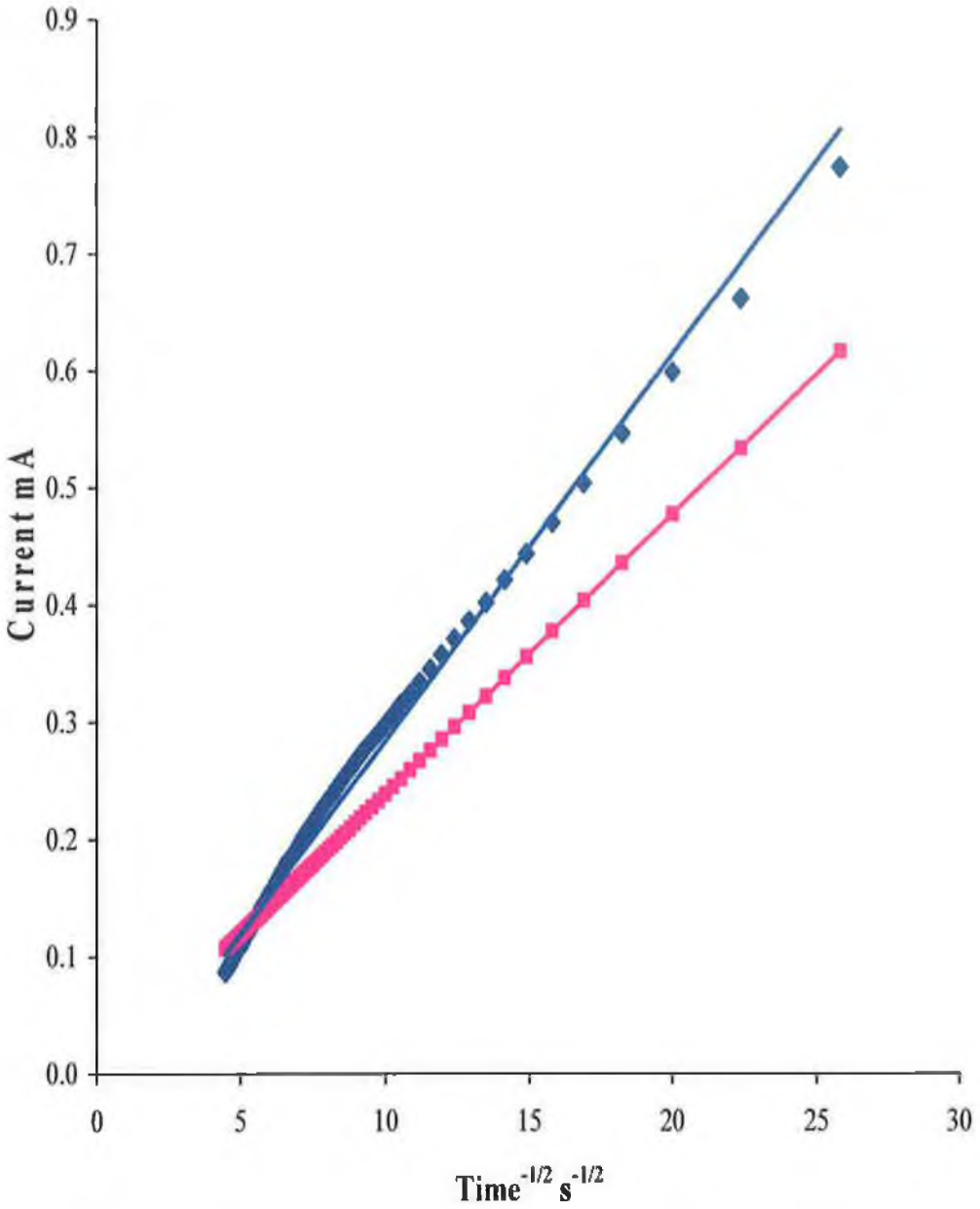

Figure 2.32: *Chronoamperometric response to potential step for 1.97 x 10^{-9} mol cm^{-2} (pink) and 1.34 x 10^{-9} mol cm^{-2} (blue) surface coverages of $[Ru(bpy)_2(PVP)_{10}]^{2+}$ thin layer in 20 mM PBS. Standard deviations remained small, at less than 2%.*

Figure 2.32 shows the chronoamperometric response of $[Ru(bpy)_2(PVP)_{10}]^{2+}$ films of both low and high surface coverage. The low surface coverage shows an interesting deviation from the theoretical Cottrell response. There seem to be two separate responses, one occurring between 5 to 10 $s^{-1/2}$ and the second between 10 to 25 $s^{-1/2}$. This is possible due to finite diffusion occurring at the early part of the plot due to mass transport limitations, after which semi-infinite conditions occur.

In contrast to H_2SO_4, the voltammetric behaviour in $HClO_4$ electrolyte showed a somewhat different pattern. In this electrolyte much slower cyclic voltammetric scan rates, (<1 mVs^{-1}) and higher electrolyte concentration (1.0 M) were required in order to observe the finite diffusional behaviour observed in sulphuric acid up to *circa* 30 mVs^{-1}. The charge transport properties of these layers in contact with $HClO_4$ although not investigated in detail, also appear quite different to H_2SO_4.

These results point to quite a different layer structure when in contact with this electrolyte, the dependence of D_{CT} on electrolyte concentration may indicate that the rate of charge propagation is limited by the ingress and egress of charge compensating counter-ions required to maintain electro-neutrality during redox switching, suggesting a less permeable layer structure than is the case in sulphuric acid. The longer C.V. time-scales required to observe thin layer behaviour would support this contention.

Indeed, the nature of the polymer / electrolyte interaction is commonly found to be of importance in determining charge transport rates.[60,61] Previous studies have indicated that the ClO_4^- ion can interact strongly with polyelectrolytes, resulting in compact, highly cross-linked, dehydrated layer structures[62,63,64] this would also explain the higher rates of charge transport observed in $HClO_4$, in terms of reduced inter-site separation. Also the strong interaction between the Ru^{2+} centres and ClO_4^- ions will decrease the electrostatic repulsion between sites resulting in increased configurational entropy for the polymer segments. The fact

that the layers in this electrolyte are compact and unswollen results in a layer structure that would reder the partition of substrate into the film very difficult.

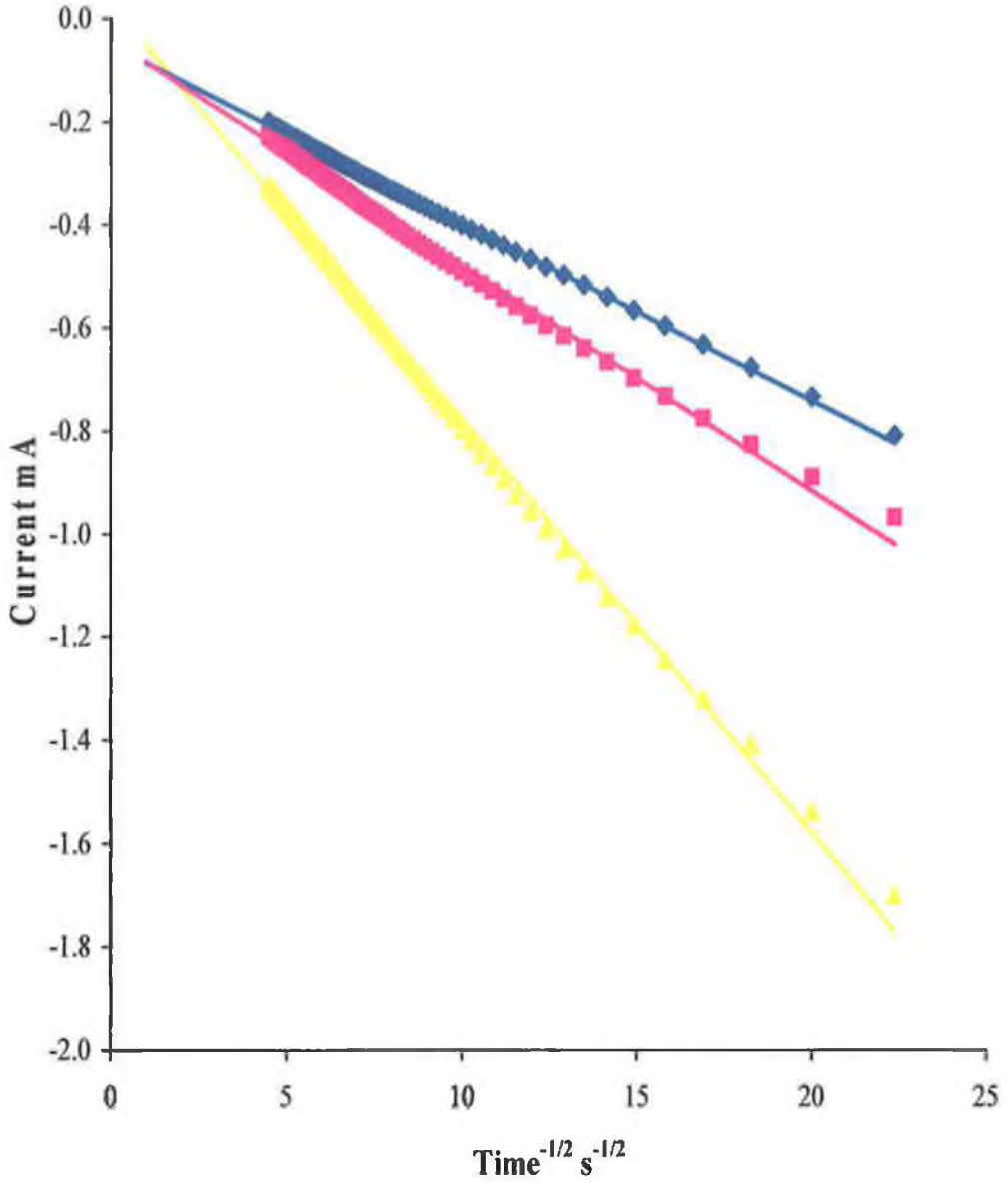

Figure 3.33: *Chronoamperometric response of polymer layer in contact with 1 M (triangles), 0.5 M (squares) and 0.1 (diamonds) M $HClO_4$.*

The rate of charge transport through the osmium metallopolymer was also investigated. Under the same conditions described above, plots of peak current varied linearly with the square root of scan rate over the range $100 \geq v \geq 500$ mVs^{-1}. Typical cyclic voltammetric scan rate dependency and Randles-Sevcik plots are shown in Figure 2.34. The metallopolymer, as with its ruthenium counterpart, showed no significant variation in D_{ct} for varying electrolyte concentration. Average Cathodic D_{ct} values for high surface coverage (2.724×10^{-4} Mol cm^{-2}) and low surface coverage (4.414×10^{-5} Mo lcm^{-2}) were 9.27×10^{-10} and 1.213×10^{-10} cm^2s^{-1} respectively, with average anodic values of 1.057×10^{-10} and 1.213×10^{-10} cm^2s^{-1}. However, these values suggest that charge transport through the osmium centres was faster than that of the ruthenium centres. There is little difference between the cathodic and anodic D_{CT} values indicative of a reversible one electron reaction.

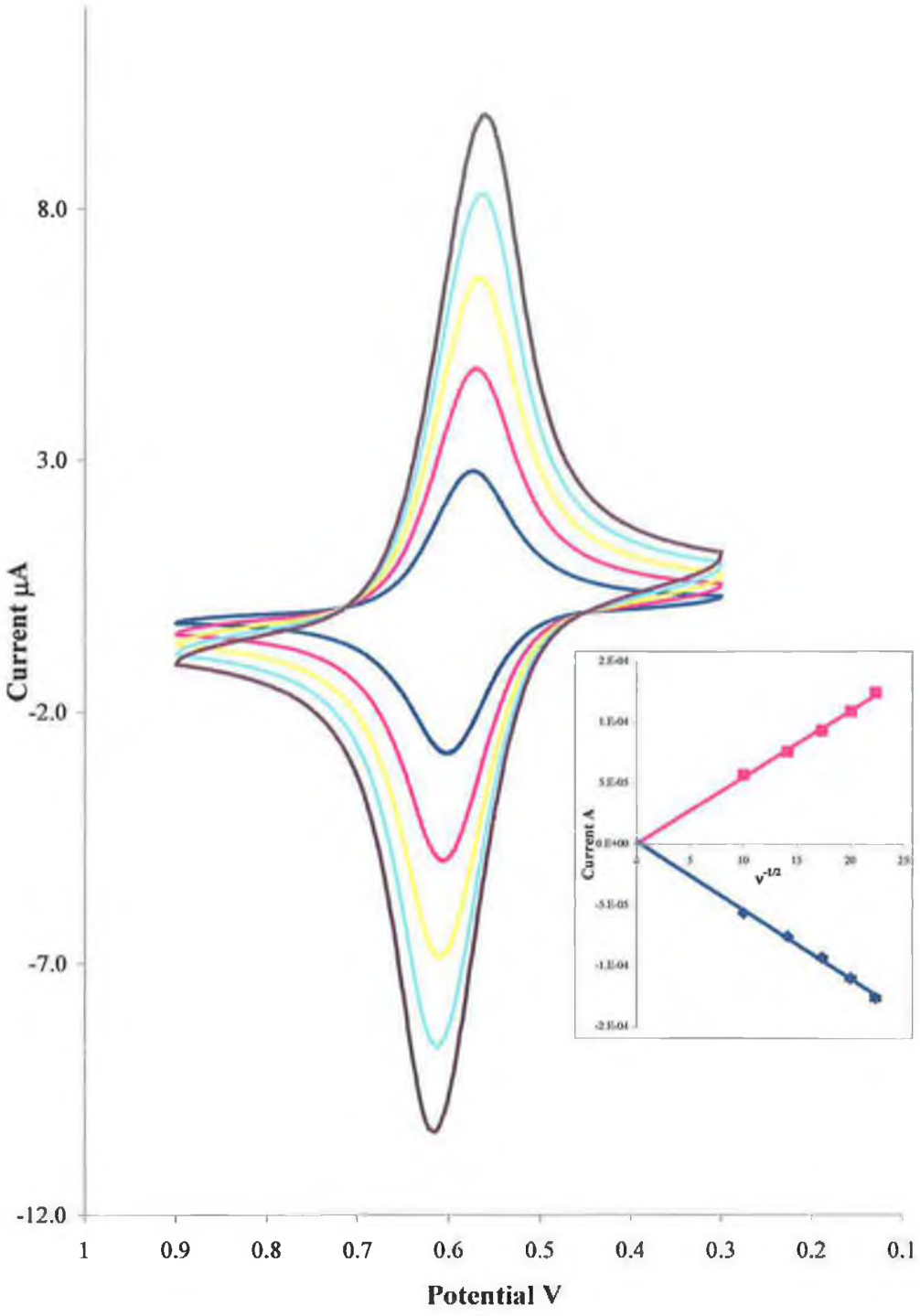

Figure 2.34: *Scan rate dependency of the metallopolymer in 0.1 M H_2SO_4 electrolyte. The insert shows Randles-Sevich plots for $[Os(bpy)_2(PVP)_{10}]^{2+}$ in 0.1 M H_2SO_4, $100<n<500\ mVs^{-1}$.*

Films containing both metallopolymers showed similar results for both high and low surface coverages. D_{ct} values for these mixed films showed no significant differences to those obtained for the unmixed films. Figure 2.35 shows the Cottrell behaviour for electrodes modified with $[Ru(bpy)_2(PVP)_{10}]^{2+}/[Os(bpy)_2(PVP)_{10}]^{2+}$ in 20 mM PBS . This clearly shows that the rate of charge propogation through the polymer phase via the osmium centres is more rapid than that through the ruthenium centres; average D_{ct} values were 1.66×10^{-9} and 4.2×10^{-10} cm^2s^{-1} for the osmium and ruthenium centres, respectively. Similar values were obtained for the corresponding polymers containing only osmium or ruthenium centres where the redox centre concentration was the same. These results suggest that there is little or no interaction between the redox centres.

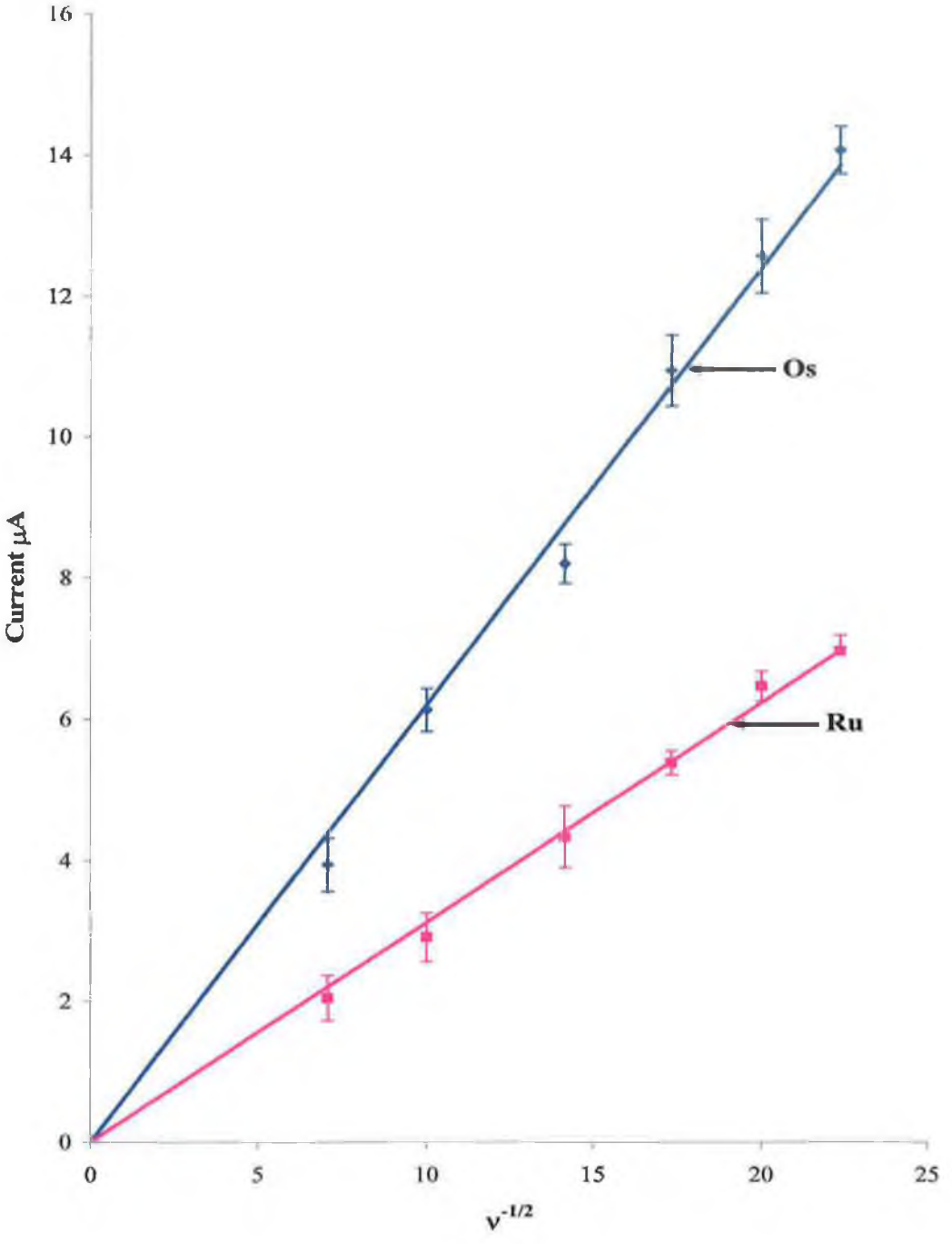

Figure 2.35: *Randles-Sevcik cathodic branch plots for the Os(II) and Ru(II) oxidation for a film containing the metallopolymers* $Ru(bpy)_2(PVP)_{10}^{2+}$ *and* $Os(bpy)_2(PVP)_{10}^{2+}$ *in 20 mM PBS electrolyte. Potentials were 1.22 and 0.74 V respectively. Total surface coverage is* 2×10^{-8} *mol* cm^{-2}.

2.6 *Mediated Oxidation of Guanine by $[Ru(bpy)_2(PVP)_{10}]^{2+}$:*

$Ru(bpy)_3^{3+}$ mediated oxidation of guanine can be described by the two step mechanism:[65]

$$[Ru(bpy)_3]^{2+} \rightarrow [Ru(bpy)_3]^{3+} + e^- \quad \textbf{(16)}$$

$$[Ru(bpy)_3]^{3+} + DNA \xrightarrow{k_2} [Ru(bpy)_3]^{2+} + DNA_{ox} \quad \textbf{(17)}$$

Where DNA_{ox} represents a DNA strand that has a guanine molecule which has been oxidised through a one electron transfer reaction. $[Ru(bpy)_3]^{3+}$ is first generated at the electrode by applying a high positive potential. The $[Ru(bpy)_3]^{3+}$ is subsequently reduced to $[Ru(bpy)_3]^{2+}$ by guanine and the regenerated reduced mediator is again oxidised at the electrode, completing a catalytic cycle.[66]

In contrast to direct oxidation of guanine at an electrode, the electron transfer reaction between $[Ru(bpy)_3]^{3+}$ and guanine is very fast (second order rate constant was measured to be roughly 1 x 10^6 M^{-1} s^{-1}).[67] The major reason for rapid electron transfer is that the oxidation potential of guanine is almost identical to that of $Ru(bpy)_3^{2+}$, being 1.1 V vs. SCE, however, if the driving force was larger then k could also be larger.[68]

Guanine oxidation has been studied in detail because oxidative damage of cellular DNA is viewed as an important factor in the onset of many disease processes and aging. There have been numerous studies into the mechanisms involved in the oxidation of guanine[69,70] by several types of damaging agents and by catalysts such as $[Ru(bpy)_3]^{2+}$. The first step in this process is a one-electron oxidation to yield a guanine radical cation that typically undergoes rearrangement or reacts with nearby molecules to form products that are oxidised more readily than guanine, e.g. 8-oxo-guanine.[71] In this manner, multiple electrons can be transferred from each guanine residue. The ability of the guanine base to undergo multiple oxidation reactions and the fact that there are multiple guanine residues in a target nucleic acid sequence provides signal amplification and contributes to the high sensitivity of mediated

electrochemical nucleic acid detection of the guanine residues in the nucleic acid sequence.[66] The effects of base stacking on guanine electron transfer have been determined by digital simulation of cyclic voltammograms of $[Ru(bpy)_3]^{2+}$ in the presence of oligonucteotides.[72] These studies showed that sequences containing isolated guanine gave a rate constant of 1.4 x $10^5 M^{-1}s^{-1}$ while sequences containing a 5'-GG segment gave an overall rate constant of 7.5 x 10^5 $M^{-1}s^{-1}$, both rate constants were independent of DNA concentrations in the simulations. The redox pathways in DNA oxidation have also been thoroughly investigated.[73]

Guanine has a formal potential of 1.29 V vs the NHE, which is approximately 1.10 V vs. Ag/AgCl[74], given the formal potential of $[Ru(bpy)_2(PVP)_{10}]^{2+}$ redox polymer it is expected that it will mediate the oxidation of substrates with redox potentials more negative than 1.05 V vs. Ag/AgCl, including the DNA base, guanine. The qualitative aspects of mediated electrocatalysis are most conveniently observed using cyclic voltammetry. Figure 2.27 shows that guanine is at potentials where the Ru^{3+} oxidant-catalyst sites are produced in the polymer film, also the absence of a return peak on addition of the guanine is an indication that catalysis is efficient and that a large number of the mediator sites are involved in the catalytic reaction. The absence of the reduction peak is due to the fact that the Ru^{3+} is involved in the reaction with guanine, that is it has already been reduced to Ru^{2+} by giving its electron to the oxidation of guanine.

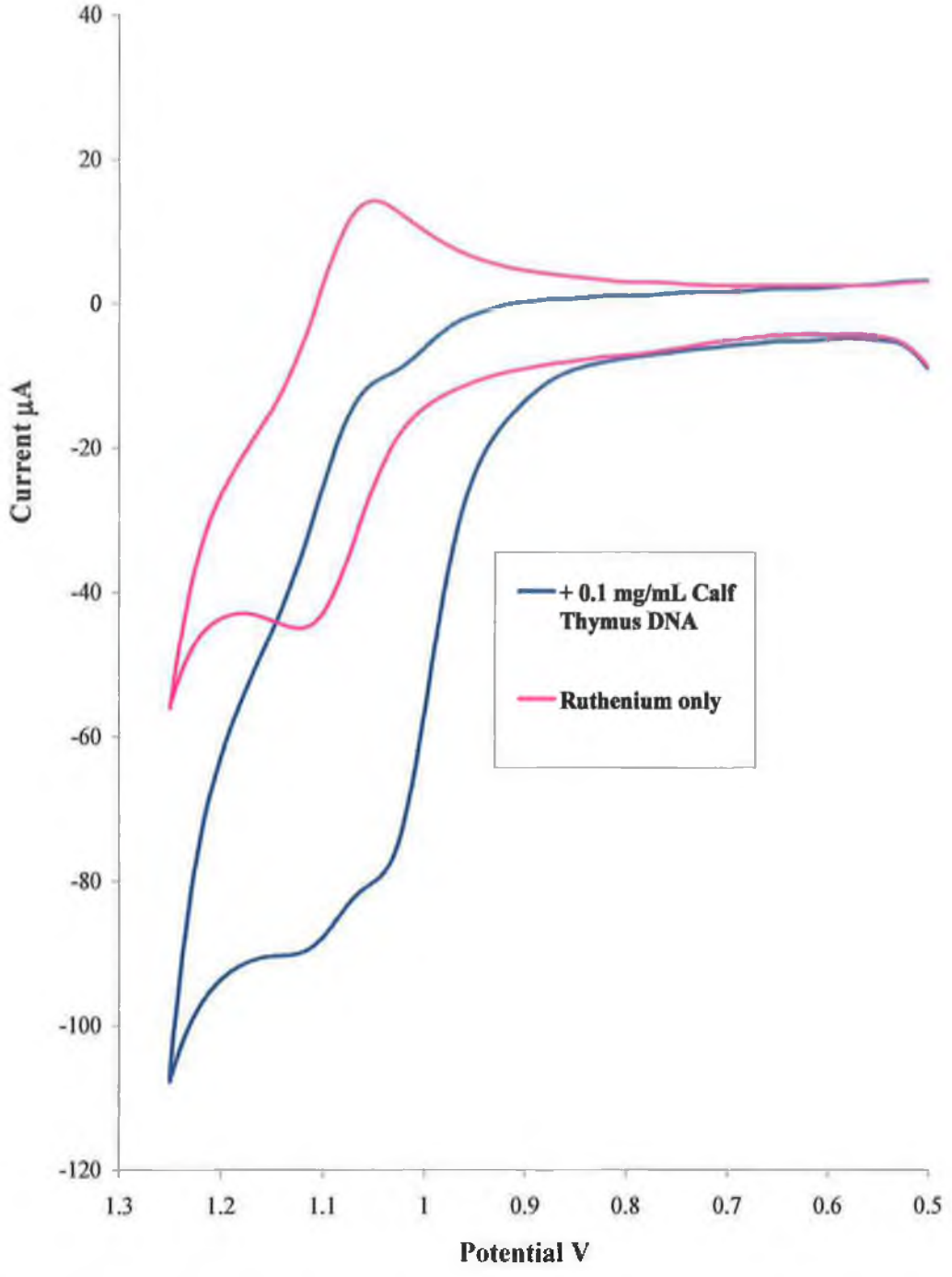

Figure 2.36: *Effect of addition of 0.1 mg/mL calf thymus DNA on the cyclic voltammogram of the ruthenium modified electrode, $\Gamma = 1.05 \times 10^{-8}$ molcm^{-1}. Scan rate 5 mVs^{-1}, 20 mM PBS electrolyte.*

The oxidation for 8-oxo-guanine, which is a product of chemical reaction that follows electron oxidation of guanine itself, is more favourable and is an intermediate in G → T transversions and other natural DNA modifications.[75] The potential for the 8-oxoG nucleoside oxidation is approximately 0.85 V in solution[76], and in fact, an electrochemical detection scheme is normally used to detect small quantities of 8-oxoG against a large background of normal guanine.[77] $[Os(bpy)_3]^{2+}$ has a much lower redox potential ($E_{1/2}$ = 0.62 V) than $[Ru(bpy)_3]^{2+}$. It has previously been shown that osmium (III) does not oxidise guanine in DNA,[78,79,80] but selectively catalysis the oxidation of 8-oxoG in both the presence and absence of guanine;

$$[Os(bpy)_3]^{2+} \rightarrow [Os(bpy)_3]^{3+} + e^- \quad \textbf{(18)}$$

$$[Os(bpy)_3]^{3+} + \text{8-oxoG} \rightarrow [Os(bpy)_3]^{2+} + \text{8-oxoG}^+ \quad \textbf{(19)}$$

Thorp *et al.* showed that cyclic voltammograms of $[Os(bpy)_3]^{2+}$ exhibited current enhancement, consistent with equation 19, when 8-oxoG was present, similar enhancement was not obeserved for normal guanine, providing a means in the that study, for the detection of mismatch selective oxidation at a single base oligonucleotides containing guanine. The rate of oxidation of 8-oxoG in the perfect GC duplex by Os(III) is approximately an order of magnitude faster than that of guanine by Ru(III) due to the larger driving force involved in the Os(III) reaction with 8-oxoG.[81]

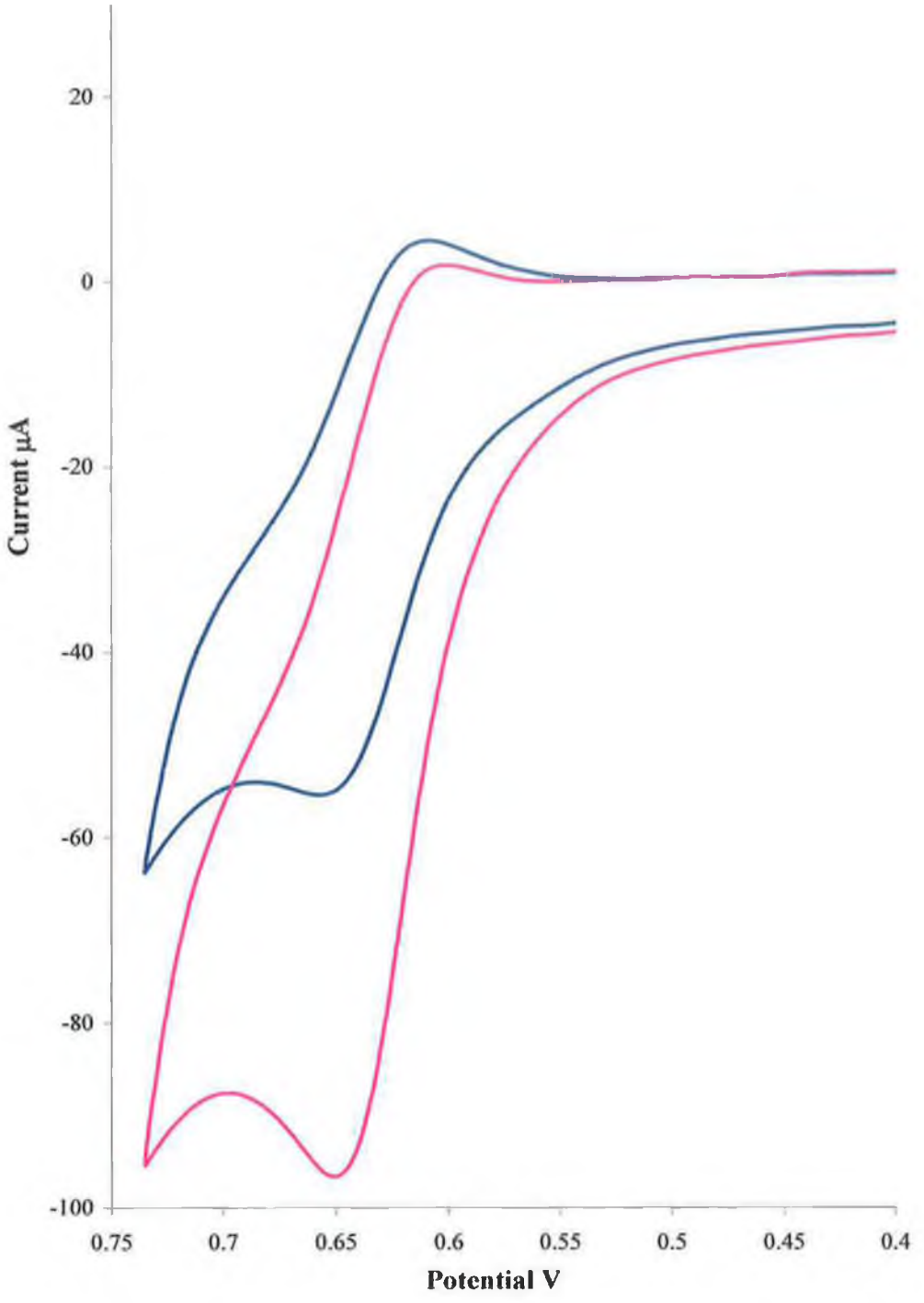

Figure 2.37: *Effect of addition of 0.1 mM 8-oxoguanine on the cyclic voltammogram of the osmium metallopolymer monolayer. Scan rate 5 mVs^{-1}, 20 mM PBS electrolyte.*

Figure 2.38 shows oxidation of 8-oxoG by $[Os(bpy)_2(PVP)_{10}]^{2+}$. The selective oxidation of 8-oxoG by $[Os(bpy)_2(PVP)_{10}]^{2+}$ is discussed in Section 3. Cyclic voltammograms were measured on mixtures of the osmium and ruthenium metallopolymer films. It was suspected that the osmium metallopolymer only oxidises the 8-oxoG, whereas, the ruthenium metallopolymer should be able to oxidise both 8-oxoG and guanine. Figure 2.39 shows the responses of the mixed films with either 8-oxoG or guanine. The reaction with guanine gives current enhancement only for the Ru (II/III) redox couple but not for the Os redox couple, showing that Os(III) is not an effective oxidant of guanine under conditions where Ru(III) oxidises guanine effectively. However, when 8-oxoG is present, current enhancement for both waves is observed. Thus, Os(III) oxidises only the 8-oxoguanine whereas Ru(III) is an effective oxidant of both the 8-oxoguanine and guanine.

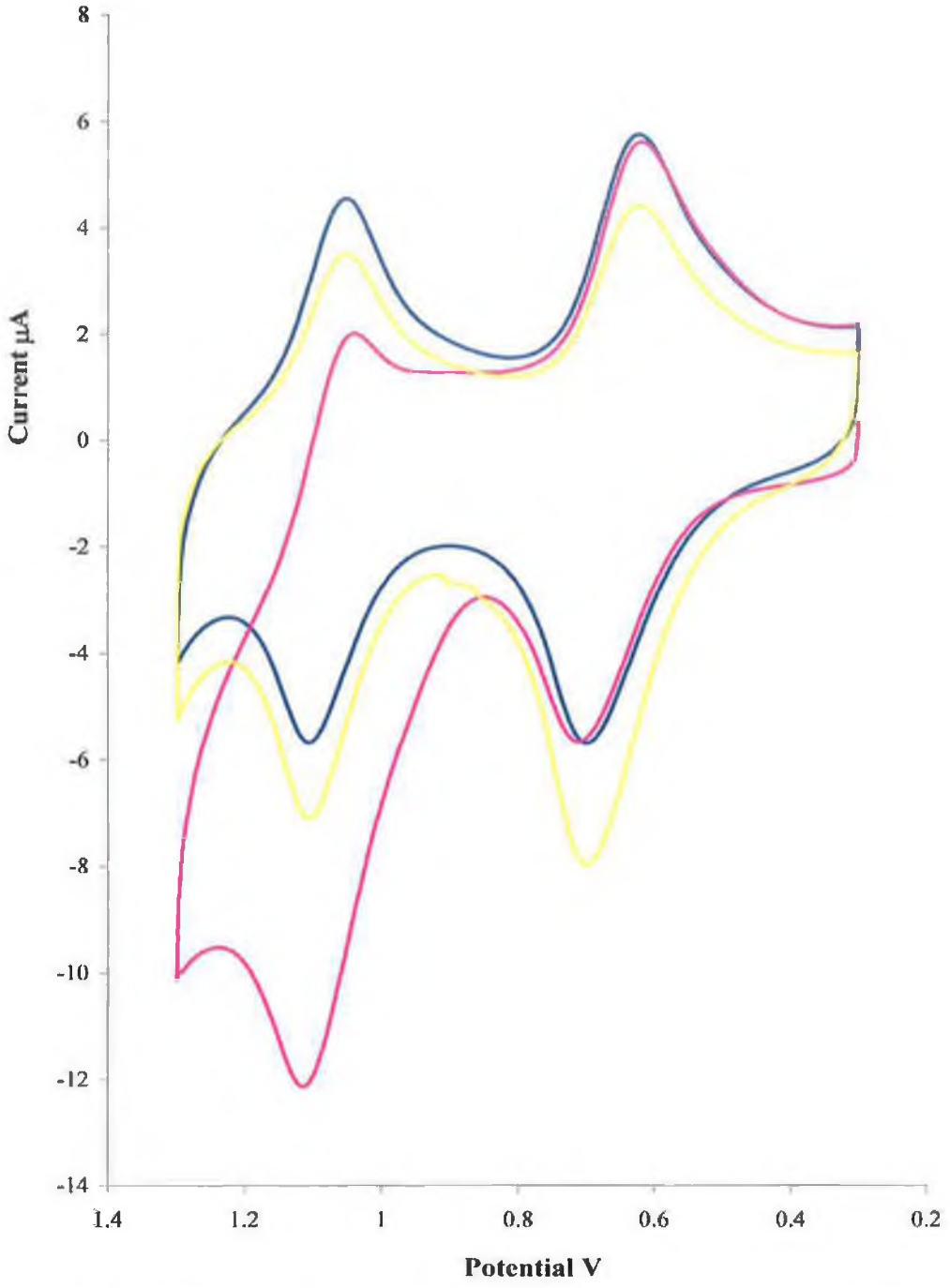

Figure 2.39: *Effect of addition of 0.1 mM 8-oxoguanine (yellow), of 0.2 mM guanine (pink) on the cyclic voltammogram of the mixed metallopolymer monolayer. Scan rate 5 mVs^{-1}, 20 mM PBS electrolyte. The metallopolymer film in blank buffer is also shown (blue).*

2.7 Conclusion:

The ruthenium and osmium metallopolymers were successfully synthesised and characterised through viscometry, spectroscopy and electrochemistry. For the most part the spectrochemical and electrochemical properties of the analogous monomeric complexes, $[M(bpy)_3]^{2+}$ and $[M(bpy)_2(pic)_2]^{2+}$, are also observed for the polymeric material. Notable exceptions are the excited state lifetime of the metallopolymer which was at least an order of magnitude lower than that of $[Ru(bpy)_3]^{2+}$ (580ns) under similar conditions, although it was similar to that of $[Ru(bpy)_2(pic)_2]^{2+}$.[24] A similar trend was observed for the osmium complexes. The quantum yield of photoluminescence, was also considerably lower for the polymer and the picoline complex than for $[M(bpy)_3]^{2+}$. Characterisation of thin layers of the metallopolymer immobilised on an electrode surface showed that they exhibited features typical of surface bound redox sites, that is the FWHM is close to the theoretical value of 90.6 mV and the peak to peak separation is close to unity, $|(I_p)_a/(I_p)_c| \approx 1$.

It has also been shown that the redox polymer $[M(bpy)_2(PVP)_{10}]^{2+}$ as a thin layer immobilised on a glassy carbon electrode has a charge transfer diffusion coefficient (D_{ct}) of the order 1 x 10^{-10} cm^2s^{-1} in PBS electrolyte. This is insensitive to electrolyte concentration, though there is some dependence on polymer layer thickness with a lower surface coverage giving an increased rate. The charge transport rates observed for the 2.9 x 10^{-8} mol cm^{-2} surface coverage are in good agreement with those previously reported for this polymer,[82] though the increase at small coverage was not observed. Although the D_{ct} in sulphuric acid electrolyte is very similar to that of the PBS electrolyte, suggesting a porous film, that observed in $HClO_4$ is quite different. The layers are compact and un-swollen in this electrolyte resulting in a difficult partition of the substrate into film. The data on these charge transports suggests that the rate of charge propagation through the layer is limited by the rate of electron hopping rather than ion movement.

Charge transport rates are important, as they have a direct bearing on the overall response time of a sensor which is dependent on the rate at which the catalytically active (M(III)) form of the layer can be generated and on the rate at which the mediating sites are regenerated. Guanine reacts with Ru^{3+} centres throughout the film; in this respect, the investigated system is a good example of the interest of redox polymer coatings in the catalysis of electrochemical reactions deriving from the three dimensional dispersion of catalytic centres. This situation is also the most favourable for developing sensitive sensors based on polymeric layers.

2.8 *References:*

1 Forster, R.J., Vos, J.G.; *J. Chem. Soc. Faraday Trans,* **1991**, *87*, 1863.

2 Doherty, A.P., Forster, R.J., Symth, M.R., Vos, J.G.; *Anal. Chim. Acta,* 1991, *255*, 45.

3 Lyons, C.H., Abbas, J., Lee, K., Rubner, M.F., *J. Electroanal. Chem.,* **1998**, *120*, 12100.

4 Shardon-Noblat, S., Deronzier, A., Ziessel, R., Zsoldos. D., *J. Electroanal. Chem.,* **1998**, *444*, 253.

5 Haas, O., Kriens, M., Vos, J.G., *J. Am. Chem. Soc.,* **1981**, *103*, 1318.

6 Kelly, D.M., Vos, J.G., *Electroactive Polymer Chemistry, Part 2: Methods and Applications,* Lyons, M. (Ed.); Plenum Press, New York, **1996**, Ch. 8.

7 Ziessel, R., *Advances in Chemical Conversions forMitigating Carbon Dioxide,* **1998**, *114*, 219.

8 Juris, A., Balzani, V., *Coordin. Chem. Rev.,* **1988**, *84*, 85-277.

9 Yagi, M., Mitsumoto, T., Kaneko, M., *J. Electroanal. Chem.,* **1998**, *448*, 131.

10 Martin, C.R., Rubinstein, I., Bard, A.J., *J. Am. Chem. Soc.,* **1982**, *104*, 4817.

11 Majda, M., Faulkner, L.R., *J. Electroanal. Chem.,* **1984**, *169*, 97.

12 Hogan, C.F., Forster, R.J., *Anal. Chim. Acta,* **1999**, *369*, 13-21.

13 Abruna, H.D., Denisevich, P., Umana, M., Meyer, T.J., Murray, R.W., *J. Am. Chem. Soc.,* **1981**, *103*, 1.

14 Abruna, H.D., Bard, A.J., *J. Am. Chem. Soc.,* **1982**, *104*, 2461.

15 Bommarito, S.L. , Lowery-Bertz, S.P., Abrune, H.D., *Inorg. Chem.,* **1992**, *31*, 502.

16 Seddon, E.A., Seddon, K.R., *The Chemistry of Ruthenium,* Elsevier, New York, **1984**, Ch. 15, 1180.

17 Forster, R.J., Vos, J.G., *Macromolecules*, **1990**, *23*, 4372.

18 Forster, R.J., Vos, J.G., *J. Electrochem. Soc.,* **1992**, *130*, 1503.

19 Wilson, R.W., Bailey, L., Cubitt, R., Gonsalves, M., Glide, A., Hillman, R.A., Vos, J.G., Hogan, C., Webster, J.R.P., *J. Phys. Chem.,* **1999**, *1*, 843.

20 Friesen, D.A., Kajita, T., Danielson, E., Meyer, T.J., *Inorg. Chem.,* **1998**, *37*, 2756.

21 Geraty, S.M., Vos, J.G., *J. Chem. Soc. Dalton Trans.,* **1987**, 3037.

22 Calvert, J.M., Meyer, T.J., *Inorg. Chem.,* **1981**, *20*, 27.

23 Rusling, J., *Biomolecular Films*, Dekker, *in press*, Ch. 1, p.1-61.

24 Hogan, C., *Ph.D. Thesis,* Dublin City University, **1999**.

25 Sullivan, B.P., Salmon, D.J., Meyer, T.J., *Inorg. Chem.,* **1978**, *17*, 3334.

26 Kelly, J.M., O'Connell, C.M., Vos, J.G., *J. Chem. Soc. Dalton Trans.,* **1986**, 253.

27 Buckingham, D.A., Dwyer, F.P., Goodwin, H.A., Sargeson, A.M., *Aust. J. Chem.,* **1964**, *17*, 325.

28 Casper, J.V., Meyer, T.J., *J. Am. Chem. Soc.,* **1983**, *105*, 5583.

29 Buckingham, D.A., Dwyer, F.P., Goodwin, H.A., Sargeson, A.M., *Aust. J. Chem.,* **1978**, *17*, 325.

30 Durham, B., Wilson, S.R., Hodgson, D.J., Meyer, T.J., *J. Am. Chem. Soc.,* **1980**, *102*, 600.

31 Clarke, A.P., *Ph.D. Thesis,* Leiden University, **1991**, Ch. 1, 10.

32 Forster, R.J., Vos, J.G., *Marcomolecules,* **1990**, *23*, 4372-4377.

33 Clear, J.M., Kelly, J.M., O'Connell, C.M., Vos, J.G., *J. Chem. Res.,* **1981,** 3039.

34 Geraty, S.M., Vos, J.G., *J. Chem. Soc., Dalton Trans.,* **1987**, 3073.

35 Sullivan, B.P., Salmon, P.J., Meyer, T.J., *Inorg. Chem.,* **1978**, *17*, 3334.

36 Johnston, E.C., Sullivan, B.P., Salmon, S.A., Adeyemi, S.A., Meyer, T.J., *Inorg. Chem.,* **1978**, *17*, 2211.

37 Kober, E.M., Marshall, J.L., Dressick, W.L., Sullivan, B.P., Caspar, J.V., Meyer, T.J., *Inorg. Chem.,* **1985**, *24*, 2755.

38 Kober, E.M., Caspar, J.V., Lumpkin, R.S., Meyer, T.J., *J. Phys. Chem.,* **1986**, *90*, 3722.

39 Atkins, *Physical Chemistry,* Ch. 23, p. 691.

40 Berokwitz, J.B., Yamin, M., Fuoss, R.M., *J. Polymer Sci.,* **1958**, *28*, 69.

41 Durham, B., Casper, J.V., Nagle, J.K. Meyer, T.J., *J. Am. Chem. Soc.,* **1982**, *104*, 4803.

42 Casper, J.V., Meyer, T.J., *J. Am. Chem. Soc.,* **1983**, *105*, 5583.

43 Clarke, A.P., Vos, J.G., Bandey, H.L., Hillman, A.R., *J. Phys. Chem.,* **1995**, 99, 15973.

44 Hage, R., *Ph.D. Thesis*, Leiden University, **1991**, Ch. 1, 10.

45 Juris, A., Balzani, V., Barigelletti, F., Campagna, S., Belser, P., Von Zelewsky, A., *Coord. Chem. Rev.,* **1988**, *84*, 85.

46 Kelly, D.M., Vos, J.G., *Electroactive polymer Chemistry, Part 2: Methods & Applications,* Ch. 8, Lyons, M. (Ed.) Plenum press, New York, **1996.** (and references therein).

47 Crosby, G.A., Klassen, D.M., Sabath, S.L., *Mol. Cryst.,* **1966**, *1*, 453.

48 Bard, A.J., Keszthelyi, C.P., Tachikawa, H., Tokel, E., *Chemiluminescence and Bioluminescence,* **1973**, *3*, 193.

49 Rozhitshii, N.N., *J. Anal. Chem. USSR,* **1992**, *47*, 1238.

50 Birch, Imhof, 1991

51 Tokel, N.E.; Bard, A.J. *J. Am. Chem. Soc.* **1972**, 94, 2862.

52 Reference, p.52.

53

54 Forster, R.J., Vos, J.G.; *Langmuir*, **1994**, 10, 4330.

55 Forster, R.J., Vos, J.G., *Macromol.,* **1990**, *23*, 4372.

56 Forster, R.J., Kelly, A.J., Vos, J.G., Lyons, M.E.G., *J. Electroanal. Chem.,* **1989**, *270*, 365.

57 Faulker, L.R., *Meth. Enzymol.*, **1978**, *57*, 494.

58 Abruna, H.D., Bard, A.J., *J. Am. Chem. Soc.,* **1982,** *104,* 2641.

59 Rubenstein, I., Bard, A.J., *J. Am. Chem. Soc.,* **1980,** *102,* 6642.

60 Forster, R. J.; Vos, J. G.; Lyons, M. E. G. *J. Chem. Soc. Faraday Trans.***1991**, 87, 3761.

61 Forster, R. J.; Vos, J. G. *J. Electrochem. Soc.* **1992**, 139, 1503.

62 Eisenberg, A. *Macromolecules* **1970**, 3, 147.

63 Bowden, E. F.; Dautartas, M. F.; Evans, J.F. *J. Electroanal. Chem.* **1987**, 219, 49.

64 Oh, S. M.; Faulkner, L. R. *J. Am. Chem. Soc.* **1989**, 111, 5613.

65 Szalai, V.A.; Thorp, H.H.; *J. Phys. Chem. B,* **2000**, 104, 6851.

66 Popovich, N.D.; Eckhardt, A.E.; Mikulecky, J.C.; Napier, M.E.; Thomas, R.S.; *Talanta*, **2002**, 56, 821-282.

67 Sistaire, M.; Holmberg, R.; Thorp, H.H.; *J. Phys. Chem.*, **1999**, 103, 10718-10728.

68 Juris, A.; Balzani, V.; Barigelletti, F.; Campagna, S.; Belser, P.; von Zelewsky, A.; *Coord. Chem. Rev.*, **1988**, 84, 85-277.

69 Burrows, C.J.; Muller, J.G.; *Chem. Rev.*, **1998**, 98, 1109-1151.

70 Steenken, S.; *Chem. Rev.*, **1989**, 89, 503-520.

71 Halliwell, B.; Gutteridge, J.M.C.; *Free Radicals in Biology and Medicine: 2nd Ed.:* Oxford University Press: Oxford, **1989**, Ch. 2.53, Ch. 8.

72 Sistare, M.F.; Codden, S.J.; Heimlich, G.; Thorp, H.H.; *J. Am. Chem. Soc.,* **2000**, 122, 4742.

73 Farrer, B.T.; Thorp, H.H.; *Inorg. Chem.,* **2000**, 39, 44.

74 Baik, M-H, Silverman, J.S., Yang, I.V., Ropp, P.A., Szalai, V.A., Yang, W., Thorp, H.H., *J. Phys. Chem.,* **2001**, *105*, 6437.

75 Duarte, V., Muller, J.G., Burrows, C.J., *Nucleic Acids Res.,* **1999**, *27*, 496-502.

76 Bernstein, R., Prat, F., Foote, C.S., *J. Am. Chem. Soc.,* **1999**, *121*, 464-465.

77 Helbock, H.J., Ames, B.N., *Proc. Natl. Acad. Sci. USA,* **1998**, *95*, 288-293.

78 Welch, T.W., Corbett, A.H., Thorp, H.H., *J Phys. Chem.,* **1995**, *99*, 11757-11763.

79 Welch, T.W., Thorp, H.H., *J. Phys. Chem.,* **1996**, *100*, 13829-13836.

80 Stemp, E.D.A., Arkin, M.R., Barton, J.K., *J. Am. Chem. Soc.,* **1995,** *117,* 2375-2376.

81 Ropp, P.A., Thorp, H.H., *Chem. Biol.,* **1999**, *6*, 599-605.

82 Clarke, A.P. *Thesis, Dublin City University*, **1992**, Ch. 2.

CHAPTER 3

SIMULTANEOUS DIRECT ELECTROCHEMILUMINESCENCE & CATALYTIC VOLTAMMETRY DETECTION OF DNA IN THIN FILM

"The most exciting phrase to hear in science, the one that heralds new discoveries, is not Eureka! (I found it!) but rather, "hmm.... that's funny...."

Isaac Asimov

3.1 Introduction:

Sensitive, selective detection of specific DNA sequences is central to clinical tests, pathogen detection, and other methods utilising polymerase chain reaction (PCR), to genetic disease screening based on oligonucleotide hybridisation, and to molecular genotoxicity studies.[1,2,3,4,5,6,7,8,9] For example, DNA forms adducts with many carcinogenic chemicals and anti cancer drugs, requiring the development of rapid sensitive assays.[10,11] Human liver cytochrome P450 enzymes convert lipophilic pollutants and drugs to metabolites that can often form covalent adducts with DNA.[12,13,14,15,16,17] These adducts serve as important markers of human exposure to environmental and occupational mutagens and carcinogens.[18,19,20]

In this study, styrene oxide is utilised to chemically damage DNA. Styrene 7,8-oxide (SO) is a major metabolite of styrene,[21] a widely used chemical monomer. It has been shown to form DNA adducts *in vitro* and *in vivo* which may be the cause of the mutagenic and carinogenic properties of the chemical.[22,23,24,25,26] Under physiological conditions, the main alklyation sites for aliphatic mono-substituted epoxides, such as styrene oxides, are the ring nitrogens at N7-guanine.[27,28,29,30,31] This reaction takes place through the β carbon of the epoxides by S_N2 type reaction mechanisms.[8] Although alkylation occurs preferentially at this site, other adducts have also being identified including those at the N2- and O6-guanine, N1- and N6-adenine and N3-cytosine, the structures of which are shown in Figure 3.8, but to a much lesser extent.[32] Once styrene oxide forms adducts with DNA, it disrupts the helical structure and as such guanine is more readily available for reaction with the ruthenium catalyst.

Electrochemistry provides simple, sensitive and inexpensive approaches to detecting DNA hybridization and damage.[33-36] One of the most sensitive approaches was first reported by Thorp *et al.*, who showed that ruthenium tris(2,2'-bpyridyl) [$Ru(bpy)_3^{2+}$] oxidizes guanine bases in DNA and oligonucteotides in an electrochemical catalytic pathway described in section 1.5.[37,38] Cycling $Ru[(bpy)_3]^{3+}$

to $[Ru(bpy)_3]^{2+}$ by the fast chemical step provides a greatly enhanced catalytic oxidation current in voltammetry. In solution, guanines reacted with $[Ru(bpy)_3]^{3+}$ at rate constants of 9 x 10^3 $M^{-1}s^{-1}$ in double stranded (ds) calf thymus (CT) DNA, and 2 x 10^5 $M^{-1}s^{-1}$ in single stranded (ss) CT-DNA[37] Guanines in various base-mismatched hybridized oligomers reacted at rate constants intermediate between the ds- and ss-DNA values. The rate of oxidation and the resulting catalytic peak current measured in voltammetry depend greatly on DNA structure and guanine sequence, providing selectivity in DNA analyses.[39-44] Damage of DNA by the formation of chemical adducts of nucleobases also alters the native ds-DNA structure, resulting in an increased reaction rate with $[Ru(bpy)_3]^{3+}$. Capitalising on this fact, sensors were developed to detect chemical DNA damage in ultrathin films using soluble[45] $[Ru(bpy)_3]^{2+}$ and a poly(vinylpyridine) (PVP)-$RuCl(bpy)_2^+$ polymer[46,47] as catalysts for square wave voltammetry.

Electrochemiluminescence (ECL) using $[Ru(bpy)_3]^{2+}$ bound to DNA as a luminescent label provides a sensitive method of detection.[48-54] The $[Ru(bpy)_3]^{2+}$ labels on DNA are oxidized to $[Ru(bpy)_3]^{3+}$, and ECL is generated by using a sacrificial reductant, often tripropylamine (Figure 3.1). ECL depends on generation of photoexcited $[Ru(bpy)_3]^{2+}$* in a process involving reaction of a radical form of the reductant with electrochemically generated $[Ru(bpy)_3]^{3+}$.[55,56]Alternatively, $[Ru(bpy)_3]^{+}$ is formed by reduction of $[Ru(bpy)_3]^{2+}$ by the radical, followed by reaction of Ru^{I} and Ru^{III} species to give $[Ru(bpy)_3^{2+}]$*.[57] Decay of $[Ru(bpy)_3^{2+}]$* to the ground state with luminescent emission at ~610 nm is measured in the detection step.

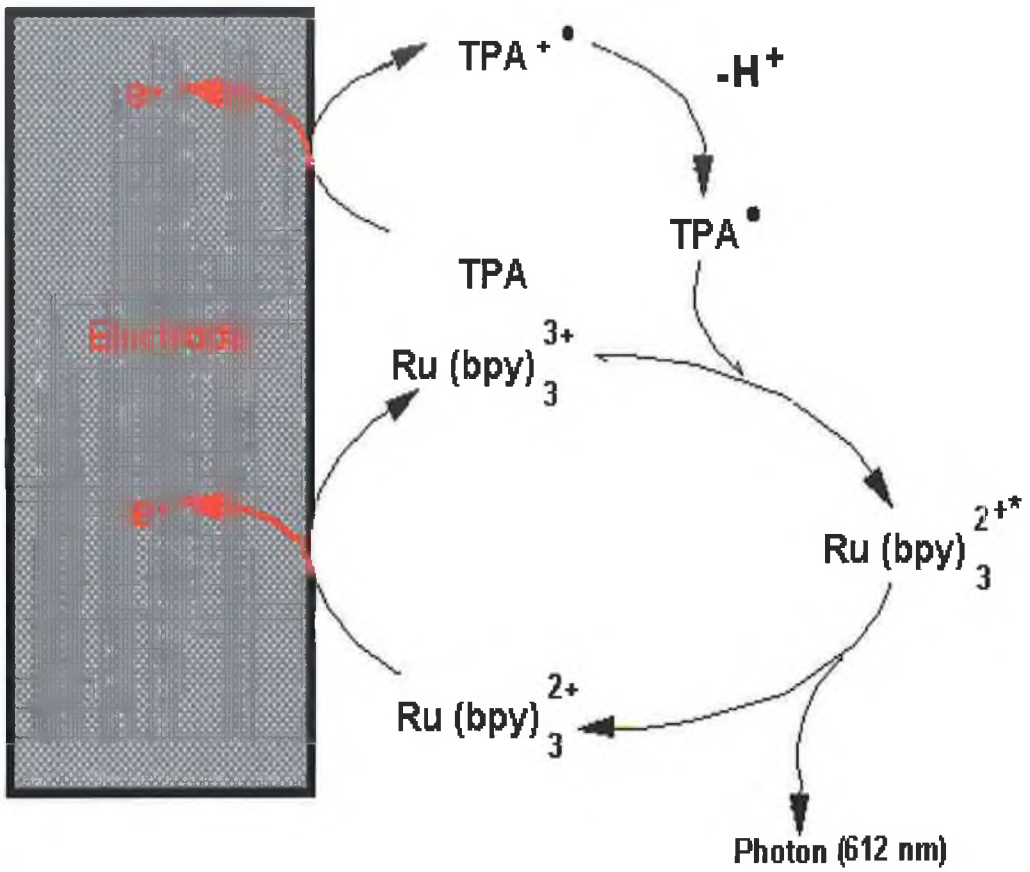

Figure 3.1: *Schematic diagram of $Ru(bpy)_3^{2+}$- tripropylamine (TPA) reaction.*

One-electron oxidation of guanine in DNA is well known to give guanine cation radicals,[58] which can also be oxidized by $[Ru(bpy)_3]^{3+}$. It was suspected that the reaction of guanine with $[Ru(bpy)_3]^{3+}$ or related species on a metallopolymer could also lead to a photoexcited Ru moiety and generate ECL as already shown in a previous chapter. Further, the rate and yield of this process might be enhanced by utilising films on electrodes with high local concentrations of Ru-catalyst and guanine. The ultrathin films of the catalytic polymer $[Ru(bpy)_2(PVP)_{10}](ClO_4)_2$ and oligonucleotides on electrodes can generate direct ECL signals that were sensitive to hybridization and chemical damage of DNA. ECL can be monitored simultaneously with catalytic electrochemical voltammograms in a simple apparatus.

3.2 Apparatus and Reagents:

Preparation and characterisation of the *bis*- substituted metallopolymer $[Ru(bpy)_2(PVP)_{10}](ClO_4)_2$ is described in chapter 2.

Calf Thymus (CT) double stranded (ds) DNA (Sigma, type XV, 13,000 avg. base pairs, 41.9% G/C), CT ss-DNA, Salmon Testes (ST) ds-DNA (Sigma, ~2,000 avg. base pairs, 41.2% G/C), ST ss-DNA, polyguanadylic acid (5') (Poly [G]), polycytidylic acid (5') (Poly [C]), polyadenylic acid (5') (Poly [A]), styrene oxide and toluene were from Sigma. Water was purified with a Hydro Nanopure system to specific resistance 18 $M\Omega cm^{-1}$. All other chemicals were reagent grade.

Simultaneous square wave voltammetry (SWV)-ECL measurements were made in a glass 3-electrode electrochemical cell at 37.0±0.5 °C using a CH Instruments Model 660 electrochemical analyzer. The cell employed a saturated calomel reference electrode (SCE), a Pt wire counter electrode, and a 4 mm diameter disk of basal plane pyrolytic graphite (PG, Advanced Ceramics) as working electrode placed close to the cell bottom. The electrolyte solution was 10 mM acetate buffer, pH 5.5, containing 50 mM NaCl. SWV conditions were 4 mV step height, 25 mV pulse height, and frequency 5 Hz. The cell was protected from light by coating with a black cloth to avoid external optical background interference and possible photodecomposition of the ruthenium metallopolymer. Solutions were purged with oxygen free nitrogen for 15 min prior to each series of experiments and a nitrogen atmosphere was maintained during data collection. A different electrode was used for each catalytic film analysis, as the oxidative analysis modifies the nucleic acids in the films.

A photomultiplier tube detector and data collection system from Labmaster Coherent Ultima was used to record emitted light from the electrode (610 nm) via

an optical fiber positioned directly underneath the DNA/metallopolymer electrode outside the flat bottom of the glass cell, as shown in Figure 3.3.

DNA-metallopolymer films were constructed by the layer-by-layer electrostatic assembly method.[9,45,47] Basal plane PG electrodes were polished with 400 grit SiC paper and then with 0.3 μm α-alumina slurries on Buehler Microcloth, washed with water and sonicated in ethanol for 15 min, then sonicated in water for 15 min. Layers were constructed by placing a 30 μL drop of 0.2% (w/v) aqueous $[Ru(bpy)_2(PVP)_{10}](ClO_4)_2$ onto each PG electrode, allowing 15 min to achieve saturated adsorption,[45] then washing with water. Subsequently, 30 μL of DNA solution (2 mg mL^{-1} DNA in 5 mM pH 5.5 acetate buffer + 0.05 M NaCl) was placed on this PG surface, allowed to adsorb 15 min, then washed with water. This sequence was repeated to obtain films with 2 metallopolymer/DNA bilayers. Films containing ss-DNA and other polynucleotides were also assembled in this way.

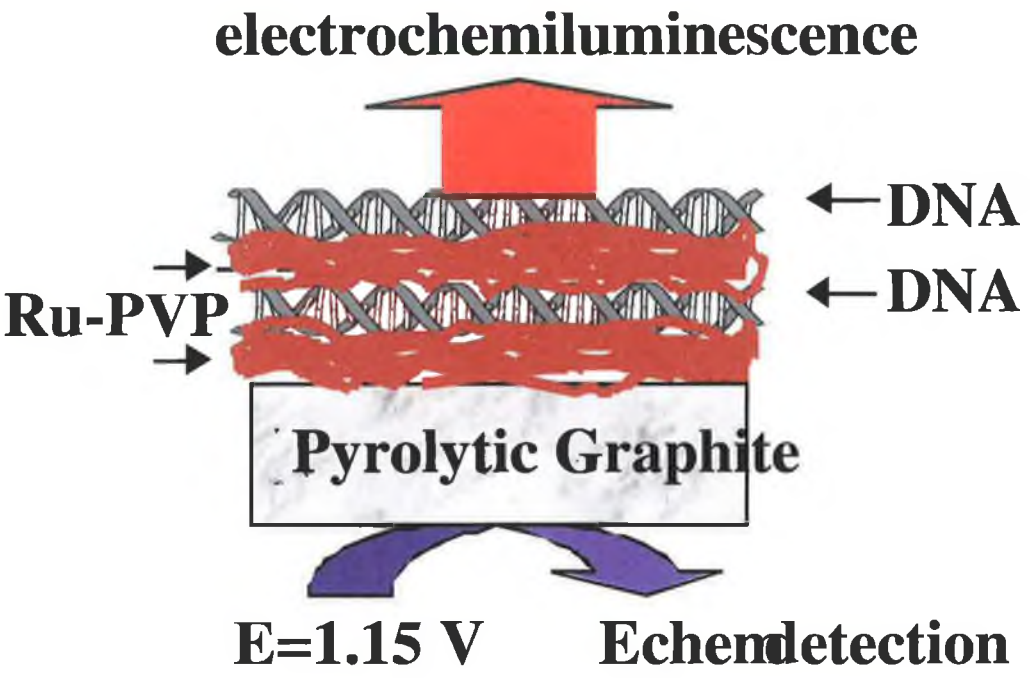

Figure 3.2: *Diagram of layer-by-layer film.*

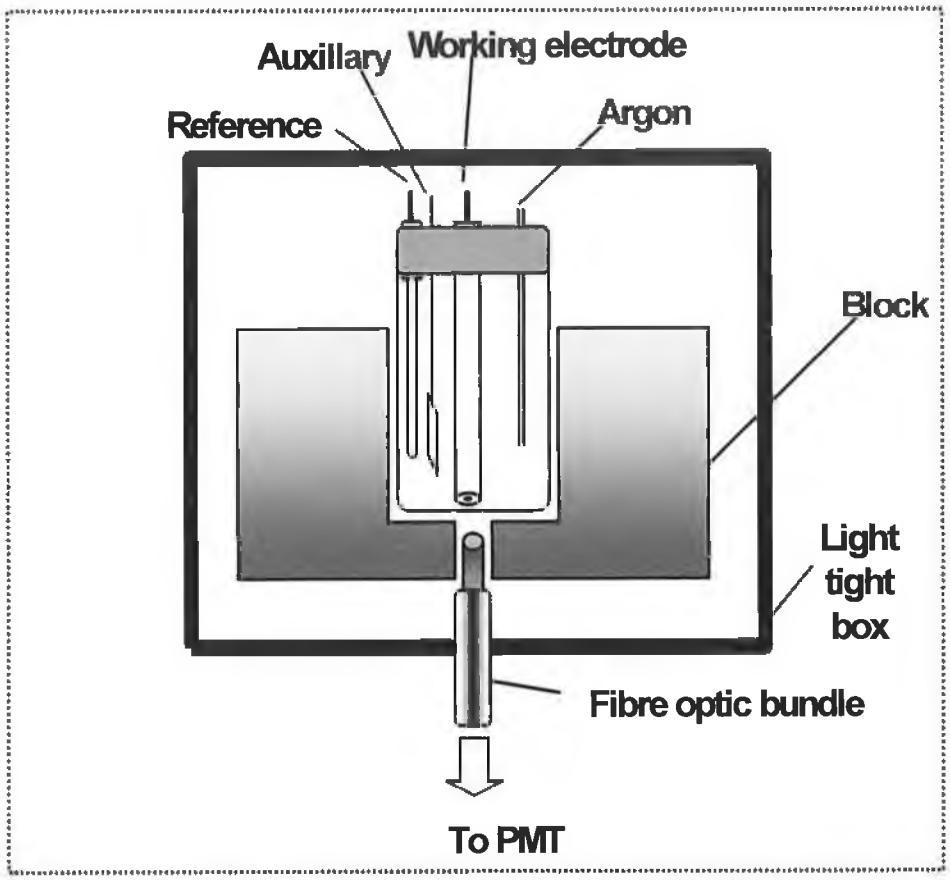

Figure 3.3: *Diagram of ECL Cell Set-up.*

Assembly of films was monitored using a quartz crystal microbalance (QCM, USI Japan) using 9 MHz QCM resonators (AT-cut, International Crystal Mfg.). To mimic the carbon electrode surface, a negative monolayer was made by treating gold-coated (0.16±0.01 cm^2) resonators with 0.7 mM 3-mercapto-1-propanol and 0.3 mM 3-mercaptopropionic acid in ethanol.[45] Films were assembled as for PG electrodes. Resonators were dried in a stream of nitrogen before measuring the frequency change (ΔF). Absorbed mass was estimated with the Sauerbrey equation,[59] for 9 MHz quartz resonators, giving dry film mass per unit area M/A as:

$$M/A \text{ (g cm}^{-2}) = -\Delta F \text{ (Hz)} / (1.83 \times 10^8) \quad \textbf{(1)}$$

The nominal thickness (d) of dry films was estimated with an expression confirmed by high resolution electron microscopy:[60]

$$d \text{ (nm)} \approx (-0.016 \pm 0.002)\, \Delta F \text{ (Hz)} \quad \textbf{(2)}$$

Incubations of films were done in styrene oxide solutions in a stirred reactor at 37.0±0.5 °C. 120 μL neat styrene oxide or toluene (as control) was added to 10 mL acetate buffer, pH 5.5 + 50 mM NaCl to give saturated solutions.[45] Previous studies shown that pH 5.5 gave optimum reaction rates of DNA with styrene oxide[47] and also allows efficient ECL production.[57] PG electrodes coated with polynucleotide or DNA films were incubated in the stirred emulsion, then rinsed with water and transferred to the electrochemical cell containing pH 5.5 buffer for SWV/ECL analysis.

3.3 *Results:*

3.3.1 *QCM Monitoring of Film Assembly*

Films were constructed for SWV/ECL measurements by the layer-by-layer electrostatic assembly method[45] with two bilayers of CT-DNA and metallopolymer $[Ru(bpy)_2(PVP)_{10}](ClO_4)_2$ deposited, denoted $(PVP\text{-}Ru/DNA)_2$. These films were first characterized by measuring QCM frequency shifts during film growth. ΔF values varied linearly with layer number for ss-DNA and ds-DNA layers alternated with Ru-PVP (Figure 3.4), suggesting regular film growth with reproducible layers of DNA and polymer. ΔF-values with eq 34 were used to obtain the weights of Ru-PVP and DNA deposited. Equation 2 was used to estimate the average nominal thickness of the films (Table 3.1). About 20% DNA and 30% more metallopolymer were incorporated in films when ss-DNA was used compared to ds-DNA. The mole ratio of guanine to ruthenium in these films was approximately 1.6:1.

Table 3.1: *Average characteristics of metallopolyion/DNA films from QCM.*

Film	*Nominal thickness, nm*	*mass DNA, $\mu g\ cm^{-2}$*	*mass Ru-PVP, $\mu g\ cm^{-2}$*
$(PVP\text{-}Ru/ST\text{-}ds\text{-}DNA)_2$	10 ± 2	1.6 ± 0.3	1.9 ± 0.4
$(PVP\text{-}Ru/ST\text{-}ss\text{-}DNA)_2$	14 ± 1.6	1.9 ± 0.5	2.6 ± 0.6

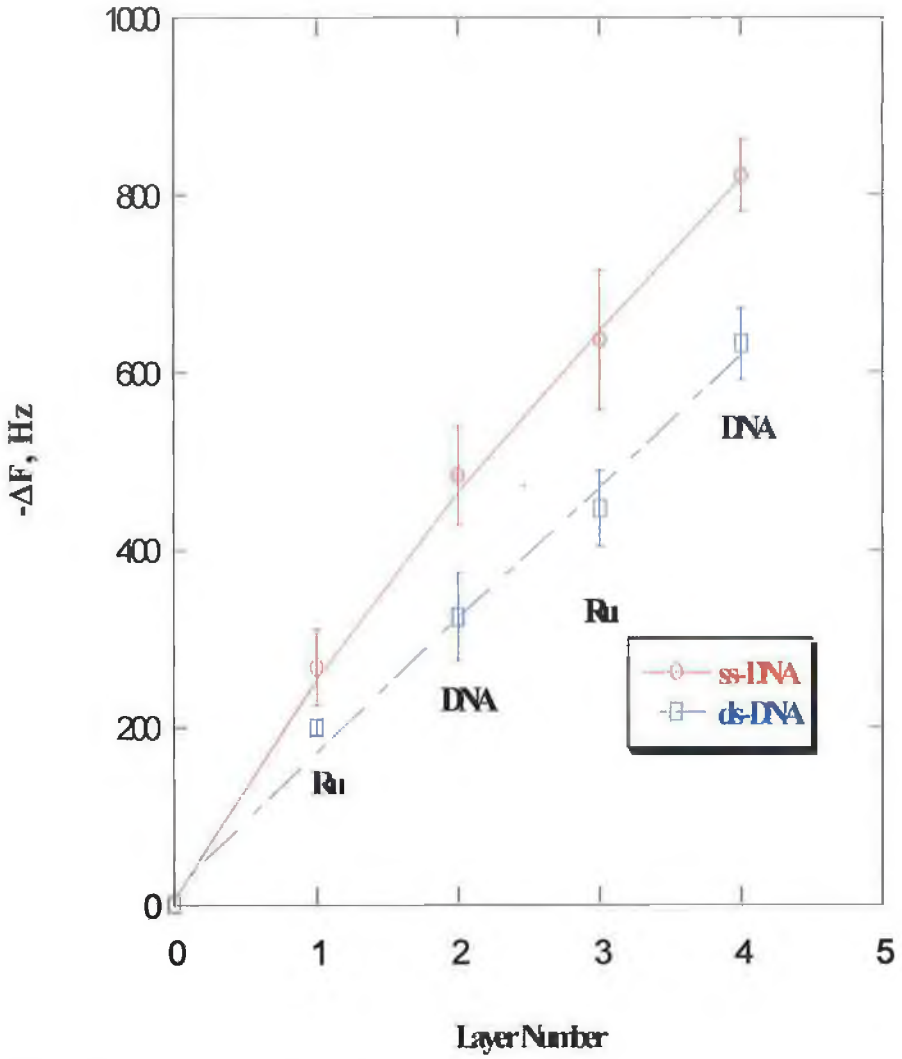

Figure 3.4: *QCM frequency shifts for cycles of alternate PVP-Ru and CT-DNA gold-quartz resonators coated first with mixed monolayers of mercaptopropionic acid/mercaptopropanol for ss-DNA and ds-DNA (Avg. values for 3 replicate films).*

3.3.2 ECL and SWV Measurements

A method in which voltammetric or amperometric current was measured simultaneously with ECL at electrodes coated with $[Ru(bpy)_2(PVP)_{10}]^{2+}$ for oxalate detection was reported previously.[61] A similar approach was utilised in this work, by scanning the potentials at which the Ru^{II} redox centres in the metallopolymer are not oxidised through values at which Ru^{II} is oxidized to Ru^{III} ($E^{o'}$ ~ 1.15 V vs. SCE), activating the catalytic cycle. Preliminary results showed that measurable ECL signals could be observed in pH ~6 buffer containing dissolved $Ru(bpy)_3^{2+}$ and guanosine monophosphate, polyguanylic acid (poly[G]) or ds-DNA while scanning voltammograms through the potential region where $Ru(bpy)_3^{2+}$ is oxidised to $Ru(bpy)_3^{3+}$. In contrast to the solution phase approach, here films were designed to contain all the necessary components for ECL generation with DNA. These ultrathin films feature the reactive species in high concentrations, ~ 1 M, in a tiny reaction volume, nL, estimated from film thickness (Table 3.1) and electrode area at ~0.2 μL.

Similar to previous reports, $[Ru(bpy)_2(PVP)_{10}]^{2+}$ adsorbed on PG electrodes gave reversible redox peaks,[62] with formal potential ca. 1.15 V vs. SCE at pH 5.5 measured by cyclic voltammetry and SWV, and surface concentration of 6×10^{-11} mol cm^{-2} obtained for electroactive ruthenium by integration of CVs at 5 mV s^{-1} this corresponds to roughly half a monolayer. The QCM data gave the approximate amount of polymer present by mass, by assuming the structure $[Ru(bpy)_2(PVP)_{10}](ClO_4)_2$, the amount of ruthenium can be calculated. Comparing this value with the amount of electroactive material calculated from the 5 mVs^{-1} scans, it was estimated that 84% of the ruthenium present in this first adsorbed layer is electroactive. This value is significantly below 100% and indicates that not all the ruthenium metal centres are active.

Figure 3.5 shows that combined ECL/SWV measurements on films containing Ru-PVP, alone or in $(Ru\text{-}PVP/PSS)_2$ films, gave the Ru^{II}/Ru^{III} oxidation

peak, and a very small amount of light. However, (Ru-PVP/poly[G])$_2$ films gave a significant ECL peak, as well as a catalytic current by SWV that was much larger than the non-catalytic Ru^{II}/Ru^{III} oxidation peak for Ru-PVP films not containing poly[G]. Figure 3.5 also shows that (Ru-PVP/poly[A])$_2$ gave a small catalytic current and a very small ECL signal, slightly above the background for Ru-PVP films. This may be due to the fact that poly[A] has a slow reaction with Ru^{3+}. This reaction is slower and uphill in comparsion to the reaction of guanine with Ru^{3+}, nonetheless the reaction can still occur and could be responsible for the small catalytic current observed.

The influence of hybridisation on the ECL signal was investigated by using films containing hybridised and unhybridised poly[G]. Figure 3.6 compares the ECL/SWV responses of films of (Ru-PVP/Poly [G])$_2$ and (Ru-PVP/Poly[G]/Poly[C])$_2$. The latter films were made by using a solution of poly[G] and poly[C] for which UV-Vis spectra confirmed hybridisation. Both ECL and SWV peaks are about 3-fold larger for films containing only the poly[G] layer compared to the film with the hybridised poly[G]/poly[C] layers. (Figure 3.6).

The unhybridised poly[G] films, cannot be considered entirely single-stranded in character due primarily to the its unique secondary structure. Guanines readily form bonds with other guanines. This results in the formation of a guanine quartet. Therefore, although there a much higher concentration of guanines in these films in comparsion to the films containing either single or double-stranded DNA, the response will not be as high as expected due to the present of these guanine quartet which will decrease the number of guanines present for reaction.

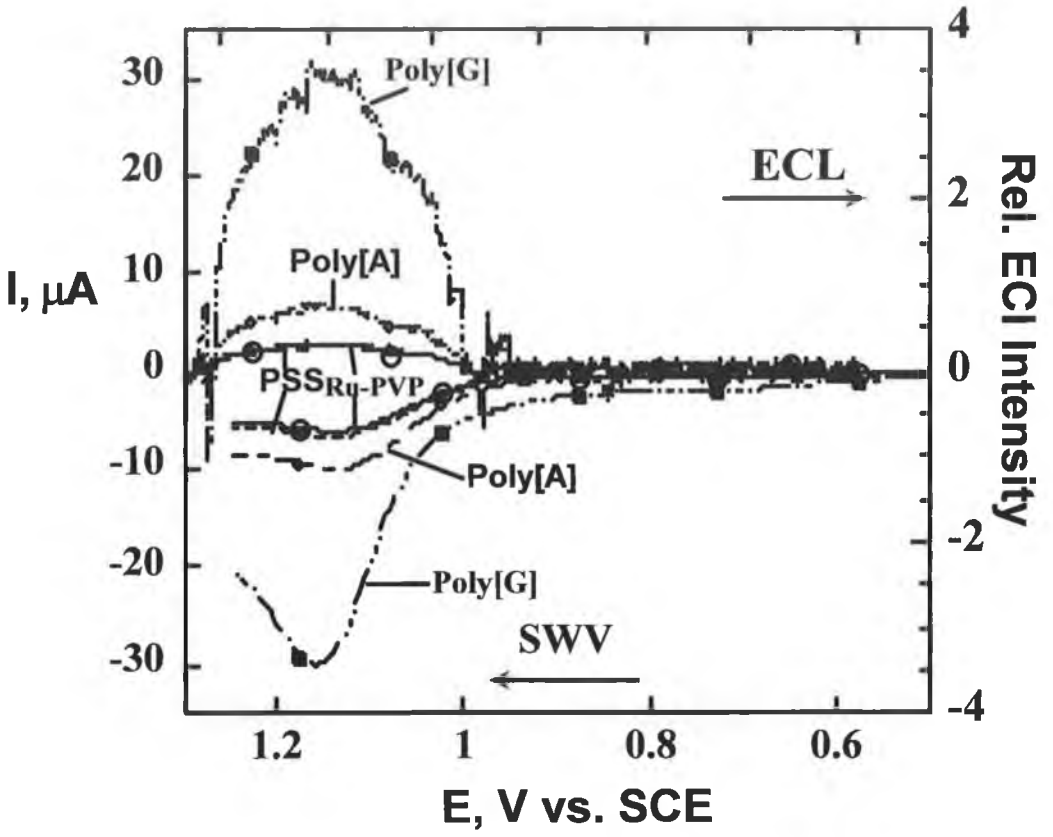

Figure 3.5: *SWV and ECL response for films containing Ru-PVP on PG electrodes in pH 5.5 buffer + 50 mM NaCl. Films are Ru-PVP alone (○), $(Ru\text{-}PVP/PSS)_2$ (◢), $(Ru\text{-}PVP/poly[A])_2$ (◇), and $(Ru\text{-}PVP/poly[G])_2$ (■). Symbols are for curve identification only.*

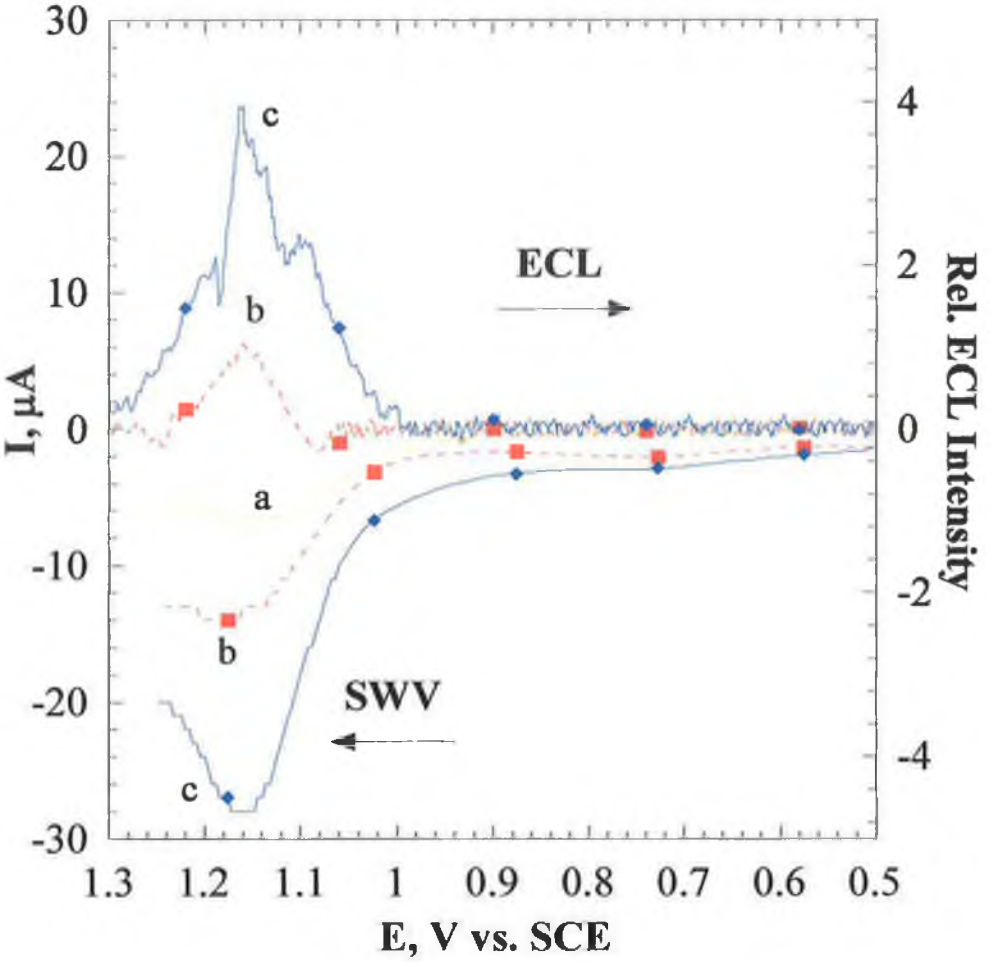

Figure 3.6: *SWV and ECL response for (a) Ru-PVP, (b) (Ru-PVP/Poly[G]/Poly [C])$_2$ and (c) (Ru-PVP/Poly [G])$_2$ films on PG electrodes in pH 5.5 buffer + 50 mM NaCl.*

Similar results were obtained when comparing ECL/SWV signals for films containing ss- and ds-DNA. (Figure 3.7). Films containing ss-DNA gave about twice the ECL signal as those made with ds-DNA. SWV peaks for the ss-DNA films were about 8-fold larger than their ds-DNA analogues. Similar results were found for calf thymus and salmon testes DNA. Films assembled with DNA and the polycation PDDA show no significant ECL peaks.

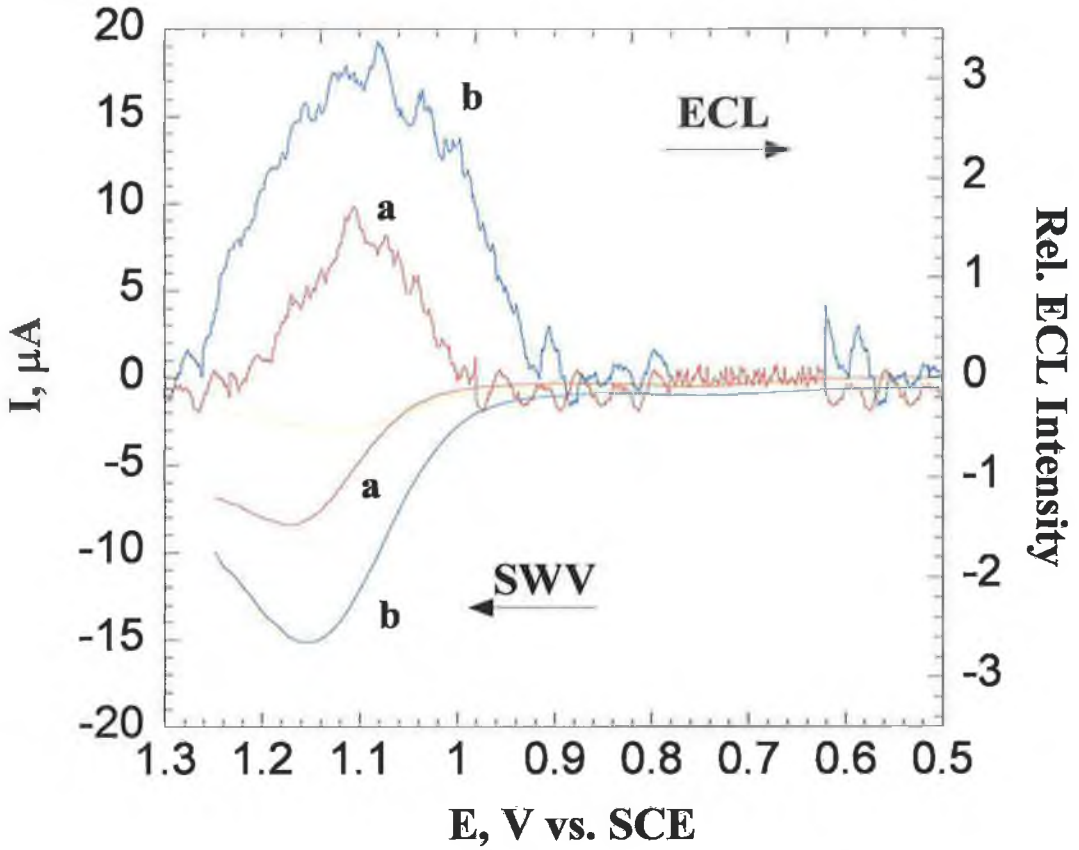

Figure 3.7: *SWV and ECL for (a) (Ru-PVP/ss-CT DNA)$_2$ films and (b) (Ru-PVP/ds-CT DNA)$_2$ films on PG electrodes in pH 5.5 buffer + 50 mM NaCl.*

3.3.3 Reaction of Nucleic Acid Films with Styrene Oxide:

The purine bases guanine and adenine in DNA form covalent adducts with styrene oxide, with the majority of reactions occurring at guanine.[63-69] Such adducts can serve as important markers of human exposure to mutagens and carcinogens.[70,71] Further, covalent adduct formation disrupts the double helical structure of DNA, and makes the guanines more available for catalytic oxidation, even when the DNA is present in polyion films.[45] By using capillary electrophoresis and liquid chromatography-mass spectrometry to analyze enzyme- and acid- hydrolyzed DNA that had been reacted with styrene oxide, it was confirmed that styrene oxide-guanine and styrene oxide-adenine adducts form under the incubation conditions used in this work.[72,73]

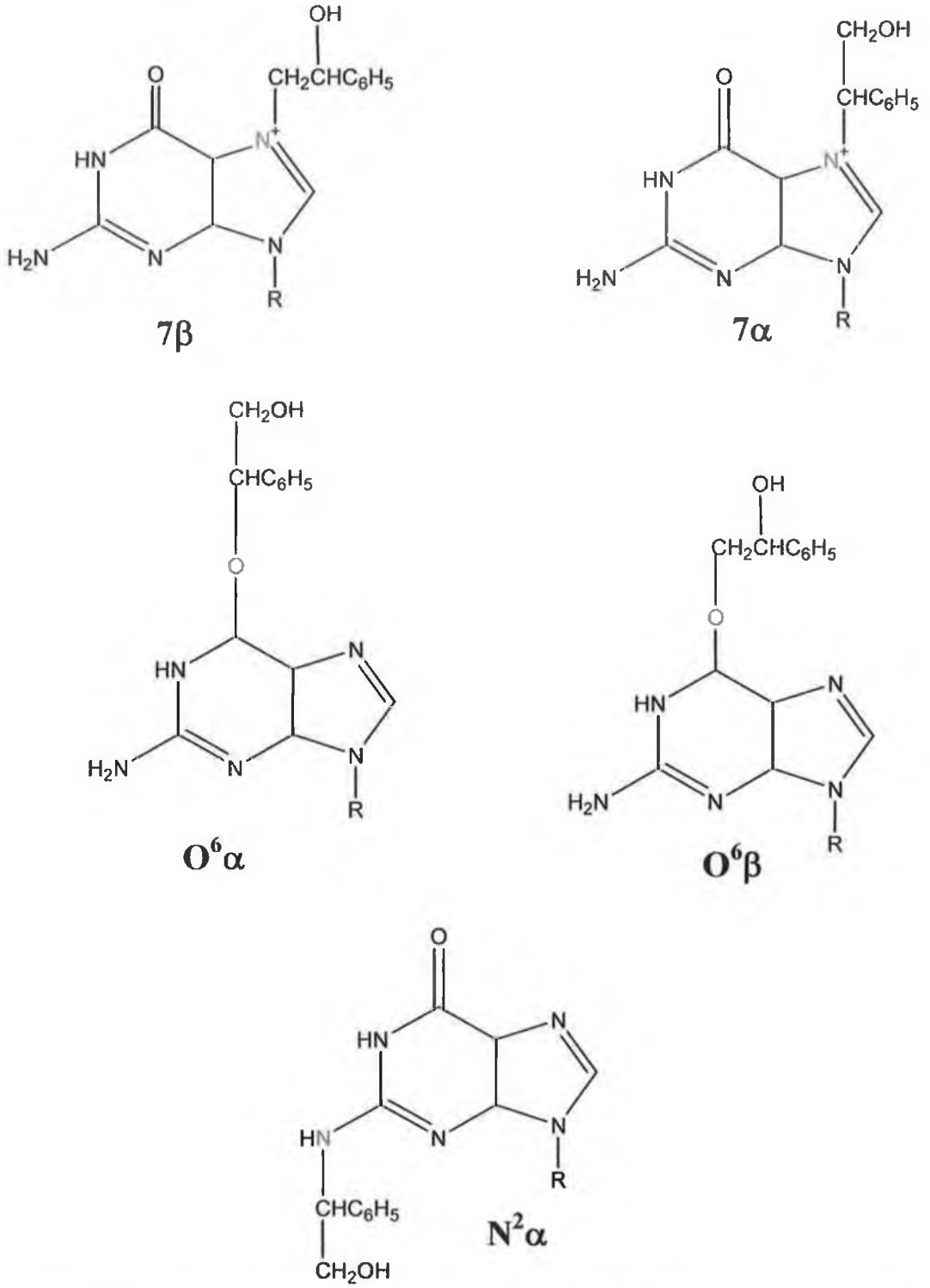

Figure 3.8: *Structures of styrene oxide-guanine derivatives. Adapted from Pavel Vodicka and Kari Hemminki, Carcinogensis,* ***1988****, 9, 1657-1660*

When $(Ru\text{-}PVP/ds\text{-}DNA)_2$ films were incubated with styrene oxide, then scanned by SWV, increases in the ECL and the SWV peaks were observed with increasing incubation time (Figure 3.9). As a control these films were also incubated in toluene and buffer over the same time scales, these films showed no significant change over the course of the study. Average peak currents for the ds-DNA films incubated in styrene oxide increased linearly with incubation time for about the first 20 min, followed by a slight decrease (Figure 3.10). Error bars in Figure 3.10 represent the electrode-to-electrode variability (n = 3). When $(Ru\text{-}PVP/ds\text{-}DNA)_2$ films were incubated with toluene, for which no chemical reactions with DNA have been reported, or in buffer only, ECL and SWV peaks remained within electrode-to-electrode variability and showed no trends with incubation time.

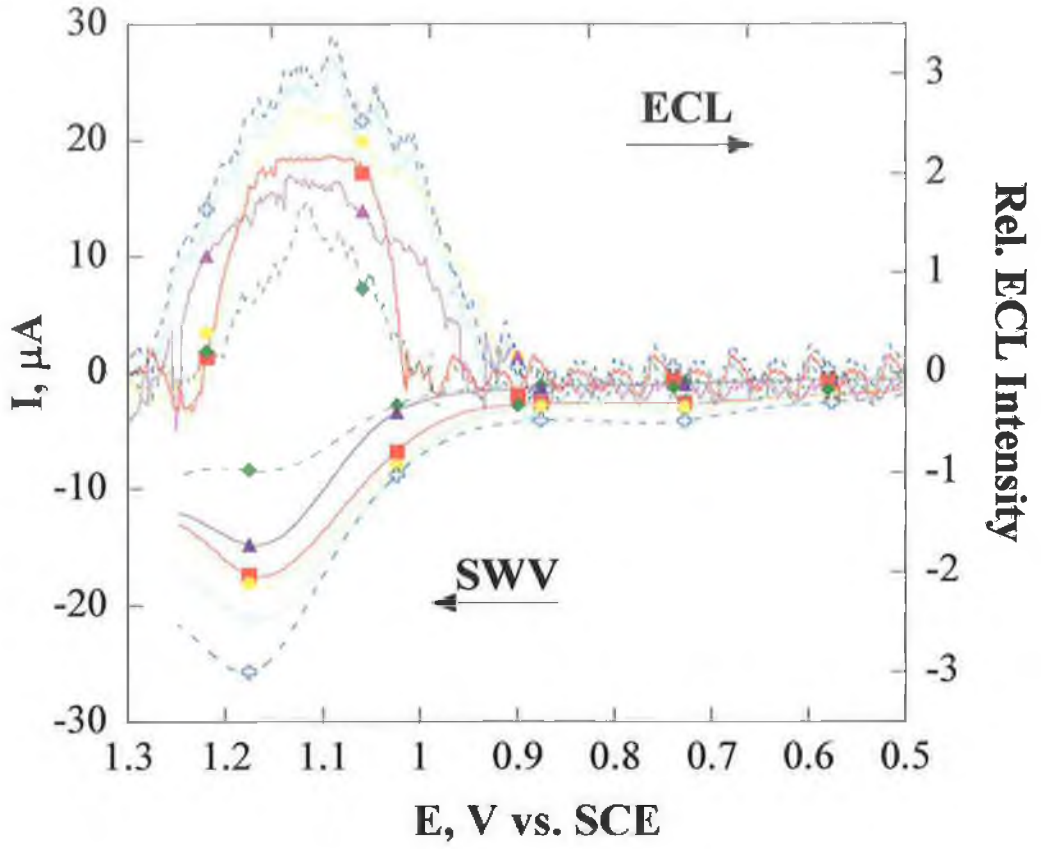

Figure 3.9: *SWV and ECL responses for (Ru-PVP/ds-CT DNA)$_2$ films on PG electrodes in pH 5.5 buffer + 50 mM NaCl after incubations 37 ℃ with saturated styrene oxide (2M). Numerical labels are incubation times in min.*

Figure 3.10: *Influence of incubation time with styrene oxide (●), toluene (▲), and buffer alone (○) on (a) average ECL signals and (b) average SWV catalytic peak currents (final response/initial response) for (Ru/ds-CT DNA)$_2$ films monitored at 610 nm and 1.15 V. Error bars represent standard deviations for three trials, one electrode per trial.*

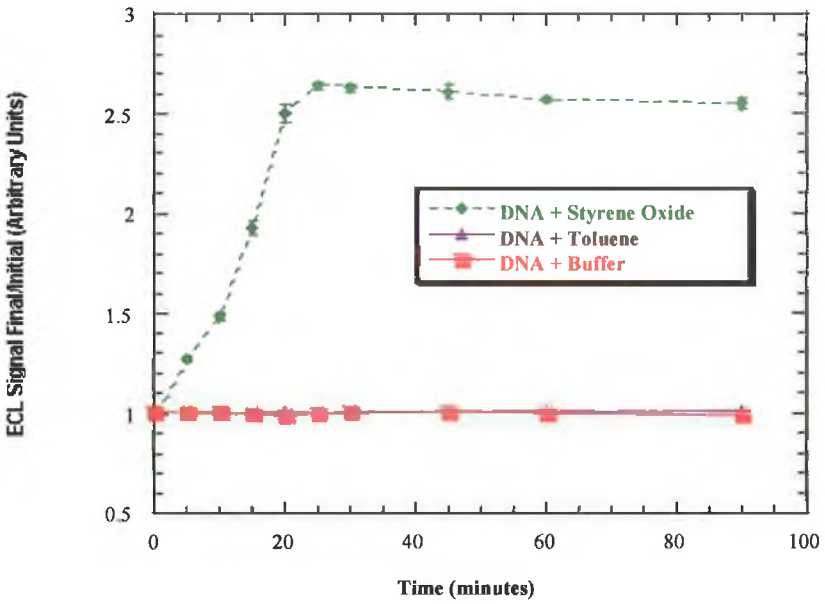

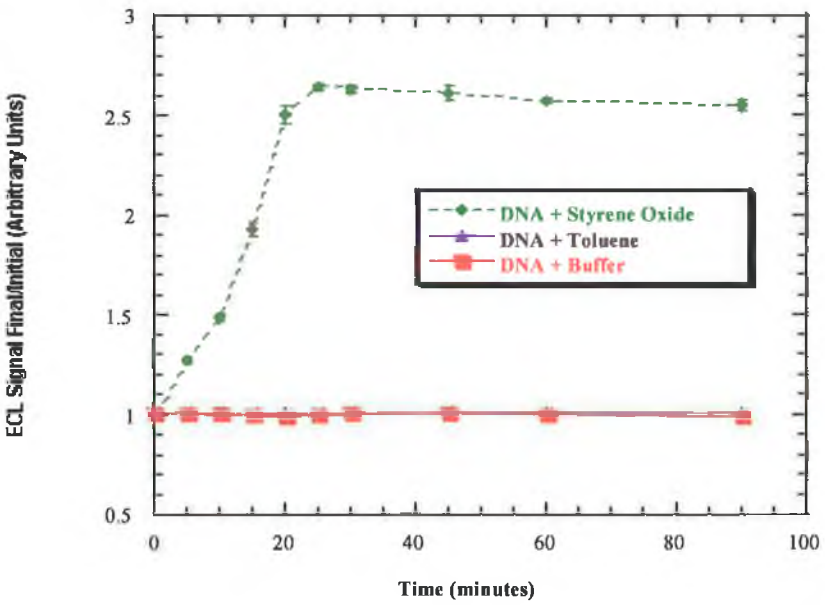

In addition to catalytic oxidation of guanines, it is possible that adducts formed on DNA by reaction with styrene oxide could be catalytically oxidised by the ruthenium metallopolymer. To assess this possibility, styrene oxide was incubated with films containing individual polynucleotides and the metallopolymer. Figure 3.11 shows that both ECL and SWV peaks increased after 10 min incubation of (Ru-PVP/poly[G])$_2$ with styrene oxide However, for films incubated with toluene, ECL and SWV peaks were nearly identical to initial values.

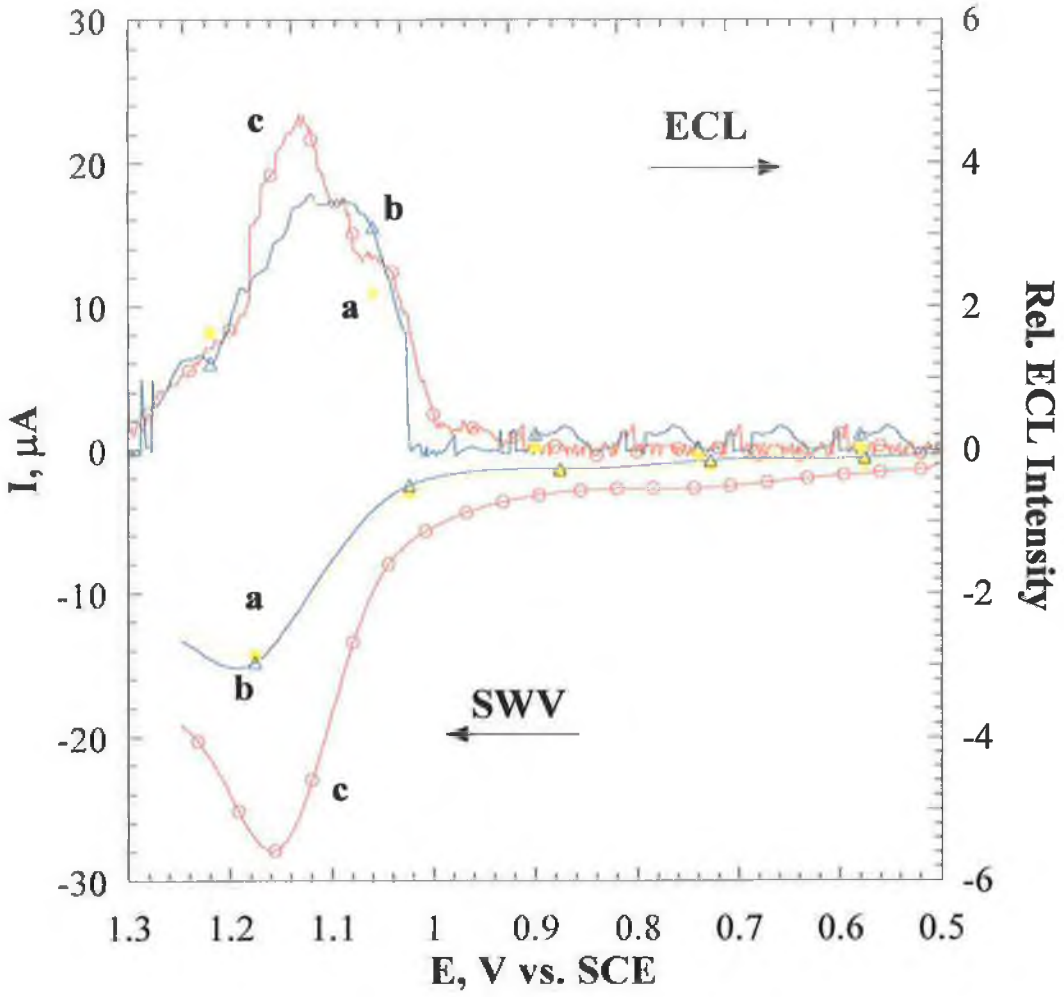

Figure 3.11: *SWV and ECL response for (Ru-PVP/poly[G])$_2$ films on PG electrodes in pH 5.5 buffer + 50 mM NaCl (a) no incubation; (b) incubated with saturated toluene control for 10 min., (c) incubated with saturated styrene oxide for 10 min.*

Similar experiments were done with films containing the other three polynucleotides. For intact Poly [A] films, only a small SWV peak for catalytic oxidation was observed. After Poly [A] was reacted with styrene oxide, a 25% increase in this peak was found. However, ECL signals for Poly [A] treated with styrene oxide were indistinguishable from the baseline before treatment. SWV of Poly[C] and Poly[T] films showed no increase in oxidation peaks either before or after 10 min incubations with styrene oxide. Poly [A] or poly[C] films did not produce significant ECL before or after incubations with styrene oxide.

3.4 Confirmation of Styrene Oxide-DNA Adduct Formation:

It was previously shown that styrene oxide is formed from styrene using Mb and cyt $P450_{CAM}$ films, the Mb and cyt $P450_{CAM}$ are the enzymes involved in the metabolised of styrene to styrene oxide.[74] However, it was necessary to confirm the formation of these adducts under the same conditions as those used for the electrochemical analysis. HPLC-MS can be used to confirm that the reaction of styrene oxide in solution under the conditions described above can produce the reported styrene oxide DNA adducts.[75] However, due to sensitivity limitations, this method required much longer analysis times than for the SWV methods.

The damaged DNA sample in solution or on the electrode surface was collected and hydrolysed with deoxyribonuclease I and phosphodiesterase I. The hydrolysates, which included DNA nucleosides and nucleosides-styrene oxide adducts, were separated and identified using either CE[76,77] or HPLC-MS.[76] UV-HPLC of damaged DNA showed the suspected dG and dA adducts as a series of peaks at t_R 15-21 mins, with the major peak in this group at ~ 18 mins. The peaks that eluted from the column at 4 min were those of the nucleosides. The peak at t_R ~ 9 min was identified as styrene oxide.

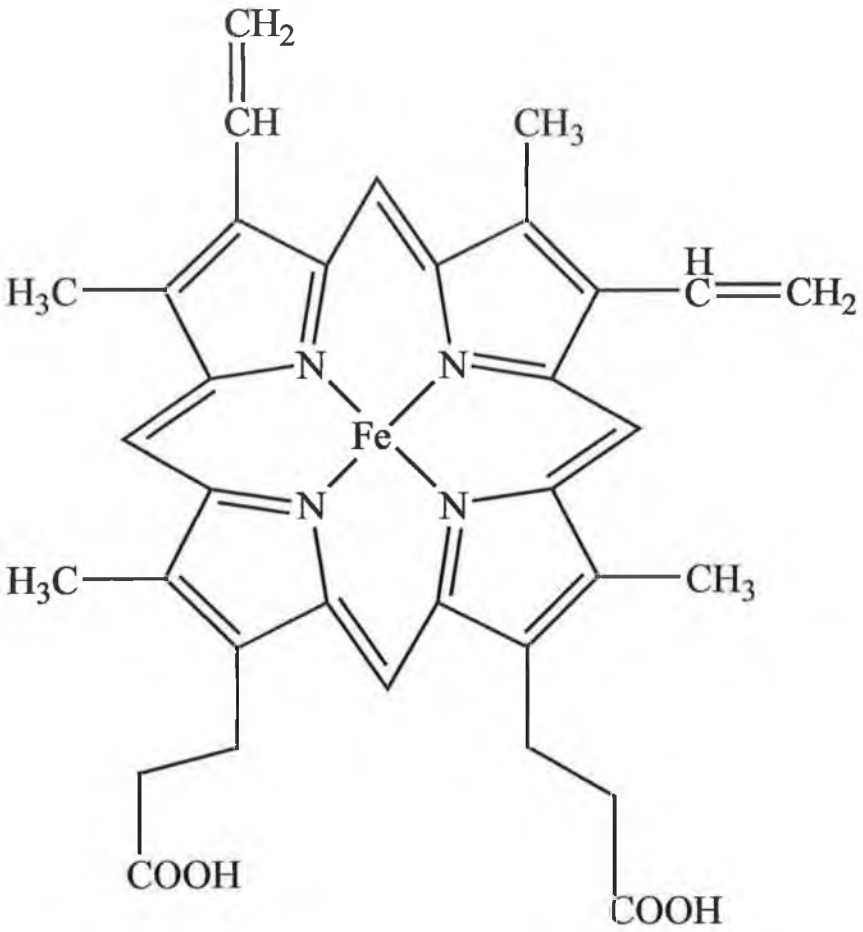

Figure 3.12: *The structures of ferroprotoporphyrin IX (heme) group in Mb and Cyt P450.*

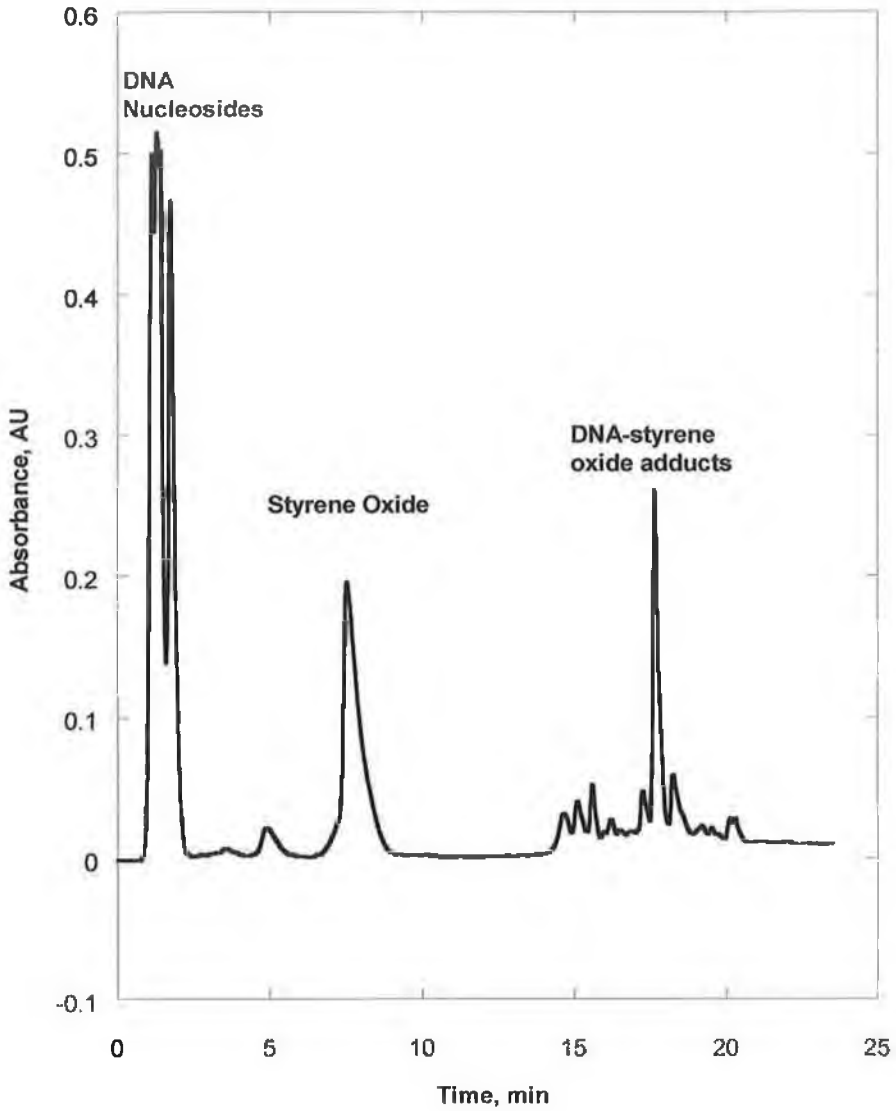

Figure 3.13: *HPLC with UV detection showing peaks of DNA-styrene oxide adducts from hydrolyzed DNA after incubation of intact ds-ST-DNA with styrene oxide for 48 hr at 37°C. HPLC experimental condition: Restek Ultra C-18 column (10 cm × 2.1 mm × 5 μm); 24% acetonitrile 76% water with 0.05% TFA as the mobile phase; 20 μL loop. Adapted from reference 78.*

Mass spectrometry provides a way to further identify the adducts. The mass spectra of the peaks at t_R 18 ± 0.2 min and 17.8 ± 0.2 min, which were thought to be to the dG-styrene oxide adduct and dA-styrene oxide adduct respectively, confirmed the production of these adducts under the experimental conditions. The molecular ions with m/Z 388 and 372 could be observed in Figure 3.14. The major product ions were 272 and 256 respectively, which correspond to the loss of a sugar from the adducts.

Single ion recording, (SIR), monitors only ions with specific m/Z. The molecular ions of the four nucleosides (dA: 252; dG: 268; dC; 228; dT: 243) and two adducts (dA-styrene oxide: 372; dG-styrene oxide: 388) were monitored. As shown in Figure 3.15, the existence of these species was recorded. However, the MS results of the relative amounts of dA-SO and dG-SO adducts formed were different from those previously reported, however, they still confirmed the guanine derivative was the most likely to be formed.[79,80] UV-HPLC showed one significant adduct peak (Figure 3.13), however, it was difficult to assign these peaks since the peaks of both dA-SO and dG-SO adducts eluted so close to each other. This analysis identified the main adducts formed under the same conditions as the electrochemical method utilised. Table 3.2 showed both the adducts and the possible fragments which were analysed during this study.

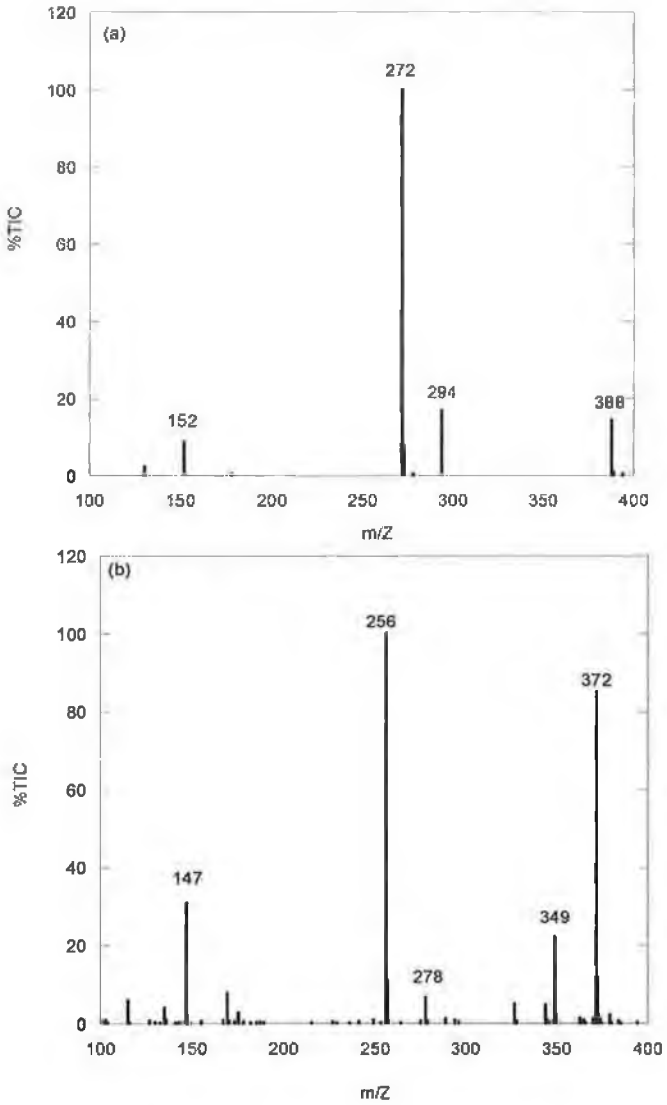

Figure 3.14: *Mass spectra of HPLC/MS for hydrolyzed DNA at t_R 18 and 17.8 ± 0.2 min. (a) T_R at 18 ± 0.2 min corresponded to the deoxyguanosine (dG)-styrene oxide adducts; (b) T_R at 17.8 ± 0.2 min corresponded to the deoxyadenosine (dA)-styrene oxide adducts. MS experimental condition: Cone voltage 15 V. Collision energy 15 eV.*

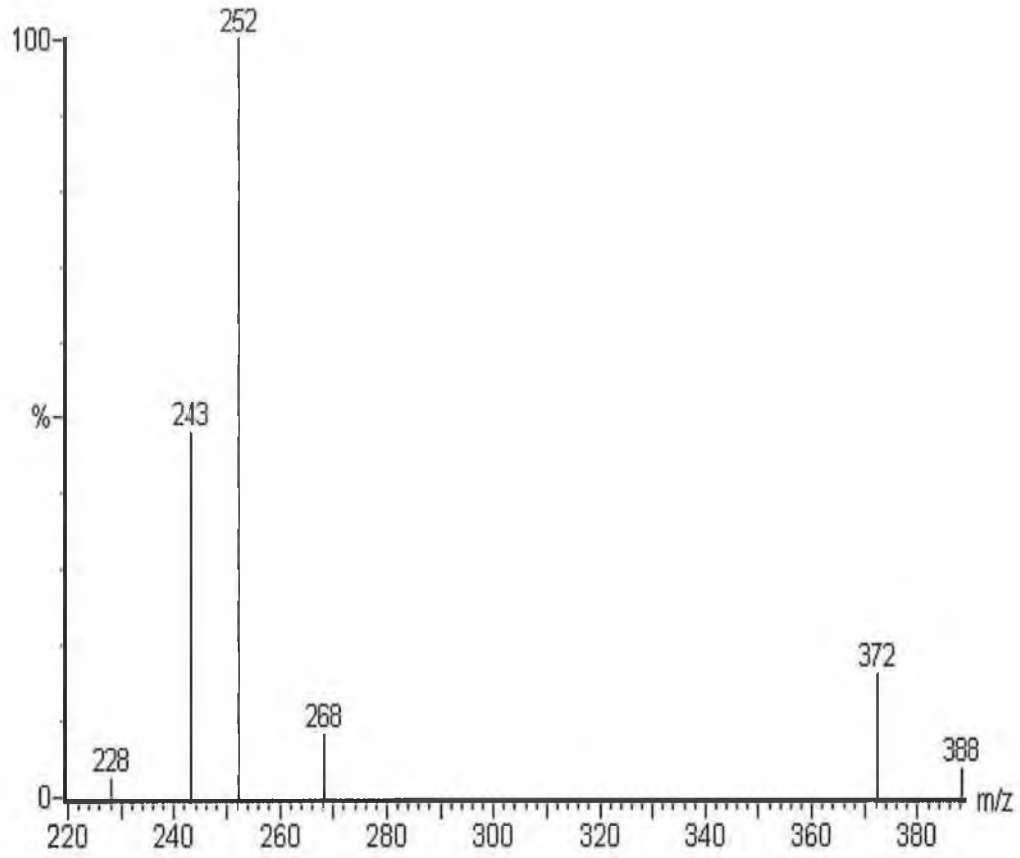

Figure 3.15: *Mass spectrum of the single ion recording (SIR) of m/Z of 228 (dC), 243 (dT), 252 (dA), 268 (dG), 372 (dA-styrene oxide adduct) and 388 (dG-styrene oxide adduct).*

Table 3.2: *Possible product ions of dG-styrene oxide adducts.*

The structure of the adduct	*Possible product ions m/z*
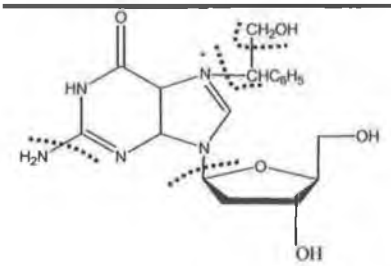	358, 343, 311, 296, 272, 268, 257, 253, 242, 227, 195, 180, 152, 137
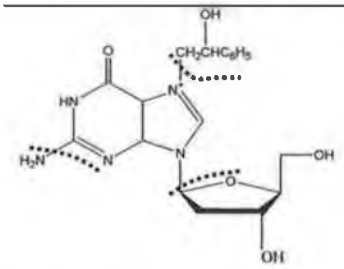	372, 357, 282, 272, 268, 267, 257, 256, 253, 195, 180, 166, 152, 151, 137
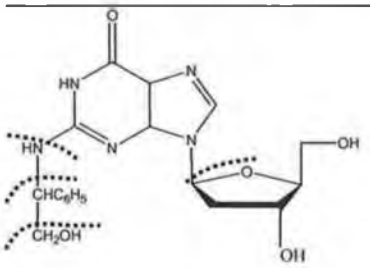	358, 311, 268, 242, 195, 152, 137
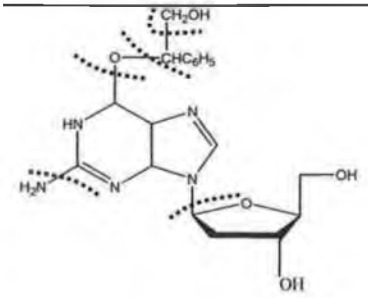	358, 343, 311, 296, 272, 268, 257, 253, 252, 242, 227, 195, 180, 152, 137, 136
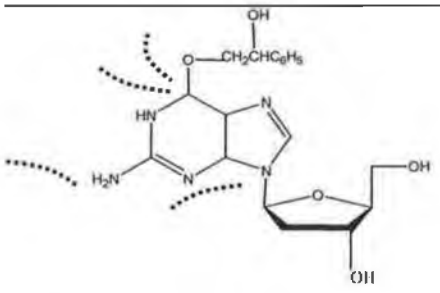	372, 357, 282, 272, 268, 267, 257, 256, 253, 252, 195, 180, 166, 152, 151, 137, 136

3.5 Discussion:

Results described herein demonstrate that ECL can be achieved by direct reaction of a Ru^{III} complex with DNA, in this case by using $[Ru(bpy)_2(PVP)_{10}]^{2+}$ in films with DNA. Alternate layer-by-layer electrostatic assembly provided Ru-PVP/ds-CT DNA films about 10 nm thick, ~ 20 Å, with intimate mixing of Ru-PVP and DNA reactants in a tiny reaction volume. Extensive intermixing of neighbouring layers in polycation/polyanion films assembled by this method has been established by neutron reflectivity studies.[59ab,81]

The ECL response appears to involve mainly the guanine bases in DNA, since no other homopolymeric nucleotides besides Poly[G] (Figure 3.11) gave significant ECL signals in films with Ru-PVP. ECL signals for Ru-PVP/Poly[G] films were 3-fold larger than for films of Ru-PVP and hybridised Poly[G]/Poly[C] (Figure 3.6). There was also a modest response from poly[A] due to Ru^{3+} oxidation of adenine. Films of metallopolymer and ss-DNA gave 2-fold larger ECL intensity than with ds-DNA (Figure 3.7), although the mass of ss-DNA in films was ~18% larger than ds-DNA (Table 3.1). Thus, the ECL yield is sensitive to the hybridisation state of oligonucleotides in the films, a key feature for detecting base mismatches.[33-36]

Figures 3.9 and 3.10 show that direct ECL in Ru-PVP/DNA films can be used to detect DNA damage. Figure 3.10a shows a nearly linear increase in ECL intensity over 20 min when Ru-PVP/ds-DNA films were reacted with styrene oxide under conditions which were confirmed to give styrene-oxide guanine and styrene-oxide adenine adducts in films and in solutions.[72,73] No enhancement of ECL signals was found when the films were incubated with toluene, which does not react with DNA (Figure 3.10). After 5 min reaction with styrene oxide, the ECL peak ratio for ds-DNA films was more than 3-fold greater than the average peak ratio for controls.

The increased ECL peak ratio for DNA films incubated with styrene oxide can be correlated with previous capillary electrophoresis results showing that under similar conditions about 1.2% damage/hr occurs for the first several hours of reaction with styrene oxide.[73] In the present study, we found that a 5 min incubation time gave an ECL peak ratio more than 3-fold larger than the noise (Figure 3.10a). This signal corresponds to an estimated practical detection limit for ECL of about 0.1% damage or 1 damaged base in 1000.

Figures 3.9 and 3.10 also show increased catalytic SWV responses to DNA treated with styrene oxide, but no current increases are observed when the films are treated with unreactive toluene or buffer in control incubations. The development of the ECL and SWV peaks with time agree very well. A similar comparison as above leads to a detection limit for catalytic SWV similar to ECL. This is about the same as for polyion/DNA films with an underlayer of $[Ru(bpy)_2Cl(PVP)_{10}]^+$,[47] which has 5 N-Ru bonds per Ru instead of 6 as in $[Ru(bpy)_2(PVP)_{10}]^{2+}$. $[Ru(bpy)_2Cl(PVP)_{10}]^+$ has a lower formal potential, about 0.8 V vs SCE as opposed to 1.15 V for $[Ru(bpy)_2(PVP)_{10}]$. However, $[Ru(bpy)_2Cl(PVP)_{10}]^+$ cannot produce ECL. Throughout the study the ECL response gave more consistent results, evident from the smaller error bars achieved. Although the ECL could be achieved using SWV or CV, the SWV system used much smaller quantities of both the ruthenium metallopolymer and DNA solutions although this could sometimes result in increased background noise. Not only is this advantageous environmentally but also eliminates problems associated with small samples.

ECL generation involves initial reaction of electrochemically generated $[Ru(bpy)_2(PVP)_{10}]^{3+}$ with a reductant to give a radical. By analogy with previously proposed mechanisms,[57,61] the pathway in these films may be represented:

$$[Ru(bpy)_2(PVP)_{10}]^{2+} \Leftrightarrow [Ru(bpy)_2(PVP_{10})]^{3+} + e^- \quad \textbf{(3)}$$

$$[Ru(bpy)_2(PVP)_{10}]^{3+} + G \rightarrow [Ru(bpy)_2(PVP)_{10}]^{2+} + G^{\bullet} \quad \textbf{(4)}$$

$$G^{\bullet} + [Ru(bpy)_2(PVP)_{10}]^{3+} \rightarrow G_{2ox} + [Ru(bpy)_2(PVP)_{10}]^{2+*} \quad (5)$$

$$[Ru(bpy)_2(PVP)_{10}]^{2+*} \rightarrow [Ru(bpy)_2(PVP)_{10}]^{2+} + h\nu \quad (6)$$

Initial oxidation by electron donation from the metallopolymer to the electrode at sufficiently positive potentials gives the Ru^{III} oxidant (equation 3), which reacts with guanines (G) in DNA to give a guanine cation radical (equation 4). This cation radical can produce Ru^{II}* sites (equation 5), representing the excited state complex, by directly reducing the Ru^{III} sites. G_{ox}^{2+} in equation 5 represents a guanine oxidised by two electrons, a reaction observed[82] in ss-DNA oxidised by dissolved $Ru(bpy)_3^{2+}$.

An alternative is shown in equations 7 and 8, where the guanine cation radical may reduce the Ru^{II} complex to Ru^{I}, which can then produce Ru^{II}* by reacting with Ru^{III}.

$$G^{\bullet} + [Ru(bpy)_2(PVP)_{10}]^{2+} \rightarrow G_{2ox} + [Ru(bpy)_2(PVP)_{10}]^{+} \quad (7)$$

$$[Ru(bpy)_2(PVP)_{10}]^{+} + [Ru(bpy)_2(PVP)_{10}]^{3+} \rightarrow [Ru(bpy)_2(PVP)_{10}]^{2+} + [Ru(bpy)_2(PVP)_{10}]^{2+*} \quad (8)$$

Ru^{2+}* represents the electronically excited state which decays to ground state by emission at ~610 nm (equation 6), providing for the simultaneous detection of ECL along with current. The onset of light emission occurs in a similar potential range as the appearance of the increased reduction current (Figures 3.4-3.9, 3.11)

Ru^{2+}* represents the electronically excited state which decays to ground state by emission at ~610 nm, providing for the simultaneous detection of ECL

along with SWV from the films. The onset of light emission occurs in a similar potential range as the appearance of the increased SWV current. The increase in ECL and SWV peaks with time of incubation with styrene oxide probably reflects a larger average rate of reaction between Ru^{III}-PVP and the chemically damaged DNA compared to the reaction with intact ds-DNA, consistent with the structurally related rate effects found by Thorp *et al.* [38,] As previous suggested when using SWV with soluble $Ru(bpy)_3^{2+}$ or the lower oxidation potential metallopolymer $[Ru(bpy)_2Cl(PVP)_{10}]^+$ to catalyse DNA oxidation in films, guanine in the ds-DNA structure must be less accessible to the oxidant than in damaged or ss-DNA. Covalent adducts of styrene oxide and guanines and adenines disrupt the double helix and allow closer contact between oxidisable moieties on the DNA and the active oxidising agent. Figure 3.11 suggests that there may also be a small contribution to the ECL by styrene oxide-guanine adducts, but the exact nature or degree of this contribution is uncertain at present.

3.6 Conclusion:

In summary, ECL can be obtained directly from the reaction of guanine bases in oligonucleotides in ultrathin films with the catalytic metallopolymer $[Ru(bpy)_2(PVP)_{10}]^{2+}$. The 10 nm films used contained <0.3 μg ds-DNA. The ECL output can be measured simultaneously with SWV catalytic oxidation peaks in a simple apparatus. ECL and SWV peaks are sensitive to oligonucleotide hybridisation and chemical damage of ds-DNA. Thus, direct ECL as described herein may find future applications in films or solutions for DNA detection in applications such as hybridisation or DNA damage estimation.

Mass spectra data confirmed that the styrene oxide-guanine derivatives are produced under similar conditions as those used for the electrochemical detection of adducts. The various adducts obtained from the attack of styrene oxide on different sites on the guanine molecule are also described. Although adducts were also formed with adenine, the guanine derivatives were more pronounced. It has already been established that styrene oxide primarily attacks the guanine base although some damage to the other bases has been observed. This study again concluded that the styrene oxide-guanine adducts were the primary products from this reaction and the formation of other adducts is considerably lower in concentration.

3.7 References:

1 (a) Cadet, J.; Weinfeld, M. *Anal. Chem.* **1993**, *65*, 675A.
(b) Santella, R. *Cancer Epidim. Biomarkers Prevent.* **1999**, *8*, 733.
(c) Primrose, S. B. *Principles of Genome Analysis*, 2nd Ed., Blackwell: Oxford, U.K. 1998.
(d) Baxevanis, A. D.; Ouellette, B. F. *Bioinformatics: Practical Guide to Analysis of Genes and Proteins*. In *Methods Biochem. Anal.* **1998**, *39*, 1.

2 S. R. Mikkelsen, *Electroanalysis*, **1996**, *8*, 15.

3 M. Yang, M. E. McGovern, M. Thompson, *Anal. Chim. Acta*, **1997**, *346*, 259.

4 H. H. Thorp, *Trends Biotechnol.*, **1998**, *16*, 117.

5 J. Wang, *J. Chem. Eur.*, **1999**, *5*, 1681.

6 X-H. Xu, A. J. Bard, *J. Am. Chem. Soc.*, **1995** , *117*, 2627.

7 W. Schrader, M. Linscheid, *J. Chromatgr. A,* **1995** , *717*, 117.

8 M. Koskinen, K. Plna, *Chem-Biol. Interact.*, **2000**, *129*, 209.

9 A. Mugweru, J. F. Rusling, *Electrochem. Commun.*, **2001**, *3*, 406.

10 W. Pauwels, H. Veulemans, *Mutat. Res.*, **1998**, *418*, 21.

11 K. Hemminki, M. Koskinen, H. Rajaniemi, C. Zhao, *Regulat. Toxicol. Pharmacol.*, **2000**, *32*, 264.

12 S. E. Beard, S. R. Caoldi, P. Gee, *Mutat. Res.*, **1996,** *371*, 1.

13 K. Hemminki, *Carcinogenesis,* **1993**, *14*, 2007.

14 E. E. McConnell, J. A. Swenberg, *Crit. Re.v Toxicol.*, **1994**, *24*, S49.

15 F. J. C. Roe, *Crit. Rev. Toxicol.*, **1994**, *24*, S117.

16 F. Jelen, E. Palacek, *Biophys. Chem.*, **1986**, *24*, 285.

17 C. Teyero, P. Perez, E. Palacek, *Bioelectrochem. Bioenerg.*, **1995**, *38*, 77.

18 P. Vodicka, L. Vodickova, K. Hemminki, *Carcinogenesis*, **1993**, *14*, 2059.

19 S. Contoreggi, W. K. Lutz, *Carcinogenesis*, **1993**, *14*, 355.

20 W. Pauwels, P. Vodicka, M. Severi, K. Plna, H. Veulemans, K. Hemminki, *Carcinogenesis*, **1996**, *7*, 2673.

21 *Monographs on the evaluation of carcinogenic risks to humans, No. 60, Some industrial chemicals,* IARC, Lyon, **1994**; pp. 45-213 and 233-346, IARC, Lyon, **1993**; K. Hemminki.

22 K. Hemminki, P. Vodicka, *Toxicol. Lett.*, **1995**, *77,* 153.

23 S. M. Rappaport, K. Yeowell-O'Connell, *Toxicol. Lett.*, **1999**, *108*, 117.

24 M. Otteneder, U. Lutz, W. K. Lutz, *Mutat. Res.*, **2002**, *500*, 111.

25 M. Koskinen, E. K. H. Schweda, K. Hemminki, *J. Chem. Soc., Perkin Trans. 2,* **1999** 2441.

26 M. Koskinen, L. Vodickove, P. Vodicka, SC. Warner, K. Hemminki, *Chem.-Biol. Interact.*, **2001**, *138*, 111.

27 F. Latif, R. C. Moschel, K. Hemminki, *Chem. Res. Toxicol.*, 1 **(1988)** 364.

28 C. Qiun, A. Dipple, *Chem. Res. Toxicol.*, **1995**, *8*, 389.

29 R. R. Selzer, A. A. Elfarra, *Arch. Biochem. Biophys.*, **1997**, *343*, 63.

30 T. Barlow, A. Dipple, *Chem. Res. Toxicol.*, **1999,** *12*, 883.

31 M. Koskinen, D. Calebiro, K. Hemminki, *Chem.-Biol. Interact.*, **2000**, *126*, 201.

32 K. Savela, A. Hesso, K. Hemminki, *Chem.-Biol. Interact.*, **1986**, 235.

33 Mikkelsen, S. R. *Electroanalysis*, **1996**, *8*, 15.

34 Thorp, H. H. *Trends Biotechnol.*, **1998**, 16, 117.

35 Wang, J. *Chem. Eur. J.* **1999**, *5*, 1681.

36 Palacek E.; Fojta, M. *Anal. Chem.* **2001,** *73*, 74A.

37 Johnston, D. H.; Glasgow, K. C.; Thorp, H. H. *J. Am. Chem. Soc.,* **1995**, *177,* 893.

38 Armistead, P. M.; Thorp, H. H. *Anal. Chem.,* **2001**, *73,*558.

39 Napier, M. E.; Thorp, H. H. *Langmuir*, **1997**, *13*, 6342.

40 Farrer, B. T.; Thorp, H. H. *Inorg. Chem.*, **2000**, *39*, 44.

41 Yang, I. V.; Thorp, H. H. *Inorg. Chem.*, **2000**, *39*, 4969.

42 Sistare, M. F.; Codden, S. J.; Heimlich, G.; Thorp, H. H. *J. Am. Chem. Soc., 122*, **2000**, 4742.

43 Szalai, V. A.; Thorp, H. H. *J. Phys. Chem. A, 104*, **2000**, 6851.

44 Onkto, A. C.; Armistead, P. M.; Kircus, S. R.; Thorp, H. H. *Inorg. Chem.,* **1999**, *38,* 1842.

45 Zhou, L.; Rusling, J. F. *Anal. Chem.,* **2001**, *73*, 4780.

46 Mugweru, A.; Rusling, J. F. *Electrochem. Commun.,* **2001**, *3,* 406.

47 Mugweru, A.; Rusling, J. F. *Anal. Chem.*, 2002, *74*, 4044.

48 Gerardi, R. D.; Barnett, N. W.; Lewis, S. W. *Anal. Chim. Acta,* **1999**, *378*, 1.

49 Fähnrich, K.A.; Pravda, M.; Guilbault, G. G. *Talanta*, **2001**, *54*, 531.

50 Xu, X.-H.; Yang, H. C.; Mallouk, T. E.; Bard, A. J. *J. Am. Chem. Soc.,* **1994**, *116*, 8386.

51 Xu, X.-H.; Bard, A. J. *J. Am. Chem. Soc.,* **1995**, *117*, 2627.

52 Leland, J. K.; Powell, M. J. *J. Electrochem. Soc.* **1990**, *137*, 3127.

53 Blackburn, G. F.; Shah, H. P.; Kenten, J. H.; Leland, J.; Kamin, R. A.; Link, J.; Petermann, J.; Powell, M. J.; Shah, A.; Talley, D. B.; Tyagi, S. K.; Wilkins, E.; Wu, T.-G.; Massey, R. J. *Clin. Chem.,* **1991**, *37*, 1534.

54 Gudibande, S. R.; Kenten, J. H.; Link, J.; Massey, R. J. *Mol. Cell Probes,* **1992**, *6*, 495.

55 Ege, D.; Becker, W. G.; Bard, A. J. *Anal. Chem.,* **1984**, *56*, 2413.

56 Kenten, J. H.; Casedei, J.; Link, J.; Lupold, S.; Willey, J.; Powell, M.; Rees, A.; Massey, R. J. *Clin. Chem,* **1991**, *37*, 1626.

57 Rubinstein, I.; Bard, A. J. *J. Am. Chem. Soc.,* **1980**, *102*, 6642.

58 Geise, B. *Acc. Chem. Res.* **2000**, *33*, 631.

59 (a) Lvov, Y. in Lvov, Y., Möhwald, H., Eds., *Proteins Architecture: Interfacing Molecular Assemblies & Immobilization Biotechnology,* Marcel Dekker: New York, **2000**, pp. 125 – 167.
(b) Lvov, Y. in Nalwa, R.W., Ed.; *Handbook Of Surfaces And Interfaces Of Materials, Vol. 3. Nanostructured Materials, Micelles And Colloids;* Academic Press; San Diego, **2001**, pp. 170 – 189.

(c) Rusling, J.F.; in Lvov, Y.; Möhwald, H., Eds., *Proteins Architecture: Interfacing Molecular Assemblies & Immobilization Biotechnology,* Marcel Dekker: New York, **2000**, pp. 337 – 354.

(d) Rusling, J.F.; Zhang, Z.; in Nalwa, R.W., Ed.; *Handbook Of Surfaces And Interfaces Of Materials, Vol. 5. Biomolecules, Biointerfaces, And Applications;* Academic Press; San Diego, **2001**, pp. 33 – 71.

60 Lvov, Y.; Ariga, K.; Ichinose, I.; Kunitake, T., *J. Am. Chem. Soc.*, **1995**, *117*, 6117.

61 Hogan, C. F.; Forster, R. J. *Anal. Chem.,* **2000**, *72*, 5578.

62 Hogan, C. F.; Forster, R. J. *Anal. Chim. Acta,* **1999**, *396*, 13.

63 Vodocka, P.; Hemminki, K. *Carcinogenesis,* **1988**, *9*, 1657.

64 Pauwels, W.; Veulemans, H. *Mutat. Res.,* **1998**, *418,* 21.

65 Hemminki, K.; Koskinen, M.; Rajaniemi, H.; Zhao, C. *Regulat. Toxicol. Pharmacol.,* **2000,** *32,* 264.

66 Hemminki, K. *Carcinogenesis,* **1993**, *14,* 2007.

67 McConnell, E. E.; Swenberg, J. A. *Crit. Rev. Toxicol.,* **1994**, *24,* S49.

68 Nestmann, E. R.; Bryant, D. W.; Carr, C. J.; Fennell, T. T.; Gorelick, N. J.; Gallagher, J. E.; Swenberg, J. A.; Williams, G. M. *Regul. Toxicol. Pharmacol.,* **1996**, *24*, 9.

69 Jelen, F.; Palacek, E. *Biophys. Chem.,* **1986**, *24,* 285.

70 Contoreggi, S.; Lutz, W. K. *Carcinogenesis*, **1993**, *14,* 355.

71 Pauwels, W.; Vodicka, P.; Severi, M.; Plna, K.; Veulemans, H.; Hemminki, K. *Carcinogenesis*, **1996**, *7,* 2673.

72 Zhou, L.; Yang, J.; Estavillo, C.; Stuart, J. D.; Schenkman, J. B.; Rusling, J. F. *J. Am. Chem. Soc.*, in press

73 Yang, J., Zhang, Z.; Rusling, J. F. *Electroanalysis.*, in press.

74 Zu, X.; Lu, Z.; Zhang, Z.; Schenkman, J. B.; Rusling, J. F. *Langmuir*, **1999**, *15*, 7372.

75 Tarcun, M.; Rusling, J. F., *Anal. Chem.,* **2004**, *submitted.*

76 Zhou, L.; Yang, J.; Estavillo, C.; Stuart, J. D.; Schenkman, J. D.; Rusling, J. F., *Am. Chem. Soc.*, **2003**, *125,* 1431.

77 Norwood, C. B.; Jackim, E.; Cheer, S., *Anal. Biochem.*, **1993**, *213*, 194.

78 Zhou, L., *Ph.D. Thesis*, University of Connecticut **2003**.

79 Koskinen, M.; Vodicka, P.; Hemminki, K., *Chem.-Bio., Interact.*, **2000**, *124,* 13.

80 Vodicka, P.; Hemminki, K., *Carcinogenesis*, **1998**, *9*, 1657.

81. Decher, G. *Science*, **1997**, *227*, 1232.

82 Armistead, P. M.; Thorp, H. H. *Anal. Chem.*, **2001**, *73,*558.

CHAPTER 4

DIRECT ELECTROCHEMILUMINESCENCE DETECTION OF OXIDISIED DNA IN ULTRATHIN POLYMER FILMS CONTAINING $[Os(bpy)_2(PVP)_{10}]^{2+}$

"The great tragedy of Science – the slaying of a beautiful hypothesis by an ugly fact"

Thomas H. Huxley

4.1 Introduction:

Direct electrochemiluminescence (ECL) involving oxidised DNA was demonstrated in ultrathin films of cationic polymer $[Os(bpy)_2(PVP)_{10}]^{2+}$ assembled layer-by-layer with DNA and oligonucleotides. A square wave voltammetric waveform oxidised Os^{II} sites in the films at ~0.6 V vs. SCE to Os^{III}. ECL was measured simultaneously with catalytic square wave voltammetry in a simple apparatus after oxidation of films with Fenton reagent (0.15 mM $FeSO_4$ + 5 mM H_2O_2). Significant ECL generation at 0.6 V occurred when oxidised guanines were present on oligonucleotides in the films, suggesting that $[Os(bpy)_2(PVP)_{10}]^{2+}$ is a specific electrochemical catalyst for 8-oxo-guanine sites in presence of guanine. This result, along with knowledge of previously suggested ECL pathways suggests, that a species initially formed by oxidation of 8-oxo-guanine by electrogenerated Os^{III} reacts with osmium sites to produce electronically excited Os^{II}*. The behaviour of thin films combining DNA, $[Ru(bpy)_2(PVP)_{10}]^{2+}$ and $[Os(bpy)_2(PVP)_{10}]^{2+}$ is presented here with the intention of the Os^{II} sites being catalytically specific for 8-oxo-guanine and Ru^{II} sites, with higher oxidising power (1.2 V), reporting on oxo-adenine formation and possible strand cleavage. The detection of both chemical and oxidative DNA damage is possible with the latter films.

Oxidative stress in mammals damages DNA,[1] generating lesions that may contribute to aging and mutagenesis.[2-5] More than 20 major oxidatively-formed DNA adducts have been characterised.[6] Oxidative DNA damage occurs from chemical reactions, irradiation, and reactive oxygen species (ROS) generated during metabolism,[7] including singlet oxygen, superoxide and hydroxyl radicals.[7c] Reaction of DNA with hydroxyl radical[7,8] causes single base modifications, yielding 8-oxoguanine (8-oxoG), 8-oxoadenine, thymine glycol and 8-hydroxycytosine, shown in Figure 4.1, as well as strand breaks and crosslinks.[9]

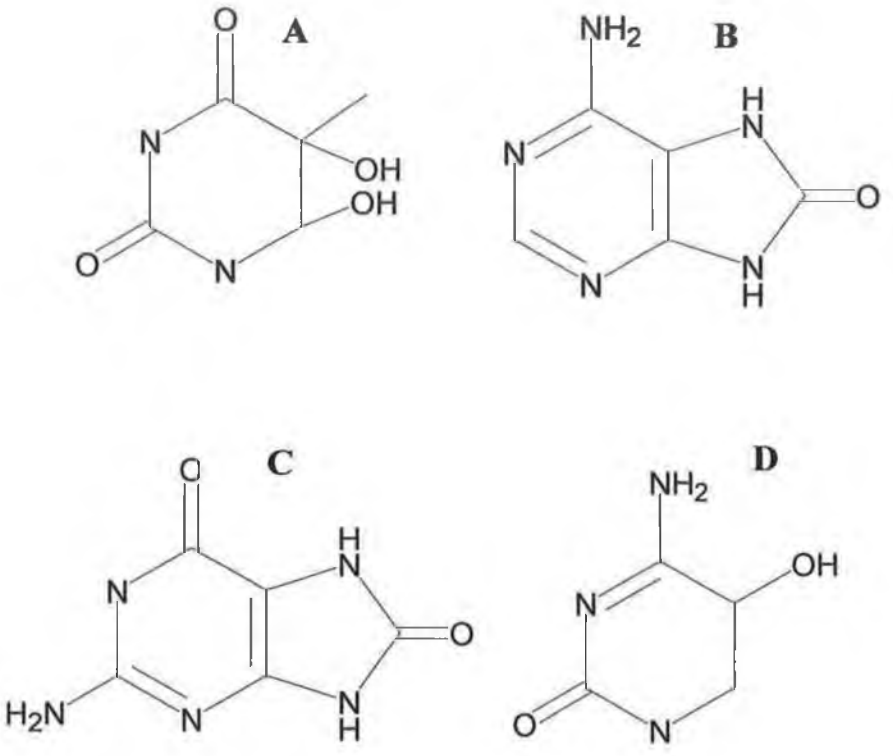

Figure 4.1: *Products of hydroxyl radical attack on the DNA bases, A is thymine glycol, B is 8-oxoadenine, C is 8-oxoguanine and D is 8-hydroxycytidine.*

Hydroxyl radicals are generated from Fe^{II} and hydrogen peroxide in the Fenton reaction.[10] Iron-mediated reactions may contribute substantially to H_2O_2-mediated damage to DNA.[11,12] H_2O_2-dependent DNA damage is thought to be due to Fenton chemistry generated by the Fe^{II} found within the human body, and used primarily for the transport of oxygen, as such it can interact readily with DNA.[13,14]

8-OxoG is one of the major products of nucleobase oxidation for which specific cellular repair enzymes exist.[7] It has been suggested as a clinical biomarker for oxidative stress.[15] When present in DNA, 8-oxoG caused G-to-T transversions, shown in Figure 4.3, and A-to-C substitutions.[16,17] While guanine is the most easily oxidised of the natural nucleobases,[18] 8-oxoG has a much lower oxidation potential[19] and is itself oxidized more easily. Its major oxidation products are guanidinohydantoin and 2-amino-4,5,6-trioxypyrimidine as shown in Figure 4.2.[20] Guanidinohydantoin in ss-DNA was recently found to be highly mutagenic and caused G-to-T transversions.[21] This is, however; an active area of research and it is clear that much additional work is yet to be preformed to determine the exact percentage of each oxidation product as well as their specific toxicities. Therefore, in Figure 4.2, all of these products could theoretically be the final product of DNA oxidation, however; this has yet to be proven that these reactions even happen *in vivo* and if they do to what extent each scheme occurs.

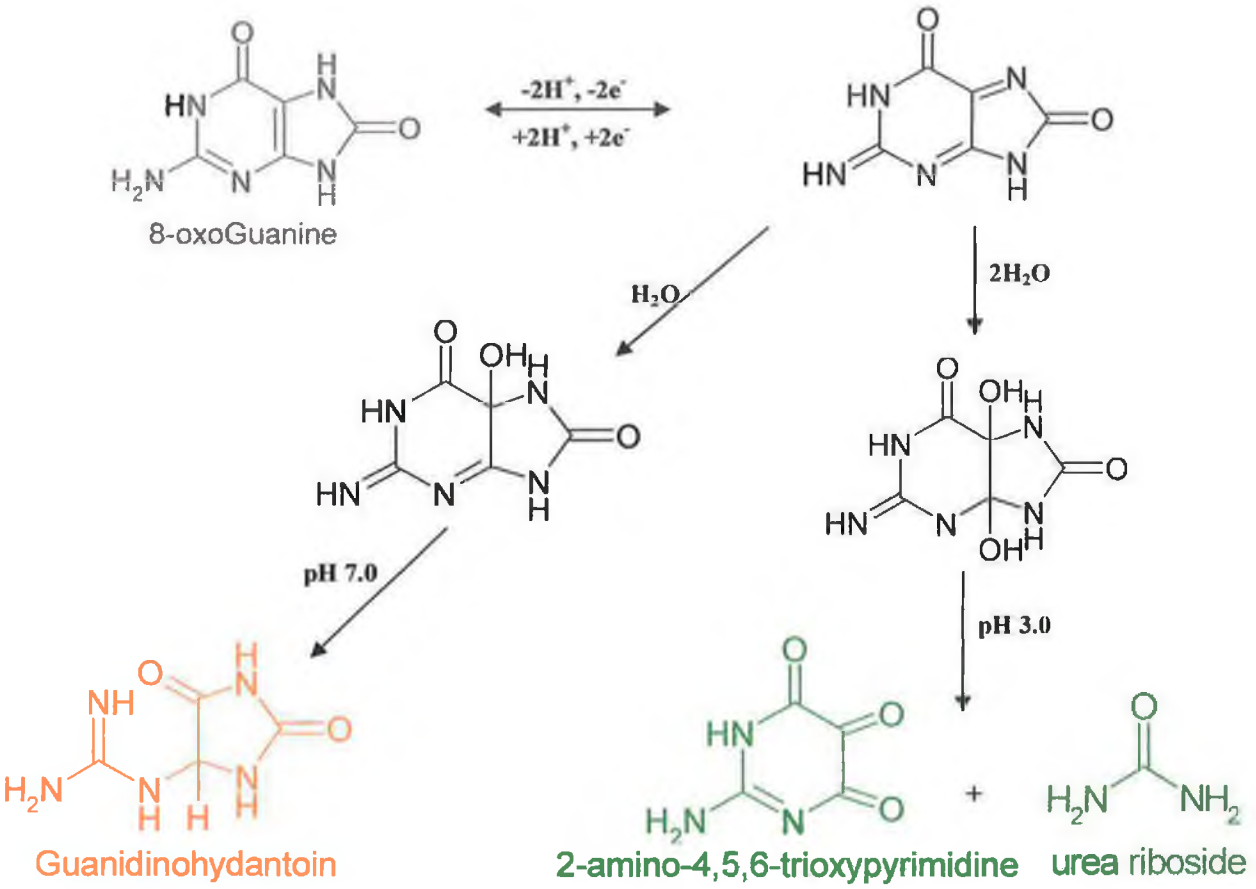

Figure 4.2: *Proposed scheme for 8-oxoGuanine oxidation. Adapted from reference 22.*

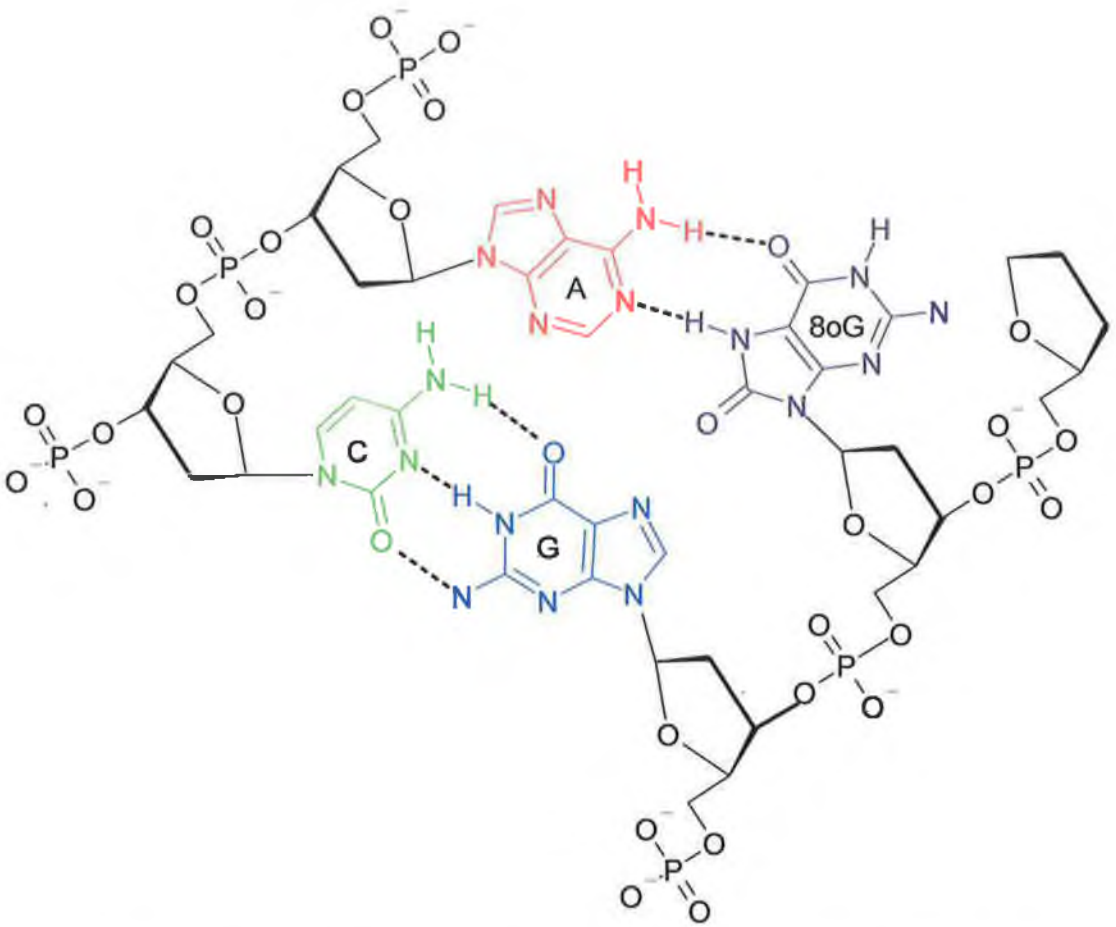

Figure 4.3: *Watson-Crick base pair C:G and Hoogsten base pair A:8-oxoG in the DNA double helix.*

The oxidation of guanine to form 8-oxoguanine has been well studied, and based on electrochemical studies, it has been concluded that it involves a two proton (2 H^+), two electron (2 e^-), oxidation. [22] It was also observed that oxidation to 8-oxoG occurs over a wide pH range, from pH 2.5 to 10.0. The initial reaction involves 1 H^+, 1 e^- oxidation of G to give the free radical, G·, which undergoes further oxidation to give 8-oxoG. The initial step was studied by Weatherly *et al.*, [23] who concluded that both the proton and the electron were removed in a single step, *i.e.* that the reaction was a proton-coupled electron transfer (PCET). G was able to transfer its proton to the solvent from within the double helix on a time scale that allowed for the coupling of the electron and proton transfers. When G oxidation occurred in a medium that did not accept protons the reaction was slowed dramatically, as it was forced to from a protonated radical cation. A proposed scheme for the two step, 2 H^+, 2 e^- oxidation of G is outlined in Figure 4.4.

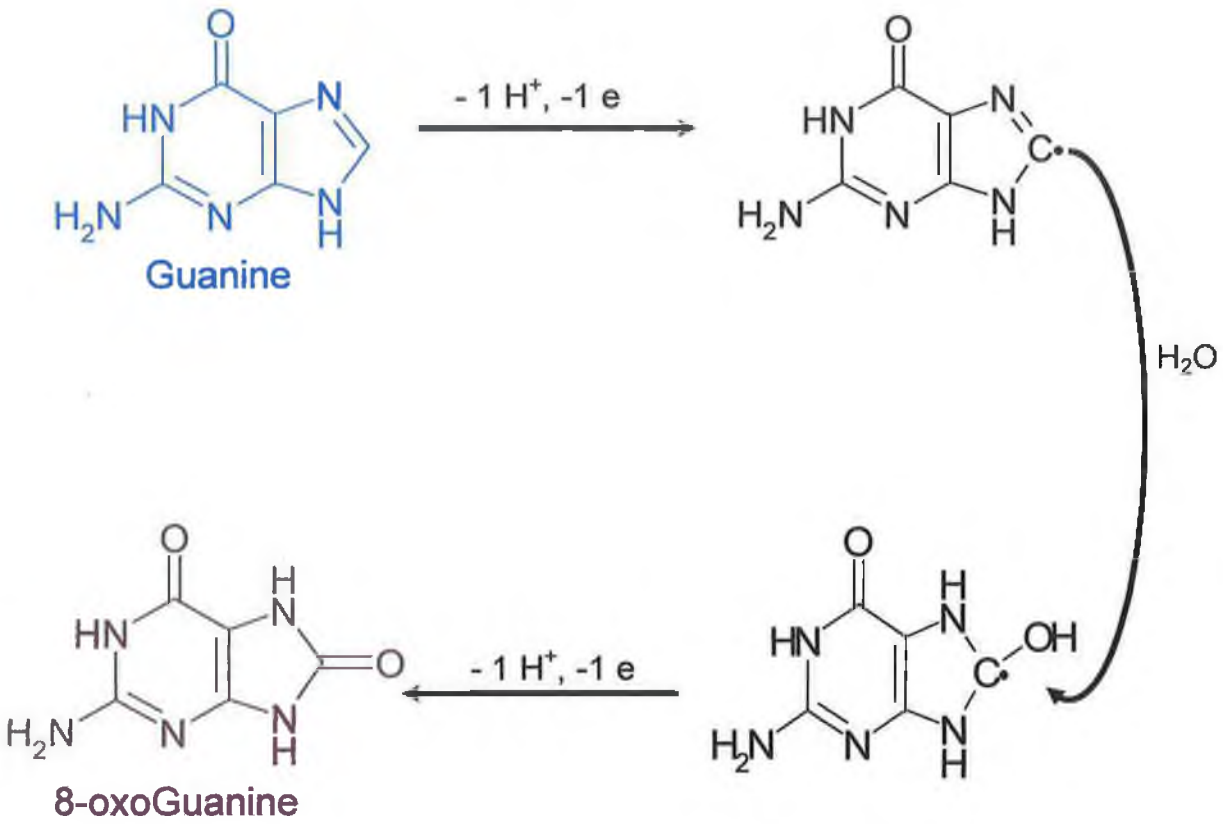

Figure 4.4: *Proposed scheme for guanine oxidation to 8-oxoguanine. Adapted from reference 24.*

8-OxoG in DNA can be determined specifically by liquid chromatography (LC) coupled to a mass spectrometer (MS) or an electrochemical (EC) detector.[15,25] The DNA requires hydrolysis and the electrochemical detector must employ a potential positive enough to oxidise 8-oxoG but low enough not to oxidise guanine, which elutes at similar retention time. LC-EC was recently used to observe the time course of 8-oxoG generation by reacting hydroxyl radicals with DNA in vitro.[26] The present requirements for hydrolysis of DNA and separation of the nucleobases make LC-based methods very labour intensive and expensive for routine clinical applications. The long-term goal of this work is to develop biosensor alternatives that can detect DNA oxidation without hydrolysis or expensive instrumentation.

Electroanalysis provides instrumentally simple, sensitive and inexpensive approaches to detect DNA hybridization and damage. [27-31] Previously it was shown that oxidation of guanines in DNA by electrochemically generated $[Ru(bpy)_2(PVP)_{10}]^{3+}$ in ultrathin films leads to photoexcited $[Ru(bpy)_2]^{2+}$* sites in the film that decays to generate electrochemiluminescence (ECL).[33] No sacrificial oxidant is required. The reaction is initiated by an electrochemical catalytic oxidation of guanine sites in DNA similar to that reported by Thorp *et al.*[34] for soluble $[Ru(bpy)_3]^{2+}$. This thin-film ECL approach was utilised to detect DNA damage from styrene oxide, as described in Chapter 3.[33]

Ropp and Thorp showed that 8-oxoG is oxidised selectively by $[Os(bpy)_3]^{3+}$ in the presence of guanine.[35] $[Os(bpy)_3]^{2+}$ has a much lower redox potential ($E_{1/2}$ = 0.62 V) than $[Ru(bpy)_3]^{2+}$, and so does not oxidise guanines in DNA. $[Os(bpy)_3]^{2+}$ catalyses the oxidation of 8-oxoG in the following catalytic pathway: [36]

$$[Os(bpy)_3]^{2+} \leftrightarrow [Os(bpy)_3]^{3+} + e^- \quad \textbf{(1)}$$

$$[Os(bpy)_3]^{3+} + DNA(8-oxoG) \rightarrow [Os(bpy)_3]^{2+} + DNA(8-oxoG^+) \quad \textbf{(2)}$$

This pathway was used to probe telomerase function in DNA using 8-oxoG placed at specific sites,[35] and to investigate intermolecular vs. intramolecular reactivity of $[Os(bpy)_3]^{2+}$-tagged oligonucleotides.[37]

$[Os(bpy)_3]^{2+}$ is capable of generating ECL if oxidised in the presence of a sacrificial reductant such as oxalate.[38] Electrochemical catalytic oxidation of 8-oxoG with $[Os(bpy)_3]^{2+}$ is analogous to the oxidation of guanine with metallopolymer $[Ru(bpy)_2(PVP)_{10}]^{2+}$ that generates ECL from DNA directly without a sacrificial oxidant. It was hypothesised that catalytic oxidation of 8-oxoG in DNA with the polymer $[Os(bpy)_2(PVP)_{10}]^{2+}$ might lead to photoexcited $[Os(bpy)_3]^{2+}$* sites to provide ECL signals, if the free energy of activation is still sufficient for 8-oxoG to generate an excited osmium site. It is reported here that ultrathin films containing $[Os(bpy)_2(PVP)_{10}]^{2+}$ and oligonucleotides on electrodes can directly generate ECL to detect oxidised guanines in DNA without using a sacrificial reductant. Films combining $[Ru(bpy)_2(PVP)_{10}]^{2+}$ and $[Os(bpy)_2(PVP)_{10}]^{2+}$ can be used to detect significantly more DNA oxidation than the previous system which incorporated the ruthenium metallopolymer only.

4.2 *Apparatus and Reagents:*

$[Ru(bpy)_2(PVP)_{10}](ClO_4)_2$ and $[Os(bpy)_2(PVP)_{10}]Cl_2$ were prepared, purified and characterised as described previously in chapter 2.[39-41]Standard time-resolved luminescence gave quantum yields and luminescence lifetimes.[42]

Calf Thymus (CT) double stranded (ds) DNA ((Sigma, type XV, 13,000 avg. base pairs, 41.9% G/C), CT ss-DNA, Salmon Testes (ST) ds-DNA (Sigma, ~2,000 avg. base pairs, 41.2% G/C), ST ss-DNA, polyguanadylic acid (5') (Poly [G]), polycytidylic acid (5') (Poly [C]), styrene oxide, toluene and iron (II) sulphate were from Sigma and polyadenylic acid (5') (Poly [A]) was from ICN Biomedical Research Products. Water was purified with a Hydro Nanopure system to specific resistance >18 mΩ-cm. All other chemicals were reagent grade.

Simultaneous square wave voltammetry (SWV)-ECL measurements were made in a 3-electrode electrochemical cell at 37.0±0.5 °C using a CH Instruments Model 660a electrochemical analyzer. The cell employed a saturated calomel reference electrode (SCE), a Pt wire counter electrode, and a 4 mm diameter disk of ordinary basal plane pyrolytic graphite (PG, Advanced Ceramics) as working electrode placed close to the glass cell bottom. The electrolyte solution was 10 mM acetate buffer, pH 5.5, containing 50 mM NaCl. SWV conditions were 4 mV step height, 25 mV pulse height, and frequency 5 Hz. The cell was covered with a black cloth to avoid external light and possible photodecomposition of the metallopolymers. Solutions were purged with pure nitrogen for 15 min prior to each series of experiments and a nitrogen atmosphere was maintained during data collection. A different electrode was used for each analysis of DNA oxidation, as the oxidative analysis modifies the nucleic acids in the film.

A Labmaster Coherent Ultima photomultiplier /monochrometer/data collection system was used to record light from the electrode (764 and 610 nm) via an optical fibre positioned directly underneath the electrode outside the flat bottom of the glass electrochemical cell, (See Figure 3.3).

DNA-metallopolymer films were constructed by layer-by-layer alternate electrostatic assembly.[43-45] Basal plane PG electrodes were polished with 400 grit SiC paper and then with α-alumina slurries on Buehler Microcloth, washed with water and sonicated in ethanol for 15 min, then sonicated in water for 15 min. Layers were constructed by placing 30 μL drops of 0.2% aqueous 50:50 $[Ru(bpy)_2(PVP)_{10}]^{2+}$:$[Os(bpy)_2(PVP)_{10}]^{2+}$ onto each PG electrode, allowing 15 min to achieve saturated adsorption,[45] then washing with water. Subsequently, 30 μL of DNA solution (2 mg mL^{-1} DNA in 5 mM pH 5.5 acetate buffer + 0.05 M NaCl) was placed on this PG surface, allowed to adsorb 15 min, and then washed with water. This sequence was repeated to obtain films with 2 metallopolymer/DNA bilayers. Films containing ss-DNA and polynucleotides were also assembled in this way.

Assembly of films was assessed at each step with a quartz crystal microbalance (QCM, USI Japan) using 9 MHz QCM resonators (AT-cut, International Crystal Mfg.). To mimic the carbon electrode surface, a negative monolayer was made by treating gold-coated (0.16±0.01 cm^2) quartz resonators with 0.7 mM 3-mercapto-1-propanol and 0.3 mM 3-mercaptopropionic acid in ethanol.[43] Films were assembled as for PG electrodes. Resonators were dried in a stream of nitrogen before measuring the frequency change (ΔF). Absorbed mass was estimated with the Sauerbrey equation,[45] for 9 MHz quartz resonators, giving dry film mass per unit area M/A as:

$$M/A \text{ (g cm}^{-2}) = - \Delta F \text{ (Hz)} / (1.83 \times 10^8) \quad \textbf{(3)}$$

The nominal thickness (d) of dry films was estimated with an expression confirmed by high resolution electron microscopy:[46]

$$d \text{ (nm)} \approx (-0.016 \pm 0.002)\ \Delta F \text{ (Hz)} \quad \textbf{(4)}$$

Films were incubated a stirred reactor at 37.0±0.5 °C. 100 μL of 15 mM $FeSO_4$ and 1 mL H_2O_2 (Fenton reagent) was added to 9 mL acetate buffer, pH 5.5 + 50 mM NaCl, to give final concentrations 0.15 mM $FeSO_4$ and 5.0 mM H_2O_2. pH 5.5 allows efficient ECL

production.[47] PG electrodes coated with polynucleotide/metallopolymer films were incubated in the stirred solutions, which had been degassed using nitrogen gas, then rinsed with water and transferred to the electrochemical cell containing fresh pH 5.5 buffer for SWV/ECL analysis.

The hydrolysis for the chromatographic analysis was slightly different to that utilised for the voltammetic analysis. 0.16 mg/mL DNA was incubated with 150 μM iron (II) sulphate and 50 mM H_2O_2 at 37 °C with constant stirring. 100 μL aliquots were taken every five minutes from 0 to 90 minutes. The reaction was quenched with 1 mL 200 proof ethanol. 50 μL 10 mM Uracil was added as an internal standard and the solution was dried immediately under a stream of nitrogen gas. It was then hydrolysed by adding 600 μL 88% (v/v) formic acid in evacuated and sealed Pierce hydrolysis tubes and heated at 140 °C for 30 minutes in a vacuum. The dried hydrosylates were refrigerated at 4 °C until further use. Prior to analysis they were re-dissolved in 1 mL 50 mM ammonium acetate buffer at pH 5.5.[26]

The HPLC system consisted of a Waters (Waters Millipore, Milford, MA) Model 660E pump, and a Waters Lambda-Max model 481 LC-spectrophotometer. A Restek Ultra C-18 reversed phase (i.d. 4.6 mm, length 250 nm, particle size 5 μm) with 1 cm guard column was used. The mobile phase comprised of 5% methanol/95% 50 mM ammonium acetate buffer, pH 5.5, run under isocratic conditions at a flow rate of 1 mL/min. For UV detection of the unmodified bases, the detector was set to 254 nm. The electrochemical detector was coupled in series with the UV detector. It consisted of a BAS CC-4 electrochemical cell and a BAS LC-4C amperometric detector. An Ag/AgCl reference electrode and a glassy carbon working electrode were used, and the potential across the cell was set at 550 mV.

For Mass spectrometry, a Micromass Quadropole II was used with a shorter Restek Ultra C-18 reversed phase (i.d. 2.1 mm, length 150 mm) with a guard column. A flow rate of 0.3 mL/min was used with a mobile phase of 5% methanol/95% 17 mM ammonium acetate buffer to prevent any ionisation suppression. Full scan spectra were taken at a cone voltage of 15 V using positive electrospray ionisation (ESI).

All chromatograms were generated using Hewlett Packard 3395 integrators. UN-SCAN-IT digitising software (Silk Scientific, Utah) was used to digitise the chromatograms which were then imported into KaleidaGraph® or MS Office Excel.

4.3 Results

4.3.1 QCM Monitoring of Film Assembly

Based on previous studies of the influence of number of layers on ECL efficiency in $[Ru(bpy)_2(PVP)_{10}]$/DNA films,[33] these studies utilised films with two bilayers of ds-DNA interspaced with $[Os(bpy)_2(PVP)_{10}]^{2+}$ (Os) or with 1:1 mixed layers of metallopolymers $[Ru(bpy)_2(PVP)_{10}]$ (Ru) and (Os) denoted $(Ru\text{-}Os/DNA)_2$. Integrity and reproducibility of film formation was first characterised by measuring QCM frequency shifts (ΔF) after each layer of film growths illustrated for films of DNA and mixed metallopolymers (Figure 4.5). $-\Delta F$ values varied linearly with layer number for ss-DNA and ds-DNA alternated with Ru-Os-PVP layers suggesting regular film growth with reproducible layers formation. The ΔF-values were used in conjunction with equations 3 and 4 to estimate weights of metallopolymers and DNA and the average nominal thickness of the films (Table 4.1). Total film thicknesses were ~16 nm, with each film containing about 3 $\mu g\ cm^{-2}$ DNA. A slightly larger amount of ss-DNA than ds-DNA was incorporated into films, as also found for DNA in films with other polycations.[43] Similar results were obtained if calf thymus was substituted for the salmon testes DNA.

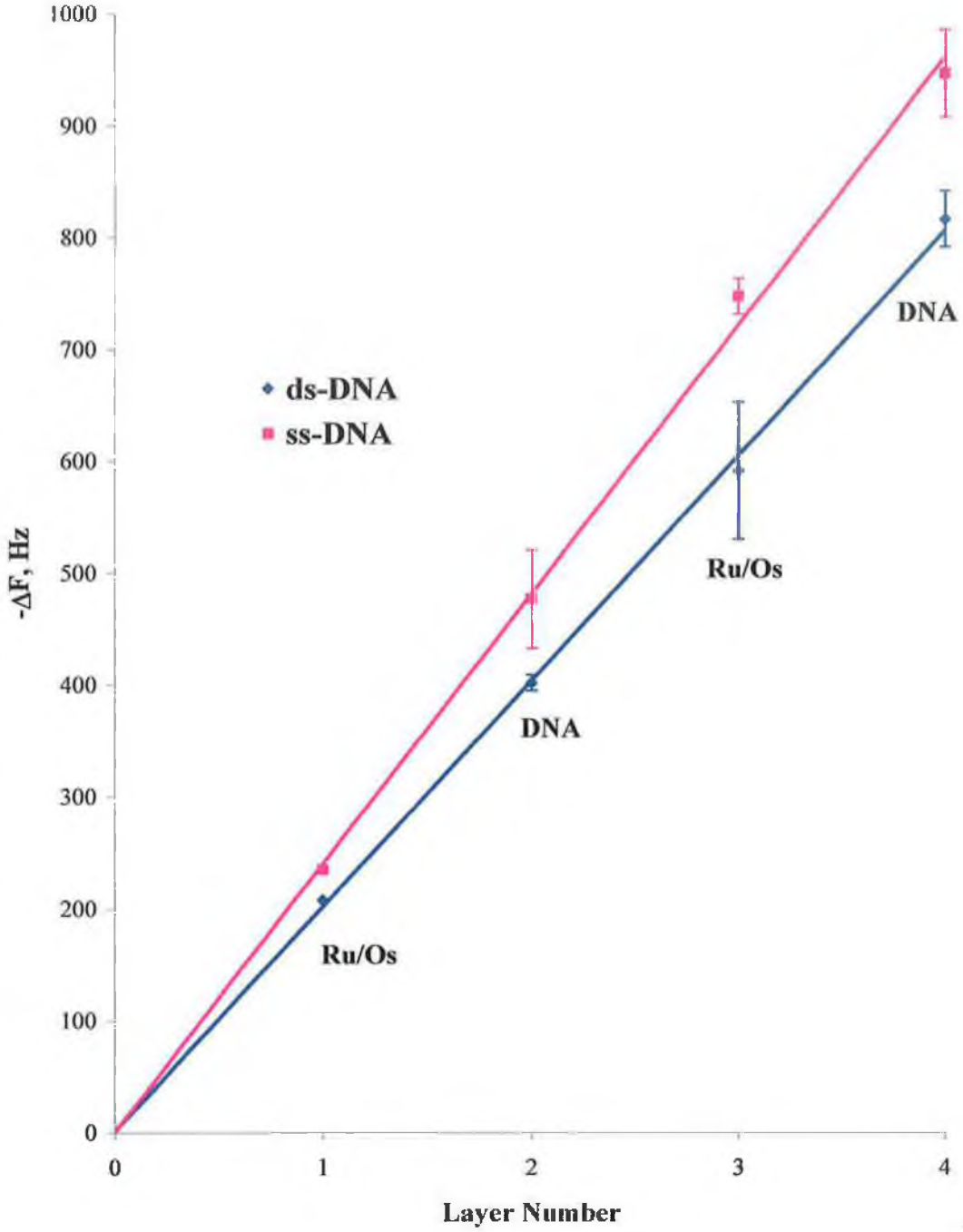

Figure 4.5: *QCM frequency shifts monitoring film formation on gold-quartz resonators coated first with mixed monolayers of mercaptopropionic acid/mercaptopropanol for alternate adsorption of 1:1* $[Os(bpy)_2(PVP)_{10}]^{2+}$:$[Ru(bpy)_2(PVP)_{10}]^{2+}$ *and salmon testes DNA (Avg. values for 3 replicate films).*

Table 4.1: *Average characteristics of metallopolyion/DNA films from QCM.*

film	*Nominal thickness nm*	*mass DNA* $\mu g\ cm^{-2}$	*mass Ru/Os-PVP* $\mu g\ cm^{-2}$
$(Ru\text{-}Os/ST\text{-}ds\text{-}DNA)_2$	15 ± 2	2.3 ± 0.5	1.9 ± 0.1
$(Ru\text{-}Os/ST\text{-}ss\text{-}DNA)_2$	17 ± 2	2.6 ± 0.4	2.2 ± 0.3

4.3.2 ECL and SWV Measurements of Osmium Metallopolymer Films:

Before proceeding to DNA, films containing homogeneous polynucleotides were examined. Upon incubation of electrodes with Fenton's reagent to oxidise the oligonucleotides, a significant increase in the ECL and SWV responses for $(Os/Poly\ G)_2$ films was found (Figure 4.6). The SWV peak occurred at 0.575 V vs. SCE and the maximum ECL signal was slightly positive of this at ~0.60 V. Fenton's reagent oxidises guanines to 8-oxoG,[17,26,48,49] which has a lower oxidation potential than guanine. 8-oxoG is presumably oxidised by $Os(bpy)_2^{3+}$ centres in the film, similar to reactions with soluble osmium complexes.[35,50]

Fenton's reagent also oxidises adenine and cytosine to products including 7-deazaadenine, 8-oxoadenine and 5-hydroxycytosine.[17,48,49] Figure 4.7 shows ECL/SWV for control films containing the Os alone, and Os with PSS, poly A and poly C, before and after incubation with Fenton's reagent. ECL and SWV curves are nearly super imposable for all these films; no significant changes were found after incubation under these oxidation conditions. Curves were similar to those for films containing Os only. The Os^{II}/Os^{III} peak reflecting the formal potential in the films is at 0.58 V vs. SCE. However, increasing the H_2O_2 concentration to 50 mM resulted in the detection of small increases in Os^{II} SWV and ECL peaks in films containing Poly A but not poly C. If oxidised forms of cytosine are formed, their oxidation potentials may be too positive[51] for them to be catalytically oxidised by $[Os(bpy)_2(PVP)_{10}]^{2+}$.

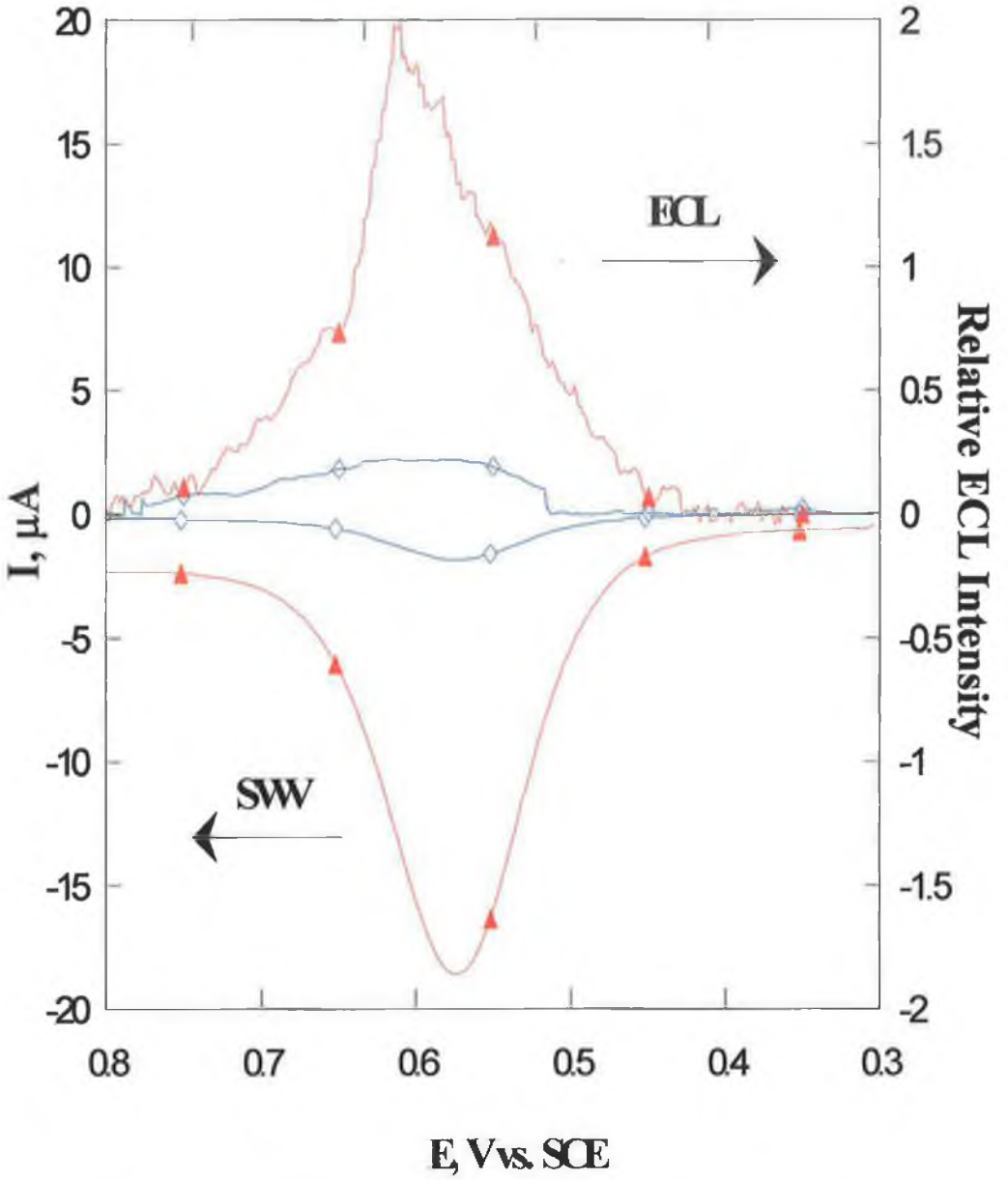

Figure 4.6: *Simultaneously measured SWV and ECL responses for $(Os/Poly\ G)_2$ films on PG electrodes in pH 5.5 buffer + 50 mM NaCl (blue) before, and (red) after 20 min incubation at 37 ±0.5 ℃ with Fenton's reagent. ECL emission monitored at 764 nm.*

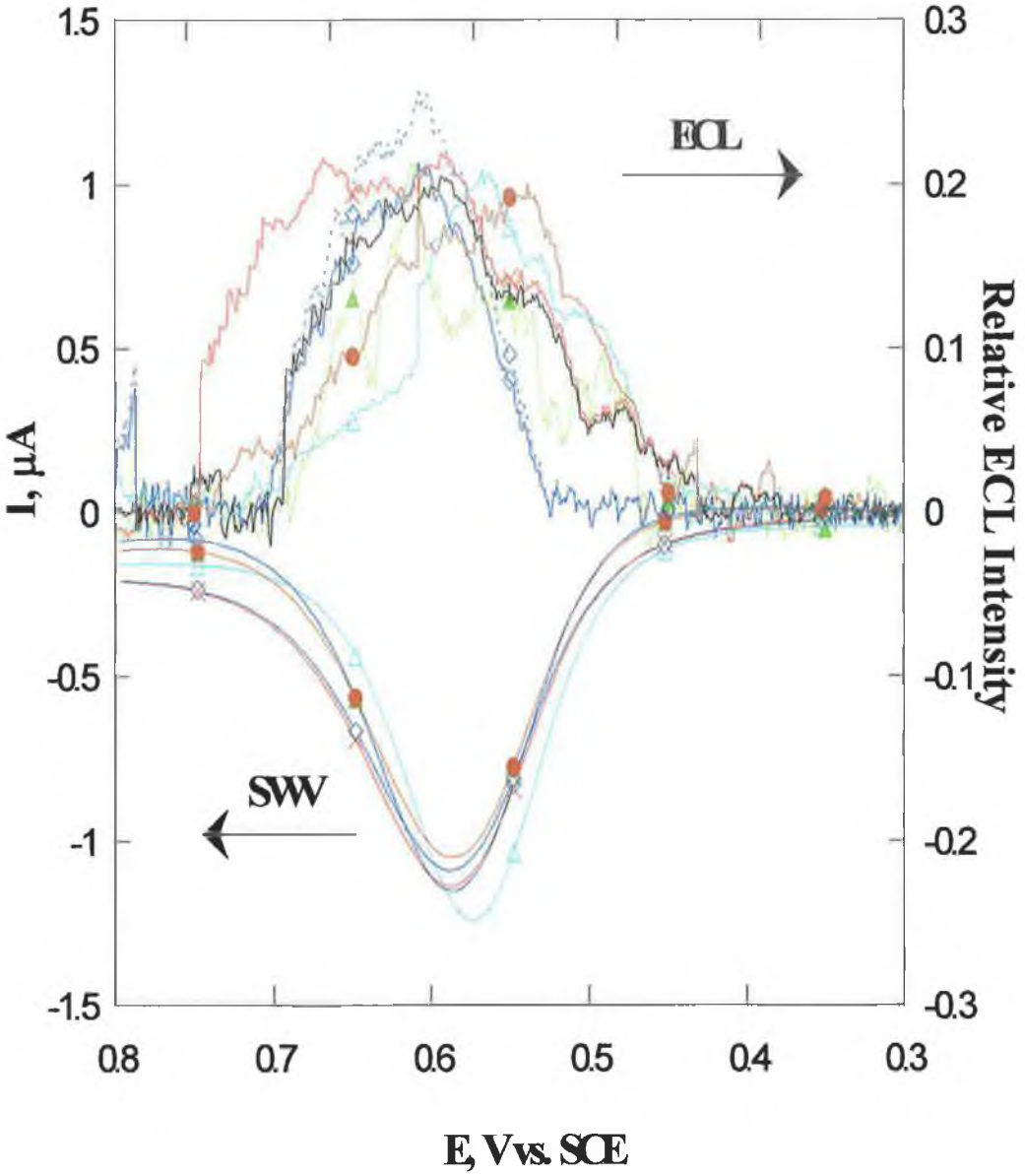

Figure 4.7: *SWV/ECL for $[Os(bpy)_2(PVP)_{10}]^{2+}$ films with polynucleotides on PG electrodes in pH 5.5 buffer before and after 20 min. incubation with Fenton reagent: $[Os(bpy)_2(PVP)_{10}]^{2+}$ alone (black, solid), $(Os\text{-}PVP/PSS)_2$ before (blue, dashed) and after (green, solid) incubation; $(Os/Poly\ A)_2$ (red, solid) before and after (red dashed) incubation; $(Os/Poly\ C)_2$ before (blue solid)and after (green dashed) incubation. ECL emission monitored at 764 nm. Poly A and Poly C are polynucleotides of adenine and cytosine respectively.*

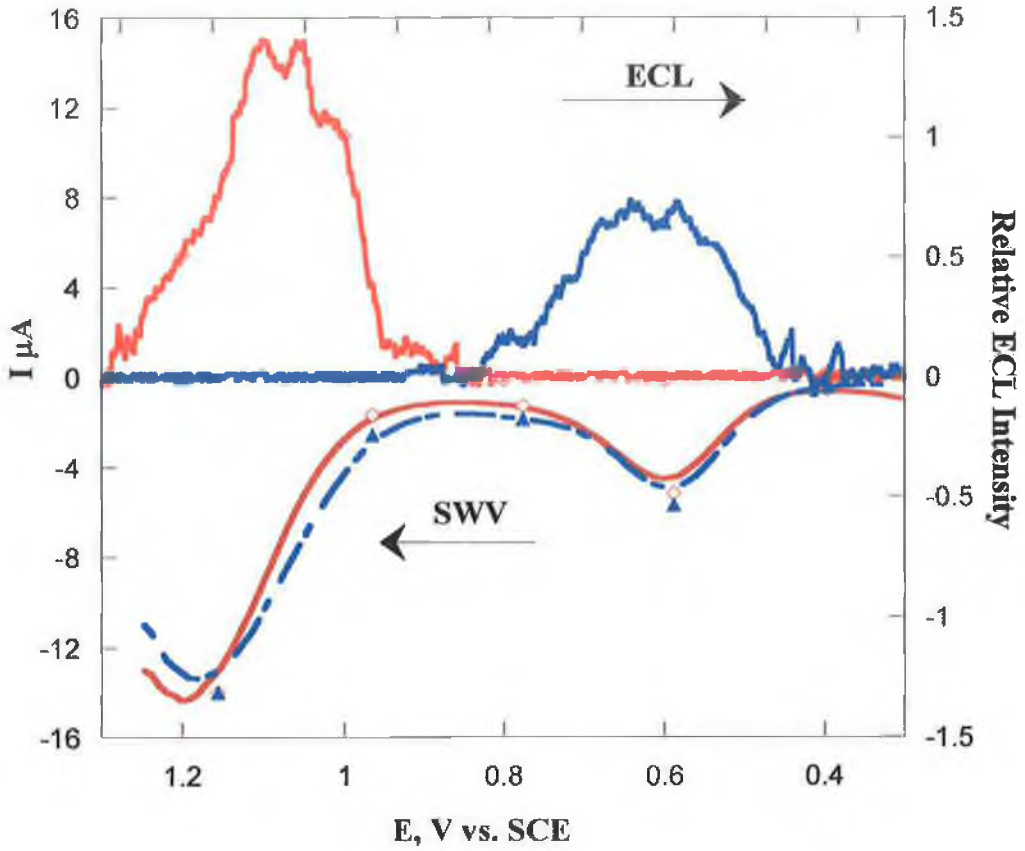

Figure 4.8: *SWV and ECL for (Os-Ru/Poly G•Poly C)$_2$ films on PG electrodes in pH 5.5 buffer after 20 min incubation at 37 °C with Fenton's reagent. ECL emission monitored at ~764 nm (blue), then monitored at ~610 nm (red).*

Since the detection wavelength was switched during the analysis, controls were run to ensure that no electron transfer, *i.e.,* that neither metal centre drove the production of the excited state of the other metal centre. Figure 4.8 shows the observed results for these controls when the detection system monitored only one wavelength. At a wavelength of 764 nm only the response from the excited state of the osmium metallopolymer is observed, however, once the detection wavelength is switched to 610 nm only the response from the excited state ruthenium metal centres is obtained.

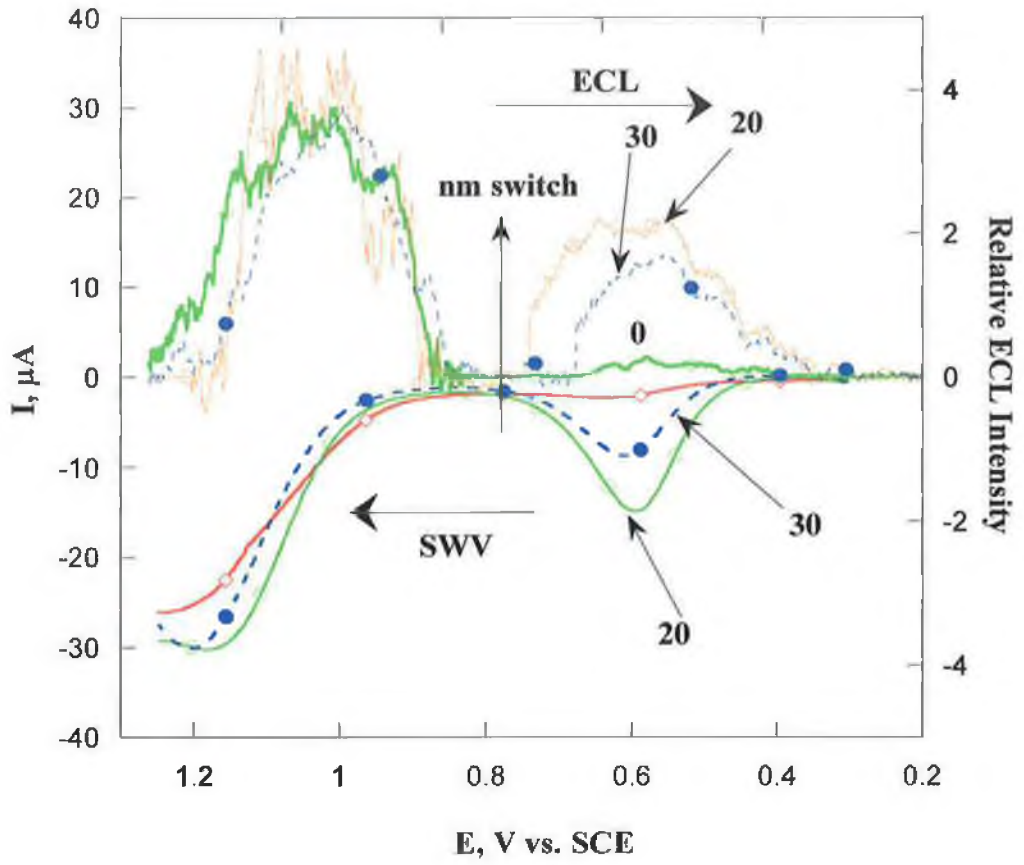

Figure 4.9: *SWV and ECL for (Os-Ru/Poly G•Poly C)$_2$ films on PG electrodes in pH 5.5 buffer before (red) and after 20 min incubation (green), and after 30 min incubation (blue), at 37 ℃ with Fenton's reagent. ECL emission at ~764 nm, then switched to ~610 nm at 0.8 V (see marker).*

Figure 4.9 shows the responses obtained for films made from the two metallopolymers and pre-hybridised poly G/poly C, *i.e.* (Os-Ru/PolyG•Poly C)$_2$. The Os^{II} catalytic peak appears at 0.6 V and the Ru^{II} peak is at ~1.2 V, reflecting the redox potentials of these polymers. ECL and SWV peaks are about 3 fold larger compared to those containing PolyG•Poly C for the Ru^{II}/Ru^{III} redox couple only. Before incubation, the Ru peak is 6-7 fold larger than the Os peak in both ECL and SWV, reflecting the fact that catalytic oxidation of guanine by Ru-centres can take place in the hybridised oligonucleotide, but that there will be little catalysis by the Os sites if the DNA is not oxidised. After incubation with Fenton's reagent, there is a dramatic increase in both the ECL and SWV peaks for the Os^{II}/Os^{III} couple in the (Os-Ru/PolyG•Poly C)$_2$ films because of catalytic oxidation of 8-oxoG formed in the incubation. However, there is only a small increase in the Ru ECL and SWV peaks.

Qualitatively, the increase in the Os peaks after incubation was larger for the films containing unhybridized Poly G (Figure 4.6) than for the (Os-Ru/PolyG•Poly C)$_2$ film (Figure 4.8). This may result from the accessibility of the bases to the reactants and the metallopolymers. However, the amount of Os in the mixed metallopolymer films is smaller in the films with only Os and poly G, and the amounts of poly G may be smaller. Thus, films of ds- and ss-DNA were compared, Figure 4.10, so as to have a system with known amounts of DNA and metallopolymers (Table 4.1). Before incubation, the ds- and ss-DNA gave nearly identical results for the Os peak. The ss-DNA gave >2-fold larger peak at the Ru potential because of enhanced oxidation by the polymer due to greater accessibility of the guanines.[33] After incubation, the ss-DNA gave somewhat larger signals than ds-DNA for both the Os and the Ru peaks. However, the differences were much smaller than that of the Ru peak for non-oxidised ss- and ds-DNA.

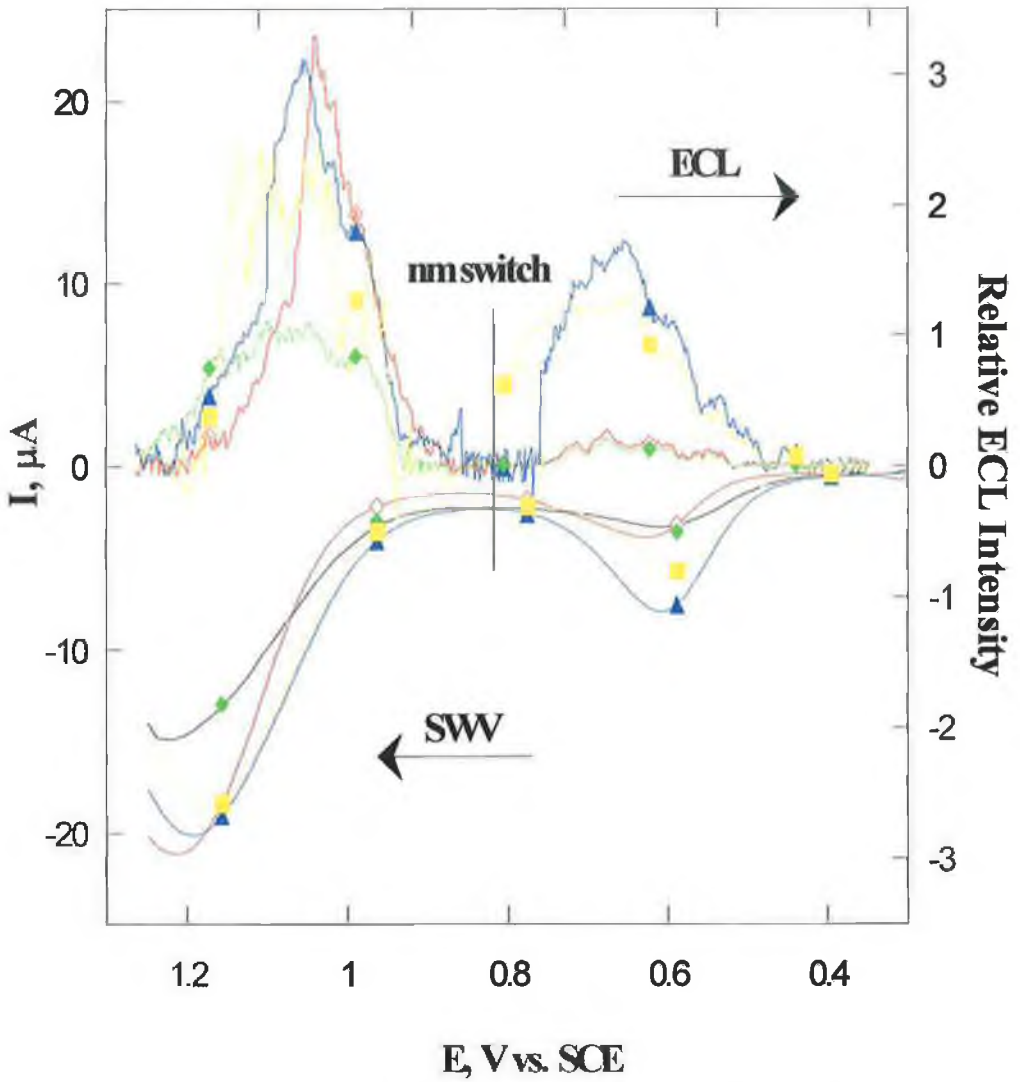

Figure 4.10: *Average SWV/ECL for (Os-Ru/ds ST DNA)$_2$ films on PG electrodes in pH 5.5 buffer before [red = ss-DNA; green = ds-DNA] and after 20 min incubation at 37 °C [blue = ss-DNA; black = ds-DNA] ECL emission monitored at ~764 nm and then switched to ~610 nm at the 0.8 V as labelled.*

When $(Os\text{-}Ru/ds\text{-}DNA)_2$ films were incubated with Fenton reagent for various times, increases in the ratios of ECL and SWV (final/initial) Os^{II} peaks were observed for up to 20 min, Figure 4.11. At longer times, dampened oscillations in these signals were observed. Controls consisting of the same types of films incubated with $FeSO_4$ alone, H_2O_2 alone or and only buffer remained at ratios within experimental error of unity.

The concentration-time profile for 8-oxoG after oxidation of DNA and of guanine by Fenton's reagent under different conditions, determining 8-oxoG after DNA hydrolysis by using LC-EC was previously shown by White *et al.*. Thus, LC-EC analysis on DNA in solution that was oxidised under exactly the same conditions as the electrodes described here for ECL/SWV, was performed. Some of the LC-EC chromatograms observed are shown in Figure 4.12, these chromatograms show the oscillating 8-oxoguanine peaks. Concentration profiles for 8-oxoG obtained by LC-EC are given in Figure 4.13. The error bars of the LC-EC results for the small amounts of [8-oxoG] found are somewhat larger than those for ECL and SWV, but the same concentration profile was found over 100 min of reaction. An initial increase in [8-oxoG] leads to a clear maximum at about 20 min.

As with pervious work performed by White *et al.*[26], the HPLC-UV-EC analysis showed an immediate generation of 8-oxoguanine, and a corresponding decrease in guanine concentration. A maximum concentration of 8-oxoguanine was reached after approximately 20 minutes, after which the overall trend was for a decrease in concentration, although this decrease was not linear. However, the maximum concentration of 8-oxoG observed for the ds-DNA was slightly later than that reported for the guanine standard. This was expected and attributed to the shielding effect of the DNA polymer backbone. The solution and film results are quite comparable, both systems producing a similar reaction profile, although exact environments and concentrations were not reproducible. Both systems showed similar trend in the first 40 minutes, subsequent results did differ slightly. This was attributed to the environment in which the results were obtained. In solution the products can more freely react with all the reactants which implied that the period was dependent on the environment in which the results were collected.

These results indicate the formation of other oxidation products from 8-oxoG. A number of compounds have been reported as possible final oxidation products of guanine. In double stranded DNA guanidinohydantoin was observed as the main product by a number of authors[52,53,54] and was found to be generated via a 5-OH intermediate of 8-oxoG. An epimer of Gn, iminoallantion (Ia), also emerged as possible oxidation products of Gn oxidation. The production of guanidinohydantoin could results in the observed results. Guanidinohydantion is not electrochemically active. Its production combined with the decrease in 8-oxoG concentrations could therefore result in a decrease in the electrochemical signals.

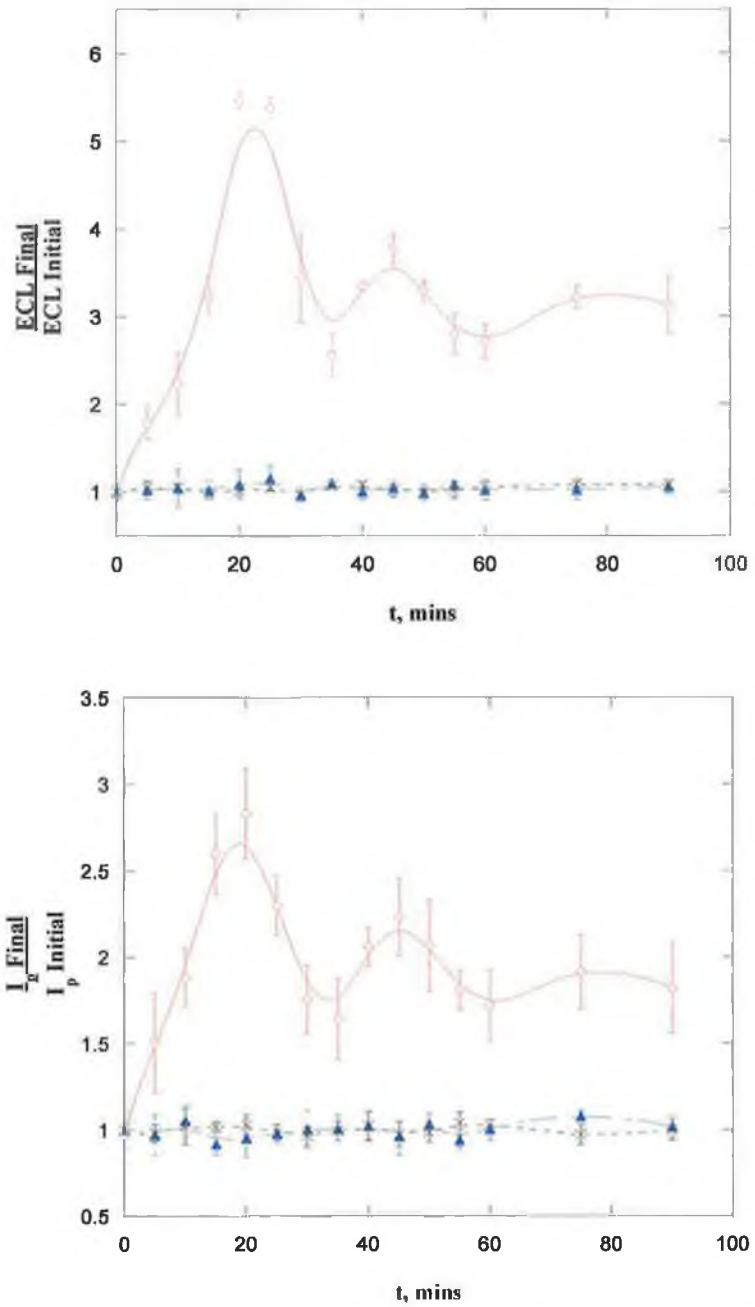

Figure 4.11: *Influence of incubation of (Os-Ru/ds-ST DNA)$_2$ films with Fenton reagent ($FeSO_4$ and H_2O_2) (red), with FeSO4 alone (blue), H_2O_2 alone (yellow), and only pH 5.5 buffer (black) on (a) average ECL signals and (b) average SWV catalytic peak currents for the Os^{II}/Os^{III} redox couple. Error bars represent standard deviations for three trials; one electrode per trial.*

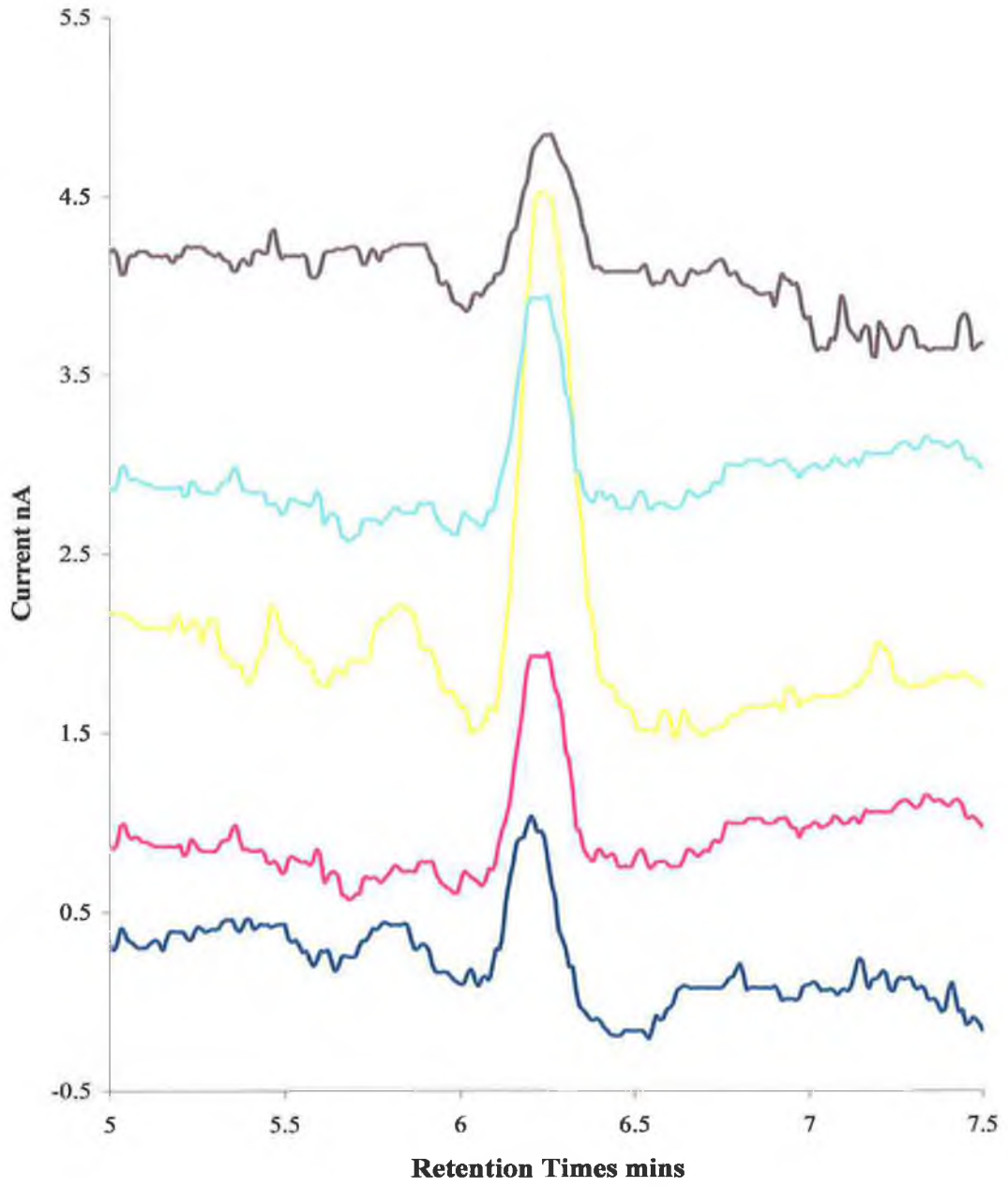

Figure 4.12: *LC-EC chromatograms of oxidation products of 1.2 mg mL^{-1} ds-DNA in pH 5.5 by Fenton reagent under same conditions as for incubation of DNA electrodes Blue plots shows [8-oxoG] peak observed after 10 mins, pink represents oxidation after 11 mins, yellow 12 mins, light blue 15 mins and purple shows [8-oxoG] peak after incubation for 18 mins. Plots are offset for clarity.*

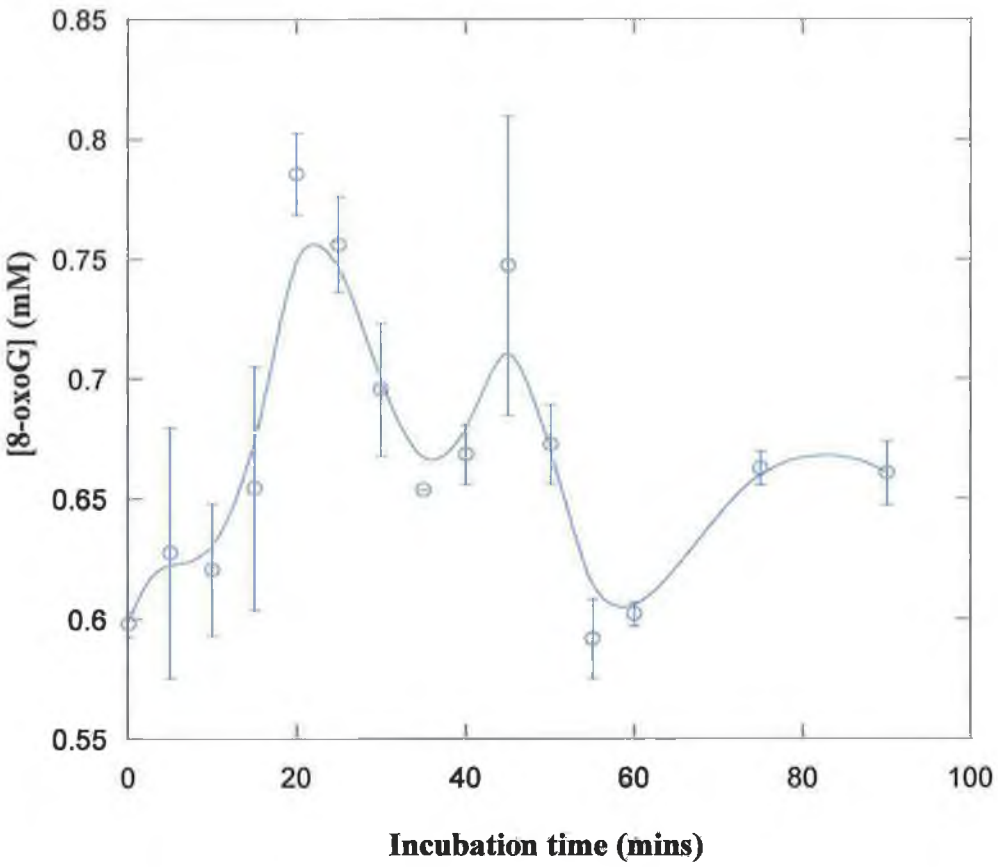

Figure 4.13: *Concentration profile of [8oxoG] determined by LC-EC during oxidation of 1.2 mg mL^{-1} ds-DNA in pH 5.5 by Fenton reagent under same conditions as for incubation of DNA electrodes (Avg. of 3 determinations).*

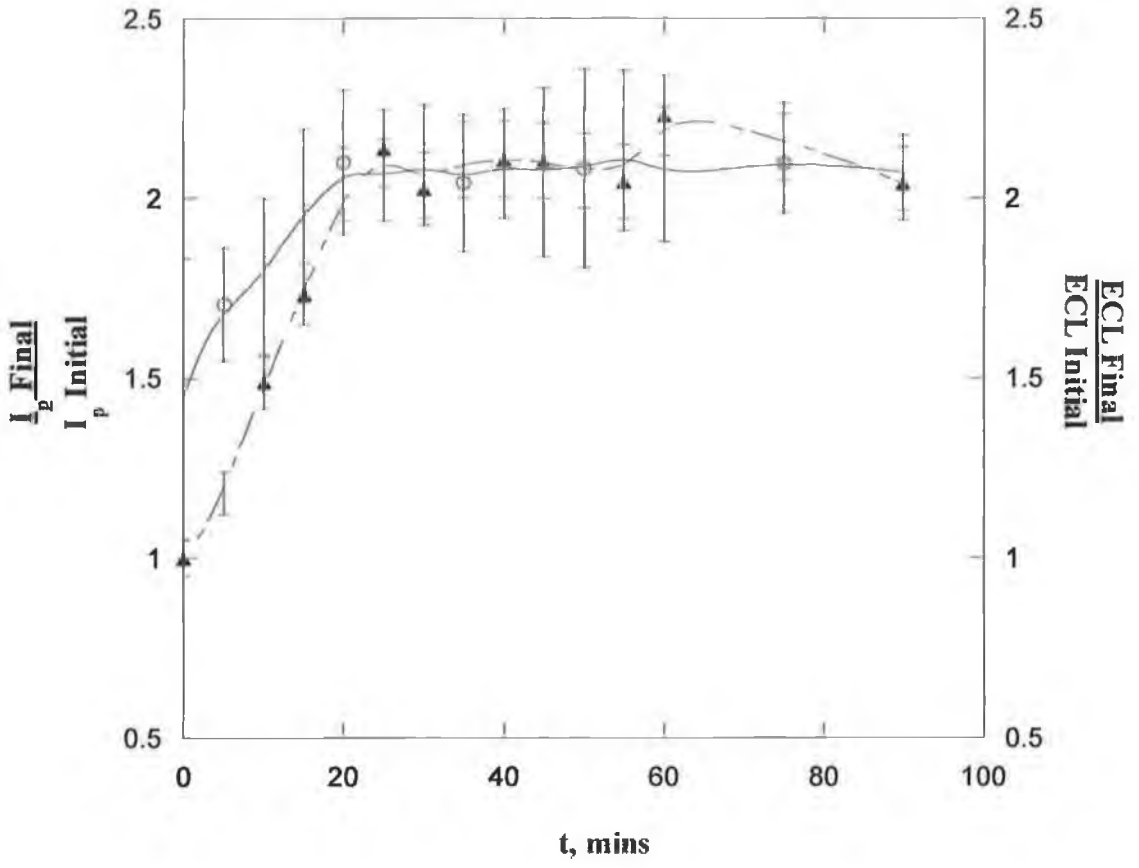

Figure 4.14: *Influence of incubation time with Fenton reagent on average ECL signals (o) and average SWV catalytic peak currents (▲) for the Ru^{II} peak for $(Os\text{-}Ru/ds\text{-}ST\ DNA)_2$ films for the same experiments in Figure 6. Avg. of 3 trials, with one electrode per trial. (Ru^{II} peaks showed no trends for any of the controls in Figure 4.12)*

The Ru^{II} ECL and SWV peak ratios (Figure 4.14) for the same films for which the Os^{II} peaks were discussed (cf. Figure 4.12) showed increases in the first 20 min of incubation with Fenton's reagent. These ratios reached limiting values slightly larger than 2 at t>20 min. The increase may be attributed to the formation of oxidised adenine derivatives or possible strand breaks either of which can result from the action of the Fenton reagents on DNA strand. The strand breaks distorted the helical structure of DNA allowing for greater interaction between the guanine base and the ruthenium metallopolymer as discussed previously in Chapter 3. No significant increases or trends for the Ru^{II} peaks were found when the films were incubated in buffer only, buffer with $FeSO_4$ only, or buffer with H_2O_2 only.

To assess the contribution to the signals from the formation of adenine or cytosine derivatives upon oxidation, films containing both the metallopolymers and either Poly A or Poly C were incubated with Fenton reagent. For the Poly C films, there was no increase in either the Os or Ru peaks upon incubation. For the film containing Poly A, there was no increase in the Os peaks, but there was ~7% increase in the Ru peaks in the SWV response after 20 min incubation. This is possible due to the formation of oxidised adenine derivatives which have similar formal potentials to guanine and as such can react with the ruthenium metallopolymer. It is likely that this reflects the oxidation of oxo-adenines by the electrogenerated Ru^{III} sites in the films. Although the concentration of these adducts would be quite low, they could result in slight structural changes. Again these changes would permit greater interaction between guanine and the ruthenium metallopolymer.

ECL and SWV of (Os-Ru/Poly $G)_2$ films before and after incubation resembled those of (Os-Ru/Poly G•Poly $C)_2$ in Figure 4.9. The ECL and SWV signals for the Os peaks increased upon incubation with Fenton's reagent, but the peak intensity for the Ru sites was not changed significantly by incubation.

4.3.3 Chemically Damaged Os-Ru/DNA Films:

The influence of chemical damage of DNA on these films was also investigated by treating them with styrene oxide, which forms covalent adducts with DNA in films mainly at the nitrogens of guanine.[43] Os-Ru/DNA films incubated with styrene oxide showed increases in the Ru^{II} SWV and ECL peaks, Figure 4.15, as previously reported for Ru/DNA films.[33] The films were also incubated in toluene, which does not react with DNA, and with buffer alone, and showed no increase or trend for the Ru or Os peaks. Films incubated with styrene oxide for 25 min gave only very small increases in the Os^{II} SWV or ECL peak signals, Figure 4.15.

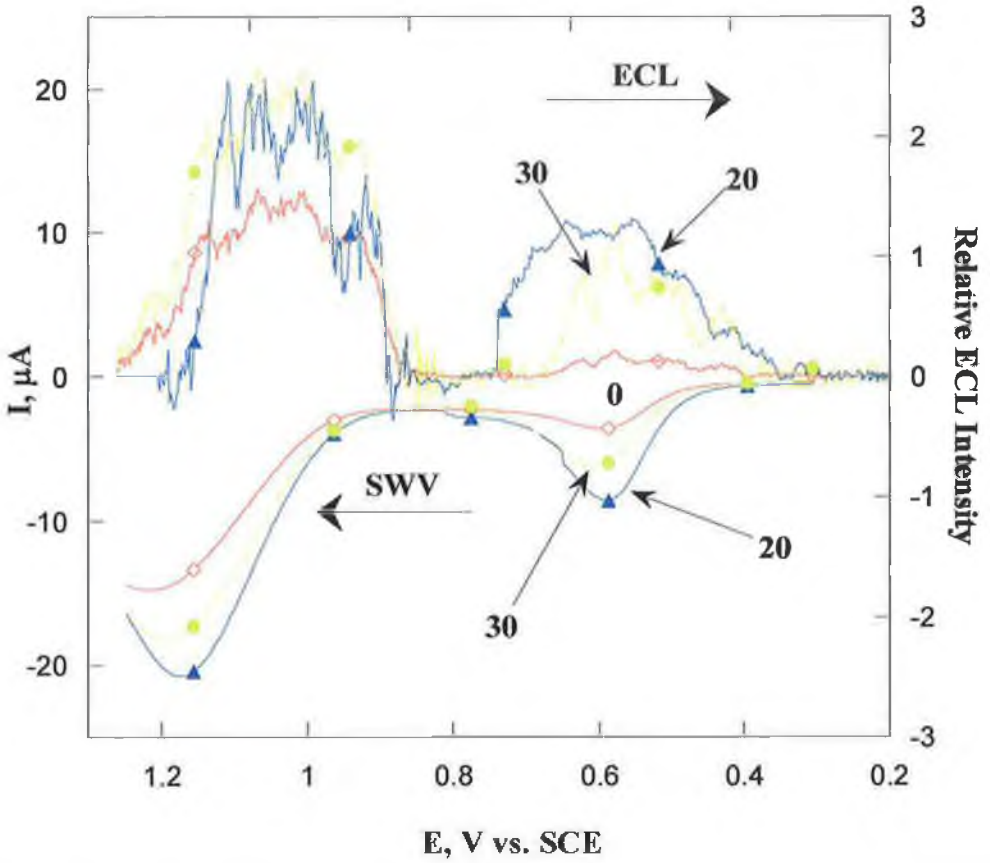

Figure 4.15: *SWV and ECL responses for (Os-Ru/ds ST DNA)$_2$ films on PG electrodes in pH 5.5 before (red) after (blue) 20 min, and (green) 30 min incubations at 37 with saturated styrene oxide. ECL emission monitored at ~764 nm and then switched to ~610 nm at the 0.8 V marker.*

4.3.4 Mass Spectroscopic analysis of 8-oxoguanine in oxidatively damaged DNA:

Mass spectrometry was utilised to confirm the production of 8-oxoguanine from the reaction studied in this analysis. In order to investigate possible products, HPLC-MS was used. Figure 4.16 shows the ion chromatograms for m/z 152 ($[G + H]^+$), m/z 168 ($[8\text{-oxoG} + H]^+$) and m/z 158 ($Gn + H]^+$) for the HPLC separation of salmon testes DNA hydrolsyates incubated with the Fenton reagents for 60 minutes. Due to different column length and flow rate, the retention times differ from the HPLC-UV-EC retention times. At a retention time of approximately 2.9 minutes guanine ions elute. There is no definite 8-oxoguanine ion, although the EC chromatogram suggests that it is present in the sample. There is however a definite elution of ions at m/z 158, suggesting the presence of guanidinohydantion (Gn) in the solution. This peak also confirms the production of 8-oxoG since Gn is an oxidation product of 8-oxoG.

Figure 4.17 shows the mass spectrum at 2.9 minutes of the total ion chromatogram from the HPLC-MS. In addition to the ions of m/z 152 and m/z 158, there are also ions of m/z 174 and m/z 190. These correspond to the ions $[G + Na]^+$ and $[8\text{-oxoG} + Na]^+$, respectively. This confirms the presence of 8-oxoguanine in the sample.

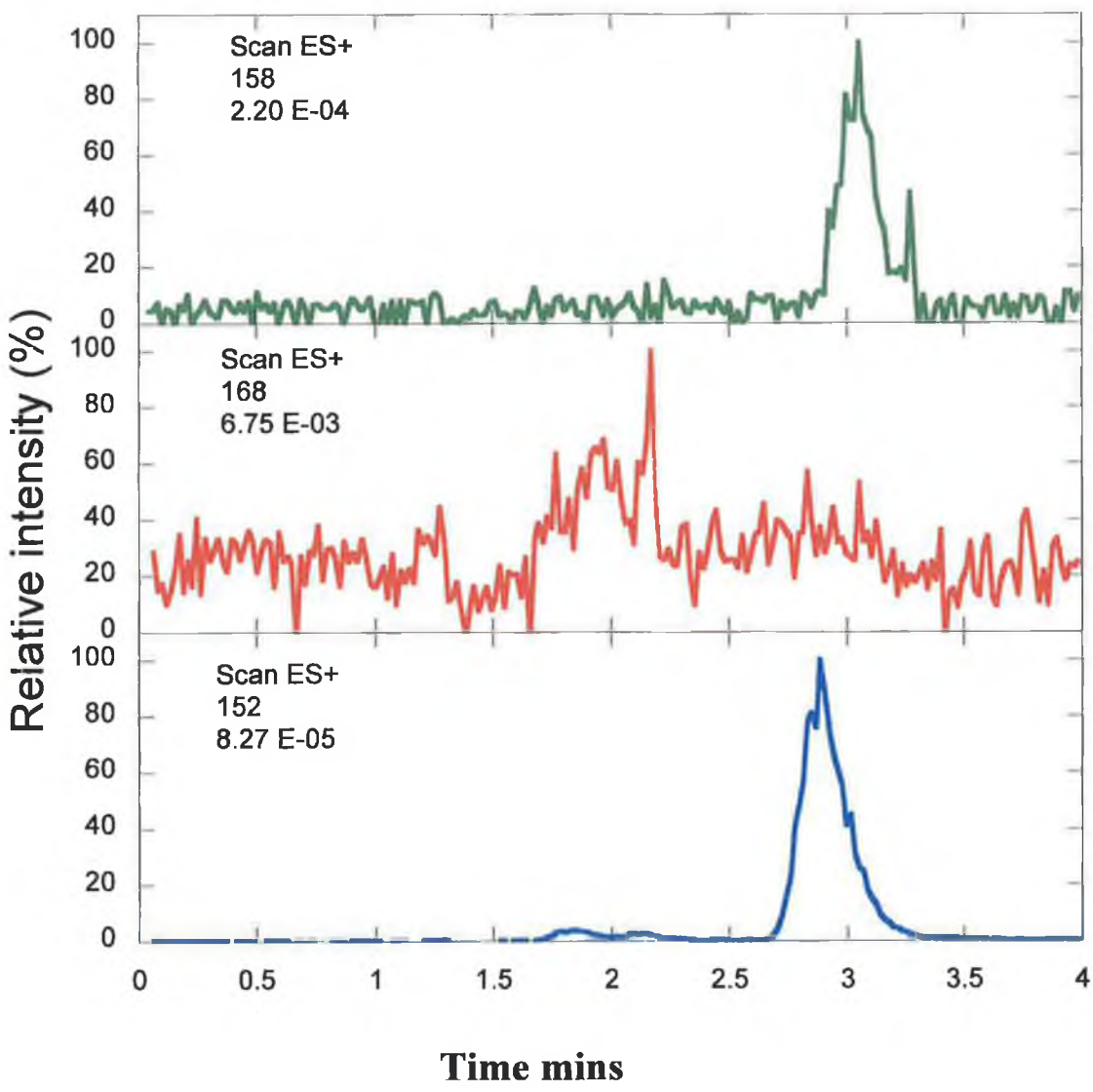

Figure 4.16: *Typical ion chromatograms m/z 158 ($[G + H]^+$), m/z 168 ($[8\text{-oxoG} + H]^+$) and m/z 158 ($[Gn + H]^+$) for salmon testes DNA incubated in solution for 60 minutes with 150 μM $FeSO_4$ and 50 mM H_2O_2.*

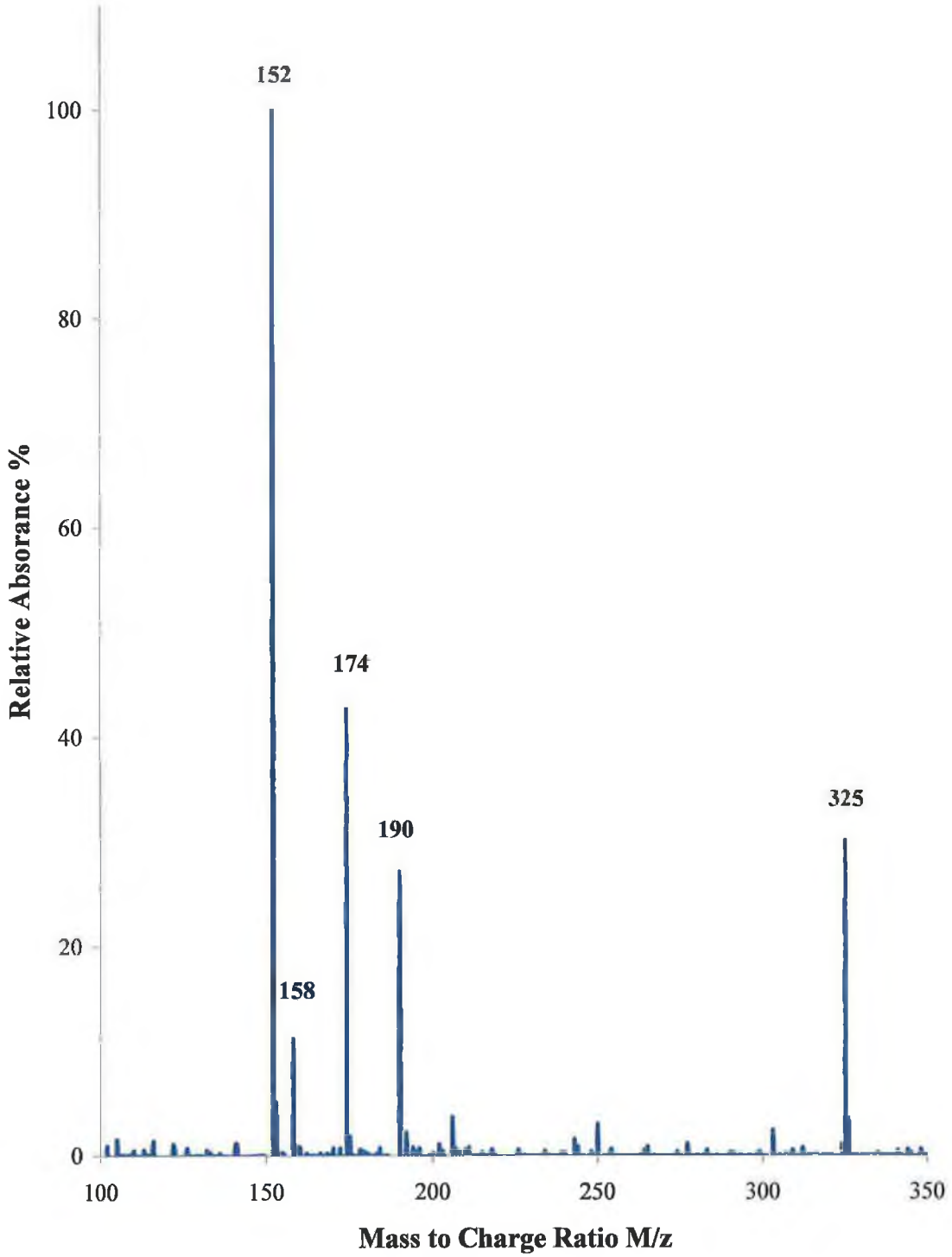

Figure 4.17: *Mass spectrum of the ion fraction eluting at 3.0 minutes of acid hydrolysed salmon testes DNA incubated with 150 μM $FeSO_4$ and 50 mM H_2O_2 for 60 minutes.*

oxidation may be related to oxidised adenines and DNA strand breaks[9] that could produce an increased amount of single strands in the films.

The formation of chemical adducts of guanine and adenine bases of DNA in films by reaction with styrene oxide under the conditions used in Figure 4.15 have been confirmed by LC-MS.[56] With the Os-Ru/DNA films, minimal increases in the Os^{II} ECL and SWV (Figure 4.15) were observed, but large increases were found for the Ru^{II} peaks as reported previously.[33] This result suggests that the Os^{II} ECL is not sensitive to formation of the DNA base adducts in this experiment.

Based on previous proposals for ECL generation pathways from reactions of metal complexes in solution or in polymer films,[38,40,47] ECL generation is likely to involve the initial reaction of electrochemically generated $[Os(bpy)_2(PVP)_{10}]^{3+}$ with a reductant to give a radical. It is suggested that that the osmium metallopolymer generates ECL signals following a pathway represented as:

$$[Os(bpy)_2(PVP)_{10}]^{2+} \Leftrightarrow [Os(bpy)_2(PVP)_{10}]^{3+} + e^- \quad \textbf{(5)}$$

$$[Os(bpy)_2(PVP)_{10}]^{3+} + 8G \rightarrow [Os(bpy)_2(PVP)_{10}]^{2+} + 8G^{\bullet} \quad \textbf{(6)}$$

$$[Os(bpy)_2(PVP)_{10}]^{3+} + 8G^{\bullet} \rightarrow [Os(bpy)_2(PVP)_{10}]^{2+*} + Gn \quad \textbf{(7)}$$

$$[Os(bpy)_2(PVP)_{10}]^{2+*} \rightarrow [Os(bpy)_2(PVP)_{10}]^{2+} + h\nu \quad \textbf{(8)}$$

Or alternatively:

$$[Os(bpy)_2(PVP)_{10}]^{2+} + 8G^{\bullet} \rightarrow [Os(bpy)_2(PVP)_{10}]^{+} + Gn \quad \textbf{(9)}$$

4.4 Discussion:

These results demonstrate for the first time that ECL can be achieved by direct reaction of an osmium complex polymer with oxidised DNA in ultrathin films, Figures 4.6, 4.7. The ECL detection equipment is simple and inexpensive, featuring a conventional voltammetric cell combined with an optical fibre that delivers light from the electrode to a monochromator/PMT detector. Osmium and ruthenium complex metallopolymers can be incorporated together in films with DNA to detect both DNA oxidation and chemical DNA damage, Figure 4.15. Alternative layer-by-layer electrostatic assembly on PG electrodes provided a hybrid or composite metallopolymer/DNA films ~15 nm thick, Table 4.1, presumably featuring intimate mixing of the metallopolymers and ds-DNA in a tiny reaction volume. This assembly approach typically results in intermixing of layers. Neutron reflectivity studies with deuterium labelled polyions, [45a,b,55] reveal that this mixing may facilitate intimate contact between the DNA and metallopolymers to achieve efficient catalytic oxidation of the DNA and efficient ECL production.

Among the homogeneous polynucleotides, only films containing poly G, Figures 4.7, gave significant increases in the Os^{II} SWV and ECL peaks upon oxidation by Fenton's reagent containing 5 mM H_2O_2, although small increases in these peaks were also found when [H_2O_2] was increased to 50 mM. Increases in the Os^{II} SWV and ECL peaks upon DNA oxidation by Fenton's reagent with 5 mM H_2O_2 appear to result mainly from oxidised guanines, presumably 8-oxoG. Oxidises adenines may contribute to the signal at higher [H_2O_2], presumably leading to more extensive DNA oxidation. Thus, the Os^{II} ECL seems to be mainly specific for 8-oxoG with minor contributions from oxidised adenines, however, we cannot exclude other oxidation products which could be partial contributors.

Again for the homogeneous polynucleotides, only films containing poly A gave increases for the Ru^{II} SWV and ECL peaks after oxidation. Films containing poly G gave increases in the Os^{II} peaks but not in the Ru^{II} peaks. The increase in the Ru^{II} peaks upon DNA

$$[Os(bpy)_2(PVP)_{10}]^{+} + [Os(bpy)_2(PVP)_{10}]^{3+} \rightarrow [Os(bpy)_2(PVP)_{10}]^{2+*} + [Os(bpy)_2(PVP)_{10}]^{2+} \quad \textbf{(10)}$$

Initial oxidation of the metallopolymer by the electrode gives the Os^{III} oxidant (equation 5), which reacts with 8-oxoG (8G) in DNA to give $8G^{\bullet}$ (equation 6), which may produce photoexcited $[Os(bpy)_2(PVP)_{10}]^{2+*}$ sites (equation 7), by directly reducing the Os^{III} sites in the film. The excited state complex $[Os(bpy)_2(PVP)_{10}]^{2+*}$ decays to the ground state by emission at ~764 nm (equation 8).[41] An alternative pathway is shown in equations 9 and 10, where G^{+} may reduce the Os^{II} sites to Os^{I}, which can then produce $Os^{II}*$ by reacting with Os^{III} sites. Further studies are underway to distinguish these possibilities.

In the early stages of the Fenton oxidation of the DNA films, both the Os^{II} and Ru^{II} ECL and SWV peak ratios increase with reaction time (Figures 4.12 and 4.14). After about 20 min reaction of the films, the Ru^{II} signals reach a steady state, but the Os^{II} peaks showed dampened oscillations up to 100 min. (Figure 4.12). LC-EC analysis of DNA after it had been oxidised under similar reaction conditions, then hydrolysed, showed an almost identical pattern of oscillations in concentration of 8-oxoG (Figure 4.13).

The oscillations of 8-oxoG concentration during Fenton oxidation of both free guanine and DNA under a variety of conditions by LC-EC-UV analysis has been previously described.[26] Detection of similar oscillations by the independent Os^{II} ECL/SWV method is presented here (Figure 4.12) that is selective for oxidised guanines and thus confirms the observation of this phenomenon. The oscillations are consistent with a competitive consecutive process in which guanine is oxidised to 8-oxoguanine, which is then rapidly oxidised to guanidinohydantoin, which was confirmed as a major product of 8-oxoG oxidation in reactions by LC-MS.[26] Here, the common oxidant •OH reacts with starting reactant guanine as well as the initial reaction product 8-oxoG. While this simple consecutive pathway must certainly be featured in the oscillations, it would typically lead to only one maximum in the concentration of the initial product.[57] Oscillatory reactions often have very complex pathways featuring several interactive catalytic cycles and multiple elementary steps;[58,59] this particular case is now under further study using additional DNA oxidants.

4.5 Conclusion:

In summary, these results show that ECL can be obtained directly from the reaction of oxidised guanine in DNA in thin films with the catalytic metallopolymer $[Os(bpy)_2(PVP)_{10}]^{2+}$. ECL and SWV peaks of the Os sites in the films are sensitive to oxidative damage that results in the formation of 8-oxoG. The apparatus is simple and inexpensive, and such sensors could be useful for the clinical detection of oxidised DNA as a biomarker for oxidative stress. The combination of ruthenium and osmium metallopolymers into the films may allow for future applications including sensors for the simultaneous detection of chemical and oxidative DNA damage.

4.6 References:

1 (a) Cross, C. E.; Halliwell, B.; Pryor, W. A.; Ames, B. N.; Saul, R. L.; McCord, J. M.; Harman, D. *Ann. Intern. Med.* **1987**, *107,* 526.
(b) Beckman, K. B.; Ames, B. N., *J. Biol. Chem.* **1997,** *272*, 19633.
(c) Kawanishi, S.; Hiraku, Y.; Oikawa, S. *Mutation Res.* **2001,** *488,* 65.

2 Ames, B.B., Shigenaga, M.K., Hagen, T.M. *Proc. Natl. Acad. Sci. USA*, **1993**, *90*, 7915.

3 Shiegenaga, M.K., Hagen, T.M., Ames, B.N., *Proc. Natl. Acad. Sci. USA*, **1994**, *91*, 10771.

4 Ames, B.N., Gold, L.S., Willett, W.C., *Proc. Natl. Acad. Sci. USA*, **1995**, *92*, 5258.

5 Beckman, K.B., Ames, B.N., *Physiol. Rev.*, **1998**, *78*, 548.

6 Henle, E.S., Luo, Y., Gassmann, W., Linn, S., *J. Biol. Chem.*, **1996**, *271*, 21177.

7 (a) Halliwell, B.; Gutteridge, J. M. C. *Biochem J.* **1984**, *219*, 1.
(b) Halliwell, B. *Mutation Res.* **1999,** *443*, 37.
(c) Cadet, J.; Delatour, T.; Douki, T.; Gasparutto, D.; Pouget, J.-P. Ravanat, J.-L.; Sauvaigo, S. *Mutation Res.* **1999**, *424*, 9.
(d) Jaeschke, H.; Gores, G. J.; Cederbaum, A. I.; Hinson, J. A.; Pessayre, D.; Lemasters, J. J. *Toxicological Sci.* **2002**, *65*, 166.

8 Pryor, W. A. *Free Rad. Biol. Med.* **1988,** *4,* 219.

9 (a) Cheng, K. C.; Cahill, D. S.; Kasai, H.; Nishimura, S.; Loeb, L. A. *J. Biol. Chem.* **1992**, *267*, 166.
(b) Olinski, R.; Gackowski, D.; Foksinski, M.; Rozalski, R.; Roszkowski, K.; Jaruga, P. *Free Rad. Biol. Med.* **2002,** *33,* 192.
(c) Floyd, R. A. *Carcinogenesis* **1990,** *11,* 1447.

10 (a) Walling, C. *Acc. Chem. Res.* **1975,** 8, 125.
(b) Aruoma, O. I.; Halliwell, B.; Gajewski, E.; Dizdaroglu, M. *J. Biol. Chem.* **1989,** *264*, 20509.
(c) Lloyd, D. R.; Phillips, D. H. *Mutation Res.* **1999,** *424*, 23.

11 Imlay, J.A., Linn, S., *Science*, **1988**, *240*, 1302.

12 Mello-Filho, A.C., Meneghini, R., *Mutat. Res.*, **1991**, *251*, 109.

13 Luo, Y-C., Han, Z-X., Chin, S.M., Linn, S., *Proc. Natl. Acad. Sci. USA*, **1994**, *91*, 12438.

14 Mello-Filho, A.C., Meneghini, R., *Biochim., Biophys., Acta,* **1984**, *781*, 56.

15 (a) Shigenaga, M. K.; Ames, B. N. *Free Rad. Biol. Med.* **1991**, *10,* 211.
(b) Lunec, J.; Holloway, K. A.; Cooke, M. S.; Faux, S.; Griffiths, H. R.; Evans, M. D. *Free Rad. Biol. Med.* **2002,** *33,* 875.
(c) Kasai H. *Mutation Res.* **1997,** *387,* 147.
(d) Halliwell, B. *Free Rad. Biol. Med.* **2002,** *32,* 968.
(e) Gedik, C. M.; Boyle, S. P.; Wood, S. G.; Vaughan, N. J.; Collins, A. R. *Carcinogenesis* **2002,** *23,* 1441.

16 Cunningham, R.P., *Curr. Biol.,* **1997**, *7*, R576.

17 Cheng, K.C., Cahill, D.S., Kasai, H., Nishimura, S., Loeb, L.A., *J. Biol. Chem.,* **1992**, *267*, 166.

18 Steenken S.; Jovanovic S. V.; *J. Am. Chem. Soc.* **1997** *119* 617.

19 (a) Goyal, R. N.; Jain, N.; Garg, D. K.; *Bioelectrochem. Bioenerg.* **1997,** *43*, 105.
(b) Duarte, V.; Muller, J. G.; Burrows C. J. *Nucleic Acids Res.* **1999,** *27,* 496.

20 (a) Duarte, V.; Muller, J. G.; Burrows C. J. *Nucleic Acids Res.* **1999,** *27,* 496.
(b) Hickerson, R. P.; Prat, F.; Foote, C. S.; Burrows, C. J. *J. Am. Chem. Soc.* **1999,** *121*, 9423.
(c) Luo, W.; Muller J. G., Rachlin, E. M.; Burrows C. J. *Chem. Res. Toxicol.* **2001**, *14*, 927.

21 Henderson, P. T.; Delaney, J. C.; Muller, J. G.; Neeley, W. L.; Tannenbaum, S. R.; Burrows, C. J.; Essigmann, *Biochemistry*, **2003**, *42*, 9257.

22 Rajendra N. Goyal, Neena Jain, Dinesh K. Garg; *Bioelectrochem. & Bioenergetics* 43 **1997** 105.

23 Stephanie C. Weatherly, Ivana V. Yang, Paul A. Armistead, H. Holden Thorp; *J. Phys. Chem. B*, **2003,** *107,* 372.

24 Goyal, R.N,; Jain, N.; Garg, D.K.; *Bioelectro. Bioenergetics,* **1997**, *43*, 105.

25 (a) Floyd, R. A.; Watson, J. J.; Wong, P. K.; Altmiller, D. H.; Rickard, R. C. *Free Rad. Res. Commun.* **1986**, *1*, 163.

(b) Helbock, H. J.; Beckman, K. B.; Shigenaga, M. K.; Walter, P. B.; Woodall, A. A.; Yeo, H. C.; Ames, B. N. *Proc. Natl. Acad. Sci.* **1998**, *95*, 288.

26 White, B., Smyth, M.R., Stuart, J. D., Rusling, J. F., *J. Am. Chem. Soc.,* **2003**, *125*, 6604.

27 Palecek, E.; Fojta, M.; Tomschik, M.; Wang, J., *Biosensors Bioelectronics*, **1998**, *13*, 621.

28 Palecek, E., *Electroanalysis* **1996**, *8*, 7.

29 Thorp, H. H., *Trends Biotechnol.*, **1998**, 16, 117.

30 Palecek, E.; Fojta, M. *Anal. Chem.*, **2001**, *73*, 74A.

31 (a) Wang, J.; Rivas, G.; Ozsoz, M.; Grant, D. H.; Cai, X.; Parrado, C. *Anal. Chem.* **1997**, *69*, 1457.

(b) Wang, J. *Chem. Eur. J.* **1999**, *5*, 1681.

32 Rusling, J. F.; Zhang, Z. in Rusling, J. F., Ed., *Biomolecular Films*, Marcel Dekker, N. Y., **2003**, pp. 1-64.

33 Dennany, L., Forster, R. J., Rusling, J.F., *J. Am. Chem. Soc.,* **2003**, *125*, 5213.

34 Johnston, D. H., Glasgow, K. C., Thorp, H. H., *J. Am. Chem. Soc.,* **1995**, *117*, 8933.

35 Ropp, P.A., Thorp, H.H, *Chem. Biol.,* **1999**, *6*, 599.

36 Szalai, V. A.; Singer, M. J.; Thorp, H. H. *J. Am. Chem. Soc.,***2002**, *124,* 1625.

37 Holmberg, R. C.; Tierney, M. T.; Ropp, P. A.; Berg, E. E.; Grinstaff, M. W.; Thorp, H. H. *Inorg. Chem.* **2003**, *42*, 6379.

38 (a) Chang, M.-M.; Sagi, T.; Bard A. J. *J. Am. Chem. Soc.,* **1977**, *99*, 5399.

(b) Rodriquez, M.; Bard A. J. *Anal. Chem.* **1990**, *62*, 2658.

39 Durham, B., Wilson, S. R., Hodgson, D. J., Meyer, T. J., *J. Am. Chem. Soc.,* **1980**, *102*, 600.

40 Hogan, C.F., Forster, R.J., *Anal. Chem.,* **1999**, *396*, 13.

41 Forster, R.J., Vos, J.G., *Macromolecules,* **1990**, *23*, 4372.

42 (a) Casper J. V.; Meyer T. J., *J. Am. Chem. Soc.*, 1983, 105, 5583.

(b) Bard, A.J., Keszthelyi, C.P., Tachikawa, H., Tokel, E., Chemilumin. & Biolumin. **1973**, *3*, 193.

43 Zhou, L., Rusling, J. F., *Anal. Chem.,* **2001**, *73*, 4780.

44 Mugweru, A., Rusling, J. F., *Electrochem. Commun.,* **2001**, *3,* 406.

45 (a) Lvov, Y. in Lvov, Y.; Möhwald, H., Eds. *Protein Architecture: Interfacing Molecular Assemblies and Immobilization Biotechnology,* Marcel Dekker: New York, **2000**, pp. 125.

(b) Lvov, Y. in Nalwa, R.W., Ed., *Handbook Of Surfaces And Interfaces Of Materials, Vol. 3. Nanostructured Materials, Micelles and Colloids,* Academic Press. San Diego, **2001**, pp. 170.

(c) Rusling, J. F. in Lvov, Y.; Möhwald, H., Eds. *Protein Architecture: Interfacing Molecular Assemblies and Immobilization Biotechnology,* Marcel Dekker: New York, **2000**, pp. 337.

(d) Rusling, J. F.; Zhang, Z. in Nalwa, R.W., Ed., *Handbook Of Surfaces And Interfaces Of Materials, Vol. 5. Biomolecules, Biointerfaces, And Applications,* Academic Press. San Diego, **2001**, pp. 33.

46 Lvov, Y.; Ariga, K.; Ichinose, I.; Kunitake, T., *J. Am. Chem. Soc.*, **1995**, *117*, 6117.

47 Rubinstein, I., Bard, A.J., *J. Am. Chem. Soc.,* **1980**, *102*, 6642.

48 Henle, E.S., Lou, Y., Linn, S., *Biochem.,* **1996**, *35*, 12212.

49 Henle, E.S., Linn, S., *J. Biol. Chem.,* **1997**, *272*, 19095.

50 Baik, M-H., Silverman, J.S., Yang, I.V., Ropp, P.A., Szalai, V.A., Yang, W., Thorp, H.H., *J. Phys. Chem. B,* **2001**, *105*, 6437.

51 Jovanaic, S.V., Simic, M.G., *J. Phys. Chem.,* **1986**, *90*, 974.

52 Floyd, R.A.; West, M.S.; Eneff, K.L.; Schneider, J.E.; Wong, P.K.; Tingey, D.T.; Hogsett, W.E.; *Anal. Biochem.,* **1990**, *188*, 155.

53 Goyal, R.N.; Jain, N.; Garg, D.K.; *Bioelectrochem. Bioenerg.*, **1997**, *43*, 105.

54 Hickerson, R.P.; Prat, F.; Muller, J.G.; Foote, C.S.; Burrows, C.J.; *J. Am. Chem. Soc.,* **1999**, *121*, 9423.

55 Decher, G. *Science,* **1997**, *227*, 1232.

56 Zhou, L.; Yang, J.; Estavillo, C.; Stuart, J. D.; Schenkman, J. B., J. F. Rusling, *J. Am. Chem. Soc.* **2003**, *125*, 1431.

57 Zuman, P.; Patel, R. *Techniques in Organic Reaction Mechanisms.* Wiley: New York, 1984. pp. 96.

58 Epstein, I. R.; Kustin, K. *J. Phys. Chem.* **1985**, *89*, 2275.

59 Scheeline, A.; Olson, D. L.; Williksen, E. P.; Horras, G. A. *Chem. Rev.* **1997**, *97*, 739.

CHAPTER 5

DIRECT ELECTROCHEMILUMINESCENT PROPERTIES OF RUTHENIUM BIS(BIPTRIDYL) COMPLEXES IN SOLUTION AND WITHIN THIN FILMS

"In this house, we OBEY the laws of thermodynamics"

Homer Simpson

5.1 Introduction:

The luminescence arising from the electron transfer recombination of electrogenerated reactants known as electrochemiluminescence (ECL), has been the subject of study since the late 1960s.[1,2] Extensive studies have been performed on both organic and inorganic systems. In the case of organic systems, poly aromatic hydrocarbons such as diphenylanthracene[3,4,5] and ruberene[6] have received the most attention, while studies of inorganic ECL systems have been dominated by transition metal complexes,[7,8,9] particularly ruthenium poly(pyridyl) species, e.g., those of the general formula $Ru(L)_3^{2+}$, where L = 2,2'bipyridine,[10,11] 4,7-diphenyl-1,10-phenanthroline[12] or 2,2'-bipyrazine.[13] This is due to the attractive photophysical and electrochemical properties which these compounds typically possess.

Extensive investigations have been carried out on ECL systems including the spectral characterisation of the emission,[14] solvent[15] and temperature[16] effects, magnetic field effects[17] as well as the kinetics and thermodynamics of the processes involved.[18] There is also an extensive body of data on the modelling and simulation of these processes.[19,20] The increasing interest in the study of ECL producing systems is due to the possibility of using them for analytical applications[21] and of developing light emitting devices[22,23] and lasers.[24] Furthermore, ECL studies may help to enhance our understanding of fundamental electron transfer processes from excited states so that such studies are also of importance in the fields of photoelectrochemical conversion and storage of solar energy.

The majority of ECL systems that have been investigated have involved species dissolved in the electrolyte phase with emission occurring in the diffusion layer near the electrode surface. However, ECL has been generated in films constrained to the surface of an electrode, *e.g.*, as thin layers produced by electropolymerisation of vinyl containing monomeric species[25] or by electrostatic incorporation of the luminescent species into a pre-formed polymeric matrix.[26] Emission *via* ECL in

monolayer films formed by self assembly or Langmuir-Blodgett (LB) techniques has also been demonstrated.[27,28] The detection of emission from monolayer films on metallic and semiconductor surfaces showed that emission from excited states generated by electron transfer could compete with quenching by the electrode.

In this chapter we will give an account of our investigations into the ECL properties of a number of ruthenium poly(pyridyl) systems in both solution phase and as modifying layers on electrode surfaces. Emission from monolayers is investigated and we describe the first instance of ECL from electrodes modified with a pre-formed polymer in which the luminescent species is covalently bound to the polymeric back-bone. A significant advantage of this type of system arises from the fact that the polymer is soluble and therefore its ECL can be characterised in solution as well as in the solid-state format. The ECL properties are characterised with a view to the rational design of sensors based on these systems. The key attributes are excited state lifetimes,τ, the electron transfer rate constant, k_{et}, and ΔG_{et}. The excited states lifetimes are important since the lifetime of the light produced must be long enough so that it can be measured but not too long to create a history affect within the sensor. k_{et} and ΔG_{et} are also important as these govern the response of the sensor.

5.2 *Apparatus and Reagents:*

Absorbance and photo-luminescence were recorded using a Shimadzu UV-240 spectrophotometer and a Perkin Elmer LS-50 luminescence spectrometer respectively. Spectroelectrochemical experiments were performed in a quartz thin layer spectroelectrochemical cell using a CH instruments (Memphis TN.) Model 660 potentiostat. A platinum flag or platinum gauze (~1 cm^2) was used as the working electrode with platinum gauze and Ag/AgCl as counter and reference electrodes respectively. All other electrochemical experiments were carried out using a 3 mm diameter platinum or glassy carbon working electrode in a conventional three electrode assembly. Potentials are quoted verses Ag/AgCl, or Ag wire where stated.

Cyclic voltammetry measurements were made using the Model 660A. Measurements involving simultaneous detection of light and current utilised a CH instrument Model 660A potentiostat and an Oriel 70680 photomultiplier tube (PMT) equipped with a high voltage power supply, (Oriel, Model 70705), which was used at a bias of -850 V, and amplifier / recorder (Oriel, Model 70701). During experiments the cell was placed inside a specially made holder which positioned the working electrode in a reproducible manner directly opposite the face of a fibre optic bundle, the other end of which was coupled to the PMT. The entire electrode assembly was contained inside a light-tight box, as shown in Figure 5.1.

An Oriel Model IS520 gated intensified CCD operated at -20^{0}C, coupled to an Oriel model MS125 spectrograph was used to acquire ECL spectra. With suitable signal averaging, this configuration allows for a complete emission spectrum (spectral range 250 nm) to be obtained within times as short as 10 ns. The emission spectra were typically recorded using the average of twenty laser shots. The gatewidth, *i.e.*, the exposure time of the CCD, was never more than 5 % of the excited state lifetime. The step size, *i.e.*, the time between the acquisition of discrete spectra, was typically 5 % of the excited state half life. All solutions were

thoroughly degassed using nitrogen or Argon prior to measurements. Co-reactants, sodium oxalate ($Na_2C_2O_4$), guanine and electrolyte tetrabuthylammonium tetrafluoroborate ($TBABF_4$) were purchased from Aldrich. $TBABF_4$ was dried *in vacuo* prior to use and all solvents used were of spectroscopic grade and were stored over activated molecular sieves. All other compounds used are described in Chapter 2.

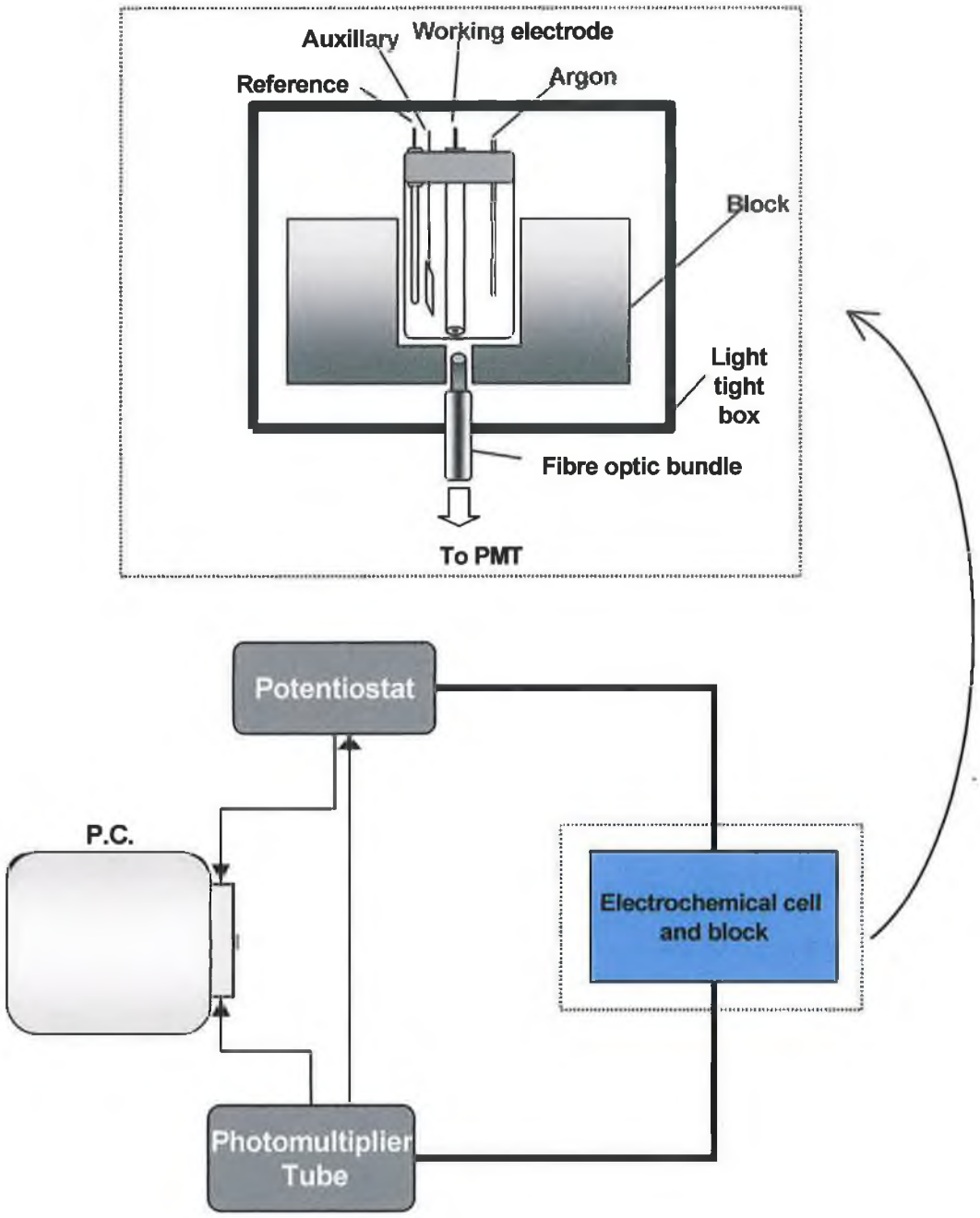

Figure 5.1: *Experimental configuration for measurements involving simultaneous detection of light and current.*

5.3 *Results & Discussion:*

5.3.1 *General:*

There are several means by which the electrochemiluminescence of transition metal complexes, such as those investigated in this study, can be observed. The first, which is referred to as the oxidative-reductive pathway, is achieved by electro-oxidising Ru^{2+} to Ru^{3+} in the presence of another species (termed a co-reactant) present in solution, with which it can react to produce the Ru^{2+} excited state,

$$Ru^{2+} - e^{-} \rightarrow Ru^{3+} \quad \textbf{(1)}$$

$$Ru^{3+} + co\text{-}reactant \rightarrow [Ru^{2+}]^{*} \quad \textbf{(2)}$$

$$[Ru^{2+}]^{*} \rightarrow Ru^{2+} + h\nu \quad \textbf{(3)}$$

This is perhaps the most convenient route, since application of only a single potential is required and steady state light emission can be achieved by maintaining a fixed potential. The intensity of the emission is controlled by the diffusional mass transport through the solution. Also the oxidation of the Ru^{2+} species normally occurs at in a potential region (~1.2V) which is easily accessible in most solvent / electrolyte systems.

Alternatively, by biasing the electrode at a suitably negative potential in order to generate the Ru^{+1} (or indeed Ru^{0} or Ru^{-1}) species in the presence of a co-reactant with suitable oxidising properties, the excited state can be generated, *i.e.,*

$$Ru^{2+} + e^{-} \rightarrow Ru^{+} \quad \textbf{(4)}$$

$$Ru^{+} + co\text{-}reactant \rightarrow [Ru^{2+}]^{*} \quad \textbf{(5)}$$

followed by reaction 3. This pathway is termed as reductive-oxidative. Although this method also involves only a single potential application, the somewhat negative potentials required for the generation of the +1 charged species renders it inaccessible in aqueous electrolyte and in some instances can lead to complications related to the relative instability of the +1 charged species or competing side reactions involving solvent decomposition products. It is also important that the formal potential of the co-reactant must be capable of reducing and oxidising the ruthenium 3+ and 1+ species respectively.

The third and final reaction pathway involves the generation of the reduced and oxidised species sequentially at the electrode surface. Here, for example if a double potential step technique is used, the oxidised species diffusing out from the electrode during the forward pulse will diffuse in toward the electrode during the reverse pulse and meet the electrogenerated reduced species in a reaction zone adjacent to the electrode, *i.e.* reactions 1 and 4 followed by:

$$Ru^{3+} + Ru^{+} \rightarrow [Ru^{2+}]^{*} + Ru^{2+} \quad \textbf{(6)}$$

proceeded by reaction 3. This route is referred to as the annihilation pathway.

5.3.2 Solution Phase ECL:

Initial ECL experiments were performed using the oxidative-reductive co-reactant pathway using 1 mM of the polymer dissolved in H_2SO_4 or DMF containing 0.1 M $TBABF_4$, as supporting electrolyte, in the presence of tripropylamine (TPA). When a potential which is more positive than the potential for the oxidation of $[Ru(bpy)_2(PVP)_{10}]^{2+}$ was applied to the platinum electrode, emission of wavelength 612 nm was observed. Emission monitored at this wavelength is "turned on" by applying a potential of 1.25 V and decreases quickly when the potential is returned to its open circuit value. Control experiments in which either the polymer or the co-reactant was absent from the test solution showed no potential switchable emission.

Spectroelectrochemistry was performed to confirm the production of a ruthenium 3+ species at the potentials utilised throughout this investigation. Figure 5.2 shows the spectral changes evident on bulk electrolysis of a 1 mM solution of $[Ru(bpy)_2(PVP)_{10}]^{2+}$ dissolved in 1 M H_2SO_4, when subjected to a potential of ~1.25 V. The formation of the ruthenium 3+ species is clearly evidenced by the decline of the peaks at 345 nm, which are metal centred (MC) transitions[29], and 460 nm, which are MLCT bands from $d \rightarrow \pi^*$ transitions, indicative of Ru^{2+} centres, and the appearance of a peak at about 310 nm, which is characteristic of the 3+ species. Visually these spectral changes are manifested by the solution changing colour from orange to green over the course of the electrolysis which is characteristic of the formation of the $Ru(N)_6^{3+}$ species. The spectral changes were fully reversible and the spectrum returned to its original form on switching the potential to a potential more negative than E^o, ~0.6 V. The decline of the Ru^{2+} peaks and appearance of a peak at ~ 310 nm which represents the formation of the Ru^{3+} species was also evident when a voltage of ~ 1.25 V was applied to a solution of $Ru(bpy)_3^{2+}$. The peak at ~ 345 nm is attributed to ligand based charge transfer. A well defined isosbectic point can be seen in Figures 5.2 and 5.3 at 325 nm. The isosbectic point

is the point at which the curves of absorbance against wavelength intersect. Isosbectic points are commonly met when electronic spectra are taken either in a solution in which a chemical reaction is in progress, in which case the two absorbing components concerned are a reactant and a product, of on a solution in which the two absorbing components are in equilibrium. If the reactant and product are single chemical species, isosbectic points will appear at all wavelengths at which their molar absorption coefficients are the same. The fact that the spectra intersect at a definite point also implies that there is no reaction intermediate between the reaction of ruthenium 2+ species to ruthenium 3+ species showing a simple conversion processes corresponding to a one electron transfer process which can also be in the cyclic voltammograms recorded for these complexes (See Figure 5.11). The isosbectic points are the same for both the ruthenium complexes.

It was also possible to generate the ruthenium(III) species chemically. On addition of a few drops of acidified lead oxide to a solution of the polymer the characteristic colour change from orange to green was observed. Solutions of the polymer which had been chemically oxidised in this manner or subject to bulk electrolysis as described previously showed luminescence when reduced by addition of guanine.

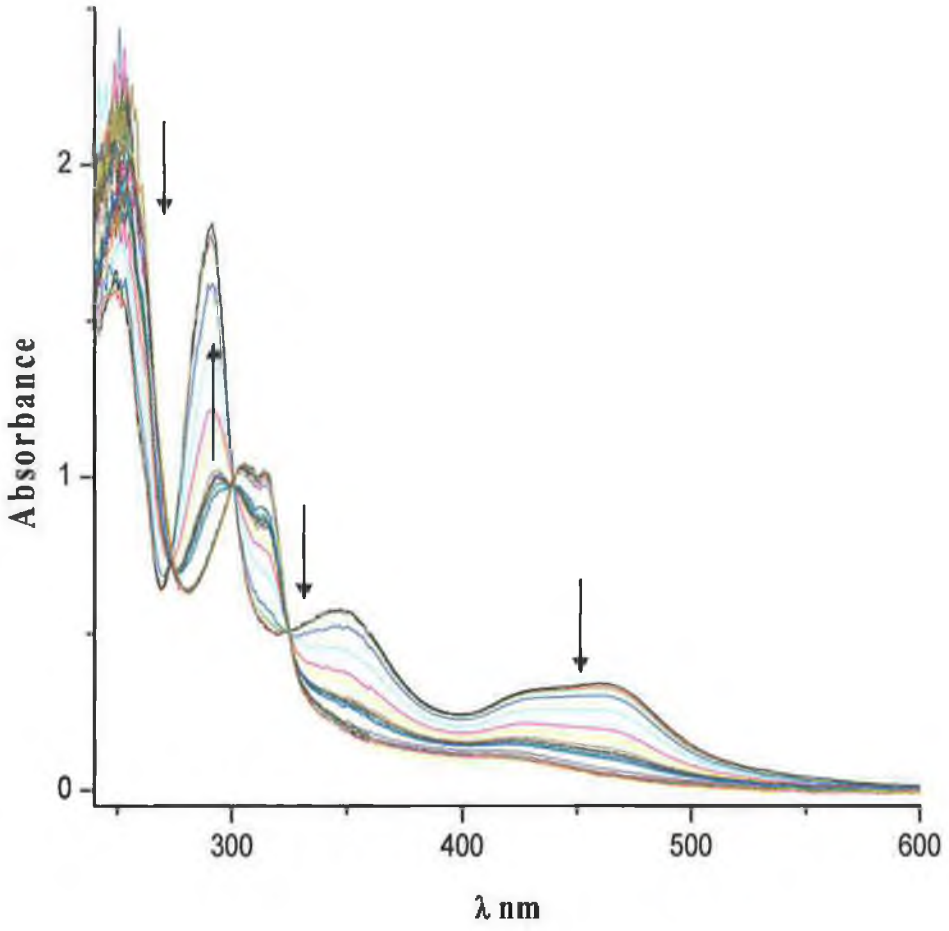

Figure 5.2: *Spectral changes induced in a 1 mM solution of* $[Ru(bpy)_2(PVP)_{10}]^{2+}$ *dissolved in 0.1 M* H_2SO_4 *by bulk electrolysis at 1.25 V for a period of approximately 150 mins.*

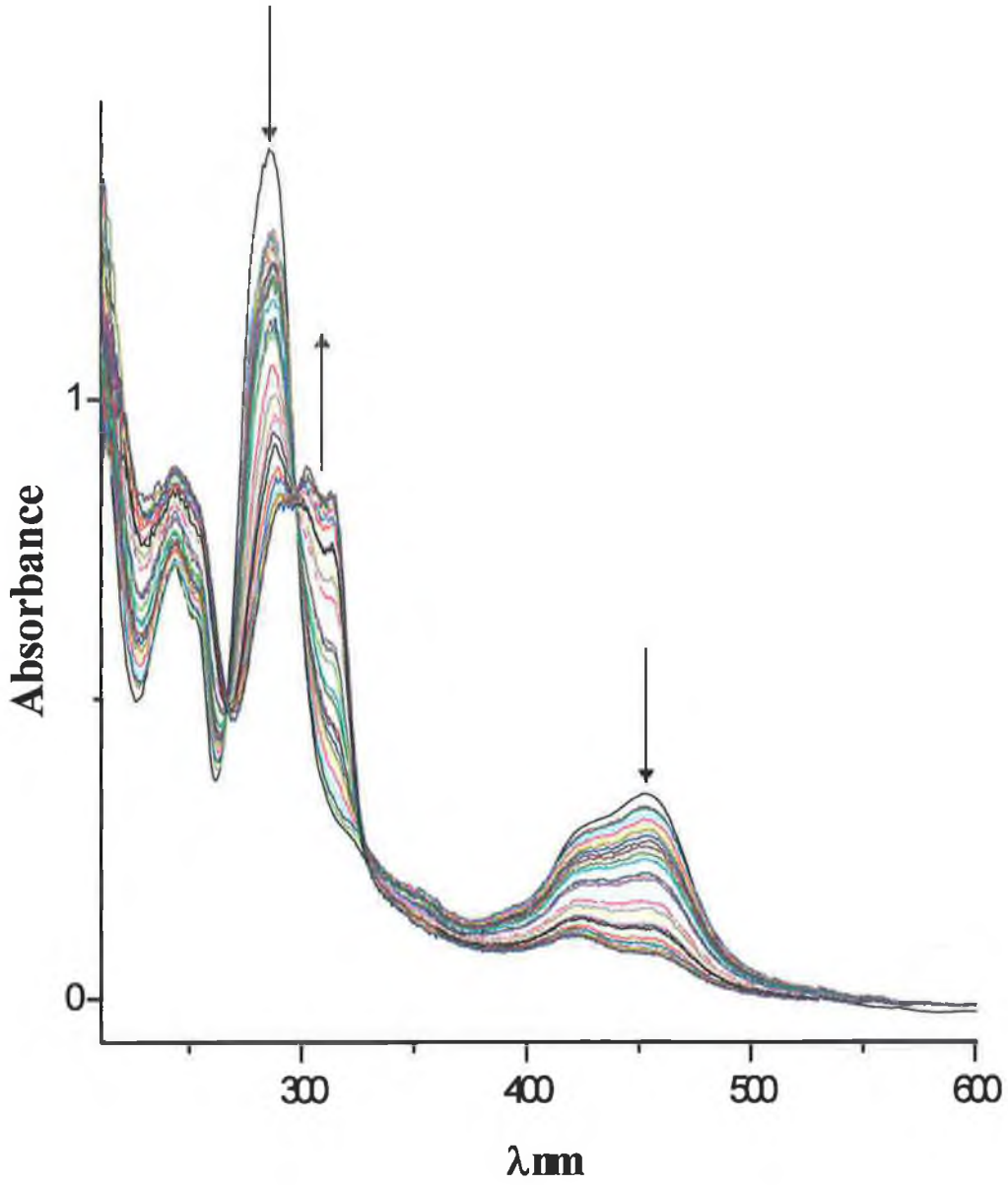

Figure 5.3: *Spectral changes induced in a 1 mM solution of* $Ru(bpy)_2^{3+}$ *dissolved in 0.1 M* H_2SO_4 *by bulk electrolysis at 1.25 V for a period of approximately 60 mins.*

Figure 5.4 shows a slow scan rate cyclic voltammogram of $Ru(bpy)_2(PVP)_{10}^{2+}$ carried out in blank supporting electrolyte. From this procedure, different concentrations of the active Ru^{3+} are created by applying suitable potentials, which was also shown from the UV spectrum obtained and described previously. Step-wise integration of this background corrected cyclic voltammogram demonstrated that the Nernst equation provides an adequate description of the potential dependence of the redox composition of the layer with a slope of 61 ± 8 mV/decade, (Figure 5.5). Using this approach, it is possible to vary the concentration of the Ru^{3+} centres from 0 to 0.8 M. It is necessary for the concentration of Ru^{3+} centres at defined potentials to be known in order to calculate the self quenching rate constant described in Section 5.3.4.

The cyclic voltammogram in Figure 5.4 shows a typical CV used for characterising modifying layers under conditions of finite diffusion. This is the condition in which the redox composition of the layer is thermodynamic equilibrium with the electrode potential (the Nernst condition), it will be observed for all electrochemical reversible reactions at sufficiently slow cyclic voltammogram scan rates, such that all electroactive centres undergo redox transformation on the time scale considered.

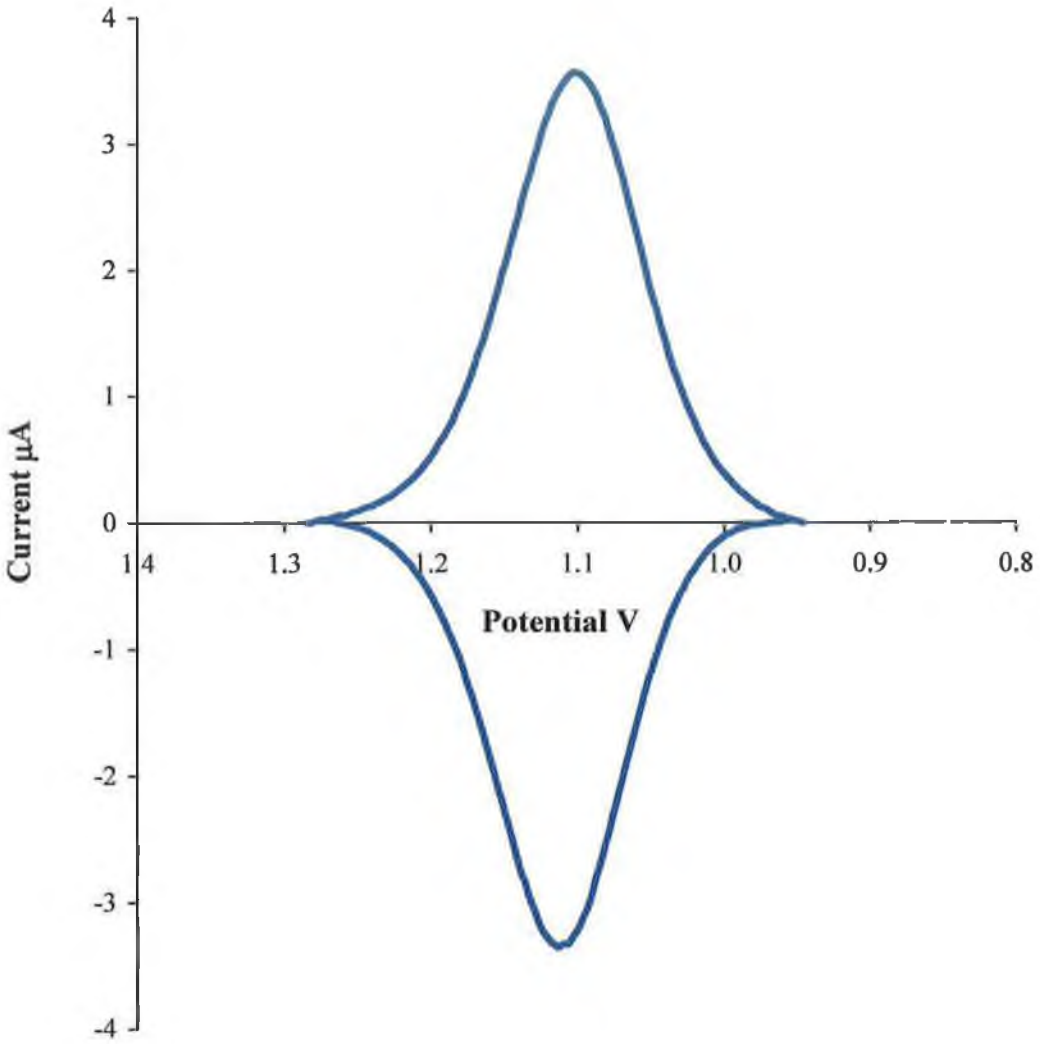

Figure 5.4: *Background corrected cyclic voltammogram of $Ru(bpy)_2(PVP)_{10}^{2+}$ thin film on a glassy carbon electrode in 0.1 M H_2SO_4 supporting electrolyte. Scan rate used was 5 mV/s.*

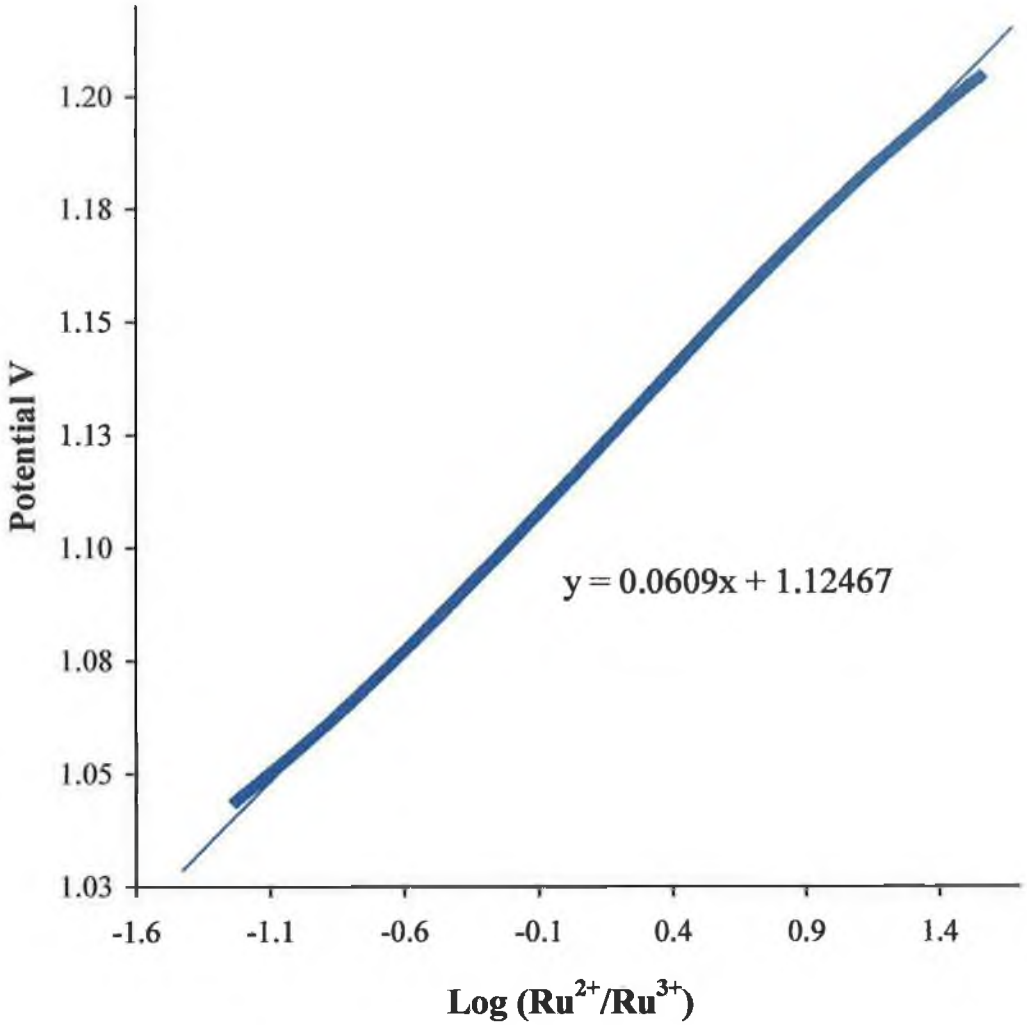

Figure 5.5: *Nernst plot derived from data in Figure 5.4. Standard deviation was less than 2%.*

Figure 5.6 shows a cyclic voltammogram of a 1 mM solution of the polymer in the presence of 0.1 M tripropylamine (TPA) with simultaneous light detection. It can clearly be seen that the onset of light emission coincides closely with the onset of oxidative current at the potential where the Ru^{3+} species is generated. The current response is typical of a mediated reaction occurring at a redox polymer layer. The current is significantly enhanced. The changes in the peak shape compared with that observed in Figure 5.4 are due to expanding diffusion layer which occurs when the Ru^{3+} species are being regenerated from the action of TPA in solution. The TPA oxidises the 3+ species and at positive potentials this is then reduced back faster and faster, extending the diffusion layer far into the bulk solution.

The light emission is attributed to the ^{3}MLCT excited state, $[Ru(bpy)_2(PVP)_{10}]^{2+}$, based on the similarity of the luminescence and ECL spectra. For example, Figure 5.7 shows an ECL spectrum of the polymer dissolved in DMF containing 0.1 M $TBABF_4$ and 0.1 M TPA at 1.2 V compared to the luminescence spectrum in which a photo-excitation wavelength of 355 nm was used.

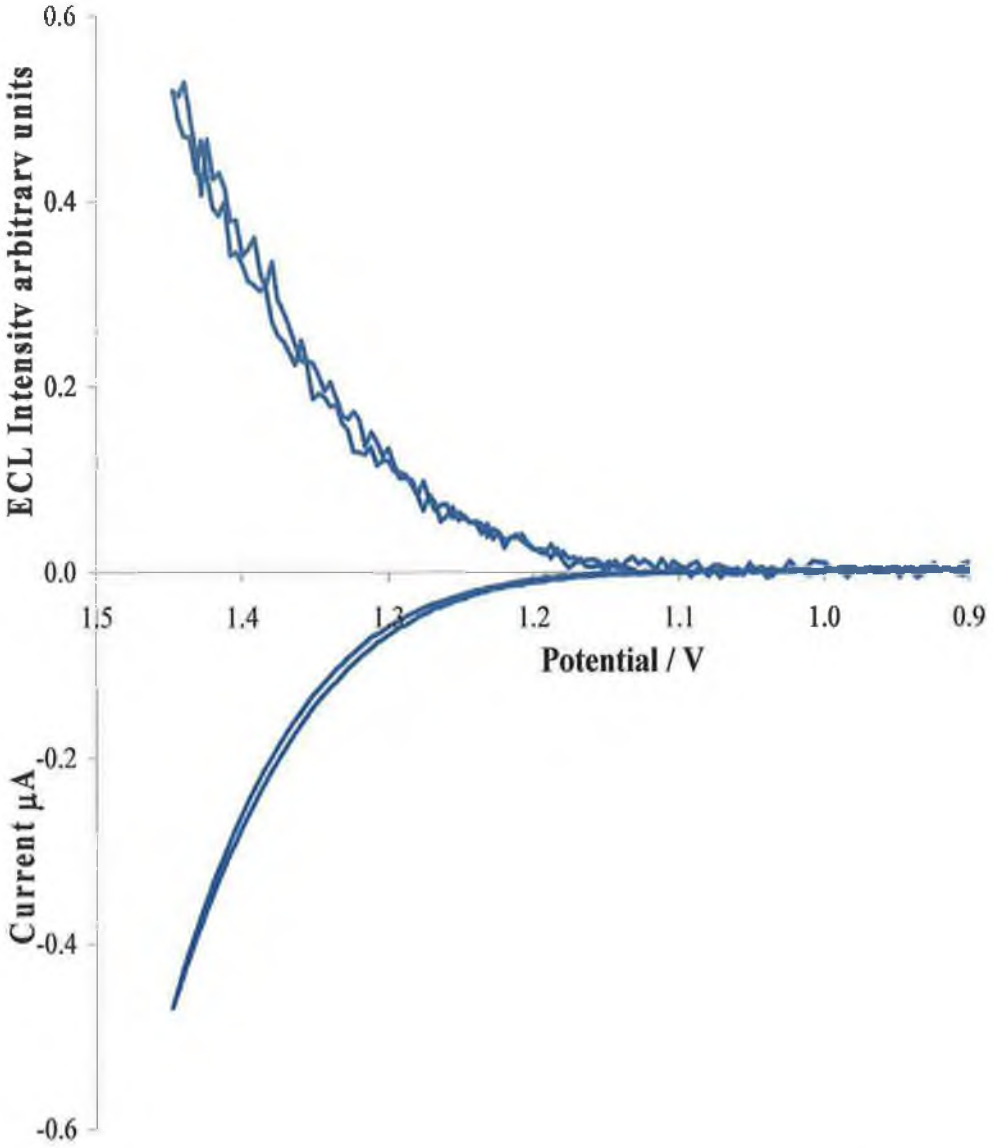

Figure 5.6: *Current and ECL – potential curves for a 1 mM solution of* $[Ru(bpy)_2(PVP)_{10}]^{2+}$ *in DMF in the presence of 0.1 M tripropylamine and 0.1 M* $TBABF_4$. *Scan rate 25* mVs^{-1}.

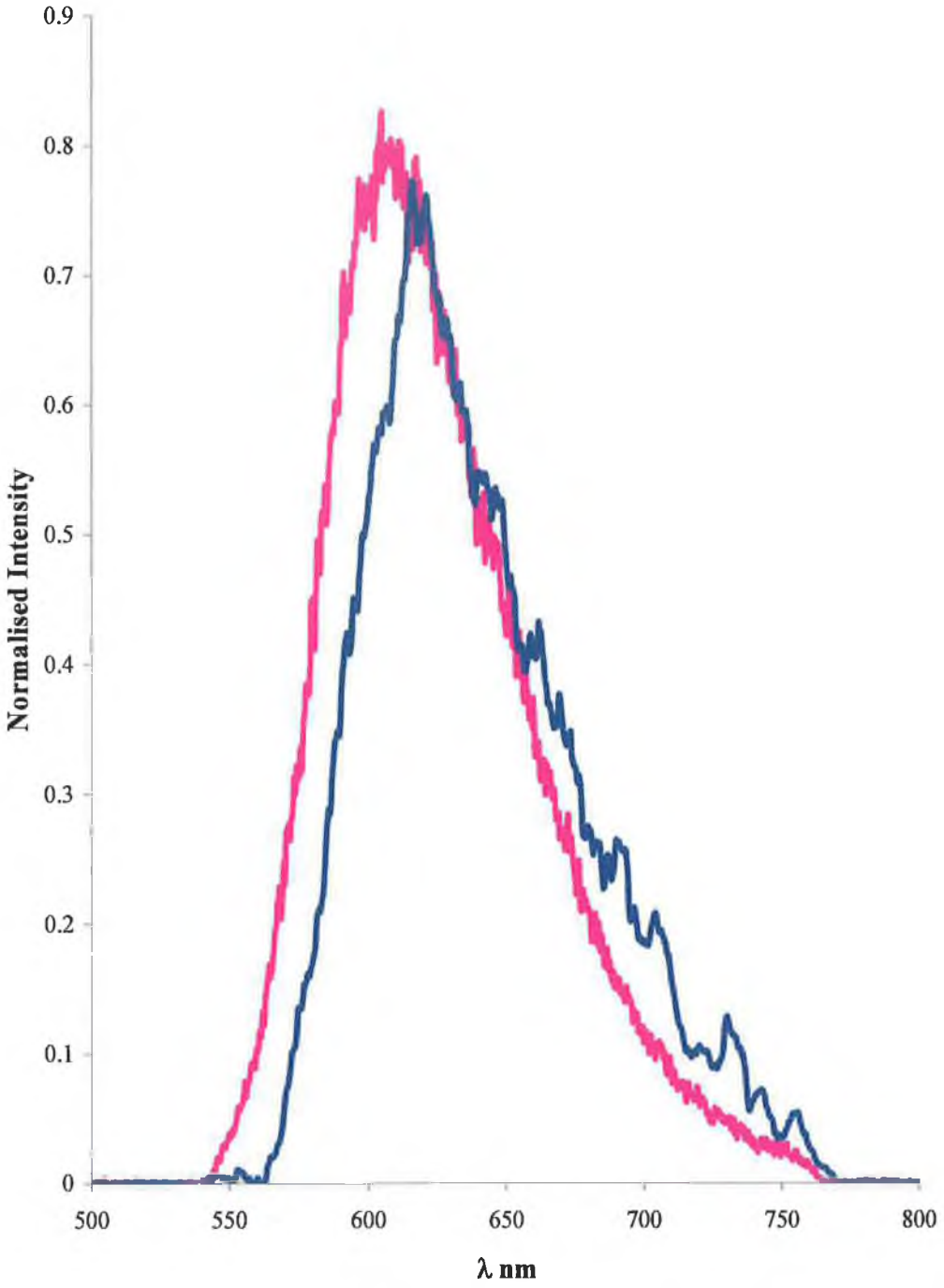

Figure 5.7: *ECL spectrum (pink) of polymer dissolved in DMF containing 0.1 M $TBABF_4$ and 0.1 M TPA. The blue line represents the photoluminescence spectrum of the same solution using a laser pulse excitation of 355 nm.*

5.3.3 ECL from Modified Electrodes:

Electrodes modified with thin films of the redox polymer $[Ru(bpy)_2(PVP)_{10}]^{2+}$, were prepared by drop casting of a 1% ethanolic solution of the polymer. Generation of ECL from polymer modified electrodes was first attempted using the annihilation pathway, i.e., pulsing between two potential limits necessary to form the Ru^{3+} and Ru^{1+} species sequentially within the layer. The experiments were carried out in acetonitrile containing 0.1 M $TBABF_4$ as supporting electrolyte. Although some ECL emission was detected using this method, it was found that the layer was unstable and desorbed from the electrode shortly after coming into contact with this solvent. Aqueous solvent mixtures containing up to 50 % water were also tried but did not improve stability.

ECL from the polymer modified electrode was more easily generated *via* the co-reactant pathway using oxalate dissolved in 0.1 M H_2SO_4. When the potential of the electrode, in contact with such a solution, is held at 1.2 V, a faint but constant orange luminescence is observed originating from the layer. A similar result was obtained for a modified electrode in contact with electrolyte containing guanine.

An ECL-potential and simultaneously monitored current-potential curve for the polymer layer in a solution containing 5 mM oxalate during a 5 mVs^{-1} potential sweep is shown in Figure 5.8. The current response is typical of a mediated reaction occurring at a redox polymer layer. The current is significantly enhanced at the formal potential of the $Ru^{2+/3+}$ couple indicating a high turnover of oxalate ions by the layer. The onset of the ECL emission occurs at precisely the same potential as the increase in current and follows a similar profile, indicating that the mediated reaction involves the formation the Ru^{2+} excited state species.

The cyclic voltammogram shows a steady state being reached at potentials more positive than the formal potential. Since there is theoretically an infinite amount of Ru^{3+} centres being recycled, the limiting factor is the amount of oxalate present. At the formal potential the maximum amount of Ru^{3+} and oxalate ions are reacting, then the amount of oxalate in the diffusion layer starts to deplete. Once this occurs oxalate from the bulk solution starts to diffuse in towards the electrode and a steady state is obtained, although this would be at potentials more positive that 1.4 V, since a steady state has not yet been reached at this potential, as can be seen in Figure 5.8.

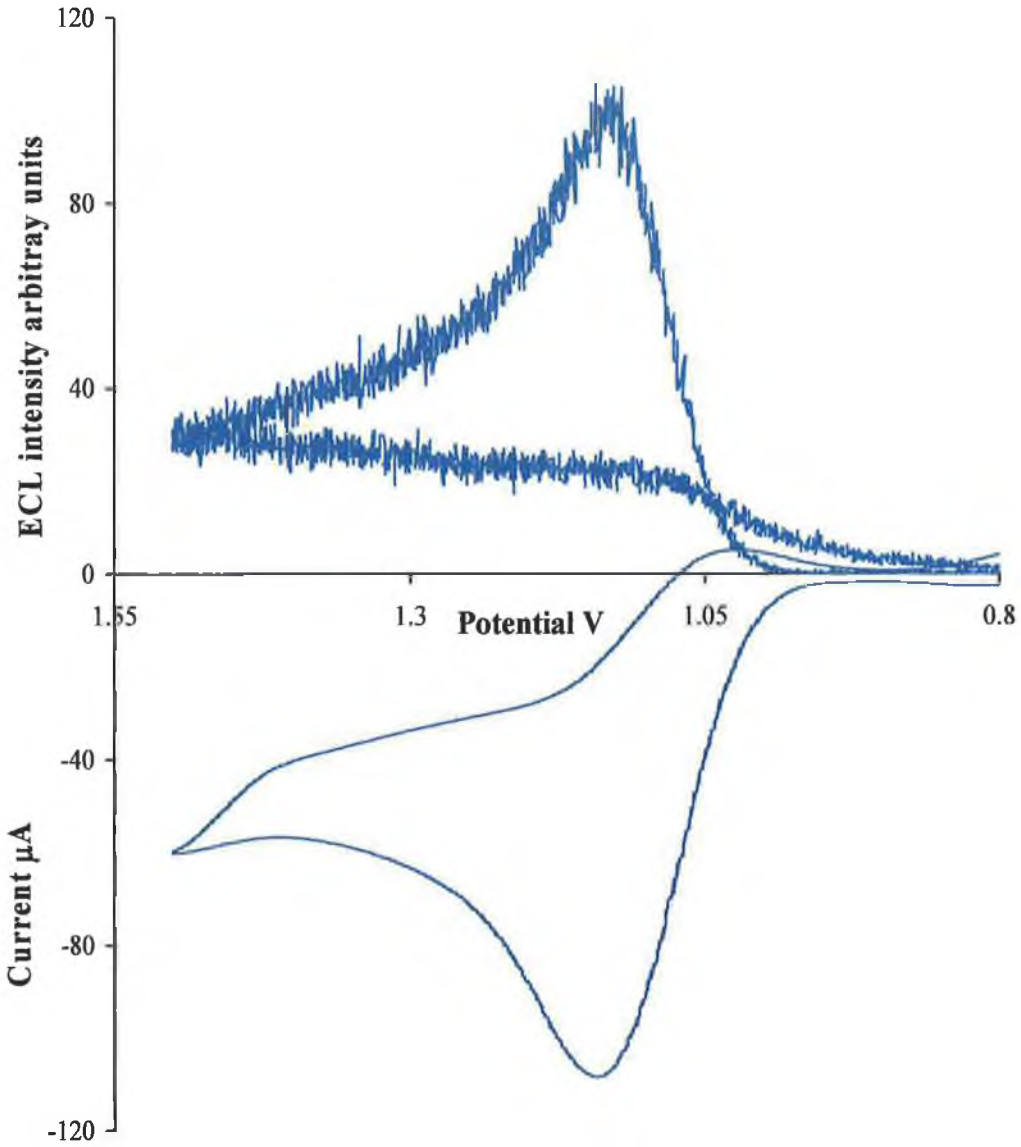

Figure 5.8: *$[Ru(bpy)_2(PVP)_{10}]^{2+}$ modified electrode (surface coverage = 2.3 x 10^{-8} mol cm^{-2}) in contact with 0.1 M H_2SO_4 electrolyte containing 5mM oxalate. Cyclic voltammetric response at 5 mV s^{-1}, with simultaneous light detection.*

Figure 5.9 shows the ECL-potential and simultaneously monitored current-potential curve for the polymer layer in a solution containing 5 mM polyguanic acid during a 5 mVs^{-1} potential sweep. It can clearly be seen that the onset of light emission coincides closely with the onset of oxidative current at the potential where the Ru^{3+} species is generated. This shows a smaller though similar response to that obtained for the solution containing oxalate indicative of a mediated reaction occurring at the redox layer. The smaller current enhancement demonstrates a lower turnover of guanine by the layer. As with the oxalate solution, the onset of the ECL emission occurs at the same potential as the increase in current and follows a similar profile, indicating that the mediated reaction involves the formation the Ru^{2+} excited state species.

The ECL response in Figure 5.9 reaches a steady state at positive potentials, which is quite different to the responses obtained in previous sections, namely Chapter 3 and 4. This is mainly due to the fact that the guanine is present in solution unlike the thin film systems. Therefore more guanine may diffuse into the electrode allowing a steady state response to be observed.

The light emission is attributed to the ^{3}MLCT excited state, $[Ru(bpy)_2(PVP)_{10}]^{2+}$, based on the similarity of the luminescence and ECL spectra. For example, Figure 5.6 shows an ECL spectrum of the polymer dissolved in PBS containing 0.1 M guanine at 1.2 V compared to the luminescence spectrum in which a photo-excitation wavelength of 355 nm was used.

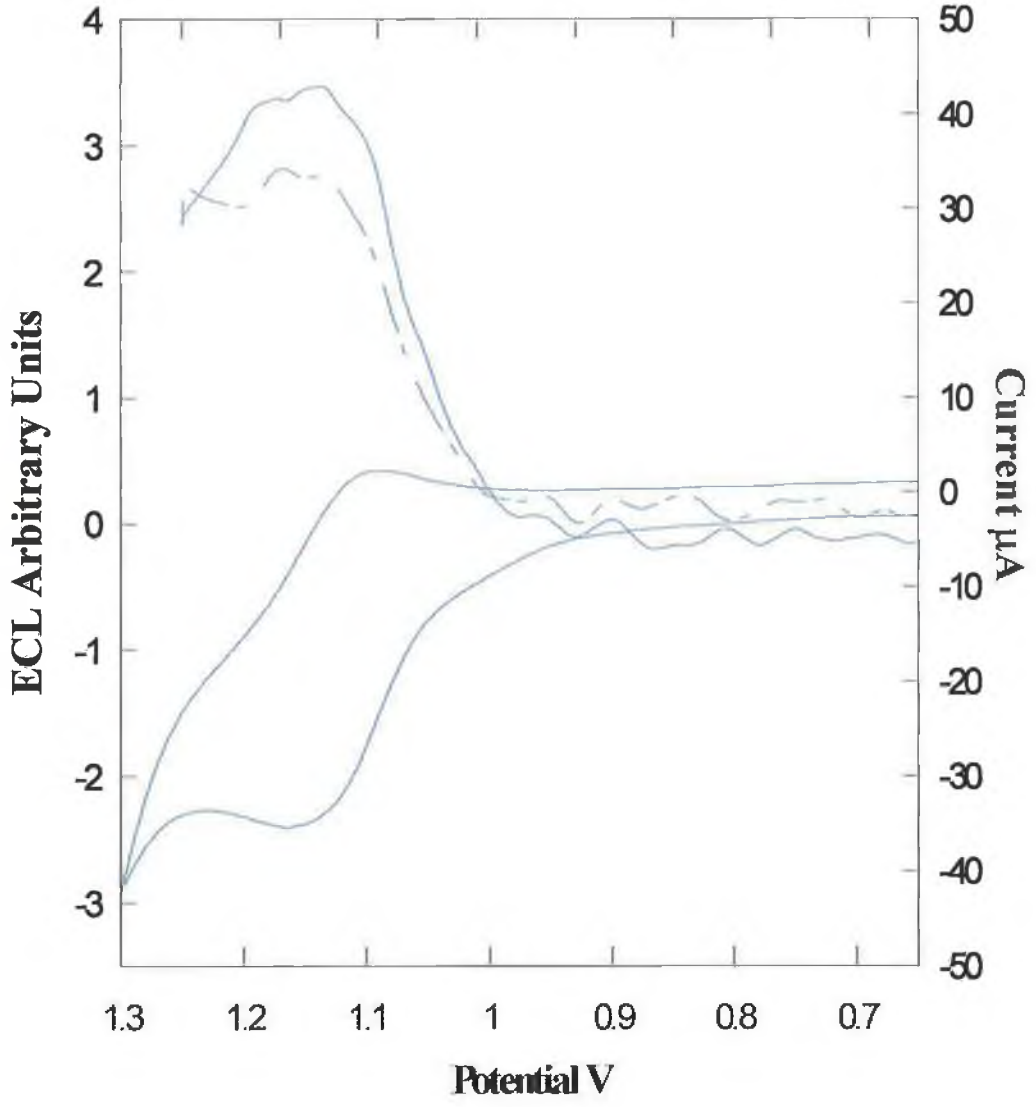

Figure 5.9: *$[Ru(bpy)_2(PVP)_{10}]^{2+}$ modified electrode (surface coverage = 2.3 x 10^{-8} mol cm^{-2}) in contact with 0.1 M PBS electrolyte containing 5 mM guanine. Cyclic voltammetric response at 5 mV s^{-1}, with simultaneous light detection.*

5.3.4 Driving Force for Photoinduced Electron Transfer:

Electron transfer is the most likely quenching mechanism in the reaction studied. It is therefore of interest to determine whether the excited state of the ruthenium moiety is quenched via oxidative or reductive electron transfer. An estimation of the thermodynamic driving force for the respective electron transfer allows for the most energetically favourable electron transfer process to be identified. If the Coulombic stabilisation energy of the products is negligible, then the thermodynamic driving force for electron transfer, ΔG^0, can be estimated from the Rehm-Weller equation[30] and the relevant formal potentials;

$$\Delta G^0 = e\left[E^0(Donor) - E^0(Acceptor)\right] - E^{00} \qquad (7)$$

where E^0(Donor) and E^0(Acceptor) are the formal potentials associated with the donor and acceptor, respectively, and E^{00} is the energy difference between the lowest vibrational levels of the ground and excited states. The value of E^{oo}, as obtained from the wavelength of maximum emission at cryogenic temperatures, is 2.07 eV. The Rehm-Weller equation can be adapted to determine the formal potential for oxidation, E^{0*}_{Ox}, and reduction, E^{0*}_{Red}, of the excited state can be calculated using the following equations;

$$E^{o*}_{Ox} = E^{o}_{Ox} + E^{oo} \qquad (8)$$

$$E^{o*}_{Red} = E^{o}_{Red} - E^{oo} \qquad (9)$$

where E^o_{Ox} and E^o_{Red} are the formal potentials associated with the first oxidation ($Ru^{2+/3+}$) and reduction ($bpy/bpy^{\bullet-}$) of the luminescent moiety in the ground state. Figure 5.10 illustrates the emission spectrum of the polymer within an ethanol:methanol solvent at 77 K. The equations above assume that all the

spectroscopic energy of the excited state (E^{00}) can be used as free energy in the redox process.[31]

The vibrational fine structure of $[Ru(bpy)_2(PVP)_{10}]^{2+}$ observed at low temperature is shown in Figure 5.10. The position of emission maximum is blue shifted by approximately 20 nm on going from 298 to 77 K, as discussed in Section 2.3.5, and a shoulder is evident at about 640 nm. The location of the peaks in this spectrum correspond closely to the emission spectrum of $[Ru(bpy)_3]^{2+}$ in EtOH:MeOH glass at 77 K.[32] The vibrational structure is assigned to a perturbed skeletal vibration of the aromatic ring, due to the removal of the π^* electron.[33]

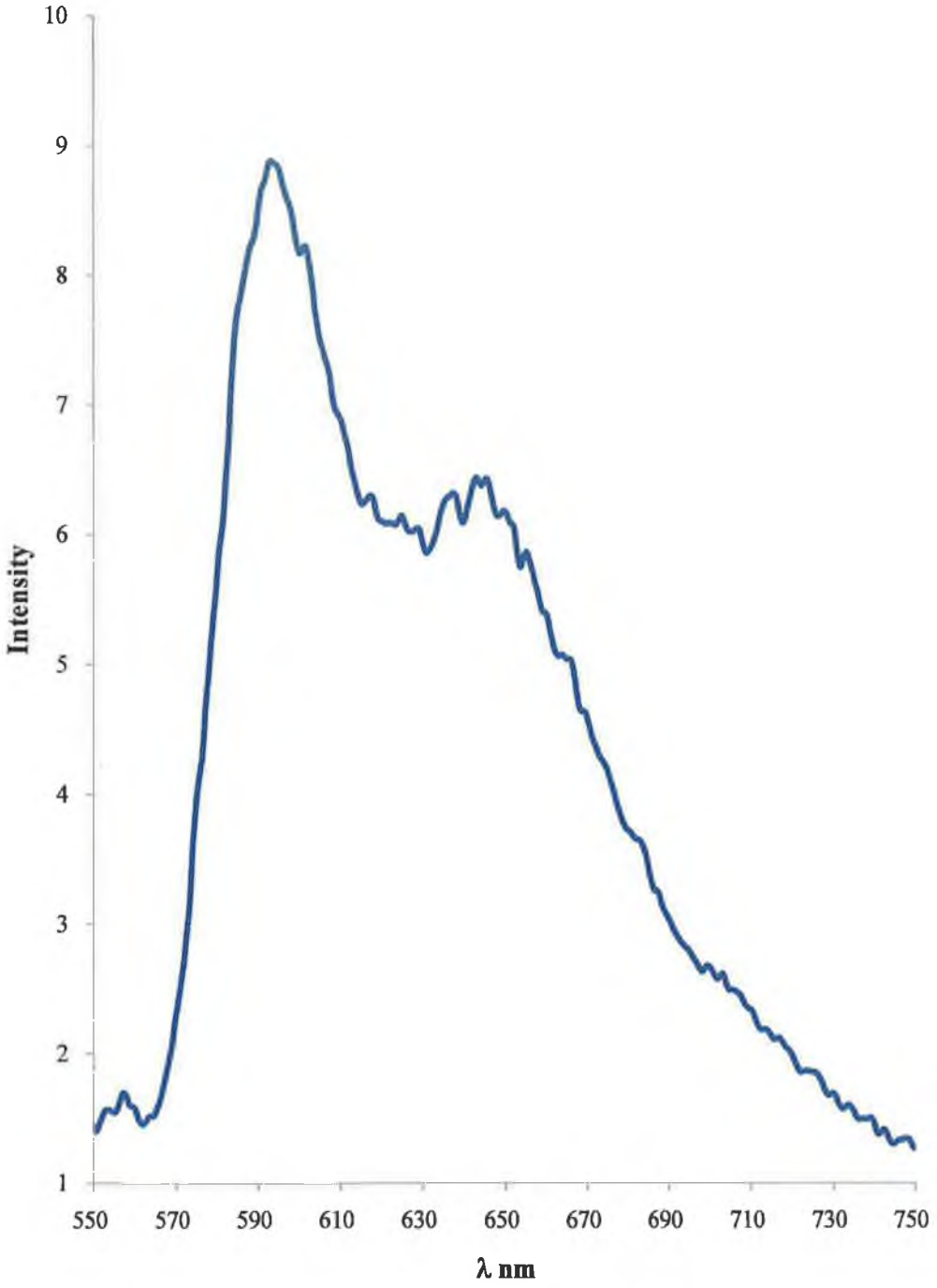

Figure 5.10: *Emission spectra of 100 μM* $[Ru(bpy)_2(PVP)_{10}]^{2+}$ *solution measured in ethanol:methanol glass at 77 K.*

In order to calculate ΔG^0, E^o_{Ox} and E^o_{Red} must be known. Figure 5.11 illustrates a solution phase cyclic voltammogram of $[Ru(bpy)_2(PVP)_{10}]^{2+}$, it demonstrates a one reversible metal based oxidation at ~ 1.26 V, consistent with a ruthenium complex containing six nitrogen donor ligands. Knowledge of the formal potentials of the ruthenium centre with the complex allows ΔG^0 for quenching to be calculated. Solution phase cyclic voltammograms indicates that E^o_{Ox} and E^o_{Red} are 1.26 and -0.84 V respectively (See Table 5.1). Using these values and equations 5.7 and 5.8 yielded values of -0.81 and 0.72 for E^{o*}_{Ox} and E^{o*}_{Red} respectively. This analysis indicated that the driving forces, ΔG^0, for oxidative and reductive quenching are -1.65 and 0.54 V respectively.

The observation that reductive quenching is thermodynamically uphill suggests that the electronically excited state is quenching following an oxidative quenching mechanism. Beyond providing an insight into the quenching mechanism, knowledge of the driving force for photoinduced electron transfer allows the electron transfer rate constants for optically and electrochemically driven processes to be compared.

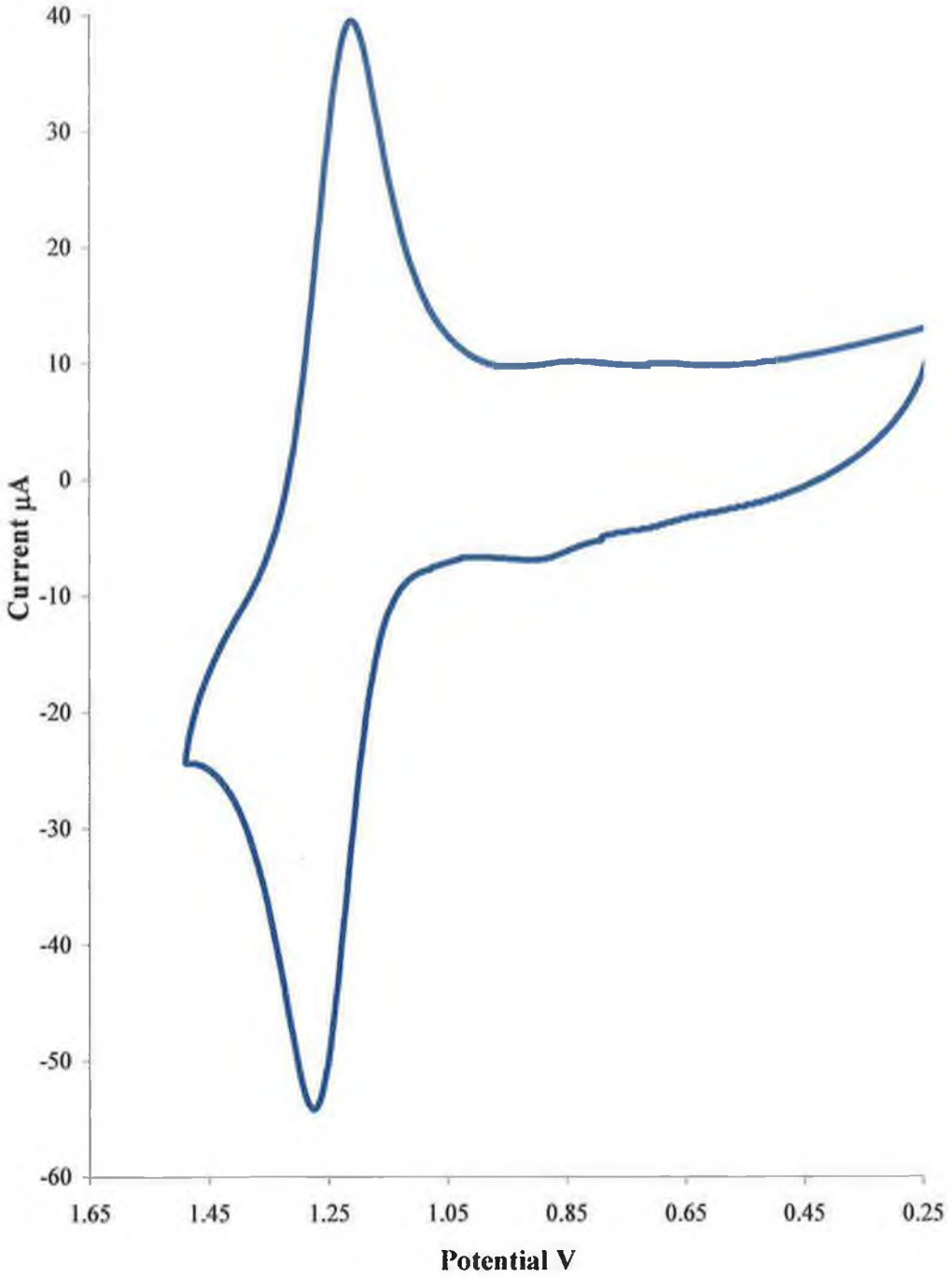

Figure 5.11: *Cyclic voltammetry of 1 mM* $[Ru(bpy)_2(PVP)_{10}]^{2+}$ *on glassy carbon (3 mm diameter), at 0.1 V* s^{-1}*. The electrolyte is 0.1 M* $TBABF_4$ *in ACN.*

The fluorescence lifetime of a substance represents the average amount of time the species remains in the excited state prior to its return to the ground state. As previously described in Section 2.3, the decay of an excited state takes place by competitive radiative and non-radiative processes. This can be expressed by the following equation;

$$\frac{1}{\tau} = k_r + k_{nr} \qquad (10)$$

where τ is the excited state lifetime and k_r and k_{nr} are the radiative and non-radiative rate constants. The fluorescent lifetime of the polymer in solution phase was measured using the laser spectroscopic system and is shown in Figures 5.12. The lifetime of $[Ru(bpy)_2(PVP)_{10}]^{2+}$ in solution was found to be 65 ± 9 ns.

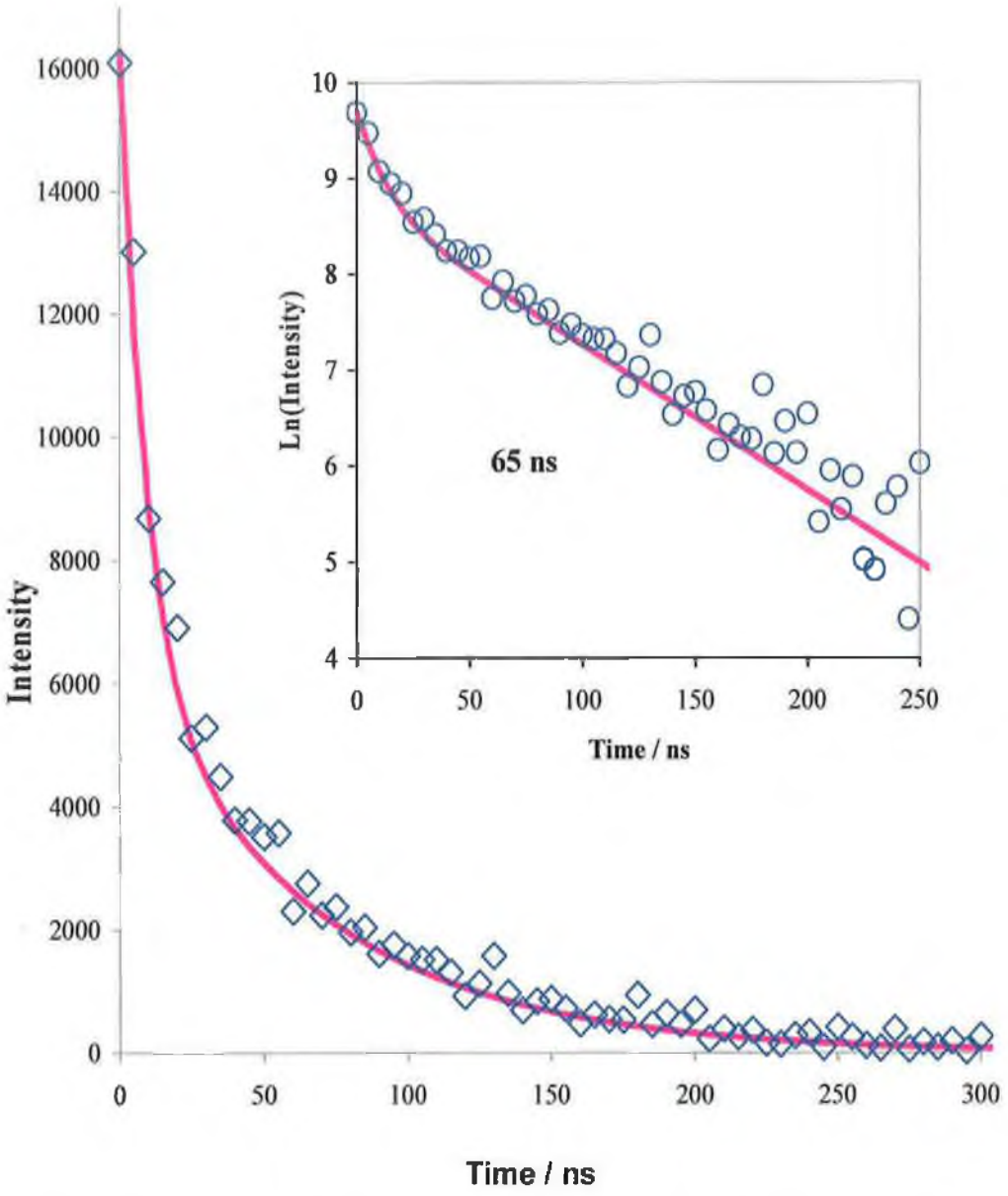

Figure 5.12: *Emission decay for a 10^{-4} M solution of $[Ru(bpy)_2(PVP)_{10}]^{2+}$ in acetonitrile monitored at 614 nm following the application of a 10 ns laser pulse of 355 nm light.*

The temperature dependence of the emission lifetime of several Ru (II) polypyridine complexes in the temperature range 1.8 – 77 K in polymethylmethacrylate matrices has been carefully investigated.[34] The luminescence was found to originate from a cluster of three closely lying levels (ΔE 10 -100 cm^{-1}) which are in Boltzmann equilibrium, each having its own radiative and non-radiative temperature independent rate constant.

In this study the temperature dependence of the luminescence lifetime for temperatures from 77 K to room temperature are investigated. For this purpose, the two levels separated by 10 cm^{-1} can be dealt with as a single level and their radiative and non-radiative rate constants account for most of the temperature independent lifetime at 77K. While the rate of the radiative transition is essentially governed by spin and symmetry factors, the radiationless rate constant generally increases with decreasing excited state energy, as expected on the basis of the energy gap law.

The temperature dependent terms can be associated with an activated surface crossing to another excited state, described by the Arrhenius equation;

$$k_{nr} = Ae^{-\Delta E / RT} \qquad \textbf{(11)}$$

By taking the natural log of this equation, it is possible to calculate the activation energy, E_a;

$$\ln k = \ln A - \frac{E_a}{RT} \qquad \textbf{(12)}$$

There is a general agreement in the literature that the Arrhenius type equation accounts for the temperature dependence of the luminescence lifetime is related to an activated surface crossing from the ^{3}MLCT manifold to a ^{3}MC level which undergoes photochemical and/or photophysical deactivation.

In systems of this kind, charge transfer may involve energy or electron transfer between molecules. Intramolecular energy transfer processes are typically temperature independent because of the small reorganisation energies involved.[35,36,37] Electron transfer is a thermally activated process involving outer sphere reorganisation energy making it sensitive to the temperature of the surrounding medium. Therefore, temperature resolved measurements of k provide a convenient means of distinguishing between photoinduced energy and electron transfer processes. Figure 5.10 illustrates a plot of ln k vs 1/T as the temperature of the ethanolic solution is systematically varied from 298 to 77 K.

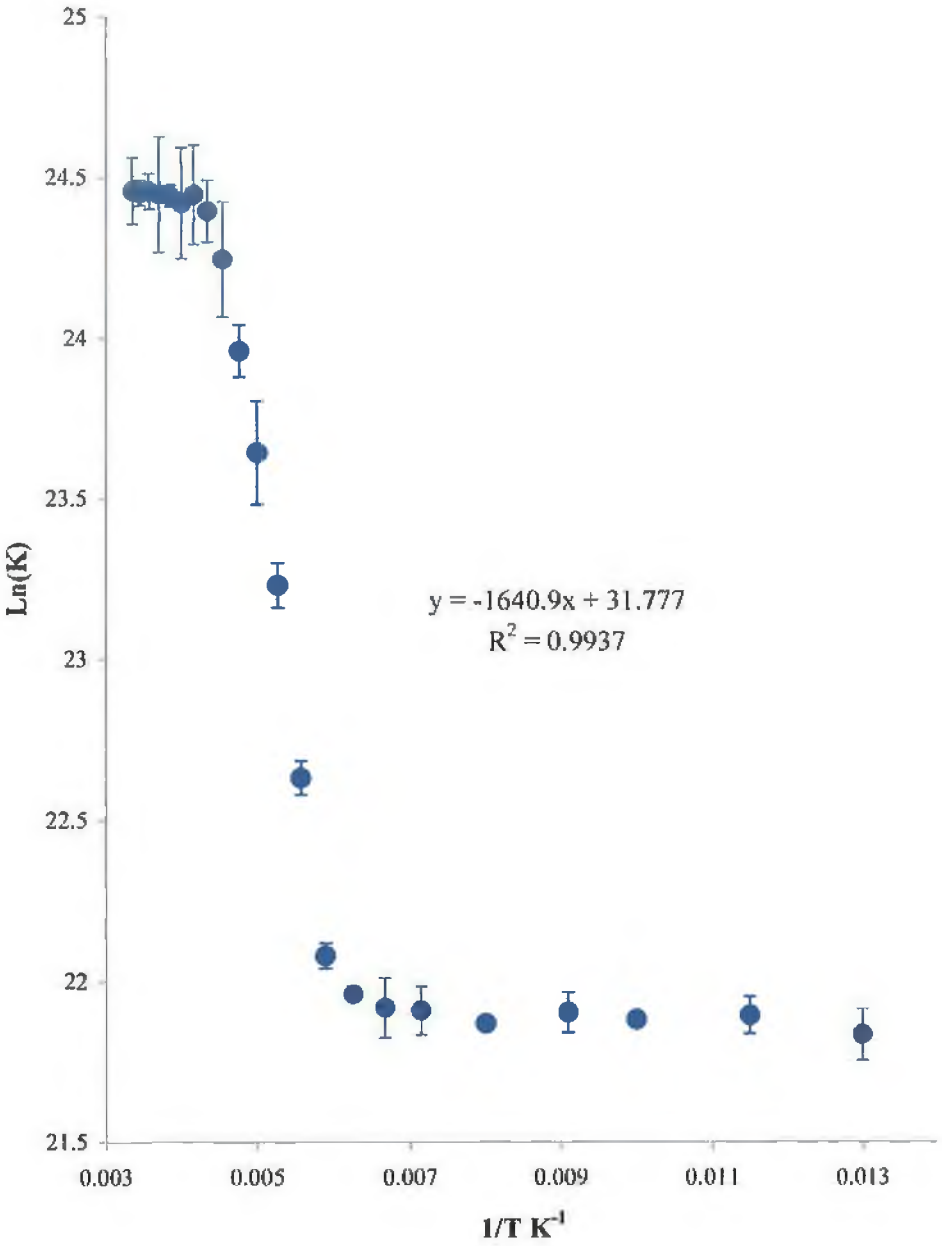

Figure 5.13: *Temperature dependence of photoinduced charge transfer for the temperature range of 77 to 298 K for a 50 mM solution of* $[Ru(bpy)_2(PVP)_{10}]^{2+}$ *degassed for 10 mins using nitrogen gas. The charge transfer rate constant, K, determined from the lifetimes of the solution at systematically varied temperatures. The equation refers to the linear part of the graph and this value is used to calculate the activation energy, Ea.*

From this graph the activation energy of the ruthenium polymer was calculated to be 12.84 $kJmol^{-1}$. This can be compared to the E_a calculated for $Ru(bpy)_3^{2+}$ under the same conditions. The E_a for 50 mM $Ru(bpy)_3^{2+}$ was determined to be 6.64 $kJmol^{-1}$. Figure 5.8 shows that the rate of charge transfer decreases rapidly with decreasing temperature on going from ~ 240 to 118 K. However, there is little change on going from 118 to 77 K. This is most likely due to temperature independent factors. The sensitivity to temperature observed in the range of 240 to 118 K indicates that photoinduced electron rather than energy transfer is the dominant quenching mechanism in this system in this temperature range.

An increase in the E_a for the ruthenium metallopolymer when compared to $Ru(bpy)_3^{2+}$ is expected, the polymer backbone being responsible for this increase.

5.3.4 Luminescent Quenching:

The photophysics and photochemistry of polypyridine complexes of ruthenium complexes, especially $Ru(bpy)_3^{2+}$, have been extensively investigated. The studies have implicated a major role for the luminescent MLCT excited state of complexes of this family. Similar conclusions have been drawn for the luminescent osmium (II) polypyridine complexes, although less data is available for this series.

The excited states of ruthenium polypyridine complexes are sufficiently long lived to undergo bimolecular collisions with other molecules. Three processes must be considered as possible quenching pathways for the polypyridine excited states:

$$ML_3^{2+*} + Q \rightarrow ML_3^{3+} + Q^- \quad \textbf{(13)}$$

$$ML_3^{2+*} + Q \rightarrow ML_3^{+} + Q^+ \quad \textbf{(14)}$$

$$ML_3^{2+*} + Q \rightarrow ML_3^{2+} + Q^* \quad \textbf{(15)}$$

The first two involve respectively oxidation and reduction of the excited state, while in equation 9, electronic excitation is transferred by an energy-transfer process to the quencher, Q. These three quenching processes, quenching by Ru^{3+}, guanine and products, may proceed in parallel so that the observed quenching rate constant may contain contributions from all three;

$$k_{q,obsd} = k_7 + k_8 + k_9 \quad \textbf{(16)}$$

Despite this complication it is possible to deduce the major quenching mechanism in the systems studied. As the electron-transfer quenching reactions are expected to be a function of the oxidation-reduction potentials of the reactants, while energy-transfer processes should depend on spectral overlap considerations. The reduction potentials and spectral data of the polypyridine complexes used in

this study are summarised in Table 5.1 and will be used as a basis for discussion in the following paragraphs.

Complex	*Ground State*		*Excited State*		*Absorbance*	*Emission*
	$E^{0}_{3,2}$ *V*	$E^{0}_{2,1}$ *V*	$E^{0*}_{3,2}$ *V*	$E^{0*}_{2,1}$ *V*	λ_{max} *nm*	λ_{max} *nm*
$Ru(bpy)_3^{2+}$	1.251	-1.28	-0.84	0.84	290, 452	605
$Ru(bpy)_2(PVP)_{10}^{2+}$	1.26	-1.35	-0.81	0.72	341, 460	612

Table 5.1: *Reduction potentials and absorption and emission maxima for* $Ru(bpy)_3^{2+}$ *and* $Ru(bpy)_2(PVP)_{10}^{2+}$.

From the previous section, it was determined that oxidative quenching was the quenching mechanism involved in this system. The Stern-Volmer equation was used to investigate further the quenching of luminescence by redox active quenchers and the direct observation if the absorption spectra of redox products formed in flash photolysis experiments. k_q can be calculated from the Stern-Volmer relationship;

$$\frac{I_0}{I} = 1 + k_q \tau_0 [Q] \qquad \textbf{(17)}$$

where I_0/I is the ratio of luminescence intensities in the absence and presence of the quencher and $[Q]$ is the quencher concentration in M. Following the quenching reactions, rapid, back electron-transfer reactions can occur between either the M(III) or the ligand reduced M(I) complexes and the reduced or oxidised forms of the quencher.

The efficiency of the electron transfer increases as spectral overlap between donor and acceptor increases. For the donor, the maximum and shape of the emission band returning the donor to ground state are considered; for the acceptor, the absorption spectrum is of relevance.

The ruthenium (II) emission spectra (λ_{max} 600 – 630 nm) overlap the absorption spectra of osmium (II) complexes (λ_{max} 590, 650 nm) so that energy transfer from the $Ru(bpy)_3^{2+}$ to $Os(bpy)_3^{2+}$ is generally expected. Quenching is thus likely to proceed by energy transfer. For this type of system electron-transfer quenching is also expected, however, most describe electron transfer quenching in osmium and ruthenium dimers linked by polypyridyl bridging ligands.[38,39]

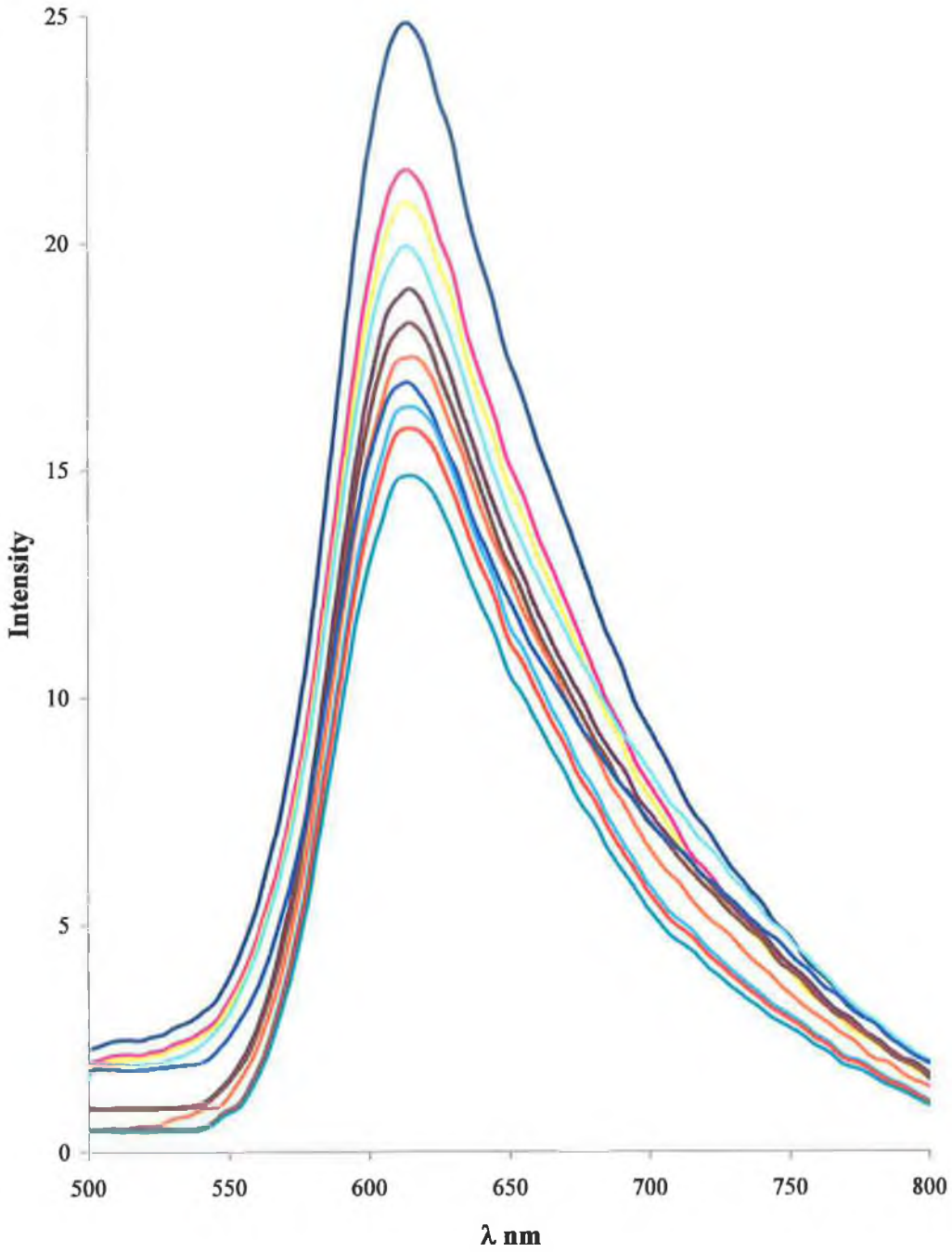

Figure 5.14: *Emission spectra of 100 μM* $[Ru(bpy)_2(PVP)_{10}]^{2+}$ *solutions containing increasing amounts of* $[Os(bpy)_3]^{2+}$ *varying from* 1×10^{-5} *to* 1×10^{-4} *M measured in ethanol at 298 K.*

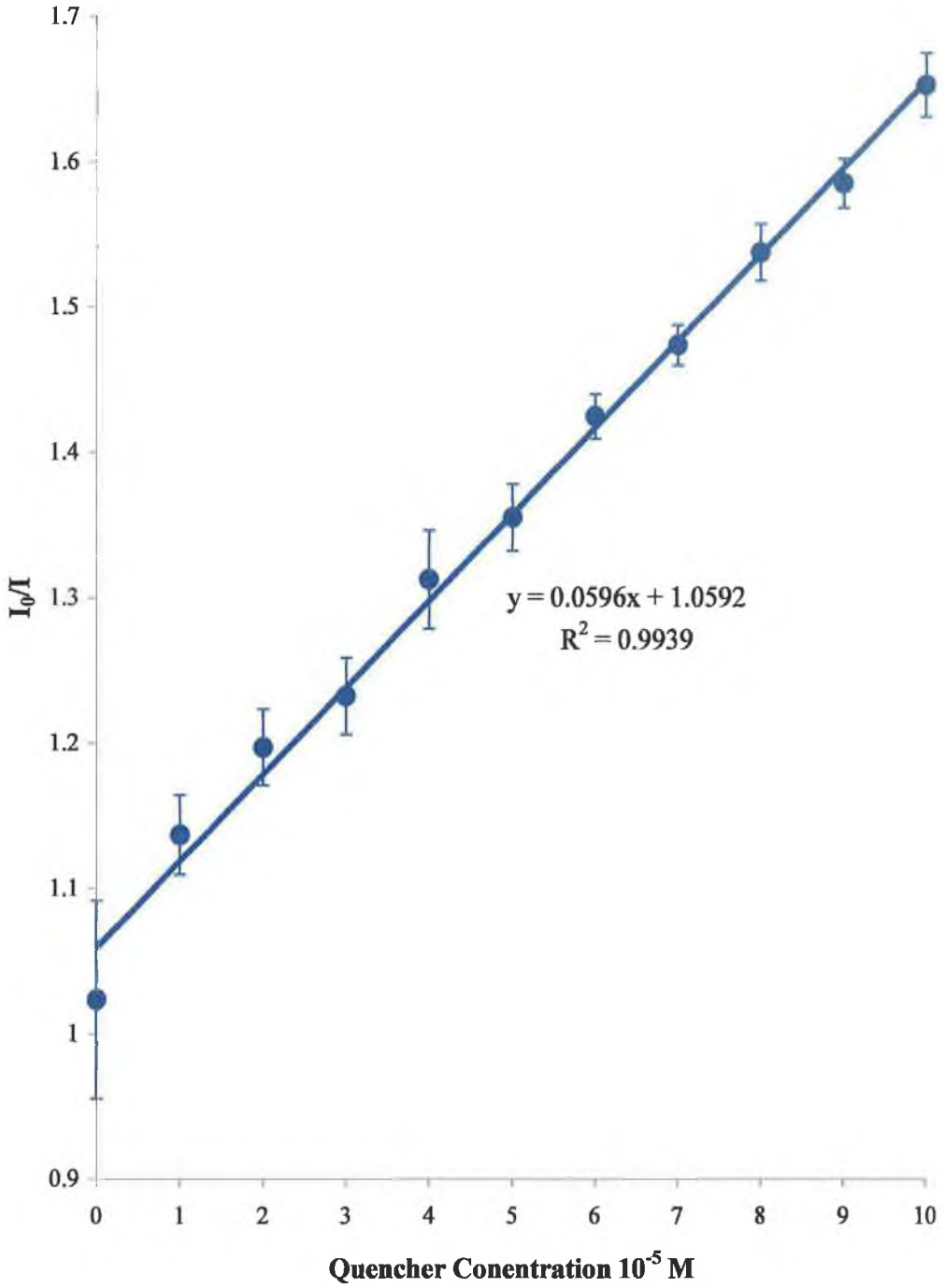

Figure 5.15: *Stern-Volmer plot derived from data in Figure 5.14.*

Figure 5.10 shows the emission spectrum of $[Ru(bpy)_2(PVP)_{10}]^{2+}$, with decreasing intensity upon addition of $[Os(bpy)_3]^{2+}$. Using the Stern-Volmer equation this data, and the emission lifetime of the ruthenium complex ,(τ = ~65 ns), was used to calculate k_q. However, the value obtained needs to be compared to that obtained from the influence of $[Os(bpy)_3]^{2+}$ on the excited state lifetime of $[Ru(bpy)_2(PVP)_{10}]^{2+}$ in order to determine if the quenching mechanism is dynamic or static.

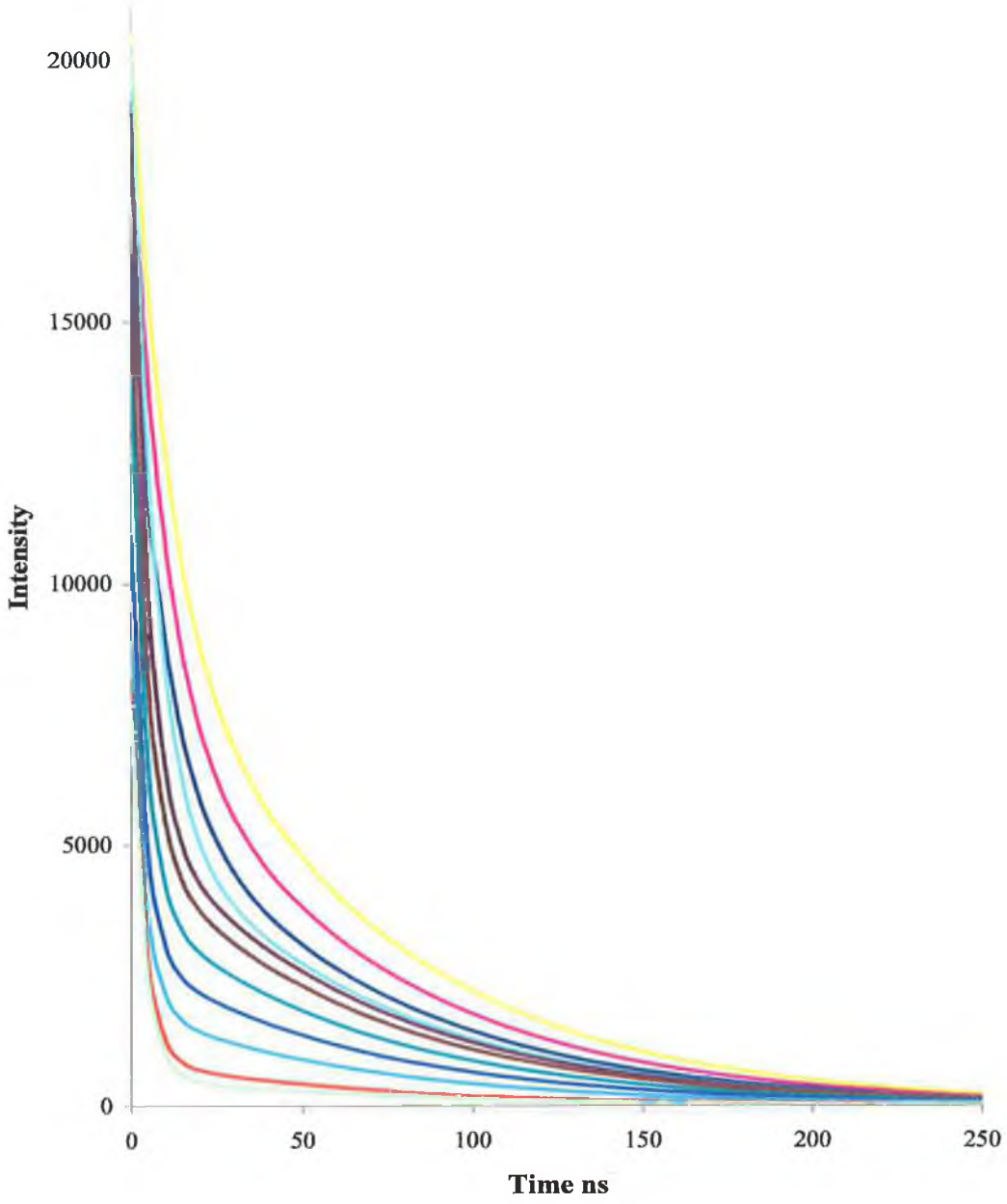

Figure 5.15: *Influence of $[Os(bpy)_3]^{2+}$ in the concentration range of 1 x 10^{-5} to 1 x 10^{-4} M on the emission decay of 10^{-4} M $[Ru(bpy)_2(PVP)_{10}]^{2+}$ in ethanol monitored at 614 nm following the application of a 10 ns laser pulse of 355 nm light.*

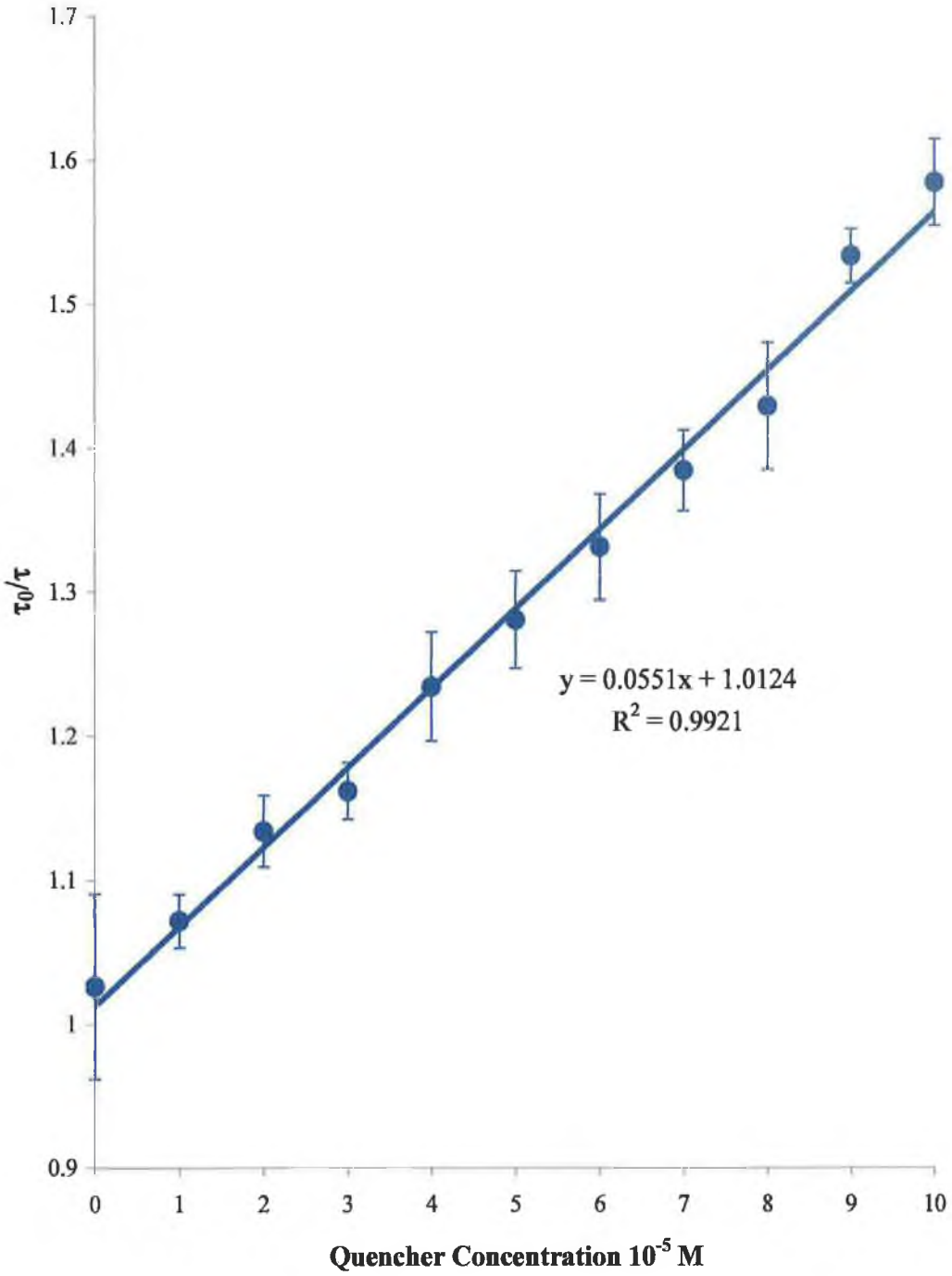

Figure 5.16: *Stern-Volmer plot derived from data in Figure 5.15.*

Excited state lifetimes can also be used to determine the quenching constant, k_q, using the Stern-Volmer relationship;

$$\frac{\tau_o}{\tau} = 1 + k_q \tau_o [Q] \qquad \textbf{(18)}$$

The comparison of the quenching constants obtained for each approach can be utilised to determine if static or dynamic quenching is involved. State quenching results in the formation of an excimer; this results in a decrease in the flourescent intensity, however, the excited state lifetimes are unaffected. This is not the case in this study, it was therefore concluded that dynamic quenching was involved in the reactions studied. Again both values indicate efficient quenching of the excited state $[Ru(bpy)_2(PVP)_{10}]^{2+*}$ by $[Os(bpy)_3]^{2+}$.

The obtained results clearly demonstrate that quenching is dynamic. This implies that no pre complex of osmium and ruthenium exists, *i.e.,* little specific interaction occurs between the two metal centres as expected. The existence of a complex may also be excluded due to the slow diffusion of the polymer in solution.

The self quenching process, namely the quenching of an excited state molecule M^* by the same chemical species in the ground state (equation 20);

$$M \xrightarrow{I_a} M^* \quad \textbf{(19)}$$

$$M^* + M \xrightarrow{k_{sq}} 2M \quad \textbf{(20)}$$

$$M^* \xrightarrow{k_r} M + h\nu \quad \textbf{(21)}$$

$$M^* \xrightarrow{k_{nr}} M \quad \textbf{(22)}$$

has been generally studied by measuring the lifetime of the excited state as a function of concentration. The lifetime τ and the concentration [M] are related through the Stern-Volmer equation as described previously. Ground state outer sphere electron transfer reactions of $RuL_3^{2+/3+}$ are very rapid. This is attributed to the low intrinsic barriers to electron transfer that obtain in this series and which are most evident in the self exchange process. Rate constants of 5×10^7 to 1×10^9 $M^{-1}s^{-1}$ in water at 25 °C have been determined for this reaction. In addition there is compelling evidence that the couples involving the charge transfer excited states of RuL_3^{2+} also possess very high self exchange rates.

Finally, both the ground state and excited state reactions respond to reaction driving force. In Table 5.2 the data for quenching by polypyridine complexes have been organised. The third and fourth columns contain values of ΔE^o for quenching according to equations 8 and 9, respectively.

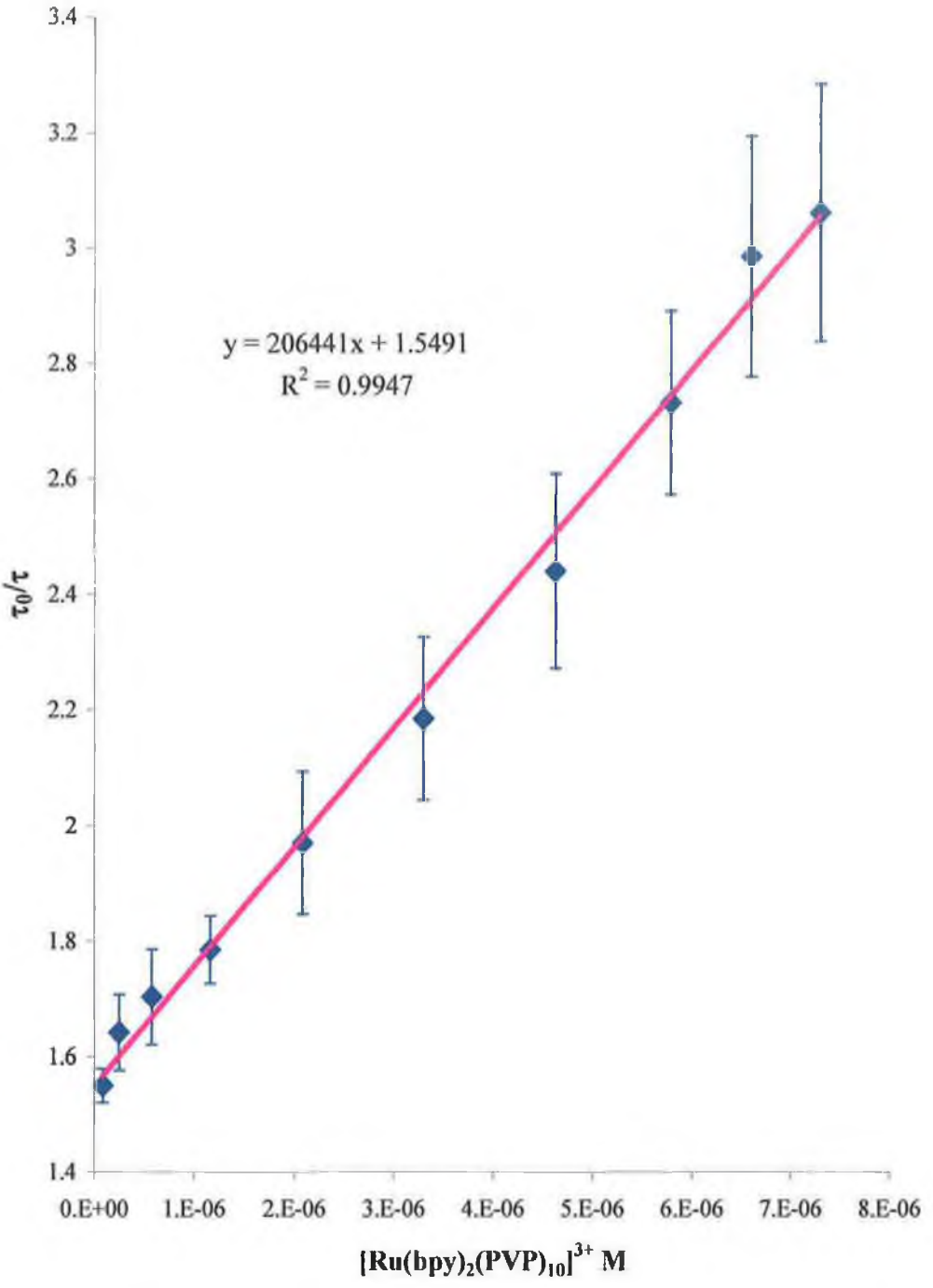

Figure 5.17: *Stern-Volmer plot of the influence of* $[Ru(bpy)_2(PVP)_{10}]^{3+}$ *on the emission decay of* 10^{-4} *M* $[Ru(bpy)_2(PVP)_{10}]^{2+}$ *in ethanol monitored at 614 nm following the application of a 10 ns laser pulse of 355 nm light.*

Energy transfer from the excited state of one RuL_3^{2+} complex to the ground state of another is not likely to be favourable thermodynamically, but rather "thermonuetral". In the RuL_3^{2+} series the absorption and emission spectra (and thus the excited state energies) are remarkably insensitive to the nature of L. Consequently energy transfer from one ruthenium complex to another is rather analogous to the self exchange process for electron transfer, except that it formally involves two simultaneous electron transfers. However, in some cases since each quenching act must regenerate an excited molecule, no net diminution in donor concentration and lifetime can result.

$$Ru(bpy)_3^{2+*} + Ru(bpy)_3^{2+} \rightarrow Ru(bpy)_3^{2+} + Ru(bpy)_3^{2+*} \qquad (27)$$

The value calculated for self quenching, $k_{sq} = \sim 7.66 \times 10^{11}\ M^{-1}s^{-1}$, is indicative of an efficient quenching mechanism and also that the electron transfer is quite fast. Although the value calculated is slightly smaller than that previously calculated for $[Ru(bpy)_2(PVP)_{10}]^{2+}$ being quenched by $Os(bpy)_3^{2+}$. However, this is expected since some self quenching may also be involved.

These results also suggest that superquenching is involved and again clearly demonstrate that the quenching mechanism in question is dynamic. The rate of quenching is faster for the polymeric material in comparison to the monomeric complex, which is unusual considering the E_a calculated for each complex. The activation energy for $[Ru(bpy)_2(PVP)_{10}]^{2+}$ is almost double that of the monomeric complex, as such the rate of quenching would be expected to be lower for the polymer. However, this is not the case, it is therefore hypothesised that the quenching is either due to superquenching or due to preconcentration of the osmium quencher from the formation of complexes with the polymer backbone which could result in restrictive and statically mixing between the ruthenium and osmium centres. The preconcentration could explain the large rate constants despite the conclusion that the quenching being diffusional.

Reactants		$-\Delta E^0$ *V*	$-\Delta E^0$ *V*	$-\Delta E^*$ *eV*	kq $M^{-1}s^{-1}$
Donor	*Quencher*				
$Ru(bpy)_3^{2+*}$	$Os(bpy)_3^{2+}$	0.38	-0.02	-0.33	$1.5x10^9$
$Ru(bpy)_2(PVP)_{10}^{2+*}$	$Os(bpy)_3^{2+}$	0.42	0.01	-0.29	$8.3x10^{11}$
$Ru(bpy)_3^{2+*}$	$Ru(bpy)_3^{2+}$	0.44	0.41	~0	$<1x10^9$
$Ru(bpy)_2(PVP)_{10}^{2+*}$	$Ru(bpy)_2(PVP)_{10}^{2+*}$	0.48	0.43	~0	$7.7x10^{11}$

Table 5.2: *Quenching Data and constants for the ruthenium complexes.*

5.4 Conclusion:

ECL was demonstrated in solution phase for the polymeric species $[Ru(bpy)_2(PVP)_{10}]^{2+}$, *via* annihilation between the electrogenerated 3+ and 1+ forms of the compound as well as *via* oxidative-reductive (TPA). ECL generated by the above methods produces spectra similar to the photoluminescence, therefore the same orbitals are presumed to be responsible, whether the excited state is formed electrochemically or photochemically. The chemiluminescence spectrum produced by chemical oxidation of the polymer and subsequent reduction with oxalate is also similar to the photoluminescence in this respect.

Electrodes modified with thin films of the redox polymer $[Ru(bpy)_2(PVP)_{10}]^{2+}$, produced ECL of greater efficiency and higher intensity than was observed for the same species freely diffusing in solution. This may be due to the layer shielding the luminescent metal centres from quenching and other processes which may be occurring in solution. Although the ECL spectrum of the polymer in solution phase was the same as the luminescence spectrum that of layer was significantly red shifted from the photoluminescence. Differences in dielectric constant of the environment of the emitters in the different experiments may be a factor here.

5.5 *References:*

1 Fleet, B.; Keliher, B. N.; Kirkbright, G. F.; Pickford, C. J. *Analyst* **1969**, 94,847.

2 Feldberg, S. W. *J. Am. Chem. Soc.* **1964**, 143, 808. **

3 Wightman, R. M.; Maness, K. M.; Bartlett, J. E. *J. Phys. Chem.* **1994**, 98, 3993.

4 Wightman, R. M.; Collison, M. M.; Paolo, P., *J. Phys. Chem.* **1994**, 98, 11942.

5 Bartelt, J. E.; Drew, S. M.; Wightman, R. M., *J. Electrochem. Soc.* **1992**, 139, 70.

6 Kapturkiewicz, A. *J. Electroanal. Chem.* **1994**, 372, 101.

7 Abruna, H. D. *J. Electroanal. Chem.* **1984**,175, 321.

8 Bonfede, S.; Ciano, M.; Fabrizio, B.; Balzani, V.; Chassot, L.; Zelewsky, A.V. *J. Phys. Chem.* **1986**,90, 3836.

9 Richter, M. M.; Debad, J. D.; Durwin, R. S.; Crosby, G. A.; Bard, A. J. *Anal. Chem.* **1996**, 68, 4370.

10 Tokel, N. E.; Bard, A. J. *J. Am. Chem. Soc.* **1972**, 94, 2862.

11 Fiaccabrino, G. C.; Koudelka-Hep, M.; Hsueh, Y.; Collins, S.D.; Smith, R. L. *Anal. Chem.* **1998**, 70, 4157.

12 Kapturkiewicz, A. *Chem. Phys. Lett.* **1995**, 236, 389.

13 Velesco, J. G.; Rubenstein, I.; Cruchley, R. J.; Lever, A. B. P.; Bard, A. J. *Inorg. Chem.* **1983**, 22, 822.

14 Faulkner, L. R.; Bard, A. J. *Electroanalytical Chemistry, Vol 10,* **1977**, Marcel Dekker, New York. (and references therein).

15 Maness, K. M.; Bartlett, J. E.; Wightman, R. M. *J. Phys. Chem.* **1994**, 98, 3993.

16 Velesco, J. G. *J.Phys.Chem.* **1988**, 92, 2202.

17 Faulkner, L. R.; Bard, A. J. *J. Am. Chem. Soc.* **1969**, 91, 209.

18 Wightman, R. M.;

19 Pastore, P.; Magno, F.; Collinson, M.M; Wightman, R. M. *J. Electroanal. Chem.* **1995**, 379, 19.

20 Bieniasz, L. K. *J. Electroanal. Chem.* **1994**, 379, 71.

21 Knight, A. W. *Trends. Anal. Chem.* **1999**, 18, 47. (and references therein).

22 Lyons, C. H.; Abbas, E. D.; Lee, J.-K.; Rubner, M. F. *J. Am. Chem. Soc.* **1998**, 120, 12100.

23 Wu, A.; Lee, J.; Rubner, M. F. *Thin Solid Films* **1998**, 327- 329, 663.

24 Horiuchi, T.; Niwa, O.; Hatakenaka, N. *Nature* **1998**, 394, 659.

25 Abruna, H. D.; Bard, A. J. *J. Am. Chem. Soc.* **1982**, 104, 2641.

26 Rubenstein, I.; Bard, A. J. *J. Am. Chem. Soc.* **1980**, 102, 6642.

27 Obeng, Y. S.; Bard, A. J. *Langmuir*, **1991**, 7,195.

28 Sato, Y.; Uosaki, K. *J. Electronal. Chem.* **1995**, 384, 57.

29 Juris, A.; Balzani, V.; Barigelletti, F.; Campagna, S.; Belser, P.; Von Zelewsky, A; *Coord. Chem. Rev.,* **1988**, *84*, 85.

30 Rehm, D.;Weller, A. *Israel J. Chem.*, **1970**, *8*, 259.

31 Ballardini, R.; Varani, G.; Indelli, M. T.; Scandola, F.; Balzani, V. *J. Am. Chem. Soc.* **1978**, *100*, 7219.

32 Casper, J.V.; Meyer, T.J.; *J. Am. Chem. Soc.,* **1983**, *105*, 5583.

33 Seddon, E.A.; Seddon, K.R.; *The Chemistry of Ruthenium,* Elsevier, New York, **1984**, Chapter 5, 1180.

34 Juris, A.; Balzani, V.; Barigelletti, F.; Campagna, S.; Belser, P.; Von Zelewsky, A; *Coord. Chem. Rev.,* **1988**, *84*, 85, and references therein.

35 Indelli, M.T., Scandola, F., Collin, J.-P., Sauvage, J.-P., Sour, A., *Inorg. Chem.,* **1996**, *35*, 303.

36 Grosshenny, V., Harriman, A., Ziessel, R., *Angew. Chem. Int. Ed. Engl.,* **1995**, *34*, 1100.

37 Ryum C.K., Schmehl, R.H., *J. Phys. Chem.,* **1989**, *93*, 7961.

38 Schanze. K. S.; Neyhart, G. A.; Meyer, T. J. *J. Phys. Chem.* **1986**, *90*, 2182.

39 Powers, M. J.; Meyer, T. J. *J. Am. Chem. Soc.* **1980**, *102*, 1289.

CHAPTER 6

CONCLUSION

"Nothing shocks me. I'm a scientist!"

Harrison Ford (as Indiana Jones)

6.1 Conclusion:

Electrochemiluminescence, the light emission arising as a result of electron transfers between electrogenerated reactants, has been of considerable interest to scientists since the phenomenon first began to be studied in detail in the late 1960s. There have been many reasons for this interest, including the fact that studies of electrochemiluminescent systems may help to enhance our understanding of fundamental electron transfer processes from excited states. These investigations are therefore important in fields such as photoelectrochemical conversion and storage of solar energy. ECL has also been shown as a promising technique as the basis for light emitting devices and lasers; also as a means of visualising electrochemical processes and surfaces, where ECL imaging is proving to be a useful technique.

However it is in the area of analysis that ECL systems have been most exploited and found most wide spread application. This is hardly surprising since, theoretically, whilst retaining the inherent advantages of sensitivity and selectivity inherent in conventional chemiluminescent methodology, ECL should potentially offer many additional advantages as an analytical technique. Some of these advantages are as follows:

- The reagents needed are generated *in situ* at an electrode, allowing greater control over the initiation, rate and course of the chemiluminescent reaction through alteration of the applied potential.
- Since the emission is concentrated close to the electrode surface, this allows optimum positioning of light measuring devices for maximum sensitivity.
- In many cases the ECL reagent is regenerated on reaction with the analyte (EC type mechanism) allowing it to be re-oxidised or reduced at the electrode and to take part in further reactions giving rise to many photons per measurement cycle.

- The emission can effectively be switched 'on and off', thus enabling signal modulation and background correction techniques to be used more effectively.
- ECL has an additional level of electrochemical selectivity because the potential at which analysis is carried out can be modulated slightly above or below the minimum required.
- Additional analytical information can be gained by simultaneously monitoring the voltammetric response with the emission.
- It is simpler to generate a chemiluminescent reagent electrochemically than to introduce it to and mix it in a reaction coil or vessel.
- Many analytes that would not normally take part in a chemiluminescent reaction become active in this respect on electrolysis.

As a result ECL has rapidly gained in importance in recent years in analytical sciences. By far, ruthenium polypyridyl complexes have received the most attention; $Ru(bpy)_3$ and related compounds have been used to detect a wide range of analytes including oxalate, alkylamines, NADH, hydrazine, amino acids, $Ru(bpy)_3$-labelled biomolecules and a variety of pharmaceutical compounds.

One limitation of ECL methods is the requirement to constantly deliver the reagent to the reaction zone. This can be overcome by employing the chemiluminescence reagent in immobilised or solid state format. The immobilisation of the reagent on a solid electrode surface lends several advantages compared with solution phase ECL systems; experimental design is made simpler and more cost effective since there is no need for an extra pump to deliver the reagent, excessive reagent consumption is eliminated and the reagent may be regenerated *in situ*.

The immobilisation approach has received some attention. Immobilised luminol has been used to quantitate hydrogen peroxide; $Ru(bpy)_3^{2+}$ elctrostatically bound in Nafion has been used with notable success to determine oxalate, amines,

NADH and glucose. However, the stability of these sensors is compromised due to $Ru(bpy)_3$ partitioning into hydrophobic regions of the film over time. Electropolymerised $Ru(vinyl\text{-}bpy)_3$ modified electrodes have been shown to have ECL properties and even exhibit diode like behaviour but their analytical usefulness is limited because of the impermeable nature of layers formed in this way. There has been growing interest in recent years in ECL reactions of organised monolayers on electrode surfaces formed by Langmuir-Blodgett or self assembly techniques, again however, stability issues as well as quenching by conductive electrode substrates have ruled out their use in an analytical context.

In this work the electrochemiluminescent and electrochemical properties of a number of ruthenium and osmium poly(pyridyl) systems, both in solution phase and as modifying layers on electrodes, have been investigated with a view to their application as sensors.

A number of ruthenium complexes and metallopolymeric materials of the general formula $[M(bpy)_2(L)_2]^{2+}$ and $[M(bpy)_2(L)Cl]^{+}$, where M is ruthenium or osmium and L is poly-vinylpyridine (PVP) or 4-methylpyridine (pic), were successfully synthesised, and characterised using viscometry, spectroscopy and electrochemistry. For the most part, the photochemical and electrochemical properties of the analogous monomeric metal complexes i.e. $[M(bpy)_3]^{2+}$ and $[M(bpy)_2(pic)_3]^{2+}$, were carried over to the polymeric material. A notable exception was the excited state life-time of $[Ru(bpy)_3]^{2+}$ which under similar conditions was lower in the monomeric complex than in the polymeric material, although it was similar to that of $[Ru(bpy)_2(pic)_2]^{2+}$ for the ruthenium complexes.

Characterisation of thin layers of the metallopolymer $[Ru(bpy)_2(PVP)_{10}]^{2+}$ immobilised on an electrode surface showed that they exhibited features typical of surface bound redox sites. The charge transport diffusion coefficient (D_{Ct}), as measured both cyclic voltammetry and chronoamperometry was approximately 2 x 10^{-11} cm^2s^{-1} and was insensitive to electrolyte concentration and layer thickness.

This result suggested a porous layer structure in which partition of charge compensating counter-ions across the layer/electrolyte interface, and their transport within the layer, was relatively unimpeded. Charge transport rates are important in so far as they have a direct bearing on the overall response time of a sensor that dictates rate at which the catalytically active, *i.e.,* Ru(III) form of the layer can be generated. Similar results were obtained for the osmium metallopolymer thin films. The characterisation of the thin layers consisting of both the ruthenium and osmium polymers also showed features of surface bound redox sites. The D_{Ct} for these layers was also determined. The investigation revealed that the rate charge propagation through the polymer phase via the osmium centres was more rapid than that through the ruthenium centres; average D_{ct} values were 1.6×10^{-9} and 4.2×10^{-10} cm^2s^{-1} for the osmium and ruthenium centres, respectively. This is possible due to a more efficient self exchange rate between the osmium metal centres in comparison to the ruthenium metal centres. Similar values were obtained for the corresponding polymers containing only osmium or ruthenium centres where the redox centre concentration was the same. These results suggested that there was little or no interaction between the redox centres.

Charge transport in $HClO_4$ electrolyte as measured by chronoamperometry was considerably faster, but showed a dependence on electrolyte concentration suggesting an ion transport limitation on D_{ct} and a considerably more compact, dehydrated layer structure in this electrolyte.

The ruthenium metallopolymer was shown to be an effective mediator for the oxidation of both guanine and 8-oxoguanine, whereas the osmium metallopolymer having a lower formal potential was shown to selectively catalyse the oxidation of 8-oxoguanine even in the presence of native guanine. Guanine reacted with Ru^{3+} centres throughout the film and 8-oxoguanine reacted with Os redox centres. In this respect the investigated system is a good example of the possibility of redox polymer coating performing electrochemical catalysis in a three dimensional

manner. This situation is also the most favourable for developing sensitive sensors based on polymeric layers.

ECL was demonstrated in solution phase for the polymeric species $[Ru(bpy)_2(PVP)_{10}]^{2+}$, *via* annihilation between the electrogenerated 3+ and 1+ forms of the compound as well as *via* oxidative-reductive (TPA) and reductive-oxidative ($S_2O_8^{2-}$) pathways. ECL generated by the above methods produced spectra similar to the photoluminescence, therefore the same orbitals were presumed to be responsible, whether the excited state was formed electrochemically or photochemically. The chemiluminescence spectrum produced by chemical oxidation of the polymer and subsequent reduction with guanine was also similar to the photoluminescence in this respect.

Electrodes modified with thin films of the redox polymer $[Ru(bpy)_2(PVP)_{10}]^{2+}$, produced ECL of slightly greater efficiency and higher intensity than was observed for the same species freely diffusing in solution even after correction for concentration differences. This may have been due to the layer shielding the luminescent metal centres from quenching and other processes, which may have occurred when the reaction took place in solution. Although the ECL spectrum of the polymer in solution phase was the same as the luminescence spectrum, that of layer was significantly red shifted from the photoluminescence. This may have been due to differences in dielectric constant of the environment of the emitters in the different experiments.

The quenching effects of the excited states of the redox polymer $[Ru(bpy)_2(PVP)_{10}]^{2+}$ was also investigated. The polymer was quenched by $Os(bpy)_2^{3+}$ through reductive quenching. The rate of quenching, k_q, was also determined to be ~8.64 x 10^{11} $M^{-1}s^{-1}$, which implied an effective quenching and fast electron transfer between the ruthenium and osmium metal centres. The self quenching was also efficient although the slightly slower than that calculated for quenching by the osmium complex, at ~ 7.5 x 10^{11} $M^{-1}s^{-1}$. Both reactions were

determined to result from dynamic quenching through comparison of the effects of the quenchers on both the fluorescent intensities and the excited state lifetimes.

Superquenching may also be involved in the quenching of the ruthenium metallopolymer. The activation energies of both the monomeric and polymeric forms were studied. The energy barrier for the metallopolymer was almost double that of the monomeric form, yet the quenching rate constants did not reflect this result. Considering the high activation energy a much slower quenching rate would be expected. Since this is not the case, superquenching may account for the faster rate constant, although further investigation into this phenomenon will be required before a complete understanding of this reaction is obtained.

The application of electrodes modified with the ruthenium redox polymer for amperometric sensing of chemical DNA damage was demonstrated using SWV. The simultaneous transaction of the chemiluminescence and current signal response of the system was demonstrated. After this was successfully preformed, the development of a sensor containing an electrode modified with a film containing both the osmium and ruthenium metallopolymers, as well as, DNA strands for simultaneous amperometric and ECL sensing of both chemical and oxidative DNA damage, was shown.

Dual transduction of amperometric and ECL signals could not only provide additional assurance of analytical results, but could provide additional information about the composition of the sample. For example, the presence of redox active species which would quench the ECL emission. Phenols, catechols, hydroquinones and bezoquinones have recently been shown to be efficient quenchers of $[Ru(bpy)_3]^{2+}$ ECL. That some analytes gave rise to good amperometric signals but no ECL is interesting since it raises the possibility of simultaneous detection of two analytes, or of providing data regarding the composition of the sample matrix.

Rapid, easy-to-use, inexpensive and sensitive assays that can screen the potential for toxicity related to a biological target (e.g., DNA) are of great importance. Pollutions from factories and exhausts from automobiles contaminate the air and the water endangering people's health. Also, certain chemicals or substances produced or used in the workplace may put people at an increased risk of developing certain types of cancers. It has been estimated that 85% of all cancers are caused by environmental pollutants. At the same time, hundreds of thousands of new chemicals are generated each year. If these chemicals are aimed at commercial development, toxicity testing becomes more and more important. It is essential to quickly identify and characterise the toxicity of chemicals and pollutants, thus reducing the uncertainties in the assessment of human exposure. A major limitation to this approach is the fact that laboratory analysis of contaminated environmental and biological samples is usually slow and expensive, which limits the number of samples that can be analysed within time and budget constraints.

The application of electrochemical methods to perform this type of analysis has received considerably interest in recent years. ECL has been exploited in this area of research although its use has been mainly through the labelling of target DNA strands or the use of a sacrificial reagent for the production of an ECL signal. The production of a direct ECL signal from the interaction of the metallopolymers and the DNA bases, namely, guanine and the biomarker 8-oxoxguanine, results in a toxicity screening sensor that is quicker and also more environmentally friendly due to the reduced amount of chemicals used in the analysis and therefore smaller amounts of waste are produced.

The application of these thin films for the detection of structural and oxidative DNA damage was established in this study. Certain chemicals react with DNA forming adduct which disrupt the helical structure, this allowed for guanine to react more readily with the ruthenium metallopolymer in the film resulting in greatly increased signals. In this fashion a chemical may be examined to determine if it forms adducts with DNA resulting in the disruption of the DNA helix. However, as

already stated, this is not the only form of DNA damage that may occur. Oxidative DNA damage may result in the formation of altered DNA bases, such as 8-oxoguanine, which do not disrupt the helical structure but cause mutations in the DNA strand. The detection of this type of DNA damage was also demonstrated. This sensor provides a quick and easy method of determining the toxicity of a particular chemical, which is also great importance with the continuing growth of new chemical each year.

Despite the obvious advantages of this sensor, there are some major opportunities for improvement. The sensor can only detect damage which causes disruption to the helical structure of DNA or to the formation of the biomarker 8-oxoguanine, DNA can be damaged in many other ways which involve the other three DNA bases. These DNA bases have quite different redox potentials and as such other polymers could be synthesised to either detect these bases or their oxidation products. This would increase the sensitivity of the current system.

Another area which would benefit from improvement is the structure of the sensor itself, namely, the carbon macroelectrode. The size of the electrode could be reduced into the nano-scaled region. These nanostructured electrodes would have the advantages of plasmonic enhancement. The possibility of using optical fibre platforms could also be studied. These could be miniaturised and have the added benefit of providing for localised measurements.

Abbreviations:

a	Flory Constant
A	Adenine
A	Electrode Area
AC	Alternating Current
ACN	Acetone
AIBN	2,2'-azobisisobutyronitrile
BD	1,3-Butadiene
BMO	Butadiene monoxide
bphb	4-bis(4'-methyl-2,2'-bipyridin-4-yl)benzene
bpy	2,2'-bipyridyl
C	Concentration
C	Cytosine
CA	Chronoamperometry
CCD	Charge coupled device
CL	Chemiluminescence
CT	Calf Thymus
CYP	Cytochrome P450 enzymes
CV	Cyclic Voltammetry
d	Layer Thickness
D	Diffusion Coefficient
DC	Direct Current
D_{ct}	Diffusion Coefficient
DNA	Deoxyribonucleic Acid
DMF	Dimethyl Formamide
DMSO	Dimethyl Sulfoxide
DPA	9,10-diphenylathracene
dp-bpy	diphenyl bipyridyl
dp-phen	diphenyl phenanthroline
ds	Double Stranded

EC	Electrochemistry
ECL	Electrochemiluminescence
EDTA	ethylenediaminetetraacetic acid
E^0	Formal Potential
E^0_{Ox}	Oxidation Potential
E_p	Potential
E^0_{Red}	Reduction Potential
ESI	Electrospray Ionisation
EtOH	Ethanol
F	Faraday's Constant
FAP_y	Formamidopyrimidine
FIA	Flow Injection Analysis
FWHM	Full width at half maximum
G	Guanine
Gn	Guanidinohydantoin
HOMO	Highest Occupied Molecular Orbital
HPLC	High performance liquid chromatography
Ia	Iminoallantoin
I_{ECL}	ECL Intensity
I_p	Current
ITO	Indium Tin Oxide
k	Reaction Rate Constant
k_{et}	Electron Transfer Rate Constant
k_{nr}	Nonradiationless Deactivation
k_r	Radiationless Deactivation
K	Flory Constant
L	Layer Thickness
LB	Langmuir-Blodgett
LC	Ligand centred charge transfer
LUMO	Lowest Unoccupied Molecular Orbital
LOD	Limit of Detection

Mb	Myoglobin
MC	Metal centred charge transfer
MeCN	Acetone
MeOH	Methanol
MLCT	Metal to ligand charge transfer
MS	Mass Spectroscopy
MW	Molecular Weight
n	Number of Electrons
N	Reaction Rate
NADH	Reduced nicotinomide adenine dinucleotide
NMR	Proton nuclear magnetic resonace
η	Intrinsic viscosity
PAH	Polyaromatic hydrocarbon
PBS	Phosphate buffer containing saline
PCET	Proton-coupled Electron Transfer
PCR	Polymerase Chain Reaction
PDDA	poly diallyldimethylammonium chloride
PG	Pyrolytic graphite
phen	phenanthroline
pic	4-methylpyridine / picoline
PMT	Photomultiplier Tube
POL	Polymer backbone
Poly	polynucleotide
PS	Polystyrene
Py	Pyrene
PVI	Poly(N-vinylimidazole
PVP	Poly-(4-vinylpyridine)
PVP/PS	Poly-4-vinylpyridine/polystyrene
Q	Quencher
$Q_{a,c}$	Anodic, cathodic Charge
QCM	Quartz Crystal Microbalance

R	Gas Constant
RDS	Relative Standard Deviation
ROS	Reactive Oxygen Species
ss	Single Stranded
SCE	Saturated Calomel Electrode
SECM	Scanning Electrochemical Microscopy
S/N	Signal to Noise Ratio
SO	Styrene Oxide
ST	Salmon Testes
SWV	Square Wave Voltammetry
T	Temperature
T	Thymine
$TBABF_4$	Tetrabutylammonium tetrafluoroborate
τ	Fluorescence Lifetime
TMPD	N,N,N',N'-tetramethyl-p-phenylenediamine
TPA	Tripropylamine
TPrA	tri-*n*-propylamine
terpy	2,2',2-terpyridine
UV	Ultra-Violet
8-oxoG	8-oxoguanine
ΔG^0	Free energy change
Γ	Surface Coverage
ϕ_{ECL}	ECL Efficiency
ϕ_{ES}	Efficiency of excited state production
ϕ_P	Quantum yield of emission
λ	Reorganisation Energy
λ_{max}	Wavelength of maximum absorbance / emission

APPENDIX:

PUBLICATIONS

J|A|C|S
ARTICLES
Published on Web 04/03/2003

Simultaneous Direct Electrochemiluminescence and Catalytic Voltammetry Detection of DNA in Ultrathin Films

Lynn Dennany,[†,‡] Robert J. Forster,*[,†] and James F. Rusling*[,‡,§]

Contribution from the National Centre for Sensor Research (NCSR), School of Chemical Sciences, Dublin City University, Dublin 9, Ireland, Department of Chemistry, University of Connecticut, U-60, 55 N. Eagleville Road, Storrs, Connecticut 06269-3060, and Department of Pharmacology, University of Connecticut Health Center, Farmington, Connecticut 06032

Received December 9, 2002; E-mail: James.Rusling@uconn.edu

Abstract: Direct electrochemiluminescence (ECL) involving DNA was demonstrated in 10 nm films of cationic polymer $[Ru(bpy)_2(PVP)_{10}]^{2+}$ assembled layer-by-layer with DNA. A square wave voltammetric waveform oxidized the Ru^{II} sites in the metallopolymer to Ru^{III}, and ECL was measured simultaneously with catalytic voltammetric peaks In a simple apparatus. Significant ECL generation occurred only when guanine bases were present on oligonucleotides in the films. This result along with knowledge of proposed ECL pathways suggests that guanine radicals initially formed by catalytic oxidation of guanines by Ru^{III} react with the metallopolymer to produce electronically exited Ru^{II*} sites in the film. ECL and catalytic SWV peaks were sensitive to oligonucleotide hybridization and chemical DNA damage. Simultaneous linear growth of ECL and SWV peaks occurred after incubation with known DNA damage agent styrene oxide over 20 min. The estimated detection limit was 1 damaged DNA base in 1000. Control incubations of metallopolymer/ds-DNA films in buffer containing unreactive toluene resulted in no significant changes of the ECL or SWV peaks.

Introduction

Sensitive, selective detection of DNA is central to clinical tests, pathogen detection, and other methods utilizing polymerase chain reaction (PCR), to genetic disease screening based on oligonucleotide hybridization, and to molecular genotoxicity studies.[1] Electrochemistry provides simple, sensitive, and inexpensive approaches to detecting DNA hybridization and damage.[2−5] One of the most sensitive approaches was first reported by Thorp et al., who showed that ruthenium tris(2,2′-bpyridyl) $[Ru(bpy)_3^{2+}]$ oxidizes guanine bases in DNA and oligonucleotides in an electrochemical catalytic pathway as in Scheme 1:[6]

Scheme 1

$$Ru(bpy)_3^{2+} \leftrightarrow Ru(bpy)_3^{3+} + e^- \quad \text{(at electrode)} \qquad (1)$$

$$Ru(bpy)_3^{3+} + DNA(guanine) \rightarrow Ru(bpy)_3^{2+} + DNA(guanine_{ox}) \qquad (2)$$

Here the one-electron oxidation product DNA($guanine_{ox}$) can be further oxidized.[7] Cycling $Ru(bpy)_3^{3+}$ to $Ru(bpy)_3^{2+}$ by the fast chemical step in eq 2 provides a greatly enhanced catalytic oxidation current in voltammetry. In solution, guanines reacted with $Ru(bpy)_3^{3+}$ at rate constants of $9 \times 10^3\ M^{-1}\ s^{-1}$ in double-stranded (ds) calf thymus (CT) DNA and $2 \times 10^5\ M^{-1}\ s^{-1}$ in single-stranded (ss) CT-DNA.[6] Guanines in various base-mismatched hybridized oligomers reacted at rate constants intermediate between the ds- and ss-DNA values. The rate of oxidation and the resulting catalytic peak current measured in voltammetry depend greatly on DNA structure and guanine sequence, providing selectivity in DNA analyses.[8−13] Recent results suggest that the initial oxidation of guanines in DNA by $Ru(bpy)_3^{3+}$ is a proton-coupled process leading to guanine radicals.[14]

Damage of DNA by the formation of chemical adducts of nucleobases also alters the native ds-DNA structure, resulting in an increased reaction rate with $Ru(bpy)_3^{3+}$. Capitalizing on this fact, we developed sensors to detect chemical DNA damage

† Dublin City University.
‡ University of Connecticut.
§ University of Connecticut Health Center.

(1) (a) Cadet, J.; Weinfeld, M. *Anal. Chem.* **1993**, *65*, 675A−682A. (b) Santella, R. *Cancer Epidimiol., Biomarkers Prev.* **1999**, *8*, 733−739. (c) Primrose, S. B. *Principles of Genome Analysis*, 2nd ed.; Blackwell: Oxford, U.K., 1998. (d) Baxevanis, A. D.; Ouellette, B. F. Bioinformatics: Practical Guide to Analysis of Genes and Proteins. *Methods Biochem. Anal.* **1998**, *39*, 1−370.
(2) Mikkelsen, S. R. *Electroanalysis* **1996**, *8*, 15−19.
(3) Thorp, H. H. *Trends Biotechnol.* **1998**, *16*, 117−121.
(4) Wang, J. *Chem.−Eur. J.* **1999**, *5*, 1681−1685.
(5) Palacek, E.; Fojta, M. *Anal. Chem.* **2001**, *73*, 74A−83A.
(6) Johnston, D. H.; Glasgow, K. C.; Thorp, H. H. *J. Am. Chem. Soc.* **1995**, *177*, 8933−8938.
(7) Armistead, P. M.; Thorp, H. H. *Anal. Chem.* **2001**, *73*, 558−564.
(8) Napier, M. E.; Thorp, H. H. *Langmuir* **1997**, *13*, 6342−6344.
(9) Furrer, B. T.; Thorp, H. H. *Inorg. Chem.* **2000**, *39*, 44−47.
(10) Yang, I. V.; Thorp, H. H. *Inorg. Chem.* **2000**, *39*, 4969−4976.
(11) Sistare, M. F.; Codden, S. J.; Heimlich, G.; Thorp, H. H. *J. Am. Chem. Soc.* **2000**, *122*, 4742−4749.
(12) Szalai, V. A.; Thorp, H. H. *J. Phys. Chem. A* **2000**, *104*, 6851−6859.
(13) Onkto, A. C.; Armistead, P. M.; Kircus, S. R.; Thorp, H. H. *Inorg. Chem.* **1999**, *38*, 1842−1846.
(14) (a) Weatherly, S. C.; Yang, I. V.; Thorp, H. H. *J. Am. Chem. Soc.* **2001**, *123*, 1236−1237. (b) Weatherly, S. C.; Yang, I. V.; Armistead, P. A.; Thorp, H. H. *J. Phys. Chem. B* **2003**, *107*, 372−378.

10.1021/ja0296529 CCC: $25.00

in ultrathin films using soluble[15] $Ru(bpy)_3^{2+}$ and a poly(vinylpyridine) (PVP)−$RuCl(bpy)_2^{+}$ polymer[16,17] as catalysts for square wave voltammetry.

Electrochemiluminescence (ECL) using $Ru(bpy)_3^{2+}$ attached to DNA provides a sensitive method of detection.[18−24] The $Ru(bpy)_3^{2+}$ labels on DNA are oxidized to $Ru(bpy)_3^{3+}$, and ECL is generated by using a sacrificial reductant, often tripropylamine. ECL depends on generation of photoexcited $[Ru(bpy)_3^{2+}]^*$ in a process involving reaction of a radical form of the reductant with electrochemically generated $Ru(bpy)_3^{3+}$.[23,25,26] Alternatively, $Ru(bpy)_3^{+}$ is formed by reduction of $Ru(bpy)_3^{2+}$ by the radical, followed by reaction of Ru^{I} and Ru^{III} species to give $[Ru(bpy)_3^{2+}]^*$.[27] Decay of $[Ru(bpy)_3^{2+}]^*$ to the ground state with luminescent emission at 610 nm is measured in the detection step. Bimetallic ruthenium complexes can give enhanced ECL intensity.[28]

One-electron oxidation of guanine in DNA is well-known to give guanine radicals,[29] which can also be oxidized by $Ru(bpy)_3^{3+}$.[7] Thus, we suspected that the reaction of guanine with $Ru(bpy)_3^{3+}$ or related species on a metallopolymer could also lead to a photoexcited Ru^{II}* moiety and generate ECL. Further, the rate and yield of this process might be enhanced by utilizing films on electrodes with high local concentrations of Ru catalyst and guanine. In this paper, we report that ultrathin films of the catalytic polymer $[Ru(bpy)_2(PVP)_{10}](ClO_4)_2$ and oligonucleotides on electrodes can generate direct ECL signals that are sensitive to hybridization and chemical damage of DNA. ECL can be monitored simultaneously with catalytic electrochemical voltammograms in a simple apparatus.

Experimental Section

Chemicals and Materials. *cis*-$[Ru(bpy)_2(H_2O)](ClO_4)_2$ was prepared and characterized by a published method.[30] The bis-substituted metallopolymer $[Ru(bpy)_2(PVP)_{10}](ClO_4)_2$ was prepared by refluxing *cis*-$[Ru(bpy)_2(H_2O)](ClO_4)_2$ with a 10-fold excess of poly(vinylpyridine) (PVP, MW 280 000) (i.e. 1 ruthenium/10 pyridine units) to give the structure below. Preparation and characterization were reported in detail previously.[31]

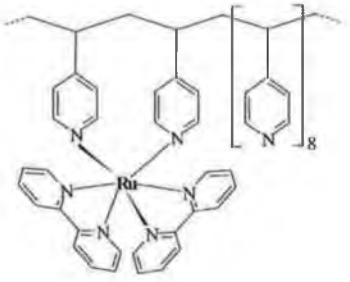

Calf thymus (CT) double-stranded (ds) DNA ((Sigma, type XV, 13 000 average base pairs, 41.9% G/C), CT ss-DNA, salmon testes (ST) ds-DNA (Sigma, ~2000 average base pairs, 41.2% G/C), ST ss-DNA, poly(guanadylic acid) (5′) (poly[G]), poly(cytidylic acid) (5′) (poly[C]), poly(adenylic acid) (5′) (poly[A]), styrene oxide, and toluene were from Sigma. Poly(dimethyldiallyammonium chloride) (PDDA, MW 200 000−350 000) was from Aldrich. Water was purified with a Hydro Nanopure system to specific resistance >16 MΩ cm. All other chemicals were reagent grade.

Apparatus. Simultaneous square wave voltammetry (SWV)−ECL measurements were made in a glass 3-electrode electrochemical cell at 37.0 ± 0.5 °C using a CH Instruments model 660 electrochemical analyzer. The cell employed a saturated calomel reference electrode (SCE), a Pt wire counter electrode, and a 4 mm diameter disk of ordinary basal plane pyrolytic graphite (PG, Advanced Ceramics) as working electrode placed close to the cell bottom. The electrolyte solution was 10 mM acetate buffer, pH 5.5, containing 50 mM NaCl. SWV conditions were 4 mV step height, 25 mV pulse height, and frequency 5 Hz. The cell was protected from light by coating with a black cloth to avoid external optical background and possible photodecomposition of the ruthenium metallopolymer. Solutions were purged with pure nitrogen for 15 min prior to each series of experiments, and a nitrogen atmosphere was maintained during data collection. A different electrode was used for each catalytic film analysis, as the oxidative analysis modifies the nucleic acids in the films.

A photomultiplier tube detector and data collection system from Labmaster Coherent Ultima was used to record emitted light from the electrode (610 nm) via an optical fiber positioned directly underneath the DNA/metallopolymer electrode outside the flat bottom of the glass cell.

Film Assembly. DNA−metallopolymer films were constructed by the layer-by-layer electrostatic assembly method.[15,17,32] Basal plane PG electrodes were polished with 400 grit SiC paper and then with 0.3 μm α-alumina slurries on Buehler Microcloth, washed with water, sonicated in ethanol for 15 min, and then sonicated in water for 15 min. Layers were constructed by placing a 30 μL drop of 0.2% aqueous $[Ru(bpy)_2(PVP)_{10}](ClO_4)_2$ onto each PG electrode, allowing 15 min to achieve saturated adsorption[32] and then washing with water. Subsequently, 30 μL of DNA solution (2 mg mL^{-1} DNA in 5 mM pH 5.5 acetate buffer + 0.05 M NaCl) was placed on this PG surface, allowed to adsorb 15 min, and then washed with water. This sequence was repeated to obtain films with 2 metallopolymer/DNA bilayers. Films containing ss-DNA and other polynucleotides were also assembled in this way.

Assembly of films was monitored at each step with a quartz crystal microbalance (QCM, USI Japan) using 9 MHz QCM resonators (AT-cut, International Crystal Mfg.). To mimic the carbon electrode surface, a negative monolayer was made by treating gold-coated (0.16 ± 0.01 cm^2) resonators with 0.7 mM 3-mercapto-1-propanol and 0.3 mM 3-mercaptopropionic acid in ethanol.[15] Films were assembled as for

(15) Zhou, L.; Rusling, J. F. *Anal. Chem.* **2001**, *73*, 4780−4786.
(16) Mugweru, A.; Rusling, J. F. *Electrochem. Commun.* **2001**, *3*, 406−409.
(17) Mugweru, A.; Rusling, J. F. *Anal. Chem.* **2002**, *74*, 4044−4049.
(18) Gerardi, R. D.; Barnett, N. W.; Lewis, S. W. *Anal. Chim. Acta* **1999**, *378*, 1−41.
(19) Fähnrich, K. A.; Pravda, M.; Guilbault, G. G. *Talanta* **2001**, *54*, 531−559.
(20) Xu, X.-H.; Yang, H. C.; Mallouk, T. E.; Bard, A. J. *J. Am. Chem. Soc.* **1994**, *116*, 8386−8387.
(21) Xu, X.-H.; Bard, A. J. *J. Am. Chem. Soc.* **1995**, *117*, 2627−2631.
(22) Leland, J. K.; Powell, M. J. *J. Electrochem. Soc.* **1990**, *137*, 3127−3131.
(23) Blackburn, G. F.; Shah, H. P.; Kenten, J. H.; Leland, J.; Kamin, R. A.; Link, J.; Petermann, J.; Powell, M. J.; Shah, A.; Talley, D. B.; Tyagi, S. K.; Wilkins, E.; Wu, T.-G.; Massey, R. J. *Clin. Chem.* **1991**, *37*, 1534−1539.
(24) Gudibande, S. R.; Kenten, J. H.; Link, J.; Massey, R. J. *Mol. Cell Probes* **1992**, *6*, 495−503.
(25) Ege, D.; Becker, W. G.; Bard, A. J. *Anal. Chem.* **1984**, *56*, 2413−2417.
(26) Kenten, J. H.; Casedei, J.; Link, J.; Lupold, S.; Willey, J.; Powell, M.; Rees, A.; Massey, R. J. *Clin. Chem.* **1991**, *37*, 1626.
(27) Rubinstein, I.; Bard, A. J. *J. Am. Chem. Soc.* **1980**, *102*, 6642−6644.
(28) Richer, M. M.; Bard, A. J.; Kim, W.; Scheinhl, R. H. *Anal. Chem.* **1998**, *70*, 310−318.
(29) Geise, B. *Acc. Chem. Res.* **2000**, *33*, 631−636.
(30) Durham, B.; Wilson, S. R.; Hodgson, D. J.; Meyer, T. J. *J. Am. Chem. Soc.* **1980**, *102*, 600−607.
(31) Hogan, C. F.; Forster, R. J. *Anal. Chim. Acta* **1999**, *396*, 13−21.
(32) (a) Lvov, Y. In *Protein Architecture: Interfacing Molecular Assemblies and Immobilization Biotechnology*; Lvov, Y., Möhwald, H., Eds.; Marcel Dekker: New York, 2000; pp 125−167. (b) Lvov, Y. In *Handbook Of Surfaces And Interfaces Of Materials, Vol. 3. Nanostructured Materials, Micelles and Colloids*; Nalwa, R. W., Ed.; Academic Press: San Diego, CA, 2001; pp 170−189. (c) Rusling, J. F. In *Protein Architecture: Interfacing Molecular Assemblies and Immobilization Biotechnology*; Lvov, Y., Möhwald, H., Eds.; Marcel Dekker: New York, 2000; pp 337−354. (d) Rusling, J. F.; Zhang, Z. In *Handbook Of Surfaces And Interfaces Of Materials, Vol. 5. Biomolecules, Biointerfaces, And Applications*; Nalwa, R. W., Ed.; Academic Press: San Diego, CA, 2001; pp 33−71.

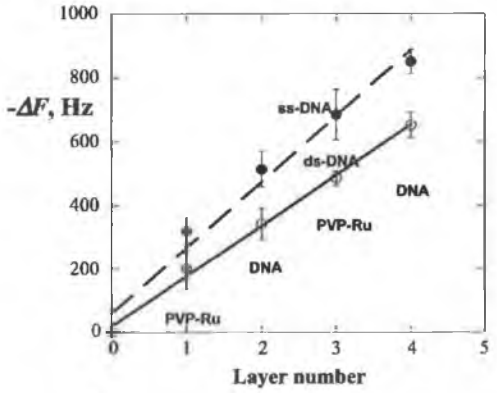

Figure 1. QCM frequency shifts for cycles of alternate PVP−Ru and CT-DNA layers on gold-quartz resonators coated first with mixed monolayers of mercaptopropionic acid/mercaptopropanol for ss-DNA (●) and ds-DNA (○) (average values for 3 replicate films).

PG electrodes. Resonators were dried in a stream of nitrogen before measuring the frequency change (ΔF). Absorbed mass was estimated with the Sauerbrey equation,[32] for 9 MHz quartz resonators, giving dry film mass/unit area M/A as

$$M/A\ (\text{g cm}^{-2}) = -\Delta F\ (\text{Hz})/1.83 \times 10^{8} \qquad (3)$$

The nominal thickness (d) of dry films was estimated with an expression confirmed by high-resolution electron microscopy:[33]

$$d\ (\text{nm}) = (-0.016 \pm 0.002)\Delta F\ (\text{Hz}) \qquad (4)$$

Reactions with Styrene Oxide. Incubations of films were done in styrene oxide solutions in a stirred reactor at 37.0 ± 0.5 °C. A 120 μL volume of neat styrene oxide or toluene (as control) was added to 10 mL of acetate buffer, pH 5.5, + 50 mM NaCl to give saturated solutions.[15] pH 5.5 gave optimum reaction rates of DNA with styrene oxide[17] and also allowed efficient ECL production.[27] PG electrodes coated with polynucleotide or DNA films were incubated in the stirred emulsion and then rinsed with water and transferred to the electrochemical cell containing pH 5.5 buffer for SWV/ECL analysis.

Safety Note: *Styrene oxide is a suspected human carcinogen and somewhat volatile. Gloves should be worn, all manipulations done under a hood, and reactions done in closed vessels.*

Results

QCM Monitoring of Film Assembly. Films were constructed for SWV/ECL measurements by the layer-by-layer electrostatic assembly method[32] with two bilayers of CT-DNA and metallopolymer $[Ru(bpy)_2(PVP)_{10}]^{2+}$ (Ru−PVP), denoted $(PVP-Ru/DNA)_2$. These films were first characterized by measuring QCM frequency shifts during film growth. ΔF values varied linearly with layer number for ss-DNA and ds-DNA layers alternated with Ru−PVP (Figure 1), suggesting regular film growth with reproducible layers of DNA and proteins. ΔF values with eq 3 were used to obtain weights of Ru−PVP and DNA. Equation 4 was used to estimate the average nominal thickness of the films (Table 1). About 20% DNA and 30% more metallopolymer were incorporated in films when ss-DNA was used compared to ds-DNA. The mole ratio of guanine to ruthenium in these films was about 1.6:1.

ECL and SWV Measurements. One of us recently reported a method in which voltammetric or amperometric current was

(33) Lvov, Y.; Ariga, K.; Ichinose, I.; Kunitake, T. *J. Am. Chem. Soc.* **1995**, *117*, 6117−6123.

Table 1. Average Characteristics of Metallopolyion/DNA Films from QCM

film	thickness, nm	DNA mass, μg cm^{-2}	RuPVP mass, μg cm^{-2}
$(PVP-Ru/ST\text{-}ds\text{-}DNA)_2$	10	1.6	1.9
$(PVP-Ru/ST\text{-}ss\text{-}DNA)_2$	14	1.9	2.6

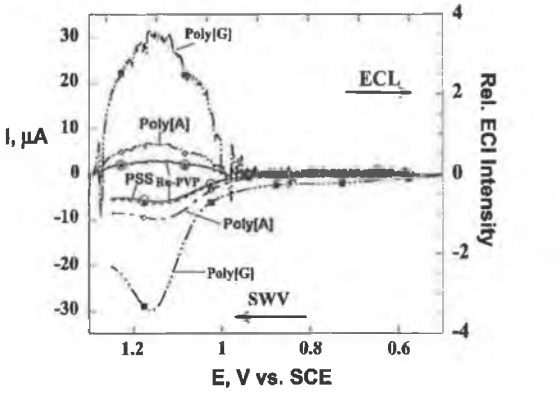

Figure 2. SWV and ECL response for films containing Ru−PVP on PG electrodes in pH 5.5 buffer + 50 mM NaCl. Films are Ru−PVP alone (○), $(Ru-PVP/PSS)_2$ (▲), $(Ru-PVP/poly[A])_2$ (◊), and $(Ru-PVP/poly[G])_2$ (■). Symbols are for curve identification only.

measured simultaneously with ECL at electrodes coated with $[Ru(bpy)_2(PVP)_{10}]^{2+}$ for oxalate detection.[34] We used a similar approach in the present work, here scanning by SWV from potentials at which the Ru^{II} redox centers in the metallopolymer are not oxidized through values at which Ru^{II} is oxidized to Ru^{III} ($E^{o\prime} \sim 1.15$ V vs SCE), activating the catalytic cycle in Scheme 1. Preliminary results showed that measurable ECL signals could be observed in pH 6 buffer containing dissolved $Ru(bpy)_3^{2+}$ and guanosine monophosphate, poly(guanylic acid) (poly[G]) or ds-DNA while scanning voltammograms through the potential region where $Ru(bpy)_3^{2+}$ is oxidized to $Ru(bpy)_3^{3+}$. Also, ECL signals were detected with nucleic acid species in solution by using a glassy carbon electrode with an adsorbed layer of $[Ru(bpy)_2(PVP)_{10}]^{2+}$. In this work, we utilized films designed to contain all the necessary components for ECL generation with DNA. These ultrathin films feature the reactive species in high concentrations in a tiny reaction volume, estimated from film thickness (Table 1) and electrode area at $\sim 2 \times 10^{-4}$ mm^3.

Similar to previous reports, $[Ru(bpy)_2(PVP)_{10}]^{2+}$ adsorbed on PG electrodes gave reversible redox peaks,[31,34] with formal potential ca. 1.15 V vs SCE at pH 5.5 measured by cyclic voltammetry and SWV and surface concentration of 6×10^{-11} mol cm^{-2} obtained for electroactive ruthenium by integration of CVs at 5 mV s^{-1}. Comparing this value with QCM results, we find that 84% of the ruthenium present in this first adsorbed layer is electroactive.

Figure 2 shows that combined ECL/SWV measurements on films containing Ru−PVP, alone or in $(PVP/PSS)_2$ films, gave the Ru^{II}/Ru^{III} oxidation peak and a very small amount of light. However, $(Ru-PVP/poly[G])_2$ films gave a significant ECL peak, as well as a catalytic current by SWV that was much larger than the noncatalytic Ru^{II}/Ru^{III} oxidation peak for Ru−PVP films not containing poly[G]. Figure 2 also shows that

(34) Hogan, C. F.; Forster, R. J. *Anal. Chem.* **2000**, *72*, 5578−5582.

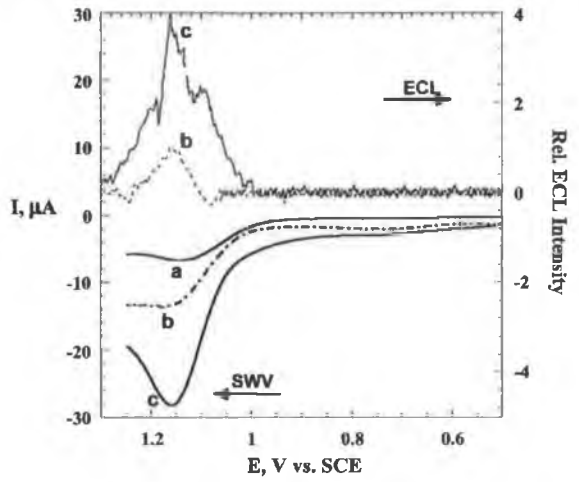

Figure 3. SWV and ECL response for (a) Ru−PVP, (b) (Ru−PVP/poly-[G]/poly[C])$_2$ and (c) (Ru−PVP/poly[G])$_2$ films on PG electrodes in pH 5.5 buffer + 50 mM NaCl.

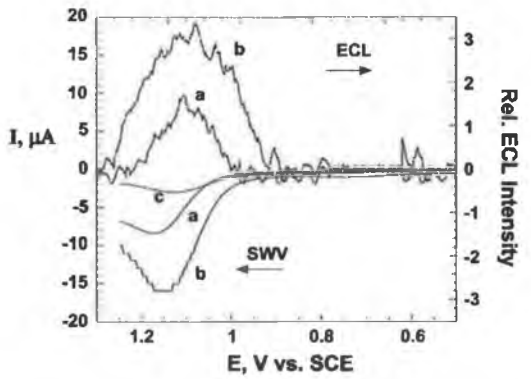

Figure 4. SWV and ECL for (a) (Ru−PVP/ds-CT DNA)$_2$ films and (b) (Ru−PVP/ss-CT DNA)$_2$ films on PG electrodes in pH 5.5 buffer + 50 mM NaCl and (c) SWV only for Ru−PVP film with no DNA.

(Ru−PVP/poly[A])$_2$ gave a small catalytic current and a very small ECL signal, slightly above the background for Ru−PVP films.

We investigated the influence of hybridization on the ECL signal by using films containing hybridized and unhybridized poly[G]. Figure 3 compares the ECL/SWV responses of films of (Ru−PVP/poly[G])$_2$ and (Ru−PVP/ poly[G]/poly[C])$_2$. The latter films were made by using a solution of poly[G] and poly-[C] for which UV−Vis spectra confirmed hybridization. Both ECL and SWV peaks are about 3-fold larger for films containing the hybridized poly[G]/poly[C] layers compared to the film with only the poly[G] layer (Figure 3).

Similar results were obtained when comparing ECL/SWV signals for films containing ss- and ds-DNA. (Figure 4). Films containing ss-DNA gave about twice the ECL signal as those made with ds-DNA. SWV peaks for the ss-DNA films were about 2.5-fold larger than their ds-DNA analogues. Similar results were found for calf thymus and salmon testes DNA. Films assembled with DNA and the polycation PDDA showed no significant ECL peaks.

There was a slight increase in the ECL signal when an additional Ru−PVP/ds-DNA bilayer was grown on top of (Ru−PVP/ds-DNA)$_2$ films, but this increase was about at the level of film-to-film variance of the 2-bilayer films. Films with

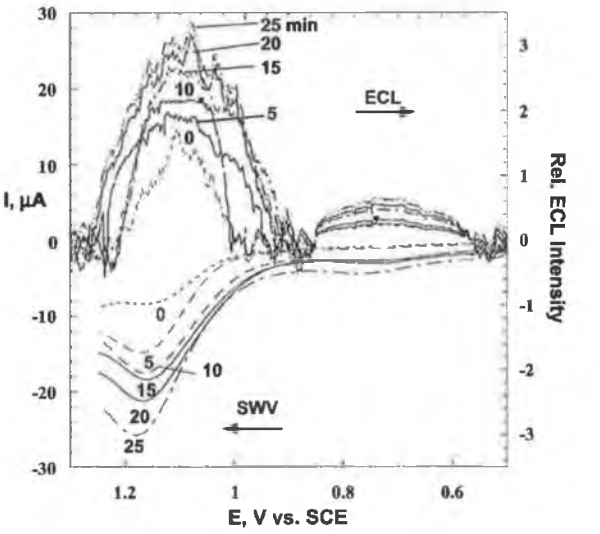

Figure 5. SWV and ECL responses for (Ru−PVP/ds-CT DNA)$_2$ films on PG electrodes in pH 5.5 buffer + 50 mM NaCl after incubations 37 °C with saturated styrene oxide. Numerical labels are incubation times in minutes.

4 bilayers, i.e., (Ru−PVP/ds-DNA)$_4$, gave smaller ECL peaks than 2-bilayer films, probably because of mass and electron transport limitations as film thickness increased similar to those observed with enzyme−polyion films.[35]

Reaction of Nucleic Acid Films with Styrene Oxide. The purine bases guanine and adenine in DNA form covalent adducts with styrene oxide, with the majority of reactions occurring at guanine.[36−42] Such adducts can serve as important markers of human exposure to mutagens and carcinogens.[43,44] Further, covalent adduct formation disrupts the double helical structure of DNA and makes the guanines more accessible for catalytic oxidation, even when the DNA is present in polyion films.[15] By using capillary electrophoresis and liquid chromatography−mass spectrometry to analyze enzyme- and acid-hydrolyzed DNA that had been reacted with styrene oxide, we previously confirmed that styrene oxide−guanine and styrene oxide−adenine adducts form under the incubation conditions used in this work.[45,46]

When (Ru−PVP/ds-DNA)$_2$ films were incubated with styrene oxide and then scanned by SWV, increases in the ECL and the SWV peaks were observed with increasing incubation time (Figure 5). Average peak currents for the ds-DNA films increased linearly with incubation time for about the first 20 min, followed by a slight decrease (Figure 6). When (Ru−PVP/

(35) Munge, B.; Estavillo, C.; Schenkman, J. B.; Rusling, J. F. *Chem. Biochem.* **2003**, *4*, 82−89.
(36) Vodocka, P.; Hemminki, K. *Carcinogenesis* **1988**, *9*, 1657−1660.
(37) Pauwels, W.; Veulemans, H. *Mutat. Res.* **1998**, *418*, 21−33.
(38) Hemminki, K.; Koskinen, M.; Rajaniemi, H.; Zhao, C. *Regul. Toxicol. Pharmacol.* **2000**, *32*, 264−270.
(39) Hemminki, K. *Carcinogenesis* **1993**, *14*, 2007−2012.
(40) McConnell, E. E.; Swenberg, J. A. *Crit. Rev. Toxicol.* **1994**, *24*, S49−S55.
(41) Nestmann, E. R.; Bryant, D. W.; Carr, C. J.; Fennell, T. T.; Gorelick, N. J.; Gallagher, J. E.; Swenberg, J. A.; Williams, G. M. *Regul. Toxicol. Pharmacol.* **1996**, *24*, 9−18.
(42) Jelen, F.; Palacek, E. *Biophys. Chem.* **1986**, *24*, 285−290.
(43) Contoreggi, S.; Lutz, W. K. *Carcinogenesis* **1993**, *14*, 355−360.
(44) Pauwels, W.; Vodicka, P.; Severi, M.; Pina, K.; Veulemans, H.; Hemminki, K. *Carcinogenesis* **1996**, *7*, 2673−2680.
(45) Zhou, L.; Yang, J.; Estavillo, C.; Stuart, J. D.; Schenkman, J. B.; Rusling, J. F. *J. Am. Chem. Soc.* **2003**, *125*, 1431−1436.
(46) Yang, J.; Zhang, Z.; Rusling, J. F. *Electroanalysis* **2002**, *14*, 1494−1500.

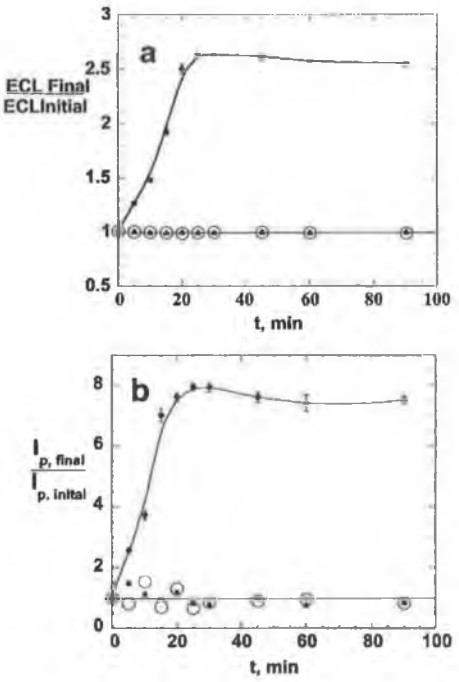

Figure 6. Influence of incubation time with styrene oxide (●), toluene (▲), and buffer alone (○) on (a) average ECL signals and (b) average SWV catalytic peak currents (final response/initial response) for (Ru/ds-CT DNA)$_2$ films. Error bars represent standard deviations for three trials, with 1 electrode/trial.

ds-DNA)$_2$ films were incubated with toluene, for which no chemical reactions with DNA have been reported, or in buffer only, ECL and SWV peaks remained within electrode-to-electrode variability and showed no trends with incubation time. Error bars in Figure 6 are mainly the result of electrode-to-electrode variability. However, both the error bars and scatter in the controls were smaller for the ECL ratios than for the SWV ratios.

In addition to catalytic oxidation of guanines, it is possible that adducts formed on DNA by reaction with styrene oxide could be catalytically oxidized by the ruthenium metallopolymer. To assess this possibility, styrene oxide was incubated with films containing individual polynucleotides and the metallopolymer. Figure 7 shows that both ECL and SWV peaks increased after 10 min incubation of (Ru−PVP/poly[G])$_2$ with styrene oxide. An 80% increase in SWV peak current and a 40% increase in ECL intensity was found. However, for films incubated with toluene, ECL and SWV peaks were nearly identical to initial values.

Similar experiments were done with films containing the other three polynucleotides. For intact poly[A] films, only a small SWV peak for catalytic oxidation was observed. After poly[A] was reacted with styrene oxide, a 25% increase in this peak was found. However, ECL signals for poly[A] treated with styrene oxide were indistinguishable from the baseline before treatment. SWV of poly[C] and poly[A] films showed no increase in oxidation peaks either before or after 10 min incubations with styrene oxide. Poly[A] or poly[C] films did not produce significant ECL before or after incubations with styrene oxide.

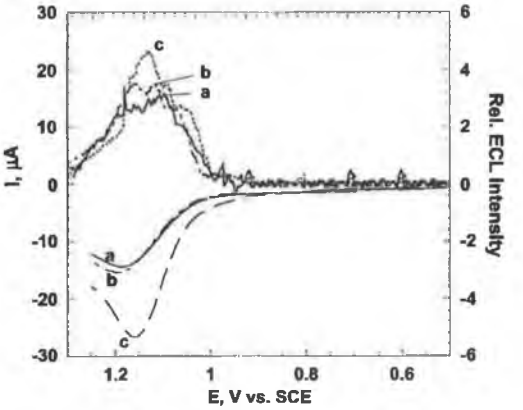

Figure 7. SWV and ECL response for (Ru−PVP/poly[G])$_2$ films on PG electrodes in pH 5.5 buffer + 50 mM NaCl: (a) no incubation; (b) incubated with saturated toluene control for 10 min.; (c) incubated with saturated styrene oxide for 10 min.

Discussion

Results described herein demonstrate for the first time, to our knowledge, that ECL can be achieved by direct reaction of a Ru^{III} complex with DNA, in this case by using $[Ru(bpy)_2(PVP)_{10}]^{2+}$ in films with DNA. Alternate layer-by-layer electrostatic assembly provided Ru−PVP/ds-CT DNA films about 10 nm thick with intimate mixing of Ru−PVP and DNA reactants in a tiny reaction volume. Extensive intermixing of neighboring layers in polycation/polyanion films assembled by this method has been established by neutron reflectivity studies.[32a,b,47]

The ECL response appears to involve mainly the guanine bases in DNA, since no other homopolymeric nucleotides besides poly[G] (Figure 2) gave significant ECL signals in films with Ru−PVP. ECL signals for Ru−PVP/poly[G] films were 3-fold larger than for films of Ru−PVP and hybridized poly-[G]/poly[C] (Figure 3). Films of metallopolymer and ss-DNA gave 2-fold larger ECL intensity than with ds-DNA (Figure 4), although the mass of ss-DNA in films was ~18% larger than ds-DNA (Table 1). Thus, the ECL yield is sensitive to the hybridization state of oligonucleotides in the films, a key feature for detecting base mismatches.[2−5]

Figures 5 and 6 show that direct ECL in Ru−PVP/DNA films can be used to detect DNA damage. Figure 6a shows a nearly linear increase in ECL intensity over 20 min when Ru−PVP/ds-DNA films were reacted with styrene oxide under conditions which were confirmed to give styrene oxide−guanine and styrene oxide−adenine adducts in films and in solutions.[45,46] No enhancement of ECL signals was found when the films were incubated with toluene, which does not react with DNA (Figure 6). After 5 min of reaction with styrene oxide, the ECL peak ratio for ds-DNA films was more than 3-fold greater than the average peak ratio for controls.

We can correlate the increased ECL peak ratio for DNA films incubated with styrene oxide with previous capillary electrophoresis results showing that under our conditions about 1.2% damage/h occurs for the first several hours of reaction with styrene oxide.[46] In the present study, we found that a 5 min incubation time gave an ECL peak ratio more than 3-fold larger than the noise (Figure 6a). This signal corresponds to an

(47) Decher, G. *Science* **1997**, *227*, 1232−1237.

estimated practical detection limit for ECL of about 0.1% damage or 1 damaged base in 1000.

Figures 5 and 6 also show increased catalytic SWV responses to DNA treated with styrene oxide but no current increases when the films are treated with unreactive toluene or buffer in control incubations. The development of the ECL and SWV peaks with time agree very well. A similar comparison as above leads to a detection limit for catalytic SWV similar to ECL. This is about the same as for polyion/DNA films with an underlayer of $[Ru(bpy)_2Cl(PVP)_{10}]^+$,[17] which has 5 N−Ru bonds/Ru instead of 6 as in $[Ru(bpy)_2(PVP)_{10}]^{2+}$ used for this work. $[Ru(bpy)_2Cl(PVP)_{10}]^+$ has a lower formal potential, about 0.75 V vs SCE as opposed to 1.15 V for $[Ru(bpy)_2(PVP)_{10}]$. However, $[Ru(bpy)_2Cl(PVP)_{10}]^+$ cannot produce significant emission at room temperature.

ECL generation involves initial reaction of electrochemically generated $[Ru(bpy)_2(PVP)_{10}]^{3+}$ with a reductant to give a radical. By analogy with previously proposed mechanisms,[27,34] the pathway in our films could be represented as in Scheme 2:

Scheme 2

$$[Ru(bpy)_2(PVP)_{10}]^{2+} \leftrightarrow [Ru(bpy)_2(PVP_{10})]^{3+} + e^- \quad (5)$$

$$[Ru(bpy)_2(PVP)_{10}]^{3+} + G \rightarrow [Ru(bpy)_2(PVP)_{10}]^{2+} + G^{\bullet} \quad (6)$$

$$G^{\bullet} + [Ru(bpy)_2(PVP)_{10}]^{3+} \rightarrow G_{2ox} + [Ru(bpy)_2(PVP)_{10}]^{2+*} \quad (7)$$

$$[Ru(bpy)_2(PVP)_{10}]^{2+*} \rightarrow [Ru(bpy)_2(PVP)_{10}]^{2+} + h\nu \quad (8)$$

Initial oxidation by electron donation from the metallopolymer to the electrode at sufficiently positive potentials gives the Ru^{III} oxidant (eq 5), which reacts with guanines (G) in DNA to give guanine radical (eq 6), consistent with the proton-coupled catalytic DNA oxidation pathway recently proposed by Thorp et al.[14] This radical may produce Ru^{II}* sites (eq 7), representing the excited state complex, by directly reducing the Ru^{III} sites. G_{2ox} in eq 7 represents a guanine oxidized by two electrons, a reaction observed[7] in ss-DNA oxidized by dissolved $Ru(bpy)_3^{3+}$.

A viable alternative is shown in eqs 9 and 10, where the guanine radical may reduce the Ru^{II} complex to Ru^{I}, which can then produce Ru^{II}* by reacting with Ru^{III}:

$$G^{\bullet} + [Ru(bpy)_2(PVP)_{10}]^{2+} \rightarrow G_{2ox} + [Ru(bpy)_2(PVP)_{10}]^{+} \quad (9)$$

$$[Ru(bpy)_2(PVP)_{10}]^{+} + [Ru(bpy)_2(PVP)_{10}]^{3+} \rightarrow [Ru(bpy)_2(PVP)_{10}]^{2+} + [Ru(bpy)_2(PVP)_{10}]^{2+*} \quad (10)$$

Ru^{II}* represents the electronically excited state which decays to ground state by emission at ~610 nm (eq 8), providing for the simultaneous detection of ECL along with SWV from the films. The onset of light emission occurs in a similar potential range as the appearance of the increased SWV current (Figures 2−5 and 7). Furthermore, similar development of final/initial peak ratios vs time of incubation with styrene oxide (Figure 6), as well as the dependence of ECL and SWV signals on hybridization of the oligonucleotides in the films (Figures 3 and 4), suggest that, as in purely voltammetric DNA oxidation with catalytic complexes,[7−9,11,12] the reaction of the Ru^{III} sites with guanines in the DNA is likely to be rate limiting (eq 6).

The increase in ECL and SWV peaks with time of incubation with styrene oxide probably reflects a larger average rate of reaction between Ru^{III}−PVP and the chemically damaged DNA compared to the reaction with intact ds-DNA, consistent with the structurally related rate effects found by Thorp et al.[7−9,11,12] As previous suggested when using SWV with soluble $Ru(bpy)_3^{2+}$ or the lower oxidation potential metallopolymer $[Ru(bpy)_2Cl(PVP)_{10}]^+$ to catalyze DNA oxidation in films, guanine in the ds-DNA structure must be less accessible to the oxidant than in damaged or ss-DNA. A smaller distance of closest approach of the Ru^{III} active sites in the polymer to the oxidizable bases presumably leads to faster reaction rates and larger catalytic peaks for damaged DNA as well as for unhybridized oligonucleotides. Covalent adducts of styrene oxide and guanines and adenines disrupt the double helix and allow closer contact between oxidizable moieties on the DNA and the active oxidizing agent. Figure 7 suggests that there may also be a small contribution to the ECL by styrene oxide−guanine adducts, but the exact nature or degree of this contribution is uncertain at present.

In summary, our results show that ECL can be obtained *directly* from the reaction of guanine bases in oligonucleotides in ultrathin films with the catalytic metallopolymer $[Ru(bpy)_2(PVP)_{10}]^{2+}$ without using a sacrificial reductant. ECL and SWV peaks are sensitive to oligonucleotide hybridization and chemical damage of ds-DNA. Both applications involve measurement of ratios, and the reproducibility of these ratios for DNA damage was slightly better for ECL (cf. Figure 6). Preliminary studies also showed that ECL can be detected for oligonucleotides in solution by using electrodes coated with $[Ru(bpy)_2(PVP)_{10}]^{2+}$. Thus, direct ECL as described herein may find future applications in films or solutions for DNA detection in applications such as hybridization or estimation of DNA damage. ECL might also be used in toxicity screening applications in films with DNA and metabolic enzymes[45] that produce metabolites that cause DNA damage. It is not necessary to measure the voltammetric signature along with the ECL output, and such approaches could simplify applications of electrode arrays for high throughput DNA analyses in which simultaneous digital imaging of ECL in multiple electrode arrays might be achieved.

Acknowledgment. This work was supported by Enterprise Ireland (R.J.F.), NCSR at Dublin City University, and by the U.S. PHS Grant No. ES03154 (J.F.R.) from the National Institute of Environmental Health Sciences (NIEHS), NIH. Its contents are solely the responsibility of the authors and do not necessarily represent the official views of NIEHS, NIH. The authors thank Blanaid White for preliminary studies, Dr. Bingquan Wang for experimental assistance with ECL apparatus, and Prof. Robert Birge and Sumi Shima for the loan of optical equipment.

JA0296529

JACS
ARTICLES
Published on Web 06/25/2004

Direct Electrochemiluminescence Detection of Oxidized DNA in Ultrathin Films Containing $[Os(bpy)_2(PVP)_{10}]^{2+}$

Lynn Dennany,[†,‡] Robert J. Forster,*[,†] Blanaid White,[†] Malcolm Smyth,[†] and James F. Rusling*[,‡,§]

Contribution from the National Centre for Sensor Research (NCSR), School of Chemical Sciences, Dublin City University, Dublin 9, Ireland, Department of Chemistry, University of Connecticut, U-60, 55 North Eagleville Road, Storrs, Connecticut 06269-3060, and Department of Pharmacology, University of Connecticut Health Center, Farmington, Connecticut 06032

Received March 10, 2004; E-mail: James.Rusling@uconn.edu

Abstract: Direct electrochemiluminescence (ECL) involving oxidized DNA was demonstrated in ultrathin films of cationic polymer $[Os(bpy)_2(PVP)_{10}]^{2+}$ [PVP = poly(vinyl pyridine)] assembled layer-by-layer with DNA or oligonucleotides. Electrochemically oxidized Os^{II} sites generated ECL from films containing oxoguanines on DNA formed by chemical oxidation using Fenton reagent. Films combining DNA, $[Ru(bpy)_2(PVP)_{10}]^{2+}$, and $[Os(bpy)_2(PVP)_{10}]^{2+}$ had Os^{II} sites that produced ECL specific for oxidized DNA, and Ru^{II} sites gave ECL from reaction with oxo-adenines, chemically damaged DNA, and possibly from cleaved DNA strands.

Oxidative stress in mammals damages DNA,[1] generating lesions that may contribute to aging and mutagenesis.[2−5] Many oxidatively formed DNA adducts have been characterized.[6] Oxidative DNA damage occurs from chemical reactions, irradiation, and reactive oxygen species (ROS) generated during metabolism,[7] including singlet oxygen, superoxide, and hydroxyl radicals.[7c] Reaction of DNA with hydroxyl radicals[7,8] causes single base modifications, yielding products including 8-oxoguanine (8-oxoG), 8-oxoadenine, thymine glycol and 8-hydroxycytosine, strand breaks, and cross-links.[9]

Hydroxyl radicals are generated from Fe^{II} and hydrogen peroxide in the Fenton reaction.[10] Iron-mediated reactions may contribute substantially to H_2O_2-mediated damage to DNA.[11,12] Such DNA damage is thought to involve Fenton chemistry generated by Fe^{II} associated with DNA.[13,14]

8-OxoG is a major product of nucleobase oxidation for which specific cellular repair enzymes exist. It has been suggested as a clinical biomarker for oxidative stress.[15] When present in DNA, 8-oxoG caused G-to-T transversions and A-to-C substitutions.[16,17] While guanine is the most easily oxidized of the natural nucleobases,[18] 8-oxoG has a much lower oxidation potential[19] and is itself oxidized more easily than guanine. The oxidation products of 8-oxoG are guanidinohydantoin and 2-amino-4,5,6-trioxypyrimidine.[20] Guanidinohydantoin in ss-DNA was recently found to be highly mutagenic and caused G-to-T transversions.[21]

8-OxoG can be determined in hydrolyzed DNA by liquid chromatography (LC) coupled to a mass spectrometer (MS) or an electrochemical (EC) detector.[15,22] We recently used LC−

† Dublin City University.
‡ Department of Chemistry, University of Connecticut.
§ University of Connecticut Health Center.

(1) (a) Cross, C. E.; Halliwell, B.; Pryor, W. A.; Ames, B. N.; Saul, R. L.; McCord, J. M.; Harman, D. *Ann. Intern. Med.* **1987**, *107*, 526−545. (b) Beckman, K. B.; Ames, B. N. *J. Biol. Chem.* **1997**, *272*, 19633−19636. (c) Kawanishi, S.; Hiraku, Y.; Oikawa, S. *Mutat. Res.* **2001**, *488*, 65−76.
(2) Ames, B. B.; Shigenaga, M. K.; Hagen, T. M. *Proc. Natl. Acad. Sci. U.S.A.* **1993**, *90*, 7915−7922.
(3) Shiegenaga, M. K.; Hagen, T. M.; Ames, B. N. *Proc. Natl. Acad. Sci. U.S.A.* **1994**, *91*, 10771−10778.
(4) Ames, B. N.; Gold, L. S.; Willett, W. C. *Proc. Natl. Acad. Sci. U.S.A.* **1995**, *92*, 5258−5265.
(5) Beckman, K. B.; Ames, B. N. *J. Biol. Chem.* **1997**, *272*, 19633−19636.
(6) Henle, E. S.; Luo, Y.; Gassmann, W.; Linn, S. *J. Biol. Chem.* **1996**, *271*, 21177−21186.
(7) (a) Halliwell, B.; Gutteridge, J. M. C. *Biochem J.* **1984**, *219*, 1−14. (b) Halliwell, B. *Mutat. Res.* **1999**, *443*, 37−52. (c) Cadet, J.; Delatour, T.; Douki, T.; Gasparutto, D.; Pouget, J.-P. Ravanat, J.-L.; Sauvaigo, S. *Mutat. Res.* **1999**, *424*, 9−21. (d) Jaeschke, H.; Gores, G. J.; Cederbaum, A. I.; Hinson, J. A.; Pessayre, D.; Lemasters, J. J. *Toxicol. Sci.* **2002**, *65*, 166−176.
(8) Pryor, W. A. *Free Radical Biol. Med.* **1988**, *4*, 219−223.
(9) (a) Cheng, K. C.; Cahill, D. S.; Kasai, H.; Nishimura, S.; Loeb, L. A. *J. Biol. Chem.* **1992**, *267*, 166−172. (b) Olinski, R.; Gackowski, D.; Foksinski, M.; Rozalski, R.; Roszkowski, K.; Jaruga, P. *Free Radical Biol. Med.* **2002**, *33*, 192−200. (c) Floyd, R. A. *Carcinogenesis* **1990**, *11*, 1447−1450.
(10) (a) Walling, C. *Acc. Chem. Res.* **1975**, *8*, 125−131. (b) Aruoma, O. I.; Halliwell, B.; Gajewski, E.; Dizdaroglu, M. *J. Biol. Chem.* **1989**, *264*, 20509−20512. (c) Lloyd, D. R.; Phillips, D. H. *Mutat. Res.* **1999**, *424*, 23−36.
(11) Imlay, J. A.; Linn, S. *Science* **1988**, *240*, 1302−1309.
(12) Mello-Filho, A. C.; Meneghini, R. *Mutat. Res.* **1991**, *251*, 109−113.
(13) Luo, Y.-C.; Han, Z.-X.; Chin, S. M.; Linn, S. *Proc. Natl. Acad. Sci. U.S.A.* **1994**, *91*, 12438−12442.
(14) Mello-Filho, A. C.; Meneghini, R. *Biochim. Biophys. Acta* **1984**, *781*, 56−63.
(15) (a) Shigenaga, M. K.; Ames, B. N. *Free Radical Biol. Med.* **1991**, *10*, 211−216. (b) Lunec, J.; Holloway, K. A.; Cooke, M. S.; Faux, S.; Griffiths, H. R.; Evans, M. D. *Free Radical Biol. Med.* **2002**, *33*, 875−885. (c) Kasai, H. *Mutat. Res.* **1997**, *387*, 147−163. (d) Halliwell, B. *Free Radical Biol. Med.* **2002**, *32*, 968−974. (e) Gedik, C. M.; Boyle, S. P.; Wood, S. G.; Vaughan, N. J.; Collins, A. R. *Carcinogenesis* **2002**, *23*, 1441−1446.
(16) Cunningham, R. P. *Curr. Biol.* **1997**, *7*, R576−R579.
(17) Cheng, K. C.; Cahill, D. S.; Kasai, H.; Nishimura, S.; Loeb, L. A. *J. Biol. Chem.* **1992**, *267*, 166−172.
(18) Steenken S.; Jovanovic S. V. *J. Am. Chem. Soc.* **1997**, *119*, 617−618.
(19) (a) Goyal, R. N.; Jain, N.; Garg, D. K. *Bioelectrochem. Bioenerg.* **1997**, *43*, 105−114. (b) Duarte, V.; Muller, J. G.; Burrows, C. J. *Nucleic Acids Res.* **1999**, *27*, 496−502.
(20) (a) Duarte, V.; Muller, J. G.; Burrows, C. J. *Nucleic Acids Res.* **1999**, *27*, 496−502. (b) Hickerson, R. P.; Prat, F.; Foote, C. S.; Burrows, C. J. *J. Am. Chem. Soc.* **1999**, *121*, 9423−9428. (c) Luo, W.; Muller, J. G.; Rachlin, E. M.; Burrows, C. J. *Chem. Res. Toxicol.* **2001**, *14*, 927−938.

EC to observe the time course of 8-oxoG generation by reacting hydroxyl radicals with DNA in vitro.[23] Requirements for hydrolysis and workup of DNA make LC-based methods too labor intensive and expensive for routine clinical measurements. A long-term goal of our work is to develop biosensor alternatives that can detect DNA damage without hydrolysis or complex instrumentation.

Electroanalysis provides instrumentally simple, sensitive, and inexpensive approaches to detect DNA hybridization and damage.[24−29] We recently reported that oxidation of guanines in DNA by electrochemically generated $[Ru(bpy)_2(PVP)_{10}]^{3+}$ {PVP=poly(vinylpyridine)} in ultrathin films leads to photoexcited $[Ru(bpy)_2^{2+}]^*$ sites that decay to generate electrochemiluminescence (ECL).[30] No sacrificial reductant is required. The reaction is initiated by electrochemical catalytic oxidation of guanines in DNA similar to that reported by Thorp et al.[31] for soluble $Ru(bpy)_3^{2+}$. This thin-film ECL approach was utilized to detect DNA damage from styrene oxide.[30]

Ropp and Thorp showed that $Os(bpy)_3^{3+}$ selectively oxidizes 8-oxoG in the presence of guanine.[32] $Os(bpy)_3^{2+}$ has a much lower redox potential (~0.62 V vs SCE) than $Ru(bpy)_3^{2+}$ and therefore does not oxidize guanine. $Os(bpy)_3^{2+}$ catalyzes the oxidation of 8-oxoG in eqs 1 and 2[33]

$$Os(bpy)_3^{2+} = Os(bpy)_3^{3+} + e^- \text{ (at electrode)} \quad (1)$$

$$Os(bpy)_3^{3+} + DNA(8\text{-oxoG}) \rightarrow Os(bpy)_3^{2+} + DNA(8\text{-oxoG}^+) \quad (2)$$

This pathway was used to probe telomerase function using 8-oxoG at specific DNA sites[32] and to investigate intermolecular vs intramolecular reactivity of Os-labeled oligonucleotides.[34]

Dissolved $Os(bpy)_3^{2+}$ is capable of generating ECL if oxidized in the presence of a sacrificial reductant such as oxalate.[35] Electrochemical catalytic oxidation of 8-oxoG with $Os(bpy)_3^{2+}$ is analogous to the oxidation of guanine with metallopolyion $[Ru(bpy)_2(PVP)_{10}]^{2+}$ that generates ECL from DNA directly without a sacrificial reductant.[30] We suspected that catalytic oxidation of 8-oxoG in DNA with $[Os(bpy)_2(PVP)_{10}]^{2+}$ could lead to photoexcited Os^{II}* sites and provide ECL signals. We report here that ultrathin films containing $[Os(bpy)_2(PVP)_{10}]^{2+}$ and oligonucleotides on electrodes directly generate ECL from oxidized DNA without using a sacrificial reductant. Films combining $[Ru(bpy)_2(PVP)_{10}]^{2+}$ and $[Os(bpy)_2(PVP)_{10}]^{2+}$ can be used to detect DNA oxidation and nucleobase adducts from chemical damage.

Experimental Section

Chemicals and Materials. Bis-$[Ru(bpy)_2(PVP)_{10}](ClO_4)_2$ and bis-$[Os(bpy)_2(PVP)_{10}]Cl_2$ were prepared, purified, and characterized as described previously.[36−38] Standard time-resolved luminescence gave quantum yields and luminescence lifetimes,[39] respectively, as follows: (1) $[Ru(bpy)_2(PVP)_{10}]^{2+}$ in cast films in pH 5.5 buffer: 0.87%, 61 ns, dissolved in solution 5.9%, 45 ns. (2) $[Os(bpy)_2(PVP)_{10}]^{2+}$ in films 0.03%, 22 ns, in solution 0.47%, 14 ns. Quantum yields and luminescence lifetimes did not show a large influence of pH.

Calf Thymus (CT) double-stranded (ds) DNA (Sigma, type XV, 13 000 av base pairs, 41.9% G/C), CT single-stranded (ss)-DNA, Salmon Testes (ST) ds-DNA (Sigma, ~2000 av base pairs, 41.2% G/C), ST ss-DNA, polyguanadylic acid (5′) (Poly [G]), polycytidylic acid (5′) (Poly [C]), styrene oxide, and toluene were from Sigma, and polyadenylic acid (5′) (Poly [A]) was from ICN Biomedical Research Products. Water was purified with a Hydro Nanopure system to specific resistance >18 mΩ cm. All other chemicals were reagent grade.

ECL Voltammetry. Simultaneous square wave voltammetry (SWV)/ECL measurements were made in a three-electrode cell at 37.0 ± 0.5 °C using a CH Instruments model 660a electrochemical analyzer. The cell employed a saturated calomel reference electrode (SCE), a Pt wire counter electrode, and a 4-mm diameter disk of ordinary basal plane pyrolytic graphite (PG, Advanced Ceramics) as working electrode placed close to the glass cell bottom. The electrolyte solution was 10 mM acetate buffer, pH 5.5, containing 50 mM NaCl. SWV conditions were 4 mV step height, 25 mV pulse height, and frequency 5 Hz. The cell was covered with a black cloth to avoid external light. Solutions were purged with pure nitrogen for 15 min prior to each series of experiments, and a nitrogen atmosphere was maintained during data collection. A different electrode was used for each analysis of DNA oxidation.

A Labmaster Coherent Ultima photomultiplier/monochromator/data collection system was used to record light from the electrode (764 and 610 nm) via an optical fiber positioned directly underneath the electrode outside the flat bottom of the glass electrochemical cell.

Film Assembly. DNA/metallopolymer films were constructed by layer-by-layer alternate electrostatic assembly.[40−42] Basal plane PG electrodes were polished with 400 grit SiC paper and then with 0.3 μm α-alumina slurries on Buehler Microcloth, washed with water and sonicated in ethanol for 15 min, and then sonicated in water for 15 min. Layers were constructed by placing 30 μL drops of 0.2% aqueous $[Os(bpy)_2(PVP)_{10}]^{2+}$ or 1:1 $[Ru(bpy)_2(PVP)_{10}]^{2+}$/$[Os(bpy)_2(PVP)_{10}]^{2+}$ onto each PG electrode, allowing 15 min to achieve saturated adsorption,[42] and then washing with water. Subsequently, 30 μL of

(21) Henderson, P. T.; Delaney, J. C.; Muller, J. G.; Neeley, W. L.; Tannenbaum, S. R.; Burrows, C. J.; Essigmann, J. M. *Biochemistry* **2003**, *42*, 9257−9262.
(22) (a) Floyd, R. A.; Watson, J. J.; Wong, P. K.; Altmiller, D. H.; Rickard, R. C. *Free Radical Res. Commun.* **1986**, *1*, 163−172. (b) Helbock, H. J.; Beckman, K. B.; Shigenaga, M. K.; Walter, P. B.; Woodall, A. A.; Yeo, H. C.; Ames, B. N. *Proc. Natl. Acad. Sci. U.S.A.* **1998**, *95*, 288−293.
(23) White, B.; Smyth, M. R.; Stuart, J. D.; Rusling, J. F. *J. Am. Chem. Soc.* **2003**, *125*, 6604−6605.
(24) Palecek, E.; Fojta, M.; Tomschik, M.; Wang, J. *Biosens. Bioelectron.* **1998**, *13*, 621−628.
(25) Palecek, E. *Electroanalysis* **1996**, *8*, 7−14.
(26) Thorp, H. H. *Trends Biotechnol.* **1998**, *16*, 117−121.
(27) Palecek, E.; Fojta, M. *Anal. Chem.* **2001**, *73*, 74A−83A.
(28) (a) Wang, J.; Rivas, G.; Ozsoz, M.; Grant, D. H.; Cai, X.; Parrado, C. *Anal. Chem.* **1997**, *69*, 1457−1460. (b) Wang, J. *Chem.−Eur. J.* **1999**, *5*, 1681−1685.
(29) Rusling, J. F.; Zhang, Z. In *Biomolecular Films*; Rusling, J. F., Ed.; Marcel Dekker: New York, 2003; pp 1−64.
(30) Dennany, L.; Forster, R. J.; Rusling, J. F. *J. Am. Chem. Soc.* **2003**, *125*, 5213−5218.
(31) Johnston, D. H.; Glasgow, K. C.; Thorp, H. H. *J. Am. Chem. Soc.* **1995**, *117*, 8933−8938.
(32) Ropp, P. A.; Thorp, H. H. *Chem. Biol.* **1999**, *6*, 599−605.
(33) Szalai, V. A.; Singer, M. J.; Thorp, H. H. *J. Am. Chem. Soc.* **2002**, *124*, 1625−1631.
(34) Holmberg, R. C.; Tierney, M. T.; Ropp, P. A.; Berg, E. E.; Grinstaff, M. W.; Thorp, H. H. *Inorg. Chem.* **2003**, *42*, 6379−6387.
(35) (a) Chang, M.-M.; Sagi, T.; Bard, A. J. *J. Am. Chem. Soc.* **1977**, *99*, 5399−5403. (b) Rodriquez, M.; Bard, A. J. *Anal. Chem.* **1990**, *62*, 2658−2662.
(36) Durham, B.; Wilson, S. R.; Hodgson, D. J.; Meyer, T. J. *J. Am. Chem. Soc.* **1980**, *102*, 600−607.
(37) Hogan, C. F.; Forster, R. J. *Anal. Chem.* **1999**, *396*, 13−21.
(38) Forster, R. J.; Vos, J. G. *Macromolecules* **1990**, *23*, 4372−4377.
(39) Casper, J. V.; Meyer, T. J. *J. Am. Chem. Soc.* **1983**, *105*, 5583−5589.
(40) Zhou, L.; Rusling, J. F. *Anal. Chem.* **2001**, *73*, 4780−4786.
(41) Mugweru, A.; Rusling, J. F. *Electrochem. Commun.* **2001**, *3*, 406−409.
(42) (a) Lvov, Y. In *Protein Architecture: Interfacing Molecular Assemblies and Immobilization Biotechnology*; Lvov, Y., Möhwald, H., Eds.; Marcel Dekker: New York, 2000; pp 125−167. (b) Lvov, Y. In *Handbook of Surfaces and Interfaces of Materials. Vol. 3: Nanostructured Materials, Micelles and Colloids*; Nalwa, H. S., Ed.; Academic Press: San Diego, CA, 2001; pp 170−189. (c) Rusling, J. F. In *Protein Architecture: Interfacing Molecular Assemblies and Immobilization Biotechnology*; Lvov, Y., Möhwald, H., Eds.; Marcel Dekker: New York, 2000; pp 337−354. (d) Rusling, J. F.; Zhang, Z. In *Handbook of Surfaces and Interfaces of Materials. Vol. 5: Biomolecules, Biointerfaces and Applications*; Nalwa, H. S., Ed.; Academic Press: San Diego, CA, 2001; pp 33−71.

DNA or oligonucleotide solution (2 mg mL^{-1} DNA in 5 mM pH 5.5 acetate buffer +0.05 M NaCl) was placed on this PG surface, allowed to adsorb 15 min, and then washed with water. This sequence was repeated to obtain films with two metallopolymer/DNA bilayers. Films containing ss-DNA and polynucleotides were also assembled in this way.

Assembly of films was assessed at each step with a quartz crystal microbalance (QCM, USI Japan) using 9 MHz QCM resonators (AT-cut, International Crystal Mfg.). To mimic the carbon electrode surface, a negative monolayer was made by treating gold-coated (0.16 ± 0.01 cm^2) quartz resonators with 0.7 mM 3-mercapto-1-propanol and 0.3 mM 3-mercaptopropionic acid in ethanol.[40] Films were assembled as for PG electrodes. Resonators were dried in a stream of nitrogen before the frequency change (ΔF) was measured. Absorbed mass was estimated with the Sauerbrey equation,[42] for 9 MHz quartz resonators, giving dry film mass per unit area M/A as:

$$M/A\ (\text{g cm}^{-2}) = -\Delta F\ (\text{Hz})/(1.83 \times 10^8) \quad (3)$$

The nominal thickness (d) of dry films was estimated with an expression confirmed by high-resolution electron microscopy:[43]

$$d\ (\text{nm}) \approx (-0.016 \pm 0.002)\Delta F\ (\text{Hz}) \quad (4)$$

DNA Oxidation. Films were incubated in a stirred reactor at 37.0 ± 0.5 °C. A 100 μL volume of 15 mM $FeSO_4$ and 1 mL of H_2O_2 (Fenton reagent) were added to 9 mL of acetate buffer, pH 5.5 and 50 mM NaCl, to give final concentrations 0.15 mM $FeSO_4$ and 5.0 mM H_2O_2. PG electrodes coated with polynucleotide/metallopolymer films were incubated in the stirred solutions, then rinsed with water and transferred to the electrochemical cell containing fresh pH 5.5 buffer for SWV/ECL analysis. pH 5.5 allows efficient ECL production.[44] Alternative hydrolysis and 8-oxoG measurement by LC–UV–EC was done by a previously described method.[23]

Results

QCM Monitoring of Film Assembly. On the basis of previous studies of the influence of number of layers on ECL efficiency in $[Ru(bpy)_2(PVP)_{10}]$/DNA films,[30] we chose two bilayers of ds-DNA/$[Os(bpy)_2(PVP)_{10}]^{2+}$ (Os–PVP) or two bilayers of DNA and 1:1 $[Ru(bpy)_2(PVP)_{10}]$ (Ru–PVP) and (Os–PVP), denoted (RuOs–PVP/DNA)$_2$. Integrity and reproducibility of film formation was characterized by measuring QCM frequency shifts (ΔF) after each layer of film growth, as illustrated for films of DNA and mixed metallopolymers (Figure 1). $-\Delta F$ values varied linearly with layer number for ss-DNA, and ds-DNA alternated with RuOs–PVP layers, suggesting regular film growth with reproducible layer formation. ΔF values with eqs 3 and 4 were used to estimate weights of metallopolymers and DNA and average nominal thickness of the films (Table 1). Total film thicknesses were ~16 nm, with each film containing ~3 μg cm^{-2} DNA. A slightly larger amount of ss-DNA than ds-DNA was incorporated into films, as also found for DNA in films with other polycations.[40]

ECL/SWV of Os–PVP/Oligonucleotide Films after Oxidation. We first examined films containing homogeneous polynucleotides and Os–PVP. Upon incubation of electrodes with Fenton's reagent to oxidize the oligonucleotides, a significant increase in the ECL and SWV responses for (Os–PVP/Poly G)$_2$ films was found (Figure 2). The SWV peak occurred at 0.58 V vs SCE, and the maximum ECL signal was slightly positive of this at ~0.60 V. Fenton's reagent oxidizes guanines to 8-oxoG,[17,23,45,46] which has a lower oxidation potential than guanine. 8-OxoG is presumably oxidized by $[Os(bpy)_2]^{3+}$ centers in the film, similar to reactions with soluble osmium complexes.[32,47]

Fenton's reagent also oxidizes adenine and cytosine to products including 7-deazaadenine, 8-oxoadenine, and 5-hy-

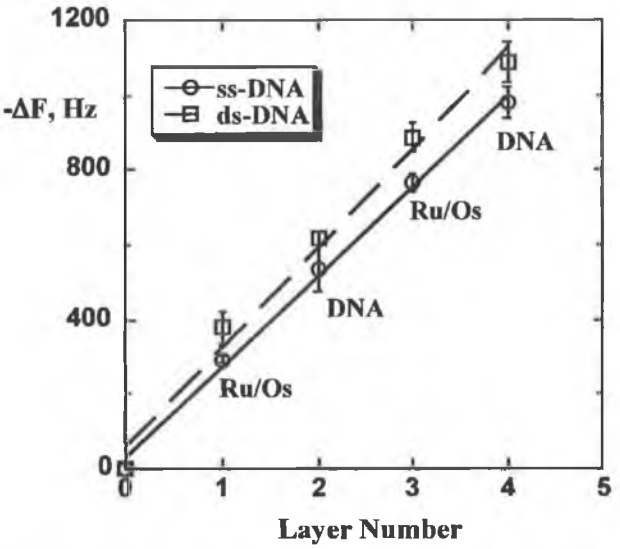

Figure 1. QCM frequency shifts monitoring film formation on gold–quartz resonators coated first with mixed monolayers of mercaptopropionic acid/mercaptopropanol for alternate adsorption of 1:1 $[Os(bpy)_2(PVP)_{10}]^{2+}$/$[Ru(bpy)_2(PVP)_{10}]^{2+}$ and salmon testes DNA (average values for three replicate films).

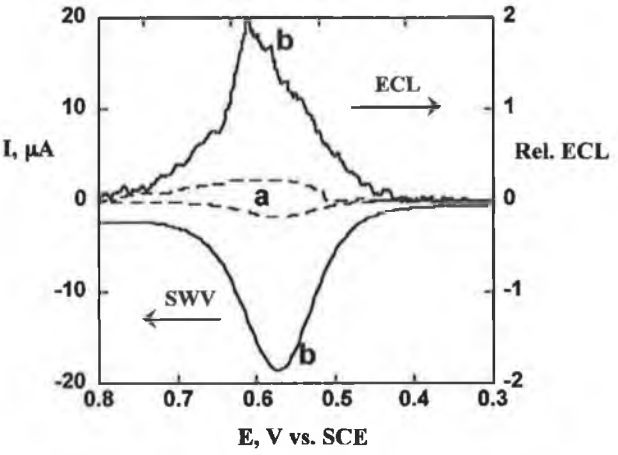

Figure 2. SWV and ECL for (Os–PVP/Poly G)$_2$ films on PG electrodes in pH 5.5 buffer and 50 mM NaCl (a) before and (b) after 20 min incubation at 37 °C with Fenton reagent. ECL emission monitored at 764 nm.

Table 1. Average Characteristics of Metallopolyion/DNA Films from QCM

film	nominal thickness, nm	mass DNA, μg cm^{-2}	mass RuOs–PVP, μg cm^{-2}
(RuOs–PVP/ST-ds-DNA)$_2$	15 ± 2	2.9 ± 0.5	1.8 ± 0.1
(RuOs–PVP/ST-ss-DNA)$_2$	17 ± 2	3.4 ± 0.4	2.0 ± 0.3

(43) Lvov, Y.; Ariga, K.; Ichinose, I.; Kunitake, T. *J. Am. Chem. Soc.* **1995**, *117*, 6117–6123.
(44) Rubinstein, I.; Bard, A. J. *J. Am. Chem. Soc.* **1980**, *102*, 6642–6644.
(45) Henle, E. S.; Lou, Y.; Linn, S. *Biochemistry* **1996**, *35*, 12212–12219.
(46) Henle, E. S.; Linn, S. *J. Biol. Chem.* **1997**, *272*, 19095–19098.
(47) Baik, M.-H.; Silverman, J. S.; Yang, I. V.; Ropp, P. A.; Szalai, V. A.; Yang, W.; Thorp, H. H. *J. Phys. Chem. B* **2001**, *105*, 6437–6444.

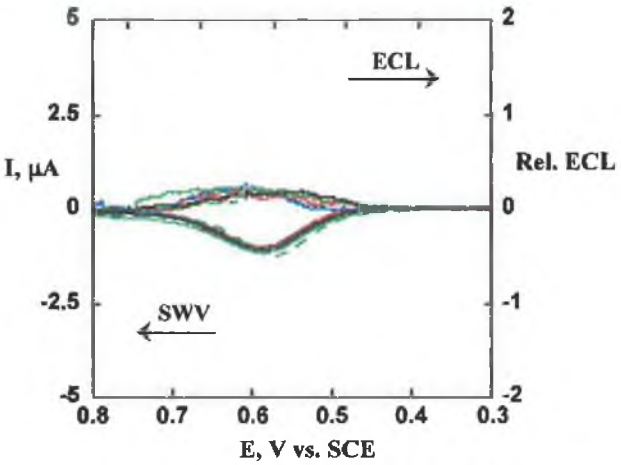

Figure 3. SWV/ECL for films containing Os−PVP but no DNA on PG electrodes in pH 5.5 buffer before and after 20 min incubation with Fenton reagent. Os−PVP alone (black, solid); $(Os−PVP/PSS)_2$ before (blue, dashed) and after (green, solid) incubation; $(Os−PVP/Poly\ A)_2$ before (red, solid) and after (red dashed) incubation; $(Os−PVP/Poly\ C)_2$ before (blue solid) and after (green, dashed) incubation. ECL emission monitored at 764 nm.

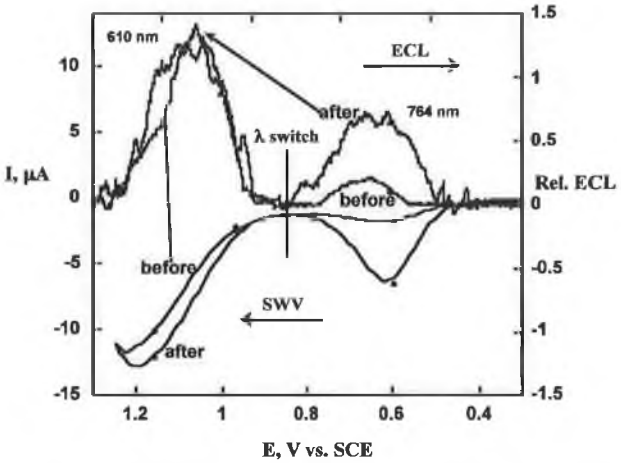

Figure 4. SWV/ECL for $(OsRu−PVP/Poly\ G{\cdot}Poly\ C)_2$ films on PG electrodes in pH 5.5 buffer before and after 20 min incubation at 37 °C with Fenton reagent. ECL emission at ~764 nm and then switched to ~610 nm at 0.8 V at marker.

droxycytosine.[17,45,46] Figure 3 shows ECL/SWV for control films containing the Os−PVP alone, as well as Os−PVP with PSS, poly A, and poly C, before and after incubation with Fenton's reagent. ECL and SWV curves are nearly superimposable for all these films; no significant changes were found after incubation under our oxidation conditions. Curves were similar to those for films containing Os−PVP only. The Os^{II}/Os^{III} peak reflecting the formal potential in the films is at 0.58 V vs SCE. However, increasing the H_2O_2 concentration to 50 mM in the Fenton reagent resulted in the detection of small increases in Os^{II} SWV and ECL peaks in films containing Poly A but not poly C. If oxidized forms of cytosine are formed, their oxidation potentials may be too positive[48] for them to be catalytically oxidized by $[Os(bpy)_2(PVP)_{10}]^{2+}$.

Figure 4 shows the responses obtained for films made from the two metallopolymers and prehybridized poly G/poly C, i.e., $(Os−Ru−PVP/PolyG{\cdot}Poly\ C)_2$. The Os^{II} catalytic peak appears

(48) Jovanaic, S. V.; Simic, M. G. *J. Phys. Chem.* **1986**, *90*, 974−978.

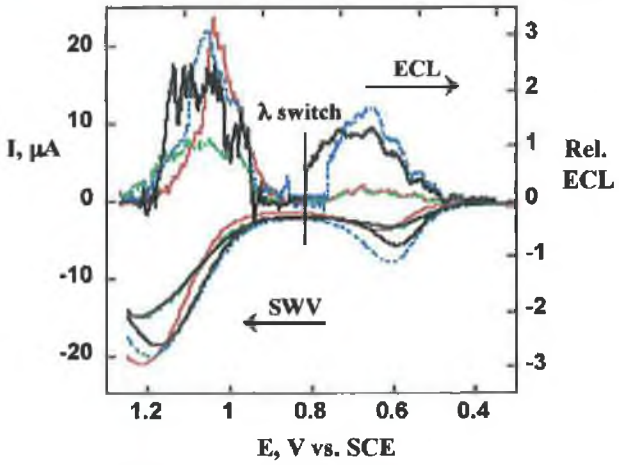

Figure 5. SWV/ECL for $(OsRu−PVP/ds\text{-}ST\ DNA)_2$ films on PG electrodes in pH 5.5 buffer before (red = ss-DNA; green = ds-DNA) and after 20 min incubation at 37 °C (blue = ss-DNA; black = ds-DNA) ECL emission monitored at ~764 nm and then switched to ~610 nm at the 0.8 V as labeled.

at ~0.6 V, and the Ru^{II} peak is at ~1.2 V, reflecting the redox potentials of these polymers. Before incubation, the Ru peak is 6- to 7-fold larger than the Os peak in both ECL and SWV, reflecting the fact that catalytic oxidation of guanine by Ru centers can take place in the hybridized oligonucleotide and that there will be little catalysis by the Os sites if the DNA is not oxidized. After incubation with Fenton's reagent, there is a dramatic increase in both the ECL and SWV peaks for the Os^{II}/Os^{III} couple in the $(Os−Ru−PVP/PolyG{\cdot}Poly\ C)_2$ films because of catalytic oxidation of 8-oxoG formed in the incubation. However, there is only a small increase in the Ru ECL and SWV peaks.

Qualitatively, the increase in the Os peaks after incubation was larger for the films containing unhybridized Poly G (Figure 2) than for the $(Os−Ru/PolyG{\cdot}Poly\ C)_2$ film (Figure 4). This may result from better accessibility of the unhybridized bases to the reactants and the metallopolymers. Thus, we compared the films of ds- and ss-DNA for which Figure 1 was obtained (Figure 5), with known amounts of DNA and metallopolymers (Table 1). Before incubation, the ds- and ss-DNA gave nearly identical results for the Os peak. The ss-DNA gave a >2-fold larger peak at the Ru potential because of enhanced oxidation by the polymer due to greater accessibility of the guanines.[30] After incubation, the ss-DNA gave somewhat larger signals than ds-DNA for both the Os and the Ru peaks. However, the differences were much smaller than that of the Ru peak for non-oxidized ss- and ds-DNA.

When $(OsRu−PVP/ds\text{-}DNA)_2$ films were incubated with Fenton reagent for various times, increases in the ratios of ECL and SWV (final/initial) Os^{II} peaks were observed for up to 20 min. (Figure 6). At longer times, dampened oscillations in these signals were observed (see Supporting Information, Figure S2, for original SWV and ECL traces). Controls consisting of the same types of films incubated with $FeSO_4$ alone, H_2O_2 alone, or only buffer had peak ratios within experimental error of unity

We previously found similar oscillating concentration−time profiles for 8-oxoG during oxidation of DNA and guanine solutions by Fenton reagent under different conditions, determining 8-oxoG after DNA hydrolysis by using LC−EC.[23] Thus,

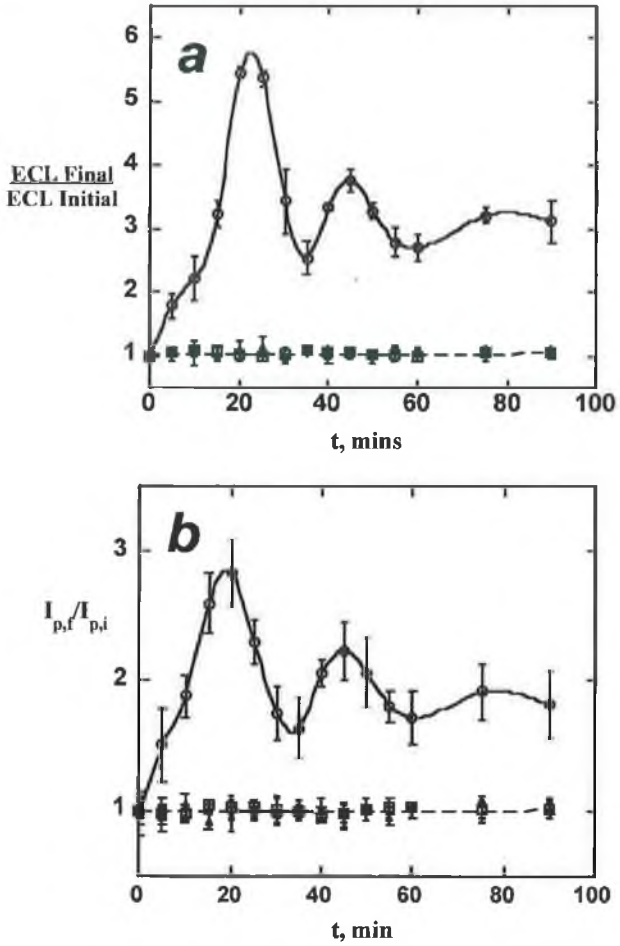

Figure 6. Influence of incubation of $(OsRu-PVP/ds\text{-}ST\ DNA)_2$ films with Fenton reagent (○), with $FeSO_4$ alone (▲), H_2O_2 alone (□), and only pH 5.5 buffer (+) on (a) average ECL signals and (b) average SWV catalytic peak currents for the Os^{II}/Os^{III} redox couple. Error bars represent standard deviations for three trials; one electrode was used per trial.

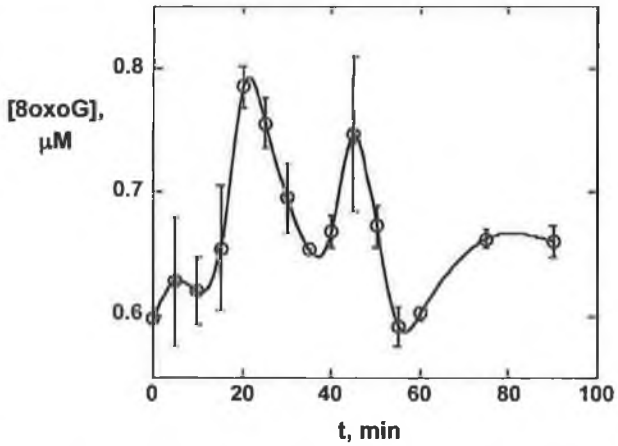

Figure 7. Concentration profile of [8oxoG] determined by LC–EC during oxidation of 1.2 mg mL^{-1} ds-DNA in pH 5.5 by Fenton reagent under same conditions as for incubation of DNA electrodes. (Average of three determinations. DNA hydrolyzed before analysis.)

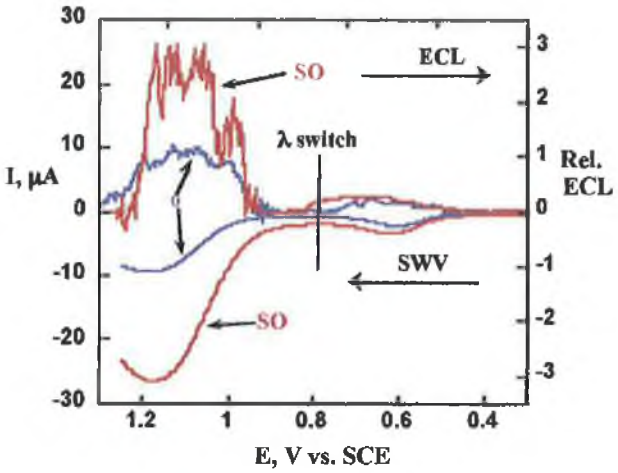

Figure 8. SWV and ECL responses for $(Os-Ru/ds\text{-}ST\ DNA)_2$ films on PG electrodes in pH 5.5 before (purple) after (red) 25 min incubations at 37 °C with saturated styrene oxide (SO). ECL emission monitored at ~764 nm and then switched to ~610 nm at the 0.8 V marker.

we repeated this LC–EC analysis on DNA in solution that was oxidized under exactly the same conditions as our electrodes for ECL/SWV. Concentration profiles for 8-oxoG obtained by LC–EC are given in Figure 7. The error bars of the LC–EC results for the small amounts of [8-oxoG] found are somewhat larger than those for ECL and SWV, but the same concentration profile was found during 100 min of reaction. An initial increase in [8-oxoG] leads to a clear maximum at about 20 min, followed by dampened oscillations in [8-oxoG] at longer times.

The Ru^{II} ECL and SWV peak ratios (Figure S3) for the same films for which the Os^{II} peaks were discussed (cf. Figure 6) showed increases in the first 20 min of incubation with Fenton's reagent. These ratios reached limiting values slightly larger than 2 at $t > 20$ min. The increase may be attributed to the formation of oxidized adenine derivatives or possible strand breaks, either of which can result from the action of the Fenton reagents on DNA. No significant increases or trends for the Ru^{II} peaks were found when the films were incubated in buffer only, buffer with $FeSO_4$ only, or buffer with H_2O_2 only.

To assess the contribution to the ECL signals from the formation of adenine or cytosine derivatives upon oxidation, films containing both the metallopolymers and either Poly A or Poly C were incubated with Fenton reagent (Supporting Information, Figure S4). For the Poly C films, there was no increase in either the Os or Ru peaks upon incubation. For the film containing Poly A, there was no increase in the Os peaks, but there was ~7% increase in the Ru peaks in both ECL and SWV after 20 min incubation. This may reflect the oxidation of oxo-adenines by the electrogenerated Ru^{III} sites in the films.

ECL and SWV of $(OsRu-PVP/Poly\ G)_2$ films before and after incubation (Supporting Information, Figure S5) resembled those of $(Os-Ru/Poly\ G{\cdot}Poly\ C)_2$ in Figure 4. The ECL and SWV signals for the Os peaks increased upon incubation with Fenton's reagent, but the peaks for the Ru sites remained about the same.

Chemically Damaged OsRu–PVP/DNA Films. The influence of chemical damage of DNA was investigated by treating films with styrene oxide, which forms covalent adducts with DNA in films mainly at the nitrogens of guanine.[40] OsRu–PVP/DNA films incubated with styrene oxide showed increases in the Ru^{II} SWV and ECL peaks (Figure 8), as previously reported for Ru–PVP/DNA films.[30] The films were also incubated in toluene, which does not react with DNA, and with

buffer alone, and they showed no increase or trend for the Ru or Os peaks. Films incubated with styrene oxide for 25 min gave only very small increases in the Os^{II} SWV or ECL peak signals (Figure 8).

Discussion

Our results demonstrate for the first time that ECL can be achieved by direct reaction of an osmium metallopolymer with oxidized DNA in ultrathin films (Figures 2, 4, and S5). The ECL detection equipment is simple and inexpensive, featuring a conventional voltammetric cell combined with an optical fiber that delivers light from the electrode to a monochromator/PMT detector. Osmium and ruthenium complex metallopolymers can be incorporated together in films with DNA to detect both DNA oxidation and chemical DNA damage (Figure 8). Alternate layer-by-layer electrostatic assembly on PG electrodes provided metallopolymer/DNA films ~16-nm thick (Table 1), presumably featuring intimate mixing of the metallopolymers and ds-DNA in a tiny reaction volume. Extensive intermixing of layers in polycation/polyanion and protein/polycation films assembled by this method has been established by neutron reflectivity studies with deuterium-labeled polyions.[42a,b,49] Such mixing facilitates intimate contact between the DNA and metallopolymers to achieve efficient catalytic oxidation of the DNA to produce ECL.

Among the homogeneous polynucleotides, only films containing poly G (Figures 4 and S5) gave significant increases in the Os^{II} SWV and ECL peaks upon oxidation by Fenton's reagent containing 5 mM H_2O_2. However, small increases in these peaks were also found in Poly A films when $[H_2O_2]$ was increased to 50 mM. Increases in the Os^{II} SWV and ECL peaks upon DNA oxidation by Fenton's reagent with 5 mM H_2O_2 appear to result mainly from oxidized guanines, presumably 8-oxoG. Oxidized adenines may contribute to the signal at higher $[H_2O_2]$ that presumably provides more extensive DNA oxidation. In general, the Os^{II} ECL in these films seems to be mainly specific for 8-oxoG, with minor contributions from oxidized adenines.

Again for the homogeneous polynucleotides, only films containing poly A gave increases for the Ru^{II} SWV and ECL peaks after oxidation (Figure S4). Films containing poly G (Figure S5) gave increases in the Os^{II} peaks but not in the Ru^{II} peaks. However, oxidized ss-DNA gave larger peaks at both Os^{II} and Ru^{II} potentials compared to oxidized ds-DNA (Figure 5). This is consistent with better accessibility of active oxidant sites in the film for their DNA-based reaction partners. In fact, oxidized ss-DNA gave peaks of about the same height as non-oxidized ss-DNA at the Ru^{II} potentials. On the basis of these observations, we rationalize the increase in the Ru^{II} peaks upon DNA oxidation (Figure 5) as related to oxidized adenines and strand breaks[9] that could produce an increased amount of single DNA strands in the films.

The formation of chemical adducts of guanine and adenine bases of DNA in films by reaction with styrene oxide under the conditions used in Figure 8 has been confirmed by LC–MS.[50] With the OsRu–PVP/DNA films, we observed minimal increases in the Os^{II} ECL and SWV (Figure 8) upon reaction with styrene oxide, but large increases were found for the Ru^{II} peaks as reported previously.[30] This result suggests that the Os^{II} ECL is not sensitive to formation of the DNA base adducts in this experiment.

On the basis of our results and previous proposals for pathways for ECL generation,[35,37,44] the initial step is likely to involve reaction of electrochemically generated $[Os(bpy)_2(PVP)_{10}]^{3+}$ with a reductant on DNA. We suggest that the osmium metallopolymer generates ECL signals following pathways represented in eqs 5–10 (8G = 8-oxoguanine site):

$$[Os(bpy)_2(PVP)_{10}]^{2+} = [Os(bpy)_2(PVP)_{10}]^{3+} + e^- \quad (5)$$

$$[Os(bpy)_2(PVP)_{10}]^{3+} + 8G \rightarrow [Os(bpy)_2(PVP)_{10}]^{2+} + 8G^+ \quad (6)$$

$$[Os(bpy)_2(PVP)_{10}]^{3+} + 8G^+ \rightarrow [Os(bpy)_2(PVP)_{10}]^{2+*} + 8G^{2+} \quad (7)$$

$$[Os(bpy)_2(PVP)_{10}]^{2+*} \rightarrow [Os(bpy)_2(PVP)_{10}]^{2+} + h\nu \quad (8)$$

Or alternatively:

$$[Os(bpy)_2(PVP)_{10}]^{2+} + 8G^+ \rightarrow [Os(bpy)_2(PVP)_{10}]^{+} + 8G^{2+} \quad (9)$$

$$[Os(bpy)_2(PVP)_{10}]^{+} + [Os(bpy)_2(PVP)_{10}]^{3+} \rightarrow [Os(bpy)_2(PVP)_{10}]^{2+} + [Os(bpy)_2(PVP)_{10}]^{2+*} \quad (10)$$

Initial oxidation of the metallopolymer by the electrode gives the Os^{III} oxidant (eq 5), which reacts mainly with 8-oxoG (8G) in DNA to give $8G^+$ (eq 6), which may produce photoexcited $[Os(bpy)_2(PVP)_{10}]^{2+*}$ sites (eq 7), by directly reducing the Os^{III} sites in the film. This excited-state Os^{II} complex decays to the ground state by emission at ~764 nm (eq 8).[38] An alternative pathway is shown in eqs 9 and 10, where G^+ may reduce the Os^{II} sites to Os^{I}, which can then produce Os^{II*} by reacting with Os^{III} sites. Further studies are underway to distinguish these possibilities.

In the early stages of the Fenton oxidation of the DNA films, both the Os^{II} and Ru^{II} ECL and SWV peak ratios increase with reaction time (Figures 6 and S3). After about 20 min reaction of the films, the Ru^{II} signals reach a steady state, but the Os^{II} peaks showed dampened oscillations up to 100 min (Figure 6). LC–EC analysis of DNA after it had been oxidized under identical conditions and then hydrolyzed showed an almost identical pattern of oscillations in concentration of 8-oxoG (Figure 7).

We previously described oscillations of 8-oxoG concentrations during Fenton oxidation of both free guanine and DNA in solution under several conditions by LC–EC–UV analysis.[23] In the present work, our Fenton's reagent contains 10-fold less H_2O_2 than previously used. Nevertheless, oxidation of DNA in solution analyzed by LC–EC gave oscillations in [8-oxoG] (Figure 7) similar to those observed with 10-fold larger H_2O_2 concentrations. Detection of oscillations by the independent Os^{II} ECL/SWV method presented here (Figure 6) that is mainly selective for oxidized guanines confirms our earlier observation of this phenomenon. Out results are consistent with a competitive consecutive process in which guanine is oxidized to 8-oxoG, which is then rapidly oxidized to guanidinohydantoin. The latter

(49) Decher, G. *Science* **1997**, *227*, 1232–1237.
(50) Zhou, L.; Yang, J.; Estavillo, C.; Stuart, J. D.; Schenkman, J. B. Rusling, J. F. *J. Am. Chem. Soc.* **2003**, *125*, 1431–1436.

was confirmed as a major product of 8-oxoG oxidation in our reactions by LC−MS.[23] Here, the common oxidant •OH reacts with starting reactant guanine as well as the initial reaction product 8-oxoG. While this simple consecutive pathway must certainly be featured in the oscillations, it would typically lead to only one maximum in the concentration of the initial product.[51] Oscillatory reactions often have very complex pathways featuring several interactive catalytic cycles and multiple elementary steps.[52,53] This particular case is now under further study using additional DNA oxidants.

In summary, ECL can be obtained directly from the reaction of oxidized guanines in DNA in thin films with the catalytic metallopolymer $[Os(bpy)_2(PVP)_{10}]^{2+}$. ECL and SWV peaks of the Os sites in the films are sensitive to oxidative damage that results in the formation of 8-oxoG. The ECL measurement is simple and inexpensive, and the approach may be useful for the detection of oxidized DNA as a biomarker for oxidative stress. The combination of ruthenium and osmium metallopolymers in the films can allow for future applications to the simultaneous detection of chemical and oxidative DNA damage.

Acknowledgment. This work was supported by Enterprise Ireland (R.F.), NCSR at Dublin City University, and by U.S. PHS Grant No. ES03154 (J.R.) from the National Institute of Environmental Health Sciences (NIEHS), NIH, U.S.A. We thank Prof. Robert Birge and Sumie Shima for the loan of optical equipment.

Supporting Information Available: Five additional figures presenting reversible cyclic voltammetry of mixed metallopolymer films and ECL/SWV results on oligonucleotide films reacted with Fenton reagent. This material is available free of charge via the Internet at http://pubs.acs.org.

JA048615+

(51) Zuman, P.; Patel, R. *Techniques in Organic Reaction Mechanisms*; Wiley: New York, 1984; pp 96−100.
(52) Epstein, I. R.; Kustin, K. *J. Phys. Chem.* **1985**, *89*, 2275−2282.
(53) Scheeline, A.; Olson, D. L.; Williksen, E. P.; Horras, G. A. *Chem. Rev.* **1997**, *97*, 739−756.